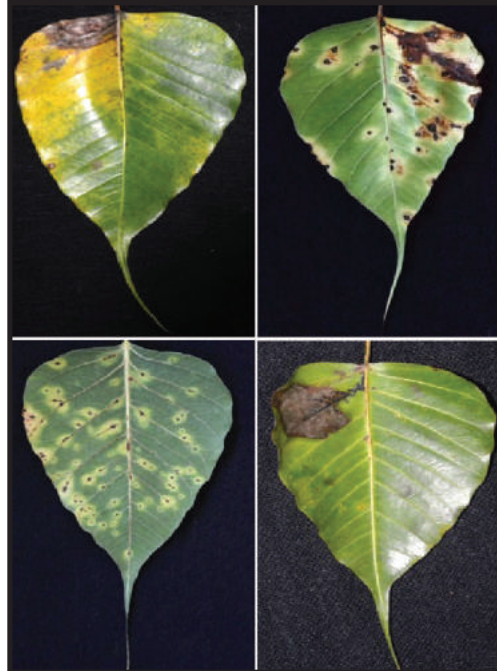


Journal of the National Science Foundation of Sri Lanka



**JOURNAL OF THE
NATIONAL SCIENCE FOUNDATION
OF SRI LANKA**

Volume 49 Number 4

December 2021

C O N T E N T S

EDITORIAL

- 467 **What is ‘organic’? organic chemistry, organic fertilizer and organic agriculture**
Ajit Abeysekera
-

RESEARCH ARTICLES

- 469 **Evaluation of insecticide resistance and underlying resistance mechanisms in selected whitefly populations in Sri Lanka**
JP Marasinghe and SHPP Karunaratne
- 479 **Occurrence of enrofloxacin and ciprofloxacin residues in broiler meat sold in Sri Lanka**
NB Karunaratna, IA Perera, NT Nayomi, DMS Munasinghe, SSP Silva, I Strashnov and BR Fernando
- 493 **Energy deposition and dose enhancement using Monte Carlo derivative sampling: applications in brachytherapy**
H Khan, ZU Koreshi, U Aziz, SR Sheikh and SA Ahmad
- 503 **Recognition of handwritten characters using deep convolution neural network**
S Arivazhagan, M Arun and D Rathina
- 513 **Mechanical and barrier properties of flexible packaging materials after the flexo printing process**
P Balaban, D Viduka, V Ristic, M Maksin, V Radic, R Vladisavljevic, M Vulic, M Josimovic and NZ Radivojevic
- 525 **Effect of priming with neem seed extract on seeds of four traditional rice varieties of Sri Lanka; Kaluheenati, Kurulurthuda, Madathawalu and Maa-wee**
MO Galappaththi, KMGG Jayasuriya and NS Gama-Arachchige
- 539 **Numerical prediction of early age concrete temperature via 3D finite difference simulation**
MP Dissanayaka and HD Yapa
- 551 **Acaricide resistance in the spinose ear tick, *Otobius megnini* (Acari: Argasidae) infesting racehorses in Sri Lanka**
GCP Diyes, KMUJ Bandara, RS Rajakaruna and SHPP Karunaratne
- 563 **Production and characterization of β -galactosidase from the fungus *Thielaviopsis ethacetica* Went.**
DMS Dissanayaka, SNT De Silva, DPSTG Attanayaka and EMM Vimukthi

- 573 **A new foliar disease of *Ficus religiosa* caused by *Diaporthe acutispora*, identified using molecular phylogeny based multigene DNA sequence analyses**
N Adikaram, S Maharachchikumbura, ISK Vithanage, D Yakandawala and L Jayasinghe
- 583 **Low dose radioiodine therapy: A review of dosimetry and evaluation of potential shielding materials for neck collars**
S Mubarak, D Nanayakkara, C Jayalath and V Sivakumar
- 593 **Effects of particle size and concentration on the pulsation characteristics of transformer oil**
C Bin and L Ge
- 607 **Bioethanol production from Palmyrah (*Borassus flabellifer*) wastes using yeast**
EJSBA Christy, S Mahilrajan, G Chandrasena and R Kapilan

617 **List of Referees**

I **Author Index**

IX **Subject Index**

Guidelines for Contributors



Cover: *Diaporthe* leaf disease in *Ficus religiosa*
See *J.Natn.Sci. Foundation Sri Lanka* 2021 49(4): 573–581

EDITORIAL

What is 'organic'? organic chemistry, organic fertilizer and organic agriculture

The historical connotation of the word 'organic' was a connection with processes in nature involving life. Thus, 'organic chemistry' was the chemistry of natural substances obtained from animals and plants. These substances were considered to possess a *vital force* which made them different from substances obtained from non-living matter such as minerals. The idea of a vital force gradually receded with the realization that at least some of the substances produced by living organisms could also be produced in the laboratory, starting from inorganic materials. Wöhler's observation in 1828, that urea could be obtained by heating ammonium cyanate, was a landmark experiment in this narrative. As the vast majority of the so-called organic compounds contained carbon, and the compounds of carbon exceed in number those of all the other elements, the term 'organic chemistry' has evolved to its current meaning today, to be the chemistry of carbon containing compounds.

The term 'organic agriculture' uses the word 'organic' in its original sense of connection with living processes in a holistic manner. Thus, one of the key principles of organic agriculture is that the farming of food crops should be carried out in a way which sustains and enhances the health of soil, plants, animals and humans; and should be based on living ecological systems and cycles.

However, the use of the word 'organic' in the term 'organic fertilizer' is ambiguous, unlike in the terms

'organic chemistry' and 'organic agriculture'. For example, urea, which is widely used as a fertilizer is produced industrially by the reaction of ammonia (from the Haber process) with carbon dioxide, is also produced by mammals as a by-product of protein metabolism.

There has been much controversy recently in Sri Lanka, regarding the importation and utilization of fertilizer, after the government of Sri Lanka stated its policy of converting to organic agriculture. It was taken for granted (incorrectly) that organic agriculture requires only 'organic fertilizer'. The controversy was partly due to the usage in public debate, of the Sinhala language word for 'organic' (which can be transcribed as "carbonica") which connotes a relationship to the element carbon, rather than to 'living' or 'natural'. The usage of the vague term 'chemical fertilizer' in the sense of being the opposite of 'organic fertilizer' confused the debate further. For example, was urea an organic fertilizer or a chemical fertilizer? Was a mineral containing potassium an organic fertilizer, chemical fertilizer or a different kind altogether called an inorganic fertilizer?

Most of the protagonists in this controversy, like Humpty-Dumpty in Lewis Carroll's story, "Through the Looking Glass" have used the word 'organic' to mean just what they "choose it to mean". As in any scientific debate, definition and agreement on the meaning of the terms used is necessary for clarity of thought required to arrive at sound conclusions.

Ajit Abeysekera

RESEARCH ARTICLE

Evaluation of insecticide resistance and underlying resistance mechanisms in selected whitefly populations in Sri Lanka

JP Marasinghe¹ and SHPP Karunaratne^{2*}

¹ Horticulture Research and Development Institute, Department of Agriculture, Peradeniya.

² Department of Zoology, Faculty of Science, University of Peradeniya, Peradeniya.

Submitted: 25 November 2020; Revised: 22 February 2021; Accepted: 23 April 2021

Abstract: Whiteflies *Bemisia tabaci* and *Trialeurodes vaporariorum* cause high economic damage to commercial crops in Sri Lanka. Insecticide resistance was tested in *B. tabaci* collected from Kandy, Anuradhapura, Badulla, Matale and Hambantota districts and *T. vaporariorum* collected from Puttlam District against six insecticides using leaf dip bioassays. LC₅₀ values and percentage mortalities for the recommended dosages were determined by log-probit mortality curves. Metabolic resistance caused by increased activities of esterases, glutathione S-transferases and cytochrome P₄₅₀-monooxygenases, and the insensitive target site resistance caused by acetylcholinesterases were evaluated by biochemical assays. Overexpression of CYP6CM1 monooxygenase protein in *B. tabaci* was tested using a lateral flow assay kit. The highest and the lowest resistance factors (RFs) were obtained for etofenprox (1311) and profenofos (4), respectively. Resistance percentages of whitefly populations to the recommended dosages were 37–83% for thiamethoxam, 50–83% for acetamiprid, 71% for imidacloprid, 2–36% for profenofos, 15–53% for carbosulfan and 68–89% for etofenprox. Anuradhapura, Badulla and Matale populations had elevated esterases, all populations had elevated GST activities and Badulla population had elevated monooxygenase activities. Populations were homozygous resistant or heterozygous for altered acetylcholinesterase mechanism. High esterase activities were parallel to high neonicotinoid resistance. CYP6CM1 overexpression was linked to thiamethoxam resistance than to acetamiprid resistance. Both the enhanced esterases and altered target sites were associated with high carbosulfan resistance. This is the first report on the insecticide resistance mechanisms of whiteflies in Sri Lanka. The outcome of the present study can be effectively utilized for a proper whitefly control programme in Sri Lanka, avoiding indiscriminate insecticide usage.

Keywords: CYP6CM1, insecticide resistance, insensitive acetylcholinesterases, metabolic resistance, whiteflies.

INTRODUCTION

Whiteflies in vegetables cause extensive economic damage. The silverleaf whitefly, *Bemisia tabaci* (Gennadius) (Insecta: Hemiptera: Aleyrodidae) is an injurious pest in agriculture (Bedford *et al.*, 1994) and listed as one of the 100 worst invasive species in the world (Global Invasive Species Database, <http://www.issg.org/database>). The greenhouse whitefly, *Trialeurodes vaporariorum* (Westwood) (Insecta: Hemiptera: Aleyrodidae), although not included in the invasive species list, is considered as another injurious whitefly present globally (Brødsgaard & Albajes, 1999; Karatolos, 2011). In Sri Lanka, both *B. tabaci* and *T. vaporariorum* cause high economic damage to commercial crops. The number of host plant species of *B. tabaci* has been estimated to be more than 600 plant species (Basu, 1995) whereas *T. vaporariorum* is also known as a highly polyphagous species having a wide host plant range (Brødsgaard & Albajes, 1999). However, the host range of these pests could be even higher at present with its wider global distribution. Out of all the whiteflies, *B. tabaci* has become prominent because of its ability to transmit a large number of begomoviruses causing complete destruction of crops (Brown & Bird, 1992). *Bemisia tabaci* is now considered as a cryptic species complex, rather than different biotypes, due to

* Corresponding author (shppk@pdn.ac.lk;  <https://orcid.org/0000-0002-2537-0548>)



This article is published under the Creative Commons CC-BY-ND License (<http://creativecommons.org/licenses/by-nd/4.0/>). This license permits use, distribution and reproduction, commercial and non-commercial, provided that the original work is properly cited and is not changed in anyway.

high genetic variations found among populations (De Barro *et al.*, 2011). Both the physiological traits and genetic variations are crucial in determining its species status, and Surendran *et al.* (2019) had identified that the predominant species type of *B. tabaci* in Sri Lanka is Asia-I.

Naturally, the control of whiteflies is difficult due to their high reproductive rate, wide host range and habit of lodging underneath leaves. On top of these natural features, the acquired resistance to insecticides by them is the most challenging at present. Insecticide resistance of whiteflies is a global issue. *Bemisia tabaci* is found to be resistant to more than 40 active ingredients used worldwide (Arthropod Pesticide Resistance Database, www.pesticideresistance.org). In brief, insecticide resistance is a heritable trait acquired by a population to withstand the toxicity of an insecticide repeatedly at its recommended dosage (Insecticide resistance action committee, <https://irac-online.org/about/resistance>). High resistance of *T. vaporariorum* to many insecticide groups including pyrethroids, organophosphates and neonicotinoids has been documented elsewhere (Cahill *et al.*, 1995; Gorman *et al.*, 2002; Nauen & Denholm, 2005; Karatolos, 2011). The two major mechanisms of insecticide resistance in insects are; increased metabolism or detoxification by enzymes (mainly through esterases, mono-oxygenases and glutathione-S-transferases), and target site insensitivity by mutations (i.e. altered sodium channels for pyrethroids, altered acetylcholinesterase for organophosphates and carbamates, and altered nicotinic acetylcholine receptors for neonicotinoids) (Karunaratne, 1998; WHO, 1998).

Previously, we reported high resistance to insecticides in three whitefly populations based on laboratory bioassays raising concerns over the existing dosages recommended for chemical control (Marasinghe *et al.*, 2017). The objective of the present study was to investigate the present status of whitefly resistance to

insecticides in more detail by analysing the whitefly populations collected from six districts of the country against three neonicotinoids, one organophosphate, one carbamate and one pyrethroid. The activities of metabolic enzymes and altered acetylcholinesterase target site were also evaluated to understand the mechanisms underlying the insecticide resistance of this injurious pest category.

METHODOLOGY

Whiteflies

Bemisia tabaci populations were collected from several intensive agricultural localities from five districts belonging to four agroecological zones of Sri Lanka, i.e. Gannoruwa in Kandy, Huruluwewa in Anuradhapura, Bandarawela in Badulla, Matale in Matale, Suriyawewa in Hambantota and Kalpitiya in Puttalam. All collections were made during the 2016–2018 period and the details are given in Table 1. *Bemisia tabaci* collected from Puttalam were not enough for experiments. *Trialeurodes vaporariorum* dominated the whitefly collections from Puttalam district, and those samples were used for experiments for comparison.

Whiteflies were transported to the entomology laboratory of the Horticulture Research and Development Institute, Gannoruwa in cool boxes within few hours of collection. They were reared separately on young brinjal, tomato or cucumber plants in fine-mesh aluminium cages of 80 × 40 × 60 cm³ under room temperature up to 5–6 generations.

Species identification of both species were re-confirmed using adult/nymphal phenotypic features and the egg-laying pattern, i.e. *B. tabaci* adults are yellowish in colour and comparatively smaller with wings held vertical and parallel to body axis at rest. The fourth instar nymph (pupa) is almost circular in shape without

Table 1: Whitefly collection localities and associated host plants

Locality / district	Collected species	Agricultural zone	Host plants
Gannoruwa/Kandy	<i>Bemisia tabaci</i>	Mid country wet	Tomato, Brinjal, Cucurbits
Huruluwewa/Anuradhapura	<i>B. tabaci</i>	Low country dry	Brinjal, Cucurbits
Bandarawela/Badulla	<i>B. tabaci</i>	Up country intermediate	Brinjal, Bean, Tomato
Matale/Matale	<i>B. tabaci</i>	Mid country intermediate	Brinjal
Suriyawewa/Hambantota	<i>B. tabaci</i>	Low country dry	Brinjal
Kalpitiya/Puttalam	<i>Trialeurodes vaporariorum</i>	Low country dry	Brinjal, Cucurbits

long threads. Eggs are laid in a scattered manner on the underside of host leaf. *Trialeurodes vaporariorum* adults hold their wings in a flattened and overlapped position at rest. The fourth instar nymph is oval/ elliptical in shape with long erect threads. Eggs are laid in a circular pattern on the underside of the host leaf. Slide-mounted pupae were also examined for characteristic morphological features to differentiate the two species (Hodges & Evans, 2005). A set of specimens from each population was stored at -20 °C for biochemical assays.

Chemicals and equipment

Chemicals were purchased from Sigma Chemicals, UK unless otherwise stated. Formulated insecticides of thiamethoxam (Actara from Deccan Fine Chemicals-India Pvt Ltd.), acetamiprid (Mospilan from Nippon Soda Company Ltd.), imidacloprid (Admire from Bayer A.G. Crop Science, Germany), profenofos (Calcron from Coromandel International Ltd., India), carbosulfan (Marshal from FMC Corporation, USA), etofenprox (Trebon from Mitsui Chemicals Agro Inc., Japan) were purchased from the agrochemical sales outlets in Kandy, Sri Lanka. UVmaxELx800TM absorbance microplate reader was from Molecular devices, Bio-Tek, USA. Protein assay kit was purchased from BIO-RAD, UK. Whitefly test kit for the detection of CNI (neonicotinoid) resistance was a gift from Bayer CropScience AG, Germany.

Bioassays

Bioassays were carried out with three neonicotinoids (thiamethoxam 25% WG, acetamiprid 20% SP and imidacloprid 70% WG), an organophosphate (profenofos 500 g/L SC), a carbamate (carbosulfan 200 g/L SC) and a pyrethroid (etofenprox 100 g/L EC) using leaf dip method as previously described (IRAC, 2009; Marasinghe *et al.*, 2017). In brief, squarecut brinjal leaves (3 × 3 cm²) were immersed in aqueous solutions of insecticides for 5 s and then air dried. Thirty whiteflies were exposed to each insecticide-treated squarecut leaf held in ventilated transparent containers. The containers were kept under normal day/night conditions at room temperature for 24 h. Seven to eight concentrations of each insecticide (five replicates with 150 whiteflies per concentration) that gave mortalities between 0 to 100% were used for testing each population, i.e. thiamethoxam 10, 100, 250, 1000, 2500, 5000, 1000 ppm; acetamiprid 10, 100, 200, 500, 1000, 2000, 5000, 10000 ppm; carbosulfan 10, 100, 300, 500, 1000, 2000, 5000, 10000 ppm; imidacloprid 10, 100, 200, 500, 1000, 2000, 5000, 10000 ppm; etofenprox 10, 100, 500, 1000, 2000, 10000, 15000 ppm and profenofos

10, 50, 100, 250, 500, 800, 1000, 2000 ppm. Distilled water without insecticides was used as the control. Final mortality was assessed after the 24 h exposure period.

Biochemical assays

Adult whiteflies in batches of 20 individuals totalling up to a minimum of 200 individuals from each population were subjected to esterase, glutathione S-transferase (GST), monooxygenase, protein and acetylcholinesterase assays using a kinetic microplate reader (Bio-Tek, USA). Mass homogenates of the batches of 20 whiteflies were prepared separately in 150 µL of distilled water. Crude homogenate was directly used for acetylcholine esterase assay. The supernatant after centrifugation for 2 min at 10,000 g was used for esterase, GST, monooxygenase and protein assays. All the biochemical assays were carried out in microtiter plates. All the tests were replicated and controls were run with distilled water instead of the crude homogenate or supernatant. The assaying methods described in the Field and Laboratory Manual of the World Health Organization (WHO, 1998) were adopted with slight modifications as previously described for agricultural insect pests (Damayanthi & Karunaratne, 2005; Karunaratne & Weerakoon, 2007).

Esterase assay

Ten microlitres of homogenate was mixed with 200 µL of 1 mM p-nitrophenyl acetate (pNPA) working solution in 50 mM sodium phosphate buffer (pH 7.4). At 405 nm, the absorbance of the reaction was measured kinetically for 2 min and converted to moles using an extinction coefficient of 6.53 mM⁻¹ (corrected for a path length of 0.6 cm).

Glutathione S-transferase (GST) assay

Ten microlitres of homogenate was mixed with 200 µL of substrate solution prepared using 10.5 mM reduced glutathione (95 parts GSH in 100 mM phosphate buffer) and 63 mM 1-chloro-2,4-dinitrobenzene (CDNB) (5 parts of CDNB in methanol). The reaction rate was measured at 340 nm for 5 min. The absorbance was converted to moles using an extinction coefficient of 5.76 mM⁻¹ (corrected for a path length of 0.6 cm).

Monoxygenase assay

Twenty microlitres of homogenate was mixed with 80 µL potassium phosphate buffer (pH 7.2) + 200 µL 6.3 mM tetramethyl benzidine (TMBZ) working solution (0.01 g TMBZ dissolved in 5 mL methanol and then in 15 mL

of sodium acetate buffer at pH 5.0) + 25 μ L of 3 % H_2O_2 solution in a microtitre plate well. The mixture was left for 2 h for incubation under room temperature and the absorbance was read as an end point assay at 630 nm. The amount of monooxygenase was expressed as equivalent units of cytochrome P⁴⁵⁰ (Brogdon *et al.*, 1997).

Protein assay

Protein assays were conducted to obtain protein concentrations of the homogenates to determine specific activities of the enzymes. BIO-RAD protein determination kit, with bovine serum albumin as the standard protein was used. Ten microlitres of the homogenate was mixed with 300 μ L of BIO-RAD working solution (prepared according to the manufacturer's instructions) and after a 5 min incubation period at room temperature, the reaction was read at 570 nm as an end point assay.

Acetylcholinesterase (AChE) assay

Two \times 25 μ L of crude homogenate were placed in two consecutive wells of a microtiter plate, each containing 145 μ L of 1 % Triton buffer in 100 mM phosphate buffer at pH 7.8 with 10 μ L of 10 mM dithiobis 2-nitrobenzoic acid (0.0396 g of DTNB in 100 mM phosphate buffer at pH 7.0). An aliquote of 25 μ L of 10 mM acetylthiocholine iodide (ASCHI) (0.0578 g ASCHI in 20 mL distilled water) was added to one of the wells while 25 μ L of 10 mM ASCHI with propoxur (10 mL of 10 mM ASCHI + 20 μ L of 0.1 M propoxur in acetone) was added to the other. Acetylcholinesterase (AChE) activity was measured at 405 nm for 5 min. Results were expressed as the percentage remaining activity in the inhibited fraction compared with the control (uninhibited) activity.

Detection of the CYP6CM1 protein in *B. tabaci*

A field portable ELISA based lateral flow assay designed to detect monooxygenase CYP6CM1 protein was used following the manufacture's protocol (Bayer CropScience). Five to ten whiteflies from each population were homogenised in conjugated polyclonal antibodies in a homogenization vial. After a 2–3 min incubation, streptavidin-gold solution was added to the vial and gently inverted 3–4 times. The mixture was then poured into the sample cavity of the test strip and observed for 5 min. Respective distinct lines at C and T points indicated the expression levels of the CYP6CM1 enzyme by the control and the sample, respectively.

Data analysis

Bioassay data were used only when the control mortality was less than 20 %. Mortalities were adjusted with control mortalities using Abbott's formula (Abbott, 1987). Adjusted mortalities were Probit transformed using Sigma Plot (version 10) software and plotted against the log values of the insecticide concentrations. The LC₅₀ and the percent mortality for the Department of Agriculture recommended dosages (DOA, 2015) were estimated by regression analysis. Chi square values (χ^2) were calculated by evaluating the goodness-of-fit of the linear regression to log-probit transformed data. The software provides the slope and the 95 % confidence limits for each mortality line. Resistance factors (RF) were calculated using LC₅₀ values reported for susceptible populations of the same species elsewhere and used to evaluate resistance levels (Cahill *et al.*, 1995; Karatolos, 2011; Vassiliou, 2011).

RESULTS AND DISCUSSION

A total of 48,989 whiteflies from *B. tabaci* and *T. vaporariorum* were subjected to insecticide bioassays. Probit analysis separately done for the bioassay results obtained for the six populations with six insecticides are shown in Table 2 together with RFs. For thiamethoxam, LC₅₀ values of both *T. vaporariorum* and *B. tabaci* were in a similar range. However, the LC₅₀ values estimated for profenofos, carbosulfan and etofenprox for *T. vaporariorum* were higher than those obtained for *B. tabaci*. Among *B. tabaci* populations, the highest and the lowest LC₅₀ values for thiamethoxam were respectively detected from Badulla and Matale populations. In contrast, for acetamiprid, the highest and the lowest were respectively from Matale and Badulla populations. The highest and the lowest values for profenofos were from Badulla and Kandy populations, respectively. Matale and Hambantota populations showed the highest and lowest LC₅₀ values, respectively, for carbosulfan, whereas Kandy and Matale populations gave the highest and the lowest LC₅₀ values for etofenprox, respectively.

Chi square value (χ^2) gives the goodness-of-fit of a dose-mortality line and significant χ^2 estimates indicate deviation from linear response showing a heterogeneity of the population. For etofenprox, all the populations except Matale exhibited a heterogeneous response. For the other insecticides tested, most of the whitefly populations showed a homogeneous response (Table 2). For carbosulfan, RFs could not be calculated

since no LC_{50} s had been reported for susceptible whitefly populations. Similarly, no LC_{50} s were found for a susceptible *T. vaporariorum* for acetamiprid, profenofos

and etofenprox. RFs were very high for etofenprox (281–1311) and the lowest RFs were estimated for profenofos (4–71) (Table 2).

Table 2: Log-dose probit mortality results obtained for bioassays conducted with whitefly populations of *B. tabaci* and *T. vaporariorum* against thiamethoxam, acetamiprid, imidacloprid, profenofos, carbosulfan and etofenprox. *Trialeurodes vaporariorum* was tested only from Puttalam and *B. tabaci* was tested only from all the other districts.

Insecticide	Population	N	LC_{50} ppm	95% CI	Slope	χ^2	RF
Thiamethoxam	Kandy	1710	579	282–1123	0.61	8.9	¹ 127
	Anuradhapura	1365	294	109–447	0.56	5.7	¹ 64
	Badulla	1093	1090	578–2024	0.86	12.7	¹ 239
	Matale	1472	25	<10–70	0.68	5.0	¹ 5
	Hambantota	1751	223	53–605	1.01	30.4****	¹ 49
	Puttalam	1478	398	49–563	0.70	14.5*	² 21
Acetamiprid	Kandy	1799	230	60–605	0.87	13.3	¹ 23
	Anuradhapura	1814	1259	622–3703	0.44	3.2	¹ 125
	Badulla	1739	208	121–321	1.00	8.5	¹ 21
	Matale	1633	1753	930–4943	1.0	9.7	¹ 172
	Hambantota	2051	985	278–5231	0.76	43.1****	¹ 98
	Puttalam	NT	NT	NT	NT	NT	NC
Imidacloprid	Puttalam	1540	806	335–2240	1.35	44.9****	² 47
Profenofos	Kandy	1893	27	<10–61	1.07	12	³ 4
	Anuradhapura	1870	121	55–230	1.21	5.6	³ 20
	Badulla	1696	434	217–1562	1.51	13.5*	³ 71
	Matale	1733	88	33–183	1.55	35.7****	³ 14
	Hambantota	1432	58	16–126	1.69	11.7*	³ 10
	Puttalam	1754	509	355–817	1.89	5.2	NC
Carbosulfan	Kandy	1644	71	45–112	0.7	0.9	NC
	Anuradhapura	1775	321	211–434	0.97	1.4	NC
	Badulla	1513	237	17–531	0.81	5.4	NC
	Matale	1400	659	240–3073	0.80	17.1**	NC
	Hambantota	953	12	<10–25	0.59	0.2	NC
	Puttalam	1761	760	371–1778	0.79	12.5	NC
Etofenprox	Kandy	1988	1704	795–3225	1.02	12.6*	³ 1311
	Anuradhapura	1890	587	274–1188	0.93	15.4*	³ 452
	Badulla	1567	1314	398–9306	0.82	31.1****	³ 1011
	Matale	1558	365	240–2699	1.30	10.5	³ 281
	Hambantota	1861	371	128–2240	1.14	35.0****	³ 285
	Puttalam	1256	2512	1223–7830	0.98	18.5**	NC

N - number tested; CI - confidence intervals; χ^2 - chi square value evaluating the goodness-of-fit of the linear regression to log-probit transformed data; RF - resistance factor; * $p < 0.05$; ** $p < 0.01$; *** $p < 0.001$; **** $p < 0.0001$; ¹ susceptible data used from Vassiliou *et al.* (2011), ² from Karatolos (2011), ³ from Cahill *et al.* (1995); NT- not tested; NC- not calculated due to unavailability of susceptible data.

Mortality of whitefly populations to the insecticide dosages recommended by the Department of Agriculture (DOA) of Sri Lanka (DOA, 2015) as determined by using the mortality curves are presented in Table 3. Percentage mortalities of populations varied from 11–98 %. Whiteflies from Kandy, Matale and Hambantota gave more than 90 % mortalities for the DOA recommended profenofos dosage, and for other three districts 3–9 fold dose increment was required to achieve a 90 % mortality. All the other tested insecticides required 3– >80-fold increase of the recommended dosage to achieve

90 % mortality in these populations. *Trialeurodes vaporariorum* gave a similar mortality as for *B. tabaci* to DOA recommended dosage except for etofenprox, which showed a lower efficacy for *T. vaporariorum* (Table 3). Imidacloprid could be tested only against *T. vaporariorum* and 29 % mortality obtained for the DOA recommended dosage indicates the high imidacloprid resistance in whiteflies. In general, high resistance to all the tested insecticides is evident in whitefly populations except for profenofos in a few populations (Table 3).

Table 3: Percentage mortalities estimated for *B. Tabaci* from Kandy, Anuradhapura, Badulla, Matale, Hambantota and *T. vaporariorum* from Puttalam, to the Department of Agriculture (DOA) recommended dosages of six insecticides

Insecticide	Mode of action*	DOA recommended dosage per 16 L tank	Percentage mortality					
			Kandy	Anuradhapura	Badulla	Matale	Hambantota	Puttalam
Thiamethoxam 25 WG	4A	8 g	30 %	43 %	17 %	63 %	32 %	36 %
Acetamiprid 20 SP	4A	16 g	50 %	39 %	49 %	17 %	29 %	NT
Imidacloprid 20 SL	4A	16 ml	NT	NT	NT	NT	NT	29 %
Profenofos 50 EC	1B	32 mL	95 %	73 %	64 %	95 %	98 %	68 %
Carbosulfan 20 EC	1A	48 mL	75 %	60 %	72 %	49 %	85 %	47 %
Etofenprox 10 EC	3A	24 mL	13 %	30 %	20 %	31 %	32 %	11 %

*as described by the Insecticide Resistance Action Committee: 4A = nicotinic acetylcholinreceptor competitive modulators-neonicotinoids; 1B = acetylcholinesterase inhibitors-organophosphates; 1A = acetylcholinesterase inhibitors-carbamates; 3A = sodium channel modulators-pyrethroids; NT - not tested

Both the species, *B. tabaci* and *T. vaporariorum*, had similar activity levels in their insecticide metabolizing enzymes (Figure 1). In *B. tabaci*, specific activities of esterases and GSTs were in the ranges of 0.18–0.35 and 1.25–1.71 $\mu\text{mol}/\text{min}/\text{mg}$, respectively. For *T. vaporariorum*, the respective values were 0.17 and 1.08 $\mu\text{mol}/\text{min}/\text{mg}$. Monooxygenase amounts in *B. tabaci* were in the range 0.02–0.50 equivalent units of cytochrome P₄₅₀ and that of *T. vaporariorum* was 0.02. Vassiliou *et al.* (2011) have reported esterase and GST activities for a susceptible *B. tabaci* population. However, the esterase specific activities cannot be used to compare with the present results since the substrate used for the assay was different to that of the present study. Using the same methodology of the present study, a GST specific activity of 0.2 $\mu\text{mol}/\text{mg}/\text{min}$ has been obtained for their susceptible population, which is about 5–8 times lower than the GST activities detected in our whitefly populations (Vassiliou *et al.*, 2011). No

other enzyme activity data from susceptible strains are available for whiteflies or for any other insect pest of agriculture for comparison. However, for anopheline mosquitoes discriminating values are available in the literature for the same assays to determine the enhanced activities; above 0.25 $\mu\text{mol}/\text{mg}/\text{min}$ for enhanced esterase activity, above 0.40 $\mu\text{mol}/\text{mg}/\text{min}$ for enhanced GST activity, and 0.35 equivalent units of cytochrome P₄₅₀ for enhanced monooxygenase amounts (Perera *et al.*, 2008). According to this classification, Anuradhapura, Badulla and Matale populations have elevated esterases, all six whitefly populations have elevated GST activities and Badulla population has elevated monooxygenase activities (Figure 1). In aphids and mosquitoes, elevation of esterases is a powerful mechanism against organophosphates and carbamates, which have molecular structures rich with esterase bonds (Karunaratne *et al.*, 2018). Thiamethoxam resistant *B. tabaci* has been synergized and reversed using the esterase inhibitor

S,S,S-tributyl phosphorotrithioate (DEF) showing its importance in thiamethoxam resistance (Kandil *et al.*, 2008). The present study also reveals high esterase activity levels parallel to high neonicotinoid resistance,

indicating the contribution of esterases to neonicotinoid resistance. Although GSTs are primarily important in dechlorination of organochlorines, elevated levels of GST activity have been reported in organophosphate, organochlorine and pyrethroid resistant mosquitoes (Che-Mendoza *et al.*, 2008). High GST levels observed in the studied whitefly populations may have a wider general role giving resistance to all insecticide groups.

Results of the ELISA based lateral flow assay for CYP6CM1 monooxygenase protein also showed a clear overexpression of CYP6CM1 monooxygenase protein in Badulla *B. tabaci* population (Figure 2). The CYP6CM1 expression levels of lateral flow assay nicely matched with the biochemical assay data indicating that CYP6CM1, a typical microsomal P₄₅₀ member of CYP6 family, is a major candidate of enhanced monooxygenases of the tested whitefly populations. Imidacloprid resistance in both the B and Q biotypes of *B. tabaci* has been tightly related to the up-regulation of the cytochrome P450-dependent monooxygenase gene CYP6CM1 (Karunker *et al.*, 2008). Overexpression of CYP6CM1 gene has also been detected in thiamethoxam resistant *B. tabaci* too (Yang *et al.*, 2013). Imidacloprid resistance in *B. tabaci* has not been tested in our study and thus, the association with imidacloprid resistance could not be traced.

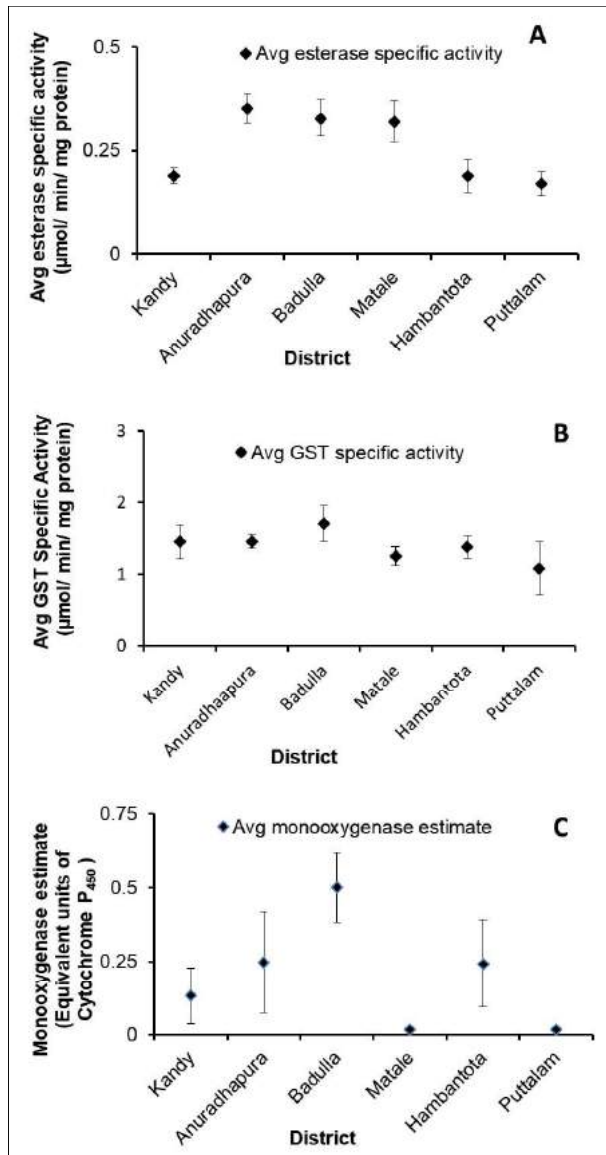


Figure 1: Insecticide metabolizing enzyme activities of whitefly populations. *Trialeurodes vaporariorum* was tested only from Puttalam and *B. tabaci* was tested only from all the other districts. A - esterase specific activity; B - glutathione-S-transferase (GST) specific activity; C - monooxygenase amounts in equivalent units of cytochrome P₄₅₀. A minimum of 100 insects (five batches, 20 individuals per batch) were tested per assay per site. Error bars indicate the standard errors.

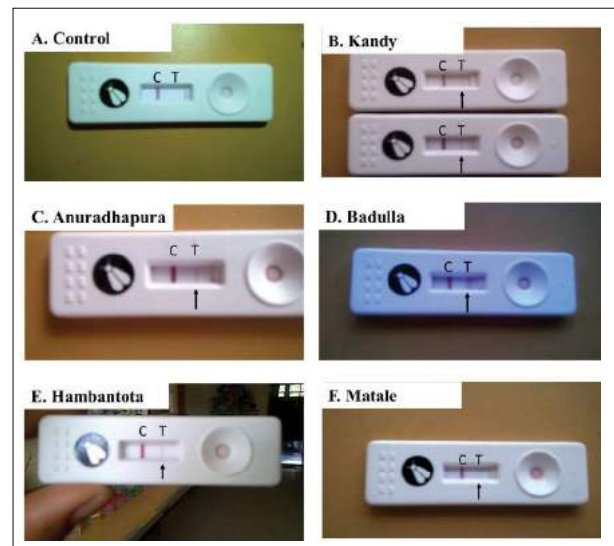


Figure 2: Monooxygenase CYP6CM1 expression level in *B. tabaci* populations from Kandy (B), Anuradhapura (C), Badulla (D), Hambantota (E) and Matale (F) as detected by the diagnostic kits. Control (A) does not show a 2nd line; C - control line; T - CYP6CM1 monooxygenase expression line

According to our bioassay results from Badulla and Matale populations, it can be concluded that CYP6CM1 is more important in thiamethoxam resistance than in acetamiprid resistance.

Percentage remaining activities of propoxur inhibited target site AChE are shown in Figure 3. The same AChE assay is used by WHO to categorize mosquito populations as susceptible homozygous (SS)

(< 30 % remaining activity), heterozygous (RS) (30–70% remaining activity) and resistant homozygous (RR) (> 70% remaining activity) for altered or insensitive AChE target site mechanism (WHO, 2016). According to these guidelines, Badulla *B. tabaci* population was homozygous resistant with > 70% remaining activity while all other populations including *T. vaporariorum* population were heterozygous for altered AChE mechanism with a remaining activity of 30–70% (Figure 3).

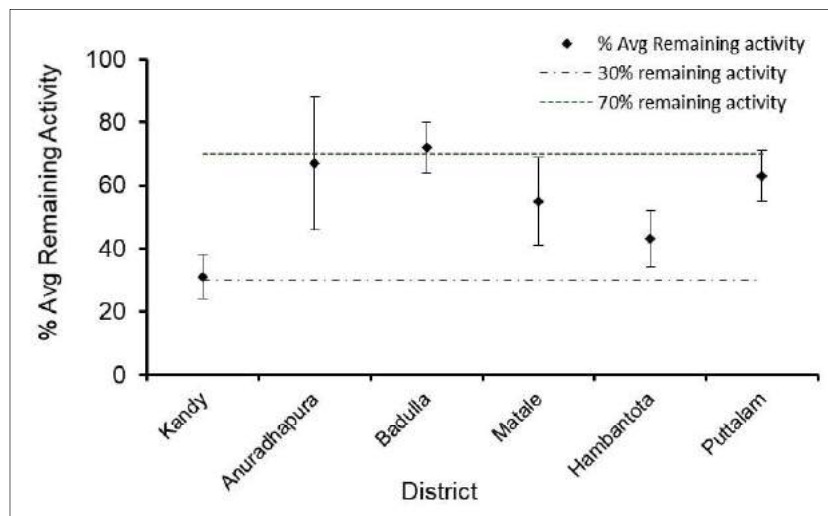


Figure 3: Percentage remaining activities of propoxur inhibited acetylcholine esterases of *B. tabaci* except for Puttalam where *T. vaporariorum* was tested. A minimum of 100 insects (five batches, 20 individuals per batch) were tested per assay per site. Two dotted lines show the WHO recommended discriminating remaining activities for mosquitoes (< 30% susceptible; 30–70% heterozygous resistance; > 70% homozygous resistance) (WHO, 2016). Error bars indicate the standard errors.

High organophosphate and carbamate resistance is expected from the altered AChE target sites and elevated esterases activities (Karunaratne *et al.*, 2018). Acetylcholinesterase insensitivity has been previously reported in OP and/or carbamate resistant whiteflies (Dittrich & Ernst, 1990; Byrne & Devonshire, 1991). Therefore, the high profenofos and carbosulfan resistance detected in Badulla and Matale districts for *B. tabaci* populations must be due to these two mechanisms.

Whitefly control has become a serious problem in agriculture due to reduced efficacy of recommended insecticides. Severity of the problem has intensified with the economical importance of *B. tabaci* being a begomovirus vector of many crops. A large number of insecticides belonging to different chemical groups have

been recommended for whitefly control in Sri Lanka (MOAAL, 1997; DOA, 2009). Organophosphates and carbamates have a long history of use for more than 4 decades. Pyrethroids were introduced in the 1990s and neonicotinoids in early years of this century for whitefly control (DOA, 2009). The popularity of neonicotinoids among farmers increased not only due to their high efficacy at the introductory phase, but also due to the wide crop range applicability and the long residual activity. The present study evaluated the efficacy of representative samples of these insecticide groups against *B. tabaci* and *T. vaporariorum* using laboratory bioassays with the leaf dip method, which resembles the foliar application method practiced in the field. The percentage mortalities estimated using probit regression lines revealed high resistance of whiteflies to all the tested insecticides,

except for profenofos. Since repeated use of less effective insecticides would further increase resistance generation with environment pollution, taking different approaches to control whiteflies at this stage is necessary. The underlying mechanisms of insecticide resistance in Sri Lankan whitefly populations were evaluated for the first time using biochemical assays. It was evident that both the metabolic resistance and insensitive target site resistance mechanisms have been developed to varying degrees in Sri Lankan whitefly populations. In *T. vaporariorum* also the resistance levels and resistance mechanisms are found to be comparable to those of *B. tabaci*.

Etofenprox is a non-ester pyrethroid having a mode of action similar to other pyrethroids, i.e. by interacting with voltage gated sodium channels (VGSC) of insect neurons. Cross resistance studies have shown no effect of enhanced metabolic enzyme activities on etofenprox toxicity in mosquitoes possibly due to the relatively simple structure of the etofenprox molecule compared to most of the other pyrethroids (Hemingway, 1995). Also, the monooxygenase synergist piperonyl butoxide (PBO) and GST synergist diethyl maleate (DEM) were able to synergize permethrin resistance, but not etofenprox resistance in *Anopheles* mosquitoes (Gross & Bloomquist, 2018). With the high resistance observed in all whitefly populations against etofenprox, and with a least chance for metabolic resistance mechanisms to be operative, there is a high possibility that knock-down type (*kdr*) target site mutations are involved in this resistance. Future studies are required to investigate the presence of *kdr*-type *VGSC* gene mutations in Sri Lankan whiteflies.

CONCLUSIONS

High percentages of the tested whitefly populations have developed resistance to the DOA recommended dosages of thiamethoxam (37–83%), acetamiprid (50–83%), imidacloprid (71%), carbosulfan (15–53%) and etofenprox (68–89%) insecticides. Least resistance was shown to the organophosphate profenofos (2–36%). Both the increased detoxification by esterases, glutathione S-transferases and monooxygenases, and AChE target site insensitivity contribute in varying degrees to the observed resistance. Involvement of *kdr* type mutations in pyrethroid resistance should be further investigated. This is the first report confirming the resistance status of Sri Lankan whiteflies with underlying resistance mechanisms and the outcome can be utilized effectively for developing a proper whitefly control programme in Sri Lanka avoiding indiscriminate use of insecticides.

Acknowledgement

Funding was provided from the National Agricultural Research Plan (NARP) for the project entitled 'Toxicity Levels of Selected Insecticides to Common Vegetable Pests'. Assistance given by S. Nawarathne for collection of insects, and the laboratory facilities provided by the Entomology Division of the Horticulture Crops Research and Development Institute, Gannoruwa and the Department of Zoology, Faculty of Science, University of Peradeniya are acknowledged.

REFERENCES

- Abbott W.S. (1987). A method of computing the effectiveness of an insecticide. *Journal of the American Mosquito Control Association* **3**(2): 302–303.
- Basu A.N. (1995). *Bemisia tabaci* (Gennadius): *Crop Pest and the Principal Whitefly Vector of Plant Viruses*, p. 183. West View Press, New Delhi, India.
- Bedford I.D., Briddon R.W., Brown J.K., Rosell R.C. & Markham P.G. (1994). Geminivirus transmission and biological characterization of *Bemisia tabaci* (Gennadius) biotype from different geographic regions. *Annals of Applied Biology* **125**: 311–325
DOI: <https://doi.org/10.1111/j.1744-7348.1994.tb04972.x>
- Brødsgaard H.F. & Albajes R. (1999). *Insect and Mite Pests: Integrated Pest and Disease Management in Greenhouse Crops* (eds. R. Albajes, M.L. Gullino, J.C. van Lenteren & Y. Elad), pp. 48–60. Kluwer Academic Publishers, Dordrecht, Netherlands.
DOI: https://doi.org/10.1007/0-306-47585-5_4
- Brogdon W.G., McAllister J.C. & Vulule J.M. (1997). Hem peroxidase activity measured in single mosquitoes identifies individuals expressing an elevated oxidase for insecticide resistance. *Journal of American Mosquito Association* **13**: 233.
- Brown J.K. & Bird J. (1992). Whitefly-transmitted geminiviruses and associated disorders in the Americas and the Caribbean Basin. *Plant Disease* **76** (3): 220–225.
- Byrne F.J. & Devonshire A.L. (1991). In vivo inhibition of esterase and acetylcholinesterase activities by profenofos treatments in the tobacco whitefly *Bemisia tabaci* (Genn.): implications for the routine biochemical monitoring of these enzymes. *Pesticide Biochemistry and Physiology* **40**: 198–204.
DOI: [https://doi.org/10.1016/0048-3575\(91\)90090-9](https://doi.org/10.1016/0048-3575(91)90090-9)
- Cahill M., Byrne F.J., Gorman K., Denholm I. & Devonshire (1995). Pyrethroid and organophosphate resistance in the tobacco whitefly *Bemisia tabaci* (Homoptera: Aleyrodidae). *Bulletin of Entomological Research* **85**: 181–187.
DOI: <https://doi.org/10.1017/S0007485300034258>
- Che-Mendoza A., Penilla R.P. & Rodríguez D.A. (2008). Insecticide resistance and glutathione S-transferases in mosquitoes: A review. *African Journal of Biotechnology* **8**(8): 1–12.

- Damayanthi B.T. & Karunaratne S.H.P.P. (2005). Biochemical characterization of insecticide resistance in insect pests of vegetables and predatory ladybird beetles. *Journal of the National Science Foundation of Sri Lanka* **33**(2): 115–122. DOI: <https://doi.org/10.4038/jnsfsr.v33i2.2341>
- De Barro P.J., Liu S., Boykin L.M. & Dinsdale A.B. (2011). *Bemisia tabaci*: A statement of species status. *Annual Review of Entomology* **56**: 1–19
- DOA (2009). *Pesticide Recommendations*. Department of Agriculture, Gannoruwa, Peradeniya.
- DOA (2015). *Pesticide Recommendations*. Department of Agriculture, Gannoruwa, Peradeniya.
- Dittrich V. & Ernst G.H. (1990). Resistance mechanisms in sweetpotato whitefly (Homoptera: Aleyrodidae) populations from Sudan, Turkey, Guatemala, and Nicaragua. *Journal of Economic Entomology* **83**: 1665–1670. DOI: <https://doi.org/10.1093/jee/83.5.1665>
- Gorman K., Hewitt F., Denholm I. & Devine G.J. (2002). New developments in insecticide resistance in the glasshouse whitefly (*Trialeurodes vaporariorum*) and the two-spotted spider mite (*Tetranychus urticae*) in the UK. *Pest Management Science* **58**: 123–130. DOI: <https://doi.org/10.1002/ps.427>
- Gross A.D. & Bloomquist J.R. (2018). Characterizing permethrin and etofenprox resistance in two common laboratory strains of *Anopheles gambiae* (Diptera: Culicidae). *Insects* **9**(4): 146. DOI: <https://doi.org/10.3390/insects9040146>
- Hemingway J. (1995). Efficacy of etofenprox against insecticide susceptible and resistant mosquito strains containing characterized resistance mechanisms. *Medical and Veterinary Entomology* **9**(4): 423–426. DOI: <https://doi.org/10.1111/j.1365-2915.1995.tb00017.x>
- Hodges G.S. & Evans G.A. (2005). An identification guide to the whiteflies (Hemiptera: Aleyrodidae) of the Southeastern United States. *Florida Entomologist* **88**(4): 518–534. DOI: [https://doi.org/10.1653/0015-4040\(2005\)88\[518:AITGTTW\]2.0.CO;2](https://doi.org/10.1653/0015-4040(2005)88[518:AITGTTW]2.0.CO;2)
- IRAC (2009). Insecticide resistance action committee susceptibility test methods series, method No. 008, version 3. Available at www.irc-online.org.
- Kandil M.A., Saleh A.Y., Wafaa E.I., Dieb W.H. & Farghaly S.F. (2008). Resistance mechanisms of whitefly *Bemisia tabaci* (Homoptera: Aleyrodidae) to thiamethoxam and profenofos. *Asian Journal of Biological Sciences* **1**(1): 33–38. DOI: <https://doi.org/10.3923/ajbs.2008.33.38>
- Karatolos N. (2011). Molecular mechanisms of insecticide resistance in the glasshouse whitefly, *Trialeurodes vaporariorum*. *PhD thesis*. University of Exeter, UK.
- Karunaratne S.H.P.P. (1998). Insecticide resistance in insects: A review. *Ceylon Journal of Science (Biological Sciences)* **26**: 73–98.
- Karunaratne S.H.P.P. & Weerakoon K.C. (2007). Involvement of metabolic and insensitive acetylcholinesterase mechanisms in insecticide resistance of rice insect pests and predatory populations from Batalagoda, Sri Lanka. *Journal of the National Science Foundation of Sri Lanka* **35**(2): 103–108. DOI: <https://doi.org/10.4038/jnsfsr.v35i2.3674>
- Karunaratne S.H.P.P., De Silva W.A.P.P., Weeraratne T.C. & Surendran S.N. (2018). Insecticide resistance in mosquitoes: Development, mechanisms and monitoring. *Ceylon Journal of Science* **47**(4): 299–309. DOI: <https://doi.org/10.4038/cjs.v47i4.7547>
- Karunker I., Benting J., Leuke B., Ponge T., Nauen R., Roditakis E., Vontas J., Gorman K., Denholm I. & Morin S. (2008). Over-expression of cytochrome P450 CYP6CM1 is associated with high resistance to imidacloprid in the B and Q biotypes of *Bemisia tabaci* (Hemiptera: Aleyrodidae). *Insect Biochemistry and Molecular Biology* **38**(6): 634–644. DOI: <https://doi.org/10.1016/j.ibmb.2008.03.008>
- Marasinghe J.P., Hemachandra K.S., Nugaliyadde L. & Karunaratne S.H.P.P. (2017). Control failure of Sri Lankan whitefly (*Bemisia tabaci* Genn) is due to high resistance development against recommended insecticides. *Journal of the National Science Foundation of Sri Lanka* **45**(1): 23–31. DOI: <https://doi.org/10.4038/jnsfsr.v45i1.8034>
- MOAAL (1997). *Pesticide Recommendations*. Department of Agriculture, Ministry of Agriculture and Lands, Sri Lanka.
- Nauen R. & Denholm I. (2005). Resistance of insect pests to neonicotinoid insecticides: current status and future prospects. *Archives of Insect Biochemical Physiology* **58**: 200–215. DOI: <https://doi.org/10.1002/arch.20043>
- Perera M.D.B., Hemingway J. & Karunaratne S.H.P.P. (2008). Multiple insecticide resistance mechanisms involving metabolic changes and insensitive target sites selected in anopheline vectors of malaria in Sri Lanka. *Malaria Journal* **7**: 168. DOI: <https://doi.org/10.1186/1475-2875-7-168>
- Surendran S.N., Marasinghe J.P., Gajapathy K., Tharmatha T., Sivabalakrishnan K., Weeraratne T.C. & Karunaratne S.H.P.P. (2019). Genotyping of *Bemisia tabaci* (Hemiptera: Aleyrodidae) reveals the presence of two genetic groups in Sri Lanka. *Journal of Entomological Science* **54**(2): 87–93. DOI: <https://doi.org/10.18474/JES18-68>
- Vassiliou V., Emmanouilidou M., Perrakis A., Morou E., Vontas J., Tsagkarakou A. & Roditakis E. (2011). Insecticide resistance in *Bemisia tabaci* from Cyprus. *Insect Science* **18**: 30–39. DOI: <https://doi.org/10.1111/j.1744-7917.2010.01387.x>
- WHO (1998). Techniques to detect resistance mechanisms (field and laboratory manual). WHO/CDS/CPC/MAL/98.6, World Health Organization, Geneva, Switzerland.
- WHO (2016). Test procedures for insecticide resistance monitoring in malaria vector mosquitoes. World Health Organization, Geneva, Switzerland.
- Yang N., Xie W., Jones C.M., Bass C., Jiao X., Yang X., Liu B., Li R. & Zhang Y. (2013). Transcriptome profiling of the whitefly *Bemisia tabaci* reveals stage-specific gene expression signatures for Thiamethoxam resistance. *Insect Molecular Biology* **22**(5): 485–496. DOI: <https://doi.org/10.1111/imb.12038>

RESEARCH ARTICLE

Occurrence of enrofloxacin and ciprofloxacin residues in broiler meat sold in Sri Lanka

NB Karunarathna¹, IA Perera², NT Nayomi¹, DMS Munasinghe³, SSP Silva⁴, I Strashnov⁴ and BR Fernando^{1*}

¹ Department of Veterinary Public Health and Pharmacology, Faculty of Veterinary Medicine and Animal Science, University of Peradeniya, Peradeniya.

² Government Veterinary Surgeon's Office, Serukele.

³ Department of Basic Veterinary Sciences, Faculty of Veterinary Medicine and Animal Science, University of Peradeniya, Peradeniya.

⁴ Department of Animal Production and Health, Peradeniya.

⁵ School of Chemistry, The University of Manchester, Oxford Road, Manchester, M13 9PL, United Kingdom.

Submitted: 06 August 2020; Revised: 19 April 2021; Accepted: 27 August 2021


Abstract: The presence of unacceptable levels of veterinary drug residues in animal-derived food is a global concern due to its negative impacts on human health. This study reports the occurrence and levels of two fluoroquinolone antimicrobials—enrofloxacin and ciprofloxacin—in broiler meat sold in Sri Lanka. A total of 129 broiler meat samples were purchased from the market, representing nine large-scale broiler meat processors (107 samples in 66 batches, branded) with an islandwide distribution and 22 small-scale processors (22 samples, unbranded). Enrofloxacin and ciprofloxacin in breast muscle were extracted following a previously published method with modifications and were subjected to High-Performance Liquid Chromatography with Fluorescence Detection analysis for the quantification of antimicrobials. Enrofloxacin residues were detected in 67 (51.9%) samples, out of which 28 had quantifiable levels (1.7–578.6 $\mu\text{g kg}^{-1}$), whereas ciprofloxacin was detected in only nine samples. Only three samples (2.3%) exceeded the European Union maximum residue limit of 100 $\mu\text{g kg}^{-1}$ for the sum of ciprofloxacin and enrofloxacin in poultry muscle. These three samples had enrofloxacin in 130.3–578.6 $\mu\text{g kg}^{-1}$ range and ciprofloxacin in 15.7–28.8 $\mu\text{g kg}^{-1}$ range. Mean enrofloxacin level in other samples was $5.9 \pm 5.3 \mu\text{g kg}^{-1}$. This study shows the widespread use of enrofloxacin in broiler meat industry in the country and the possibility of meat with harmful levels of residues entering the market. Thus, we highlight the need to establish regulations and a national-level veterinary drug residue surveillance program for animal-derived foods including broiler meat to ensure consumer safety.

Keywords: Broiler meat, ciprofloxacin, enrofloxacin, fluoroquinolone, HPLC, poultry, Sri Lanka.

INTRODUCTION

Poultry meat and eggs constitute two major animal protein sources for humans worldwide (Nkukwana, 2018). Rapid growth in global poultry production over the past few decades (McLeod *et al.*, 2009) is partly attributed to the application of veterinary drugs for health management practices, such as therapy and prophylaxis, and for growth promotion of poultry birds (Singer & Hofacre, 2006; Apata, 2009). However, irrational use of veterinary drugs can create a potential food safety risk for consumers via exposure to sub-therapeutic doses of drugs that may be present in animal-derived food (Darwish *et al.*, 2013; Gouvea *et al.*, 2015).

Enrofloxacin is a synthetic, second-generation fluoroquinolone antimicrobial used exclusively in veterinary practice (Ahn *et al.*, 2012; Janecko *et al.*, 2016). Mechanism of action of the drug is via inhibition of bacterial DNA gyrase (a type II topoisomerase), which results in interruption of the normal coiling of DNA, and rapid cell death (Mitchell, 2006). Its excellent activity against both Gram-positive and Gram-negative

* Corresponding author (ruchika@vet.pdn.ac.lk;  <https://orcid.org/0000-0003-2972-1111>)



This article is published under the Creative Commons CC-BY-ND License (<http://creativecommons.org/licenses/by-nd/4.0/>). This license permits use, distribution and reproduction, commercial and non-commercial, provided that the original work is properly cited and is not changed in anyway.

pathogens (Mitchell, 2006) has contributed to its widespread use in food-producing animals. In poultry industry, enrofloxacin is used to treat various respiratory and alimentary tract infections (Anderson *et al.*, 2003; Javadi *et al.*, 2011), including mycoplasmal infection, pasteurellosis (Bauditz, 1987), and colibacillosis (Huff *et al.*, 2004), which is an economically devastating bacterial disease in poultry worldwide (Dziva & Stevens, 2008). In many animal species, including poultry birds, enrofloxacin is biotransformed via de-ethylation to the primary metabolite ciprofloxacin (Seguin *et al.*, 2004; Dimitrova *et al.*, 2007; de Assis *et al.*, 2016). Thus, animal-derived food obtained from farm animals treated with enrofloxacin can contain residues of both enrofloxacin and ciprofloxacin. Ciprofloxacin is also a broad-spectrum second-generation fluoroquinolone antimicrobial with a similar mechanism of action as enrofloxacin (Sharma *et al.*, 2010). However, unlike enrofloxacin, ciprofloxacin is used in human medicine to treat infections of the urinary and respiratory tracts and skin, typhoid fever, and infectious diarrhea (King *et al.*, 2000).

Many previous studies have documented the presence of residues of enrofloxacin and ciprofloxacin in poultry meat, including muscle tissue, liver and kidney (Amjad *et al.*, 2005; Salehsadeh *et al.*, 2007; Pena *et al.*, 2010; Sattar *et al.*, 2014; Sultan *et al.*, 2014; Wang *et al.*, 2015; Panzenhagen *et al.*, 2016; Sarker *et al.*, 2018). Human exposure to sub-therapeutic doses of veterinary drugs can be associated with several health hazards such as hypersensitivity reactions (Kowalski *et al.*, 2005), carcinogenic, mutagenic, and teratogenic effects (Beyene, 2016; Manage 2018), and disruption of intestinal microflora (Dethlefsen *et al.*, 2008). Moreover, continuous exposure to antimicrobial agents can promote development of antimicrobial-resistant strains of bacteria in humans (Landers *et al.*, 2012; Gouvea *et al.*, 2015; Manage, 2018), which has become a global health concern. In fact, fluoroquinolone-resistance in bacteria has been reported in many parts of the world (Endtz *et al.*, 1991; Smith *et al.*, 1999), which is of medical significance since fluoroquinolones are used in human therapy as well. Such resistant bacteria can act as reservoirs of genes conferring resistance to fluoroquinolones (Manage & Liyanage, 2019), and these genes can be transmitted to other bacteria as well. Exposure of humans to ciprofloxacin through animal-derived food is also a major concern because it is one of the most widely used antimicrobials in the world (Sharma *et al.*, 2010; Conley *et al.*, 2018) and is also among the drugs of choice for human *Campylobacter* infection (McDermott *et al.*, 2004).

To safeguard consumers from adverse effects, various countries and regulatory authorities have established Maximum Residue Limits (MRL) for enrofloxacin and ciprofloxacin. European Union, for example, has established an MRL of 100 $\mu\text{g kg}^{-1}$ for the sum of enrofloxacin and ciprofloxacin in poultry muscle, skin and fat, and higher MRLs for poultry liver (200 $\mu\text{g kg}^{-1}$), and kidney (300 $\mu\text{g kg}^{-1}$; European Commission, 2010). In comparison, Japan has set a much lower MRL (10 $\mu\text{g kg}^{-1}$) for these substances in chicken tissue (Ministry of Health and Welfare, 2005), while the United States has banned the use of enrofloxacin in poultry, adopting a zero tolerance policy of the drug (FDA, 2005).

In Sri Lanka, poultry industry is the leading and fastest growing food animal sector (DAFH, 2019). It is dominated by chicken meat and egg production, while other sectors, such as turkeys, ducks, quail, and geese remain insignificant (DAFH, 2019). Chicken meat is the most widely consumed meat type in the country (De Silva *et al.*, 2010), and per capita chicken availability has doubled from 4.9 kg to 10.4 kg during the last decade (DAFH, 2010; 2019). In addition, over 90% of the meat-based value-added products are manufactured using chicken meat (DAFH, 2019). With the heavy demand for poultry products, the country's broiler sector, together with the layer sector, has grown tremendously over the past few decades and has transitioned from a backyard system into a commercial industry (Wickramarachchi *et al.*, 2017). Currently, around 80% of the poultry farms in the country operate at a commercial scale (Dandeniya *et al.*, 2018), and have contributed to the self-sufficiency in chicken meat and egg production (DAFH, 2019).

Intensive poultry production in the country has inevitably resulted in the use of a variety of veterinary drugs including antimicrobials by the poultry farmers (Herath *et al.*, 2015; 2016; Liyanage & Pathmalal, 2017; Dandeniya *et al.*, 2018; Lowe *et al.*, 2019). Enrofloxacin is among the most widely used antimicrobials by the broiler farmers in Sri Lanka (Herath *et al.*, 2015; 2016; Dandeniya *et al.*, 2018). Enrofloxacin may be used alone or together with other antimicrobials such as amoxicillin (Dandeniya *et al.*, 2018). Other antimicrobials commonly used for therapy and prophylaxis include sulfonamides, tylosin, and tetracyclines (Herath *et al.*, 2016; Dandeniya *et al.*, 2018; Lower *et al.*, 2019). These antimicrobials are commonly administered to birds via drinking water (Herath *et al.*, 2015). However, the use of antimicrobials as growth promoters in feed is now prohibited in the country (Goutard *et al.*, 2017).

Despite the extensive use of veterinary drugs, reports on their usage patterns are limited in Sri Lanka (Manage, 2018), and their presence in animal-derived food has been studied sparsely. Gunarathne *et al.* (2016) have analysed residues of five sulfonamides in broiler meat samples collected from eight districts and reported the presence of sulfadoxine and sulfadiazine in three and two samples, respectively, out of 72 samples tested, indicating the potential for commonly used drugs to present in poultry products. Lowe *et al.* (2019) have investigated the presence of eight antimicrobial residues, including ciprofloxacin, in broiler meat samples (muscle, liver and kidneys) from six large-scale broiler meat producers in the country using a bio-assay method and reported that detectable levels of residues were not found in any of the 252 samples tested.

Sri Lanka currently does not have regulations to control veterinary drug residues in animal-derived food, and no surveillance programs are in place to monitor antimicrobial residues in food. Therefore, studies pertaining to occurrence of veterinary drug residues in animal-derived food are important to ensure the consumer safety. Further, such studies will provide baseline information to employ a risk-based veterinary drug residue surveillance programmes in the country. The objective of this study was to document the occurrence and levels of enrofloxacin and its main metabolite ciprofloxacin in broiler meat sold in Sri Lanka. For that, broiler meat samples were collected from the market, representing both large-scale and small-scale broiler meat processors, and residues in breast muscle were determined, using High-Performance Liquid Chromatography with Fluorescence Detection.

METHODOLOGY

Sample collection

A total of 129 broiler meat samples (whole chicken) were collected representing large-scale broiler meat processors (n = 9, named A–I) producing an average of over 200 MT per month and small-scale processors (n = 22) in Sri Lanka from August 2018 to June 2019.

Large-scale processors provide the highest contribution to the broiler meat production in the country, and activities from pre-processing to packaging are carried out in semi-automated processing plants, where each slaughter batch include more than 1000 birds (Kottawatta *et al.*, 2017). Broiler meats produced by these processors are available throughout

the country under different brand names. From each large-scale processor, 5–23 whole chicken samples (5–10 batches) were collected comprising of a total of 107 samples (66 batches). The number of samples collected from each processor was nearly proportional to their monthly broiler meat production. Almost all of these large-scale processors are poultry buy-back operators, and therefore, a single batch of broiler meat may include broiler birds raised in different farms having different management practices. To account for this possibility, more than one sample from a single batch were purchased on several occasions.

Small-scale broiler meat processors often slaughter birds depending on the day-to-day requirement (Kottawatta *et al.*, 2017), and broiler meats are sold without a brand name at their own retail shops closer to the farms. Twenty-two broiler meat samples from small-scale processors were collected from 22 different shops (1 sample from each processor) in three districts (Kandy, Colombo, and Kurunegala) to ensure a wider coverage of small-scale processors. Although these products did not have an expiry date, they were freshly slaughtered birds. After collection, about 100 g of the breast muscle was minced using a household grinder and stored at -20°C until analysed. The breast muscle was used to determine the analytes of interest since the muscle tissues constitute the major edible portion in chicken and breast muscle is representative of all other muscle tissues in chickens (Lowe *et al.*, 2019).

Analytical method

The method described by Yorke and Froc (2000) was used with some modifications. These modifications include increasing the sample weight from 0.5 g to 3 g, and use of 6 mL of acetonitrile/acetone (70/30) as the extraction solvent instead of 200 µL of acetonitrile used in the original method. These modifications were employed to improve the recovery of the method but had a limited success. Further, 2 mL of hexane was used in two consecutive rounds to remove the fat in the sample instead of one time 300 µL of hexane used in the original method.

Reference standards

Analytical standards of enrofloxacin (purity > 98%; catalogue no. 17849) and ciprofloxacin (VETRANAL®; purity = 99%; catalogue no. 33434) were purchased from Sigma-Aldrich (St Louis, MO, USA).

Preparation of standard solutions and calibration standards

Stock standard solutions of enrofloxacin and ciprofloxacin (100 mg L^{-1}) were prepared by dissolving 10 mg of the compound with 100 μL of 1 mol L^{-1} NaOH and completing up to 100 mL with methanol (Yorke and Froc, 2000). Individual stock standard solutions were mixed and diluted with 0.05 mol L^{-1} tris(hydroxymethyl) aminomethane buffer (pH 9.1), hereafter referred to as tris buffer, to prepare a mixed standard solution containing enrofloxacin and ciprofloxacin (each at 1 mg L^{-1}), which was used to spike the quality control samples and to prepare calibration standards. This study employed an external calibration methodology, and calibration standards (1, 5, 10, 25, 50, 100, 150 and $200 \mu\text{g L}^{-1}$) were prepared by diluting the mixed standard solution (1 mg L^{-1}) with tris buffer. Stock standard solutions of enrofloxacin and ciprofloxacin were stable for at least eight months when stored at -20°C without exposure to light. Both the mixed standard solution (1 mg L^{-1}) and calibration standards were prepared freshly before the analysis.

Quality control samples

Quality control samples were prepared by spiking drug-free breast muscle samples, purchased from a reliable source, and confirmed by analysing with LC-MS/MS, for the absence of enrofloxacin and ciprofloxacin residues. The blank samples were spiked with both analytes at final tissue concentrations of 50, 100 and $150 \mu\text{g kg}^{-1}$ that are equivalent to $0.5 \times \text{MRL}$, MRL and $1.5 \times \text{MRL}$, respectively established for poultry muscle by the European Union (European Commission, 2002).

Sample extraction

Frozen minced breast muscle samples were allowed to thaw at room temperature, and $3.00 \pm 0.05 \text{ g}$ of the sample was weighed. Then, 1800 μL tris buffer was added to the sample and allowed to stand at room temperature for 10 min. For the quality control samples, to which 150, 300 or 450 μL of mixed standard solution (1 mg L^{-1}) had been added, only 1650, 1500 or 1350 μL of tris buffer was added, respectively. Then, 6 mL of acetonitrile/acetone (70/30, v/v) was added, and the sample was homogenized for 1 min using a tissue homogenizer (Ultra Turrax® T 25 basic; IKA® Werke GmbH & Co. KG, Staufen, Germany). The homogenate was centrifuged at 4,000 g for 10 min, and 2.6 mL of the supernatant

was transferred to a glass tube and evaporated at 50°C under mild flow of N_2 (purity = 99.95%), using a dry block incubator with a sample concentrator (Dri-Block® DB-3A, Techne Ltd., Cambridge, UK). The dry residue was resuspended in 1.5 mL of tris buffer solution, and vortexed for 10 s. The resuspended sample was defatted twice by adding 2 mL of n-hexane, vortexing for 30 s and discarding the upper hexane layer. Next, 0.5 mL of n-hexane was added to the sample and vortexed for 30 s. The sample was transferred to a 2-mL microcentrifuge tube, and then was centrifuged at 17,000 g for 5 min. Finally, 750 μL of the bottom aqueous layer was filtered through a $0.45\text{-}\mu\text{m}$ PVDF syringe-driven filter, and the filtrate was transferred to an amber coloured autosampler vial for injection into the HPLC system (dilution factor = 1.5).

A negative control (blank breast muscle sample) and a blank sample spiked with enrofloxacin and ciprofloxacin, each at $100 \mu\text{g kg}^{-1}$, were run with each batch of samples for recovery calculation. If antimicrobial levels in the samples exceeded the European Union MRL of $100 \mu\text{g kg}^{-1}$, those samples were confirmed by repeating the analysis.

High-performance liquid chromatography-fluorescence detection (HPLC-FLD) analysis

The HPLC analysis was performed using an Agilent 1100 series HPLC system (Agilent Technologies, Waldbronn, Germany) consisting of a micro vacuum degasser (G1379A), quaternary pump (G1311A), auto-sampler (G1313A), thermostatted column compartment (G1316A) and a fluorescence detector (G1321A, Agilent 1200 series). The mobile phase was a mixture of $0.02 \text{ mol L}^{-1} \text{H}_3\text{PO}_4$ /acetonitrile (85/15, v/v; Yorke & Froc, 2000) and was delivered isocratically at a flow rate of 1 mL min^{-1} . Reversed-phase chromatographic separation (Yorke & Froc, 2000) was performed on a C18 analytical column (Zorbax Eclipse XDB-C18, $4.6 \times 150 \text{ mm}$, particle size $5 \mu\text{m}$; Agilent Technologies, CA, USA). The analytical column was maintained at 50°C and was fitted with a guard column (Zorbax SB-C18, $4.6 \times 12.5 \text{ mm}$, particle size $5 \mu\text{m}$; Agilent Technologies, CA, USA) for protection. The injection volume of the sample was 20 μL , and the total run time was 10 min. Excitation and emission wavelengths for fluorescence detection were set at 280 nm and 450 nm, respectively (Yorke & Froc, 2000). ChemStation for LC3D software (Rev. A. 10.02) was used to control the HPLC system and analyse the output data.

Method validation

Linearity

Linearity of the analytical method was determined over the 1–200 $\mu\text{g L}^{-1}$ concentration range for each analyte, using the external calibration standards. The linearity of the standard curve was expressed using coefficient of determination (R^2) obtained through the least square linear regression.

Selectivity

Blank breast muscle samples from different sources were analysed to assess matrix interference and presence/absence of co-eluting endogenous compounds at the retention times of the two analytes. In addition, chromatographic selectivity was also assessed by calculating the resolution of the enrofloxacin and ciprofloxacin peaks following the equation given below (USFDA, 1994).

$$R_s = \frac{t_{RB} - t_{RA}}{0.85 (W_{0.5B} + W_{0.5A})} \quad \dots(1)$$

where, R_s = peak resolution, t_{RB} = retention time of peak 2, t_{RA} = retention time of peak 1, $W_{0.5B}$ = width of peak 2 at half peak height, and $W_{0.5A}$ = width of peak 1 at half peak height.

Trueness (Recovery)

The trueness of measurements was assessed through recovery of analytes spiked into a blank matrix. Blank breast muscle samples were spiked with the two analytes at $0.5 \times \text{MRL}$, MRL , and $1.5 \times \text{MRL}$ as per the validation requirements of Commission Decision 2002/657/EC (European Commission, 2002). Mean recovery at each spike level was calculated from nine replicates that were run on three different days.

Precision

Precision of the analytical procedure was determined at two levels: repeatability (intra-assay precision) and intermediate precision (within-laboratory reproducibility). To determine repeatability, blank muscle samples spiked with the two analytes at 50, 100, and 150 $\mu\text{g kg}^{-1}$ were analysed on the same day. Intermediate precision was determined by analysing spiked samples on three different days. Precision was expressed as the percent relative standard deviation (RSD%) of measured concentration of analytes.

Limit of detection and limit of quantification

Chromatograms of blank muscle samples were analysed, and signal-to-noise ratio of three and ten were considered as limit of detection (LOD) and limit of quantification (LOQ), respectively at the retention time windows of the two analytes.

Decision limit ($CC\alpha$) and detection capability ($CC\beta$)

Blank breast muscle samples spiked with enrofloxacin and ciprofloxacin, each at 100 $\mu\text{g kg}^{-1}$ (i.e., MRL), were analysed, and decision limit ($CC\alpha$) was calculated as the concentration at the permitted limit plus 1.64 times the corresponding standard deviation (i.e., $CC\alpha = \text{MRL} + 1.64\text{SD}$, $\alpha = 5\%$). To determine the detection capability ($CC\beta$), blank breast muscle samples spiked with enrofloxacin and ciprofloxacin at respective $CC\alpha$ values were analysed, and $CC\beta$ was calculated as the value of the $CC\alpha$ plus 1.64 times the corresponding standard deviation (i.e., $CC\beta = CC\alpha + 1.64\text{SD}$, $\beta = 5\%$).

Statistical analysis

Descriptive statistics, including mean, standard deviation, minimum and maximum were calculated for enrofloxacin and ciprofloxacin levels in samples above the limit of quantification. Enrofloxacin level was compared between large-scale and small-scale processors, using one-way analysis of variance (ANOVA). Before conducting ANOVA, normality of the data and homogeneity of variances were verified ($p > 0.05$) using Shapiro-Wilk and Levene's tests, respectively. Statistical analyses were conducted using Minitab 17 statistical software (Minitab Inc., State college, PA, USA) with the level of significance set at 0.05.

RESULTS AND DISCUSSION

Method validation

The HPLC-FLD method separated ciprofloxacin and enrofloxacin within less than 8 min, and the respective analytes were eluted with a mean retention time \pm standard deviation (SD) of 5.64 ± 0.08 min and 7.25 ± 0.13 min (Figure 1). Both peaks had an acceptable symmetry and were well separated from each other with a resolution of 5.6, which is higher than the minimum recommended resolution of 2 between the peaks of interest (USFDA, 1994). Chromatograms of blank muscle samples did not have any co-eluting peaks at the retention times of the

two analytes (Figure 1), which indicates the selectivity of the analytical method for the two target analytes.

All the matrix peaks eluted within five minutes of sample injection.

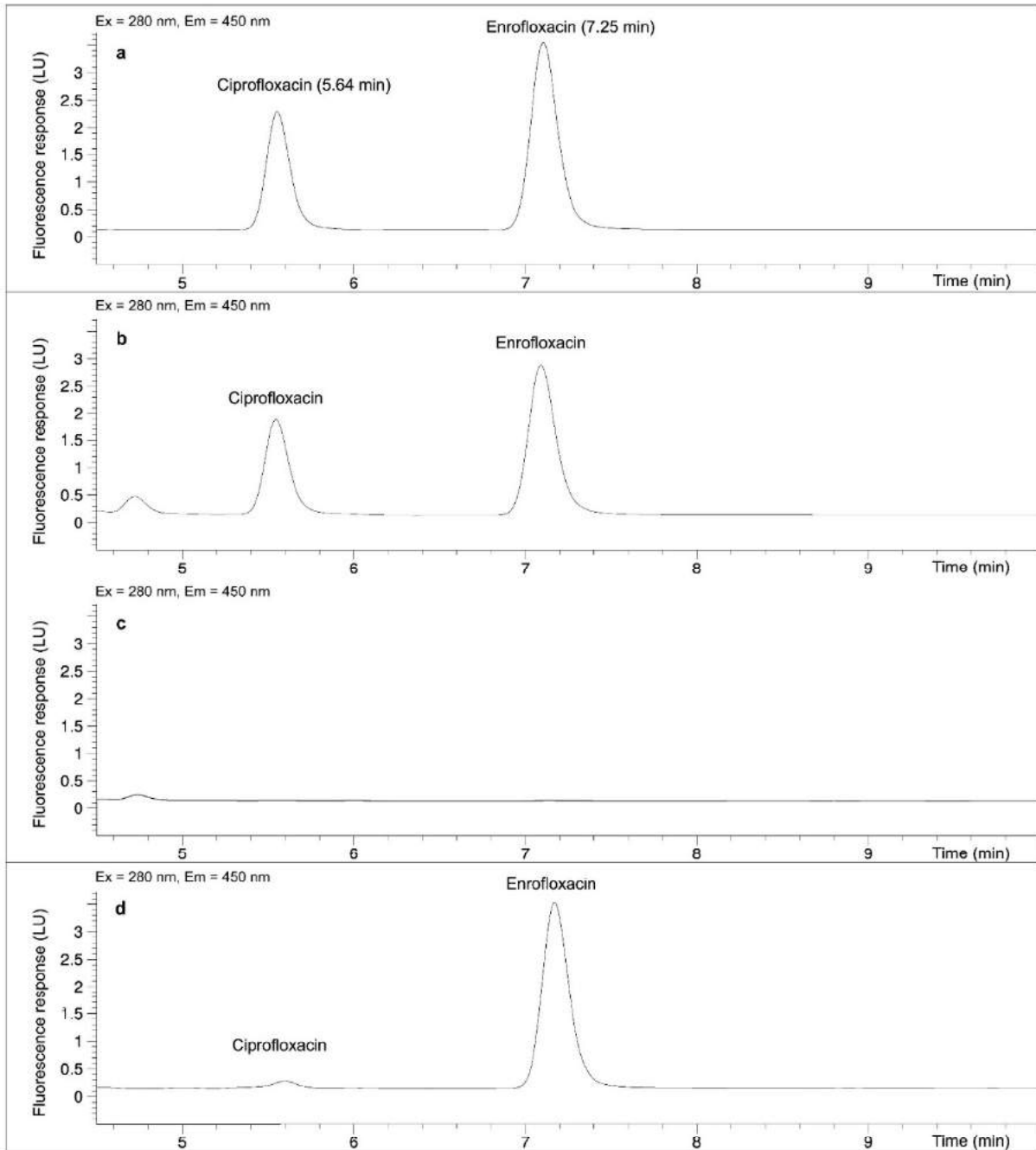


Figure 1: HPLC-FLD chromatograms. (a) Calibration standard solution containing ciprofloxacin and enrofloxacin, each at $50 \mu\text{g L}^{-1}$. Retention time is given in parentheses; (b) Broiler breast muscle sample spiked with ciprofloxacin and enrofloxacin, each at $100 \mu\text{g kg}^{-1}$; (c) Blank broiler muscle sample showing absence of endogenous compounds in the matrix at the retention times of two analytes; (d) A broiler breast muscle sample that exceeded European Union MRL ($100 \mu\text{g kg}^{-1}$) for the sum of enrofloxacin and ciprofloxacin in poultry muscle, showing the presence of both ciprofloxacin and enrofloxacin (LU = luminescence unit; dilution factor is 1.5 for b and c; dilution factor is 3 for d).

Table 1: Performance characteristics of the analytical method for determination of residues of enrofloxacin and ciprofloxacin in broiler breast muscle

Analyte	Spiked level ($\mu\text{g kg}^{-1}$)	Mean recovery \pm SD (%) ^a	RSD _r (%)	RSD _i (%)	LOD ($\mu\text{g kg}^{-1}$)	LOQ ($\mu\text{g kg}^{-1}$)	CC α ($\mu\text{g kg}^{-1}$)	CC β ($\mu\text{g kg}^{-1}$)
Enrofloxacin	50	63.3 \pm 7.1	12.3	11.2				
	100	63.1 \pm 7.1	9.0	11.2	0.5	1.6	111.6	113.1
	150	62.0 \pm 7.7	8.8	12.5				
Ciprofloxacin	50	58.6 \pm 4.0	7.9	6.9				
	100	60.9 \pm 5.2	7.2	8.5	2.2	7.5	108.5	111.2
	150	60.6 \pm 3.0	4.4	4.9				

^amean recovery from nine replicates

RSD_r - repeatability; RSD_i - intermediate precision; LOD - limit of detection; LOQ - limit of quantification; CC α - decision limit; CC β - detection capability; SD - standard deviation

Standard curves for enrofloxacin and ciprofloxacin demonstrated a good linearity over the 1–200 $\mu\text{g L}^{-1}$ concentration range with coefficients of determination (R^2) above 0.998, indicating sufficient linearity of the present analytical method. Mean recovery of enrofloxacin at the three spike levels (i.e., 50, 100, and 150 $\mu\text{g kg}^{-1}$) ranged between 62.0–63.3%, while that of ciprofloxacin varied between 58.6–60.9% (Table 1). Similar relatively low recoveries have been reported by several other authors who have used similar extraction procedure to determine quinolones in meat (Yorke & Froc, 2000; Kirbiš *et al.*, 2005). This relatively low recovery rate of the analytical method could affect detection of very low levels of analytes (<0.8 $\mu\text{g kg}^{-1}$ of enrofloxacin and <3.7 $\mu\text{g kg}^{-1}$ of ciprofloxacin) in the samples.

Repeatability RSD% for enrofloxacin and ciprofloxacin at the three spike levels were in the ranges of 8.8–12.3% and 4.4–7.9%, respectively, with lower RSD% values observed at higher spike levels (Table 1). Intermediate precision RSD% for the two analytes at three spike levels varied between 4.9 and 12.5%. According to the guidelines of Commission Decision 2002/657/EC, intermediate precision RSD% should not exceed the RSD% calculated by the Horwitz equation, and the repeatability RSD% should not exceed two thirds of the RSD% calculated by the Horwitz equation (European Commission, 2002). The repeatability RSD% and intermediate precision RSD% of the present analytical method met these performance criteria, indicating acceptable precision, as the RSD% values calculated by Horwitz equation were 25.1, 22.6, and 21.3% for 50, 100, and 150 $\mu\text{g kg}^{-1}$ levels, respectively.

Based on the signal-to-noise ratio method, limit of detection (LOD) and limit of quantification (LOQ) of

enrofloxacin were 0.5 and 1.6 $\mu\text{g kg}^{-1}$, respectively, while those of ciprofloxacin were comparatively higher (2.2 and 7.5 $\mu\text{g kg}^{-1}$). The LODs and LOQs obtained for the two analytes were sufficiently below the European Union MRL (100 $\mu\text{g kg}^{-1}$) and even Japanese MRL (10 $\mu\text{g kg}^{-1}$). These LODs and LOQs are similar to those reported by Yorke and Froc (2000). Decision limits (CC α) for enrofloxacin and ciprofloxacin were 111.6 $\mu\text{g kg}^{-1}$ and 108.5 $\mu\text{g kg}^{-1}$ respectively, and detection capabilities (CC β) were 113.1 $\mu\text{g kg}^{-1}$ and 111.2 $\mu\text{g kg}^{-1}$ for the respective analytes. These CC α and CC β of the two analytes are also comparable with those reported in other similar studies (de Assis *et al.*, 2016).

Occurrence of enrofloxacin and ciprofloxacin in broiler muscle

The study revealed that 67 (51.9%) out of the 129 broiler breast muscle samples were positive for residues of enrofloxacin (range = LOD–578.6 $\mu\text{g kg}^{-1}$). Enrofloxacin was detected in samples from both large-scale (50.5%) and small-scale (59.1%) broiler meat processors. In each large-scale processor, 40.0–69.6% of the samples became positive for enrofloxacin, except in one processor (Table 2). Three breast muscle samples—one from a large-scale processor and two from small-scale processors—had residues of enrofloxacin above the European Union MRL of 100 $\mu\text{g kg}^{-1}$ (Figure 2; Table 3). The mean concentration of enrofloxacin was 5.9 \pm 5.3 $\mu\text{g kg}^{-1}$ (range = 1.7–19.3 $\mu\text{g kg}^{-1}$) in breast muscle samples with quantifiable enrofloxacin levels (excluding the samples that exceeded the MRL of 100 $\mu\text{g kg}^{-1}$). The mean enrofloxacin levels did not differ significantly between the large-scale processors (6.6 \pm 5.9 $\mu\text{g kg}^{-1}$) and the small-scale processors (3.7 \pm 2.2 $\mu\text{g kg}^{-1}$; one way ANOVA, $F_{1,23} = 1.34$, $p = 0.259$).

Table 2: Occurrence of residues of enrofloxacin and ciprofloxacin in broiler breast muscle collected from nine large-scale (A–I) and small-scale broiler meat processors

Broiler meat processor	No. of samples analysed	Enrofloxacin		Ciprofloxacin	
		No. of positive samples ^a	Percentage of positive samples (%)	No. of positive samples ^a	Percentage of positive samples (%)
A	23	16	69.6	0	0.0
B	15	6	40.0	1	6.7
C	15	8	53.3	0	0.0
D	12	7	58.3	1	8.3
E	12	6	50.0	0	0.0
F	10	1	10.0	0	0.0
G	10	5	50.0	2	20.0
H	5	2	40.0	0	0.0
I	5	3	60.0	0	0.0
Small-scale processors	22	13	59.1	5	22.7
Total	129	67	51.9	9	7.0

^anumber of samples above LOD**Table 3:** Residue levels of enrofloxacin and ciprofloxacin in the three broiler breast muscle samples that exceeded European Union MRL of 100 µg/kg for sum of ciprofloxacin and enrofloxacin in poultry meat

Sample	Type of processor	Ciprofloxacin level (µg kg ⁻¹)	Enrofloxacin level (µg kg ⁻¹)	Sum of enrofloxacin and ciprofloxacin (µg kg ⁻¹)
1	Small-scale	15.9	130.3	146.2
2	Small-scale	15.7	259.2	274.9
3	Large-scale	28.8	578.6	607.4

Ciprofloxacin residues were detected (i.e., above the LOD) in nine (7.0%) out of 129 breast muscle samples (Table 2). Five of these samples belonged to small-scale broiler meat processors, and the remaining four belonged to large-scale processors. Ciprofloxacin residues could be quantified only in the three samples that had enrofloxacin residue levels above the European Union MRL. Ciprofloxacin levels in those three samples ranged from 15.7–28.8 µg kg⁻¹ (mean ± SD = 20.1 ± 7.5 µg kg⁻¹). Ciprofloxacin residue levels were 8–20 times lower than the enrofloxacin levels in those three samples.

The presence of enrofloxacin in 51.9% of the breast muscle samples and detection of enrofloxacin in both large- and small-scale broiler meat processors indicate the widespread use of enrofloxacin by broiler farmers. There are previous reports on high usage of enrofloxacin by broiler farmers in Sri Lanka (Herath *et al.*, 2015;

2016; Dandeniya *et al.*, 2018). For example, enrofloxacin was found to be the most widely used antimicrobial in broiler farms associated with large-scale companies and medium-scale broiler farms (Dandeniya *et al.*, 2018). Previous studies conducted elsewhere have also reported the presence of enrofloxacin residues in broiler meat. The occurrence of enrofloxacin in breast muscle samples in our study (51.9%) is similar to that of Aslam *et al.* (2016), who reported that 52% of broiler muscle had residues of enrofloxacin in a study conducted in Pakistan. However, various studies have reported occurrences of enrofloxacin in broiler meat that are different from the present study [e.g., 5% by Wang *et al.* (2015), 18% by Sattar *et al.* (2014), 21% by Sarker *et al.* (2018), 22% by Panzenhagen *et al.*, (2016), 33% by Pena *et al.* (2010), and 90% by Attari *et al.* (2014)] with occurrence reaching up to 100% in certain studies (Salehzadeh *et al.*, 2007).

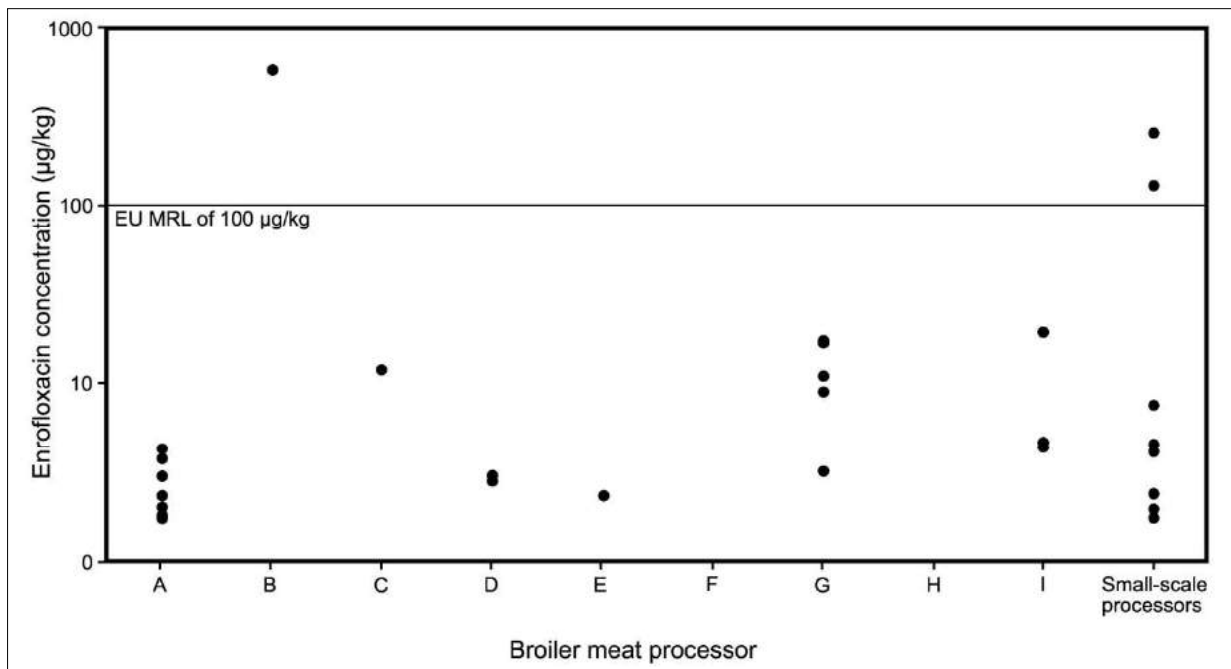


Figure 2: Levels of enrofloxacin (samples with quantifiable levels) in broiler muscle samples from large-scale processors and small-scale processors.

Ciprofloxacin is the main metabolite of enrofloxacin (Seguin *et al.*, 2004; Dimitrova *et al.*, 2007; de Assis *et al.*, 2016) and can occur in animal-derived food obtained from farm animals treated with enrofloxacin (Amjad *et al.*, 2005). In a pharmacokinetics study, where chickens were treated with enrofloxacin at 10 mg kg⁻¹ body weight, de Assis *et al.* (2016) found that ciprofloxacin levels in muscle tissue (44.6–241.7 µg kg⁻¹) were 7–12 times lower than the corresponding enrofloxacin levels (484.1–2941.8 µg kg⁻¹) and that ciprofloxacin levels became undetectable when enrofloxacin levels were around ~6 µg kg⁻¹. This explains the low levels of ciprofloxacin (15.7–28.8 µg kg⁻¹), which were 8–20 times lower compared to enrofloxacin levels (130.3–578.6 µg kg⁻¹) in our study, and the low occurrence of ciprofloxacin (7.0%) in breast muscle samples compared to enrofloxacin (51.9%). Our results are consistent with other studies that have shown both low occurrence and low levels of ciprofloxacin compared with enrofloxacin in broiler meat (Amjad *et al.*, 2005; Pena *et al.*, 2010; Moghadam *et al.*, 2018; Sureshkumar & Sarathchandra, 2018; Arslan-acroz & Sozibilir, 2020). Previously Lowe *et al.* (2019) have analysed ciprofloxacin in broiler meat samples (muscle, liver, and kidney) collected from Sri Lanka using a bioassay method, but ciprofloxacin residues were not detected in any of the 252 samples

analysed. It is possible that Lowe *et al.* (2019) did not find ciprofloxacin residues due to the employment of a screening bioassay technique in which the sensitivity is relatively low.

The three broiler breast muscle samples that exceeded the European Union MRL of 100 µg kg⁻¹ for the sum of enrofloxacin and ciprofloxacin in poultry muscle indicate incorrect use, and possibly abuse of enrofloxacin by certain broiler farmers. Misuse of veterinary drugs is a common problem in the animal production systems, and enrofloxacin levels above the MRLs in broiler meat have been reported in several countries including Pakistan (Aslam *et al.*, 2016), Portugal (Pena *et al.*, 2010) and Iran (Salehzadeh *et al.*, 2007). However, the situation of the broiler meat industry in Sri Lanka, as revealed by our study, is better compared with the broiler meat industry reported in the study of Aslam *et al.* (2016), in which 21 (28%) out of 75 broiler meat samples had enrofloxacin above the MRL.

The European Medicine Agency recommends a withdrawal period of 3 days for chickens treated with enrofloxacin at a dosage of 10 mg kg⁻¹ body weight (EMA, 2012). This 3-day withdrawal period has been shown to be adequate for the enrofloxacin levels in

chicken muscle tissue to deplete not only below the European Union MRL of 100 $\mu\text{g kg}^{-1}$ but also below the Japanese MRL of 10 $\mu\text{g kg}^{-1}$ (Shim *et al.*, 2013; de Assis *et al.*, 2016). In broiler farms in Sri Lanka, birds are treated with antimicrobials within the first 5–6 days of age and then during 18–24 days of age, and the birds are usually slaughtered around 35–36 days of age (Lowe *et al.*, 2019). Therefore, this practice, which includes a ~10-day drug-free period, alone should be adequate to prevent the occurrence of enrofloxacin levels above the MRL in broiler meat. However, the enrofloxacin levels (130.3–578.6 $\mu\text{g kg}^{-1}$) exceeding the MRL in our study indicate that the broiler birds have been treated within three days of the planned slaughter, or birds have been treated with a higher dose of enrofloxacin than the recommended dose. However, it is difficult to predict the exact cause for the higher enrofloxacin levels without examining the treatment records of birds. Misuse of veterinary drugs can occur in broiler farms in Sri Lanka due to the lack of knowledge on the importance of adhering to withdrawal periods (Lowe *et al.*, 2019) and the use of antimicrobials without professional advice (Karunarathna *et al.*, 2013; Herath *et al.*, 2015).

In our study, 97.7% of breast muscle samples had no enrofloxacin or enrofloxacin levels below the MRL of 100 $\mu\text{g kg}^{-1}$, indicating that these products are within safe limits for human consumption from a toxicological point of view. Nevertheless, widespread use of enrofloxacin in broiler meat industry, as evident from our study, may have important implications on development of antimicrobial resistance in bacteria. Development of fluoroquinolone-resistance is well known in *Campylobacter* sp., which is a major cause of food-borne illnesses worldwide (Tauxe, 2002). In several parts of the world, authorization of enrofloxacin in poultry was found to be responsible for the emergence of fluoroquinolone-resistant *Campylobacter* sp. (Endtz *et al.*, 1991; Smith *et al.*, 1999). In the United States, such fluoroquinolone-resistant *Campylobacter* isolates were found to have transferred to humans, causing fluoroquinolone-resistant *Campylobacter* infections, and consequently, the US banned the use of fluoroquinolones in poultry industry in 2005 (Nelson *et al.*, 2007). In Sri Lanka also, emergence of such resistance remains a possibility because of the widespread use of enrofloxacin and high prevalence of *Campylobacter* in broiler flocks and chicken meat in the retail market (Kalupahana *et al.*, 2013, 2018; Kottawatta *et al.*, 2017). In fact, some studies have shown that more than 80% of *Campylobacter* isolates obtained from broiler birds and chicken meat in Sri Lanka were resistant to quinolones (Kottawatta *et al.*, 2017). In addition to *Campylobacter* sp., resistance

to fluoroquinolones has been observed in *Escherichia coli* isolated from chickens as well (Dissanayake & Wijewardana, 2005). Bacteria resistant to enrofloxacin have been reported in poultry litter and poultry manure in Sri Lanka (Herath *et al.*, 2015; 2016; Lowe *et al.*, 2019). The practice of using poultry manure as fertilizers in vegetable cultivation (Herath *et al.*, 2015; 2016), can contribute to spread of antimicrobial resistance in the environment (Dandeniya *et al.* 2018). Wastewater from poultry farms can spread not only antimicrobials into the environment but also antimicrobial-resistant bacteria as well (Liyanage & Pathmalal, 2017).

Although many countries have regulations to control veterinary drug residues including fluoroquinolones in animal-derived food (European Commission, 2010), Sri Lanka currently does not have such regulations/legislations. As a result, poultry processors are not required to test their products for presence of veterinary drug residues. Our study, in which 2.3% of broiler meat samples had enrofloxacin levels exceeding the European Union MRL, indicates the possibility of broiler meat with harmful levels of drug residues entering the market. Therefore, it is important to establish regulations and surveillance programmes to ensure the chemical safety of animal-derived food in the country and to improve consumer confidence. Many broiler farms associated with large-scale companies in the country have discontinued or minimized the use of tetracyclines as its extensive use has led to the development of resistance in bacteria (Dandeniya *et al.*, 2018; Lowe *et al.*, 2019). Given the level of resistance building up in bacteria against enrofloxacin, it has been suggested that poultry industry in Sri Lanka will have to abandon the use of enrofloxacin in the near future (Dandeniya & Caucci, 2020). Therefore, a mechanism is required to monitor the usage of veterinary drugs in the country and to ensure prudent use of antimicrobials in the animal production by educating the farmer community.

CONCLUSION

This study reports a high occurrence of fluoroquinolone residues, especially enrofloxacin, in broiler meat with an occasional violation of MRLs established elsewhere. Therefore, it is necessary to establish regulations in Sri Lanka (including MRLs) to control veterinary drug residues in animal-derived food and a risk-based surveillance program to ensure consumer safety and build consumer confidence which in turn will benefit the poultry industry. Further, prudent use of antimicrobials in animal-derived food is essential to combat development of antimicrobial

resistance against valuable antimicrobials reserved for human medicine such as ciprofloxacin.

Competing interest

Authors declare none.

Acknowledgements

Authors thank Innovation Commercialization Enhancement (ICE) grant of the Faculty of Veterinary Medicine and Animal Science (6026-LK/8743-LK) under the Accelerating Higher Education Expansion and Development project of the Ministry of Higher Education, Sri Lanka. Authors also thank International Atomic Energy Agency's Technical Cooperation Projects SRL 5048, RAS 5078 and INT 5154. We thank Mr. Malinda Dissanayake for assistance in laboratory.

REFERENCES

- Ahn Y., Linder S.W., Veach B.T., Yan S.S., Fernández A.H., Pineiro S.A. & Cerniglia C.E. (2012). In vitro enrofloxacin binding in human fecal slurries. *Regulatory Toxicology and Pharmacology* **62**(1): 74–84.
DOI: <https://doi.org/10.1016/j.yrtph.2011.11.013>
- Amjad H., Iqbal J. & Naeem M. (2005). Analysis of some residual antibiotics in muscle, kidney and liver samples of broiler chicken by various methods. *Proceedings of the Pakistan Academy of Sciences* **42**(4): 223–231.
- Anderson A.D., Nelson J.M., Rossiter S. & Angulo F.J. (2003). Public health consequences of use of antimicrobial agents in food animals in the United States. *Microbial Drug Resistance* **9**(4): 373–379.
DOI: <https://doi.org/10.1089/107662903322762815>
- Apata D.F. (2009). Antibiotic resistance in poultry. *International Journal of Poultry Science* **8**(4): 404–408.
- Arslan-acaroz D. & Sozibilir N.B. (2020). Investigation of enrofloxacin and ciprofloxacin residues by LC-MS/MS in chicken liver marketed in Afyonkarahisar. *Ankara Universitesi Veteriner Fakültesi Dergisi* **67**(2): 137–142.
- Aslam B., Kousar N., Javed I., Raza A., Ali A., Khaliq T., Muhammad F. & Khan, J.A. (2016). Determination of enrofloxacin residues in commercial broilers using high performance liquid chromatography. *International Journal of Food Properties* **19**(11): 2463–2470.
DOI: <https://doi.org/10.1080/10942912.2015.1027922>
- Attari V.E., Abbasi M.M., Abedimanesh N., Ostadrahimi A. & Gorbani A. (2014). Investigation of enrofloxacin and chloramphenicol residues in broiler chickens carcasses collected from local markets of Tabriz, North Western Iran. *Health Promotion Perspectives* **4**(2): 151–157.
DOI: <https://dx.doi.org/10.5681%2Fhpp.2014.020>
- Bauditz R. (1987). Results of clinical studies with Baytril in poultry. *Veterinary Medical Review* **2**: 130–136.
- Beyene T. & Tesega B. (2014). Rational veterinary drug use: Its significance in public health. *Journal of Veterinary Medicine and Animal Health* **6**(12): 302–308.
DOI: <https://doi.org/10.5897/JVMAH2014.0332>
- Conley Z.C., Bodine T.J., Chou A. & Zechiedrich L. (2018). Wicked: The untold story of ciprofloxacin. *PLoS Pathogens* **14**(3): e1006805.
DOI: <https://doi.org/10.1371/journal.ppat.1006805>
- Dandeniya W.S. & Caucci S. (2020). Composting in Sri Lanka: Policies, Practices, Challenges, and Emerging Concerns. In: *Organic Waste Composting through Nexus Thinking* (eds. H. Hettiarachchi, S. Caucci & K. Schwarzel), pp. 61–89. Springer Nature, Switzerland.
- Dandeniya W.S., Herath E.M., Kasinthar M., Lowe W.A.M. & Jinadasa R.N. (2018). Prevalence of antibiotic resistant bacteria in poultry litter-based manures and potential threats on food safety for carrot (*Dacuscarotova*). In: *Be the Solution to Soil Pollution. Proceedings of the Global Symposium on Soil Pollution*, Rome, Italy, 2–4 May. Food and Agriculture Organization of the United Nations, pp. 309–314.
- DAPH (2010). *Annual Report*. Department of Animal Production and Health, Peradeniya, Sri Lanka. Available at http://www.daph.gov.lk/web/images/content_image/publications/annual_reports/annual_report_2010.pdf, Accessed 31 May 2021.
- DAPH (2019). *Annual Report*. Department of Animal Production and Health, Peradeniya, Sri Lanka. Available at http://daph.gov.lk/web/images/content_image/publications/annual_reports/2019/daph_annualReport_9_18_compressed.pdf, Accessed 31 May 2021.
- Darwish W.S., Eldaly E.A., El-Abbasy M.T., Ikenaka Y., Nakayama S. & Ishizuka M. (2013). Antibiotic residues in food: the African scenario. *Japanese Journal of Veterinary Research* **61**(Supplement): S13–S22.
DOI: <http://doi.org/10.14943/jjvr.61.suppl.s13>
- de Assis D.C.S., da Silva G.R., Lanza I.P., Ribeiro A.C.D.S.R., Lana Â.M.Q., Lara L.J.C., de Figueiredo T.C. & Cançado S.D.V. (2016). Evaluation of the presence and levels of enrofloxacin, ciprofloxacin, sulfaquinoxaline and oxytetracycline in broiler chickens after drug administration. *Plos One* **11**(11): e0166402.
DOI: <https://doi.org/10.1371/journal.pone.0166402>
- De Silva P.H.G.J., Atapattu N.S.B.M. & Sandika A.L. (2010). A study of the socio-cultural parameters associated with meat purchasing and consumption pattern: a case of Southern Province, Sri Lanka. *The Journal of Agricultural Sciences* **5**(2): 71–79.
- Dethlefsen L., Huse S., Sogin M.L. & Relman D.A. (2008). The pervasive effects of an antibiotic on the human gut microbiota, as revealed by deep 16S rRNA sequencing. *PLoS Biology* **6**(11): e280.
DOI: <https://doi.org/10.1371/journal.pbio.0060280>
- Dimitrova D.J., Lashev L.D., Yanev S.G. & Pandova B. (2007). Pharmacokinetics of enrofloxacin in turkeys. *Research in Veterinary Science* **82**(3): 392–397.
DOI: <https://doi.org/10.1016/j.rvsc.2006.09.004>

- Dissanayake D.R.A. & Wijewardana T.G. (2005). Indigenous chickens as sentinels for antimicrobial resistance to *Escherichia coli* in Sri Lanka. *Proceeding of the Peradeniya University Research Sessions, Sri Lanka*, 10 November, pp. 160.
- Dziva F. & Stevens M.P. (2008). Colibacillosis in poultry: unravelling the molecular basis of virulence of avian pathogenic *Escherichia coli* in their natural hosts. *Avian Pathology* **37**(4): 355–366.
DOI: <https://doi.org/10.1080/03079450802216652>
- Endtz H.P., Ruijs G. J., van Klingeren B., Jansen W.H., van der Reyden T. & Mouton R.P. (1991). Quinolone resistance in *Campylobacter* isolated from man and poultry following the introduction of fluoroquinolones in veterinary medicine. *Journal of Antimicrobial Chemotherapy* **27**(2): 199–208.
DOI: <https://doi.org/10.1093/jac/27.2.199>
- European Commission (2002). Commission Decision 2002/657/EC of 12 August 2002 implementing Council Directive 96/23/EC concerning the performance of analytical methods and the interpretation of results. *Official Journal of the European Communities* **50**: 8–36.
- European Commission (2010). Commission Regulation (EU) No 37/2010 of 22 December 2009 on pharmacologically active substances and their classification regarding maximum residue limits in foodstuffs of animal origin. *Official Journal of the European Union* **15**: 1–72.
- European Medicine Agency (2012). Baytril 10% oral solution and associated names: Annex I, II, III, IV. Available at https://www.ema.europa.eu/en/documents/referral/baytril-10-oral-solution-associated-names-annex-i-ii-iii-iv_en.pdf. Accessed 31 May 2021
- FDA (2005). *Withdrawal of Approval of the New Animal Drug Application for Enrofloxacin in Poultry*. Docket number 2000N–1571. Department of Health and Human Services, United States Food and Drug Administration.
- Goutard F.L., Bordier M., Calba C., Erlacher-Vindel E., Góchez D., de Balogh K., Benigno C., Kalpravidh W., Roger F. & Vong S. (2017). Antimicrobial policy interventions in food animal production in Southeast Asia. *BMJ* **358**: 36–41.
DOI: <https://doi.org/10.1136/bmj.j3544>
- Gouvêa R., dos Santos F.F., de Aquino M.H.C. & Pereira V.L. (2015). Fluoroquinolones in industrial poultry production, bacterial resistance and food residues: a review. *Brazilian Journal of Poultry Science* **17**(1): 1–10.
DOI: <http://dx.doi.org/10.1590/1516-635x17011-10>
- Gunarathne L., Fernando R., Munasinghe D.M.S. & Abeynayake P. (2016). Detection of sulfonamides residues in broiler meat in Sri Lanka. *Proceedings of South Asian Symposium on Sustainable Environment Management*, 17–18 March. Center for Environment Studies, University of Peradeniya, Sri Lanka, pp. 14.
- Herath E.M., Dandeneya W.S., Samarasinghe A.G.S.I., Bandara T.P.M.S.D. & Jinadasa R.N. (2015). A preliminary investigation on methods of reducing antibiotic resistant bacteria in broiler litter in selected farms in mid country, Sri Lanka. *Tropical Agricultural Research* **26**(2): 409–414.
- Herath E.M., Palansooriya A.G.K.N., Dandeneya W.S. & Jinadasa R.N. (2016). An assessment of antibiotic resistant bacteria in poultry litter and agricultural soils in Kandy district, Sri Lanka. *Tropical Agricultural Research* **27**(4): 389–398.
- Huff W.E., Huff G.R., Rath N.C., Balog J.M. & Donoghue A.M. (2004). Therapeutic efficacy of bacteriophage and Baytril (enrofloxacin) individually and in combination to treat colibacillosis in broilers. *Poultry Science* **83**(12): 1944–1947.
DOI: <https://doi.org/10.1093/ps/83.12.1944>
- Janecko N., Pokludova L., Blahova J., Svobodova Z. & Literak I. (2016). Implications of fluoroquinolone contamination for the aquatic environment-A review. *Environmental Toxicology and Chemistry* **35**(11): 2647–2656.
- Javadi A., Mirzaie H. & Khatibi S.A. (2011). Effect of roasting, boiling and microwaving cooking methods on Enrofloxacin residues in edible tissues of broiler. *African Journal of Pharmacy and Pharmacology* **5**(2): 214–218.
DOI: <https://doi.org/10.5897/AJPP.9000118>
- Kalupahana R.S., Kottawatta K.S.A., Kanankege K.S.T., Van Bergen M.A.P., Abeynayake P. & Wagenaar J.A. (2013). Colonization of *Campylobacter* spp. in broiler chickens and laying hens reared in tropical climates with low-biosecurity housing. *Applied Environmental Microbiology* **79**(1): 393–395.
DOI: <https://dx.doi.org/10.1128%2FAEM.02269-12>
- Kalupahana R.S., Mughini-Gras L., Kottawatta S.A., Somarathne S., Gamage C. & Wagenaar J.A. (2018). Weather correlates of *Campylobacter* prevalence in broilers at slaughter under tropical conditions in Sri Lanka. *Epidemiology and Infection* **146**(8): 972–979.
DOI: <https://doi.org/10.1017/S0950268818000894>
- Karunarathna K.G.R.N., Arulkanthan A. & Jayasena N.U.A. (2013). Antimicrobial resistance patterns in *Escherichia coli* of poultry origin in the Kandy district. *Proceedings of the Peradeniya University Research Sessions, Sri Lanka*, 4 July, pp. 99.
- King D.E., Malone R. & Lilley S.H. (2000). New classification and update on the quinolone antibiotics. *American Family Physician* **61**(9): 2741–2748.
- Kirbiš A., Marinšek J. & Flajs V.C. (2005). Introduction of the HPLC method for the determination of quinolone residues in various muscle tissues. *Biomedical Chromatography* **19**(4): 259–265.
DOI: <https://doi.org/10.1002/bmc.435>
- Kottawatta S.A.K., Van Bergen M.A.P., Abeynayake P., Wagenaar, J.A., Veldman K.T. & Kalupahana R.S. (2017). *Campylobacter* in broiler chicken and broiler meat in Sri Lanka: Influence of semi-automated vs. wet market processing on campylobacter contamination of broiler neck skin samples. *Foods* **6**(12): 105.
DOI: <https://doi.org/10.3390/foods6120105>
- Kowalski T.J., Henry M.J. & Zlabek J.A. (2005). Furazolidone-induced pulmonary hypersensitivity. *Annals of Pharmacotherapy* **39**(2): 377–379.
DOI: <https://doi.org/10.1345%2Faph.1E080>

- Landers T.F., Cohen B., Wittum T.E. & Larson E.L. (2012). A review of antibiotic use in food animals: perspective, policy, and potential. *Public Health Reports* **127**(1): 4–22. DOI: <https://doi.org/10.1177%2F003335491212700103>
- Liyanage G.Y. & Pathmalal M. (2017). Risk of prophylactic antibiotics in livestock and poultry farms—a growing problem for human and animal health. *Pharmaceutical Journal of Sri Lanka* **7**(1):13–22.
- Lowe W.A.M., Samarakone T.S., Vidanarachchi J.K., Dandeniya W.S. & Edirisinghe N. (2019). Antibiotic residue free broiler meat; Prevalence of antibiotic residues in broiler meat and resistant bacteria in poultry litter in Sri Lanka and awareness on antibiotic usage. *International Journal of Food and Nutritional Sciences* **8**(4): 34–40.
- Manage P.M. (2018). Heavy use of antibiotics in aquaculture; Emerging human and animal health problems—A review. *Sri Lanka Journal of Aquatic Sciences* **23**(1): 13–27.
- Manage P.M. & Liyanage G.Y. (2019). Antibiotics induced antibacterial resistance. In: *Pharmaceuticals and Personal Care Products: Waste Management and Treatment Technology*, pp. 429–448. Butterworth-Heinemann, Oxford, UK.
- McDermott P.F. *et al.* (27 authors) (2004). Development of a standardized susceptibility test for *Campylobacter* with quality-control ranges for ciprofloxacin, doxycycline, erythromycin, gentamicin, and meropenem. *Microbial Drug Resistance* **10**(2): 124–131. DOI: <https://doi.org/10.1089/1076629041310064>
- McLeod A., Thieme O. & Mack S.D. (2009). Structural changes in the poultry sector: will there be smallholder poultry development in 2030? *World's Poultry Science Journal* **65**(2): 191–200. DOI: <https://doi.org/10.1017/S0043933909000129>
- Ministry of Health and Welfare (2005). *Specifications and Standards for Food, Food Additives*. Notification no. 499. Ministry of Health and Welfare, Tokyo, Japan.
- Mitchell M.A. (2006). Enrofloxacin. *Journal of Exotic Pet Medicine* **15**(1): 66–69.
- Moghadam N.R., Arefhosseini S.R., Javadi A., Lotfipour F., Ansarin M., Tamizi E. & Nemati M. (2018). Determination of enrofloxacin and ciprofloxacin residues in five different kinds of chicken tissues by dispersive liquid–liquid microextraction coupled with HPLC. *Iranian Journal of Pharmaceutical Research* **17**(4): 1182–1190.
- Nelson J.M., Chiller T.M., Powers J.H. & Angulo F.J. (2007). Fluoroquinolone-resistant *Campylobacter* species and the withdrawal of fluoroquinolones from use in poultry: a public health success story. *Clinical Infectious Diseases* **44**(7): 977–980. DOI: <https://doi.org/10.1086/512369>
- Nkukwana T.T. (2018). Global poultry production: Current impact and future outlook on the South African poultry industry. *South African Journal of Animal Science* **48**(5): 869–884. DOI: <https://doi.org/10.4314/sajas.v48i5.7>
- Panzenhagen P.H.N., Aguiar W.S., Gouvêa R., de Oliveira A.M., Barreto F., Pereira V.L.A. & Aquino M.H.C. (2016). Investigation of enrofloxacin residues in broiler tissues using ELISA and LC-MS/MS. *Food Additives & Contaminants: Part A* **33**(4): 639–643. DOI: <https://doi.org/10.1080/19440049.2016.1143566>
- Pena A., Silva L.J.G., Pereira A., Meisel L. & Lino C.M. (2010). Determination of fluoroquinolone residues in poultry muscle in Portugal. *Analytical and Bioanalytical Chemistry* **397**(6): 2615–2621. DOI: <https://doi.org/10.1007/s00216-010-3819-0>
- Sarker Y.A., Hasan M.M., Paul T.K., Rashid S.Z., Alam M.N., & Sikder M.H. (2018). Screening of *Veterinary and Animal Research* **5**(2): 140–145. DOI: <http://doi.org/10.5455/javar.2018.e257>
- Sattar S., Hassan M.M., Islam S.K.M.A., Alam M., Al Faruk M.S., Chowdhury S. & Saifuddin A.K.M. (2014). Antibiotic residues in broiler and layer meat in Chittagong district of Bangladesh. *Veterinary World* **7**(9):738–743. DOI: <https://doi.org/10.14202/vetworld.2014.738-743>
- Seguin M.A., Papich M.G., Sigle K.J., Gibson N.M. & Levy J.K. (2004). Pharmacokinetics of norfloxacin in neonatal kittens. *American Journal of Veterinary Research* **65**(3): 350–356. DOI: <https://doi.org/10.2460/ajvr.2004.65.350>
- Sharma P.C., Jain A., Jain S., Pahwa R. & Yar M.S. (2010). Ciprofloxacin: review on developments in synthetic, analytical, and medicinal aspects. *Journal of Enzyme Inhibition and Medicinal Chemistry* **25**(4): 577–589. DOI: <https://doi.org/10.3109/14756360903373350>
- Shim J.H., Shen J.Y., Kim M.R., Lee C.J. & Kim I.S. (2003). Determination of the fluoroquinolone enrofloxacin in edible chicken muscle by supercritical fluid extraction and liquid chromatography with fluorescence detection. *Journal of Agricultural and Food Chemistry* **51**(26): 7528–7532. DOI: <https://doi.org/10.1021/jf0346511>
- Singer R.S. & Hofacre C.L. (2006). Potential impacts of antibiotic use in poultry production. *Avian Diseases* **50**(2): 161–172. DOI: <https://doi.org/10.1637/7569-033106R.1>
- Smith K.E., Besser J.M., Hedberg C.W., Leano F.T., Bender J.B., Wicklund J.H., Johnson B.P., Moore K.A. & Osterholm M.T. (1999). Quinolone-resistant *Campylobacter jejuni* infections in Minnesota, 1992–1998. *New England Journal of Medicine* **340**(20): 1525–1532. DOI: <https://doi.org/10.1056/NEJM199905203402001>
- Sultan I.A. (2014). Detection of enrofloxacin residue in livers of livestock animals obtained from a slaughterhouse in Mosul City. *Journal of Veterinary Science and Technology* **5**(2): 168. DOI: <https://doi.org/10.4172/2157-7579.1000168>
- Sureshkumar V. & Sarathchandra G. (2018). Prevalence of enrofloxacin and its primary metabolite ciprofloxacin residues in broiler meat and organ samples of field origin. *Global Journal of Bioscience and Biotechnology* **7**(3): 324–326.
- Tauxe R.V. (2002). Emerging foodborne pathogens. *International Journal of Food Microbiology* **78**(1-2): 31–41. DOI: [https://doi.org/10.1016/S0168-1605\(02\)00232-5](https://doi.org/10.1016/S0168-1605(02)00232-5)
- U.S. Food and Drug Administration (1994). *Reviewer Guidance, Validation of Chromatographic Methods*, Center for Drug Evaluation and Research, Rockville, USA.

- Wang G.N., Feng C., Zhang H.C., Zhang Y.Q., Zhang L. & Wang J.P. (2015). Determination of fluoroquinolone drugs in meat by ionic-liquid-based dispersive liquid-liquid microextraction-high performance liquid chromatography. *Analytical Methods* 7(3): 1046–1052.
DOI: <https://doi.org/10.1039/C4AY02383H>
- Wickramarachchi A.R., Herath H.M.L.K., Jayasinghe-Mudalige U.K., Edirisinghe J.C., Udugama J.M.M., Lokuge L.D.M.N. & Wijesuriya W. (2017). An analysis of price behavior of major poultry products in Sri Lanka. *Journal of Agricultural Sciences* 12(2): 138–148.
- Yorke J.C. & Froc P. (2000). Quantitation of nine quinolones in chicken tissues by high-performance liquid chromatography with fluorescence detection. *Journal of Chromatography A* 882(1-2): 63–77.
DOI: [https://doi.org/10.1016/S0021-9673\(00\)00165-5](https://doi.org/10.1016/S0021-9673(00)00165-5)

RESEARCH ARTICLE

Energy deposition and dose enhancement using Monte Carlo derivative sampling: applications in brachytherapy

H Khan¹, ZU Koreshi², U Aziz^{3*}, SR Sheikh³ and SA Ahmad⁴

¹ Department of Sciences & Humanities, National University of Computer and Emerging Sciences, Islamabad, Pakistan.

² Faculty of Graduate Studies, Air University, Islamabad, Pakistan.

³ Department of Mechatronics Engineering, Air University, Islamabad, Pakistan.

⁴ Department of Strategic Studies, National Defence University, Islamabad, Pakistan.


Submitted: 23 September 2020; Revised: 24 February 2021; Accepted: 23 April 2021

Abstract: Energy deposition and radiation dose distribution by the use of gold, a high-Z biocompatible element in water solution, is estimated as a function of source energy typical of brachytherapy sources (15 keV, 20 keV, 30 keV, 40 keV, 80 keV, 90 keV, 150 keV, 300 keV, 1 MeV), solution concentration (5–25 mg Au/g H₂O), and solution placement (1–2 cm concentric shells). Monte Carlo (MC) simulations are carried out with the MCNP5 code, compared with other widely used MC codes such as PENELOPE and GEANT, to validate the dose estimates, which may vary considerably due to artifacts and data libraries, and extended to a sensitivity analysis using perturbation estimates. The energy deposition and radiation dose are estimated as a function of monoenergetic source radiation energy, and concentration of gold in solution. MC simulation is carried out in the coupled photon-electron radiation mode for x-rays emanating from a radiation source implanted in a water cell, for which results are valid for a cancer cell modelled by a spherical water phantom. For carrying out sensitivity studies, the Monte Carlo perturbation feature with material perturbations was used to sample derivatives in a single run which were used in a Taylor series to estimate both dose and Dose Enhancement Factor (DEF) from single MC runs. Close agreement was found between dose estimates from MCNP5, PENELOPE and GEANT, in spite of artifacts such as cut-offs in electron transport. It was also found that dose increases with energy of a source, and that dose enhancement, for a given concentration, decreases with source energy. The perturbation estimates result in enhanced computational efficiency.

Keywords: Brachytherapy, dose enhancement, energy deposition, gold nanoparticles, Monte Carlo simulation.

INTRODUCTION

Energy deposition from radiation is of use for several engineering and medical applications, such as the design of radiation shields and in the treatment of cancer. This research carried out simulations to estimate the dose in a water cell similar to a cancer cell in composition. In nuclear medicine, radiation nuclide therapy (RNT) is used for the treatment of organs such as the thyroid, bones, heart, liver and for the treatment of cancer in organs such as the lungs, breast, colon and rectum, prostate, stomach, and liver. Nuclear radiation, in the form of X-rays, gamma rays and charged particles, can damage the DNA (deoxyribonucleic acid) molecules of cancer cells that carry the genetic information and pass it from one generation to the next, to stop their further division. RNT is used both externally as ‘tele-therapy’ and internally as brachytherapy, or ‘short-distance therapy’. The number of cancer cases globally is expected to grow from 14.1 million in 2012 to 24 million by 2035 (Common Cancer Types - National Cancer Institute; Worldwide cancer data - World Cancer Research Fund). Improvements in cancer therapy, such as the dose enhancement by radiation and better computational methods for its estimation, the focus areas of research reported in this paper are thus of paramount importance to the science and technology of medicine. Of the 200 or more radioisotopes used in nuclear medicine (Radioisotopes in Medicine), common

* Corresponding author (umair.aziz@mail.au.edu.pk;  <https://orcid.org/0000-0002-9554-0725>)



This article is published under the Creative Commons CC-BY-ND License (<http://creativecommons.org/licenses/by-nd/4.0/>). This license permits use, distribution and reproduction, commercial and non-commercial, provided that the original work is properly cited and is not changed in anyway.

radioisotopes include technetium ^{99m}Tc , iodine ^{125}I , palladium ^{103}Pd , iridium ^{192}Ir , cesium ^{137}Cs , and cobalt ^{60}Co .

Important radionuclides for brachytherapy include the conventional encapsulated (Perez-Calatayud *et al.*, 2012) low dose rate (LDR) sources (< 200 cGy per hour) Ir-192, and high dose rate (HDR) sources (> 1200 cGy per hour) (Pisansky *et al.*, 2008; Mose *et al.*, 2013; Mobit *et al.*, 2016). Permanent brachytherapy sources (Lechtman *et al.*, 2011) such as ^{125}I and ^{103}Pd with energy < 50 keV are commonly used LDR sources, with typical implants of 50-80 metallic seeds encasing isotopes, used for the treatment of prostate cancer, uveal melanomas and brain tumours.

For calculations for dose distribution MC methods (Kalos & Whitlock, 2008) and general-purpose codes, such as EGSnrc, GEANT (Allison *et al.*, 2006), PENELOPE (Salvat *et al.*, 2006) and MCNP (Team, 2008) have been extensively used (Jabbari, 2011; Seco, 2016) for simulating the transport of radiation from radiation seeds in the medium consisting of tissue, and material in the vicinity of the cancer. These codes have produced fast and accurate results which have been experimentally validated and benchmarked.

A further development in brachytherapy has been the possibility of injecting high-Z biocompatible elements such as gold and gadolinium in solution form through fenestrations of cancer cells to improve the effectiveness of therapy. The method thus requires elements of dimensions small enough to be delivered into tumour cells so that the effects of radiation are localized and restricted to the 'bad' cells while sparing the healthy 'good' cells. The determination of radiation dose, in addition to the previously mentioned factors, now extends to a determination of the choice of element, its size and shape, and injection procedure in solution form. The requirements of particle size necessitate the range down to nanoscale ($\sim 10^{-9}$ m) which compares with the diameter of an atom ($\sim 10^{-10}$ m), thus introducing nanotechnology to the field of brachytherapy (Jain *et al.*, 2012; Chatterjee *et al.*, 2013).

In brachytherapy, the use of gold nanoparticles (GNPs) is an active area of research to determine possible dose enhancement (Bahreyni Toossi *et al.*, 2012; Brivio *et al.*, 2017; Safigholi & Song, 2018; Gray *et al.*, 2019; Jangjoo *et al.*, 2019) to make the therapy more effective. Nanoscale, at which the wavelength of incident electromagnetic radiation can become of the order of atomic dimensions casts doubts on the reliability

of simulation results from Monte Carlo codes due to several artifacts.

The effects of such artifacts for electron transport have been investigated (Almansa *et al.*, 2006; Koivunoro *et al.*, 2012; Archambault & Mainegra-Hing, 2015) with EGSnrc, GEANT and PENELOPE codes and in some cases 'large discrepancies' (> 3%) have been found between MCNP5 dose distributions and the 'reference codes' concluding that MCNP5 electron transport calculations are not accurate at all energies and in every medium by general clinical standards. Similarly, comparisons have been made (Yu *et al.*, 2017) between EGSnrc, GEANT4, MCNP5 and PENELOPE for mono-energetic electron beams in a water-filled sphere of radius varying from 0.25–4.5 cm for beam energies of 0.5 MeV, 1.0 MeV, and 5.0 MeV and found to have differences below 10% by tuning parameters associated with multiple scattering algorithms at the expense of increased computation time. It can thus be anticipated that MCNP5 may differ due to its inadequate low-energy treatment of electron transport. Šidlová and Trojek (2010) have carried out electron transport comparisons of MCNPX, Penelope and EGSnrc, for electrons of 20–450 keV in water, lead and tungsten. These comparisons were focused on bremsstrahlung, energy deposition in matter, electron ranges and production of secondary electrons by gamma radiation. Thus, preliminary runs are carried out to compare dose estimates from MCNP5 with Penelope and Geant4 (Almansa *et al.*, 2006).

Thus, benchmarking and validating MC results have become particularly relevant not only for radiation dose but also for the resulting biological absorbed dose, which is the ultimate quantity of interest varying from organ to organ. With the objective of determining radiation dose distribution and the dose enhancement factor (DEF) by the use of gold, a high-Z biocompatible element, this work carries out MC simulation, using MCNP5, for simulating coupled photon-electron radiation transport from x-rays emanating from a radiation source implanted in tumour, modelled by a spherical water phantom, to estimate the energy deposited and the subsequent biological dose. Good comparisons are presented for point mono-energetic source in water (Luxton & Jozsef, 1999; Almansa *et al.*, 2006). While water phantoms are used for representing configurations similar to soft tissue, full anthropomorphic phantoms are also used to carry out detailed simulation for the dose (Neves *et al.*, 2014)

For MC simulations in brachytherapy (Lechtman *et al.*, 2013; Mesbahi *et al.*, 2013; Asadi *et al.*, 2015) it has been shown that photon source energy and

concentration are important factors that determine DEF while the size of GNPs is not so important (above the K-edge energy). Thus, in this work, a homogenous model with considerable savings on the computational effort, as well as a sensitivity capability is used to extract crucial information on the DEF from independent parameters.

The MCNPX code has been used (Mesbahi *et al.*, 2013) for simulating mono-energetic photon beams (50–120 keV), ⁶⁰Co beam, and 6 & 18 MV photon beams, while GEANT4 simulations have been carried out (Banoqitah & Djouider, 2016) for estimating the DEF from high energy photons from ¹⁹²Ir (0.380 MeV), ¹³⁷Cs (0.662 MeV) and ⁶⁰Co (1.2 MeV) for gadolinium (Z = 64) nanoparticles in a heterogeneous model with concentrations ranging from 10-70 mg/g brain tumour.

In this work, the source energy of interest is 15 keV – 1 MeV typical of brachytherapy sources (15 keV, 20 keV, 30 keV, 40 keV, 80 keV, 90 keV, 150 keV, 300 keV, 1 MeV), while the gold particles in solution form with water were assumed to comprise a homogenous mixture with concentrations in the range 5–25 mg Au/g H₂O. While MCNP has the capability of modelling very detailed heterogeneous configurations, this paper considers a homogenous model solely to demonstrate (i) results from benchmarked problems and (ii) for obtaining MC sensitivity estimates for a ‘bulk’ material to demonstrate validity of MC perturbation and quantifying increased computational efficiency.

For comparison, dose estimates from MCNP5 were compared with published results from PENELOPE and GEANT. The second objective of this work was to estimate the effect of small changes in solution concentration on the resulting radiation dose from a single MC simulation rather than estimating changes from MC re-runs where the effect is vulnerable to be masked in the uncertainty of the estimate itself. Such MC perturbation analysis has applications in brachytherapy for estimating dose perturbations when implants are present in the vicinity of an organ receiving radiation from an implanted source (Yu *et al.*, 2017). However, it is yet to be used in simulation for brachytherapy studies and can provide great computational efficiency leading to optimal designs based on ‘best’ experimental parameters such as radiation energy, concentration of gold in solution and material placement for maximizing an objective function of interest.

There is still no consensus on the optimal size, shape and distribution of GNPs. Experimental and pre-clinical evidence for mouse tumours showing a 1-year survival rate of 86% following a dose of 26 Gy, with 1.9 nm

intravenously administered GNPs vs 20% for tumours not laden with GNPs (Jain *et al.*, 2012), indicates that nanotechnology offers promising improvements in brachytherapy. This work is aimed to further improve the understanding of determining possible improvements in delivered dose by applying Monte Carlo simulation, and the MC perturbation capability (Rief, 1984; Koreshi & Lewins, 1990), to lead to optimal experimental configurations.

METHODOLOGY

Monte Carlo simulation

The Monte Carlo code MCNP5 is used to carry out a coupled photon-electron simulation of radiation transport to estimate the dose distribution, from a point isotropic photon source typical of brachytherapy sources (30 keV for ¹²⁵I - 1.25 MeV for ⁶⁰Co) located at the origin of a sphere, in concentric shells of water of thickness 0.5 mm up to a radius of 15 cm. A solution of gold and water is then considered in the shells located 1–2 cm from the center and the F6 (energy deposition) and *F8 (pulse height) tallies are used for phantom dosimetry. Photon and electron data for air, water and gold are based on ENDF/B-VI (Release 8). In the MCNP ‘detailed physics’ simulation, coherent (Thomson) scattering is included, and fluorescent photons produced from photoelectric absorption are included and electrons produced from photon collisions are transported in a ‘condensed history’ method that accumulates the effects of many individual collisions into single steps sampled probabilistically. The F6 tally given as equation (1)

$$D = \frac{\rho_a}{m} \int dE \int dt \int dV \int d\Omega \sigma_t(E) H(E) \phi(\vec{r}, \hat{\Omega}, E, t) \text{ MeV g}^{-1} \dots(1)$$

where D is dose, m is mass, ρ_a is atomic density, t is time, E is energy, V is volume, Ω is solid angle, ϕ is scalar flux scored over volume (track length/volume) cm⁻², σ_t is microscopic total cross-section and H is heating number (MeV/collision),

from MCNP is converted from MeV/g to yield the dose in nGy cm² Bq⁻¹ hr⁻¹ to compare with Almansa *et al.* (2006). The results plotted are for $\dot{D} = \kappa r^2 D$ nGy cm² Bq⁻¹ hr⁻¹ where $\kappa = 576 \text{ nGy cm}^2 \text{ Bq}^{-1} \text{ hr}^{-1} / (\frac{\text{MeV}}{\text{g}})$.

Monte Carlo perturbation sampling

Perturbation algorithms in MC simulation (Rief, 1984) extended the capability of MC methods to sensitivity studies and optimization (Koreshi & Lewins, 1990). The

change in a response function such as dose D , due to a variation in an independent parameter, such as material density ρ , expressed as a Taylor series in equation (2)

$$D(\rho) = D(\rho_o) + D'(\rho_o)\delta\rho + \frac{1}{2!}D''(\delta\rho)^2 + \dots \quad \dots(2)$$

can be used with first- and second-order derivatives D' and D'' from a single run. Thus, when the change in a parameter is small enough to be of the order of the statistical uncertainty of a MC estimate, then the difference from two independent runs may mask the actual difference. In order to circumvent such inaccuracy, the derivatives are sampled in a single simulation. The energy deposition for a ‘perturbed’ design (D^{new}) can thus be estimated from a Taylor series in terms of a ‘reference’ design (D^{ref}).

Material composition

The material used in this work is water with gold solution which has density $\rho = 1.04 \text{ g cm}^{-3}$ very close to that of soft tissue $\rho = 1.04 \text{ g cm}^{-3}$ [with a four-component simplified composition hydrogen (H), carbon (C), nitrogen (N) and oxygen (O) with weight percentages: 10.454, 22.663, 2.49, 63.525%, respectively] and the photon cross-sections for both (water and soft tissue) are almost indistinguishable so that conclusions drawn for energy deposition would hold for both materials to a reasonably acceptable order.

RESULTS AND DISCUSSION

Benchmarking of radiation dose and dose distribution

To compare MCNP5 results for energy deposition from a mono-energetic point isotropic source at the centre of a sphere of radius 15 cm, the F6 tally in 0.5 mm thick concentric shells were used with 1 million histories for each source energy level. From the results shown in Figure 1, it is seen that there is good agreement with the results given in the literature (Almansa *et al.*, 2006). When normalized to a reference dose from a 1 MeV source, it is seen that the lowest energy, 15 keV, has an energy deposition of about 65% of the reference which falls off rapidly to less than 10% in 1.5 cm of water. With a further increase in energy, the relative intensities drop but the deposition sustains to greater depths, which is less important in brachytherapy than to give a localized deposition from a low-energy source.

MCNP simulations were carried out on an Intel(R) Core (TM) i7-2620M CPU @ 2.70GHz with an installed memory of 8.00 GB (3.24 GB usable) and 32-bit Operating system with Windows 7 Professional.

The DEF shown in Figure 2 gives the extent and magnitude as a function of source energy and concentration confirming the trend of direct variation with concentration and inverse variation with source

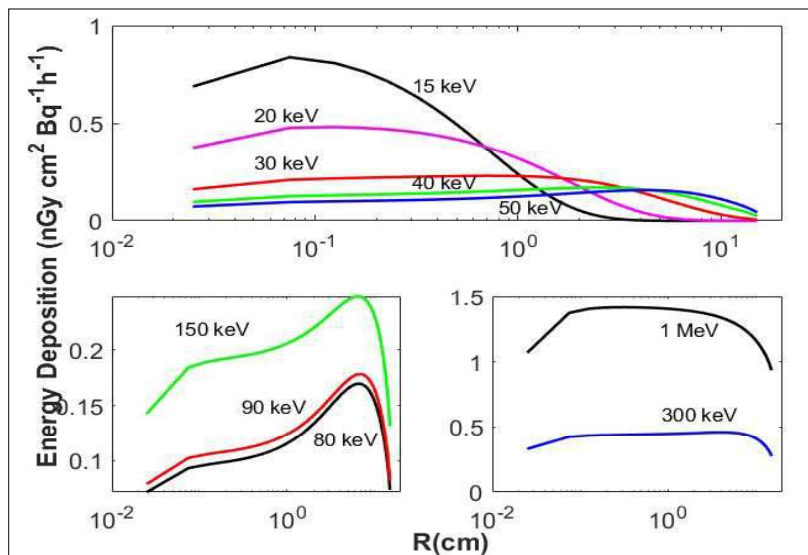


Figure 1: Energy deposition for mono-energetic photons of energy E: 15 keV-1 MeV

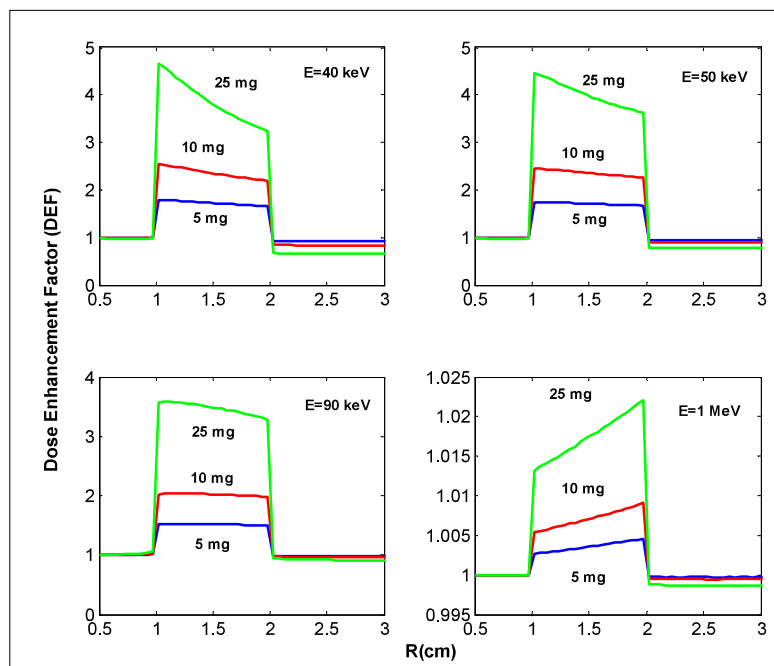


Figure 2: Dose enhancement factor (DEF) vs. distance for E = 40 keV, 50 keV, 90 keV, 1 MeV for varying concentrations 5, 10, 25 mg Au/g H₂O

energy. The rate of ‘fall’ or ‘rise’ of DEF in the solution region is indicative of the slightly longer spatial effect of the high-energy photons as compared to low-energy photons.

For ophthalmic brachytherapy with ¹²⁵I (mean energy 35.49 keV), a full three-dimensional heterogeneous model (Asadi *et al.*, 2015) simulating 10⁷–10⁹ histories, for 50 nm GNPs, estimate the DEF for 7, 10, 18 and 30 mg/g as 1.9, 2.2, 3.2 and 4.6 for the tumour phantom compared with 1.9, 2.3, 3.3 and 4.8 in the water phantom, respectively.

As given in Table 1, this work, for a water phantom with 10⁶ simulations with a maximum time ~35 minutes in a homogenous mixture model for the solution gives, for 40 keV and concentrations of 5, 10, 25 mg/g maximum DEFs (Figure 3) of 1.8, 2.5, 4.6. DEF has been found to lie in the range 1.4–3.7 with the highest DEF for 90 keV (Mesbahi *et al.*, 2013); the effect of GNP size was not considerable (Lechtman *et al.*, 2011; Mesbahi *et al.*, 2013) while concentration and energy were important. These simulations (Lechtman *et al.*, 2011; Mesbahi *et al.*, 2013) carried out for 7 and 18 mg Au/g H₂O for 30, 50, 100 nm GNPs and energies between 50–18 MeV, report highest DEF of 3.5 at 90 keV followed by 3.0 at 50 keV both for 30 nm GNPs and 18 mg/g concentration.

Table 1: Max DEF for 1M simulations vs E and concentration; CPU time (mins) shown in brackets

No.	E (keV)	$\alpha = 5$	$\alpha = 10$	$\alpha = 25$
1	40	1.7854 (33.17)	2.5398 (35.48)	4.6537 (17.86)
2	50	1.7394 (40.53)	2.4521 (42.47)	4.4529 (21.56)
3	90	1.5204 (59.56)	2.0398 (58.19)	3.5861 (31.02)
4	1000	1.0046 (98.71)	1.0091 (101.78)	1.0221 (71.46)

For high energy sources, with 10⁸ source particles simulated, it is reported (Banoqitah & Djouider, 2016) that a maximum DEF is 1.45 within the tumour when implanted with 70 mg/g Gd for the lowest energy (¹⁹²Ir), and that the DEF varies directly with concentration and inversely with source energy e.g. for a concentration of 30 mg/g it decreases from 1.24 to 1.09 when photon energy increases from 0.380 MeV (¹⁹²Ir) to 1.20 MeV (⁶⁰Co). The results for this work show similar trends at high energy (1 MeV), i.e., a maximum DEF increasing very slowly from 1.0046 to 1.0221 as concentration increases from 5 mg/g to 25 mg/g.

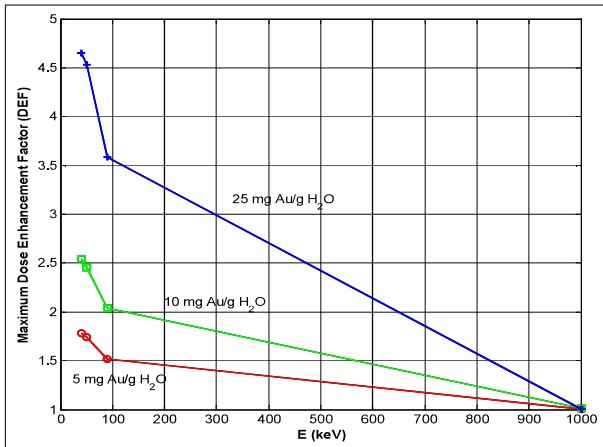


Figure 3: Maximum dose enhancement factor vs. energy for varying concentrations 5, 10, 25 mg Au/g H₂O

MC perturbation estimates

The simulations carried out for the results presented in previous sections were computationally intensive, which usually requires in excess of one hour for high energy (1 MeV). Thus, MC would be inefficient for carrying out sensitivity studies where the effect of perturbations, such as the solution concentration of gold in water, on

the DEF would be required. If a change is small then the statistical uncertainty in the results from two independent simulations, from which the change in the outcome is being estimated, could mask the effect of the change and hence produce unreliable results. Thus, perturbation MC was examined to obtain first- and second-order derivative changes, shown in Figure 4, in concentration of the gold solution in the range 5–25 mg Au/g H₂O. For this, a single run at a reference design of 5 mg Au/g H₂O was carried out and derivatives were obtained for the energy deposition to predict results for 15 mg Au/g H₂O in 35.24 minutes compared with 33.17 minutes as given in Table 1.

The 1st and 2nd order perturbation results, 15 mg (1PT) and 15 mg (2PT) respectively, for estimating the energy deposition at 15 mg/g are almost identical due to the small magnitude of the perturbation rendering the 2nd derivative an almost insignificant contribution. A better idea of the differences from re-run estimates $(\Delta D)_r$ compared with perturbation theory estimates $(\Delta D)_p$ is depicted in Figure 5, where the ratio γ , given by equation (3), remains ~ 1 in the gold solution region (1-2 cm) but at the boundary where there is a sharp jump, the perturbation estimates are also unreliable, since the magnitude of the perturbation exceeds the validity of 2nd order Taylor series.

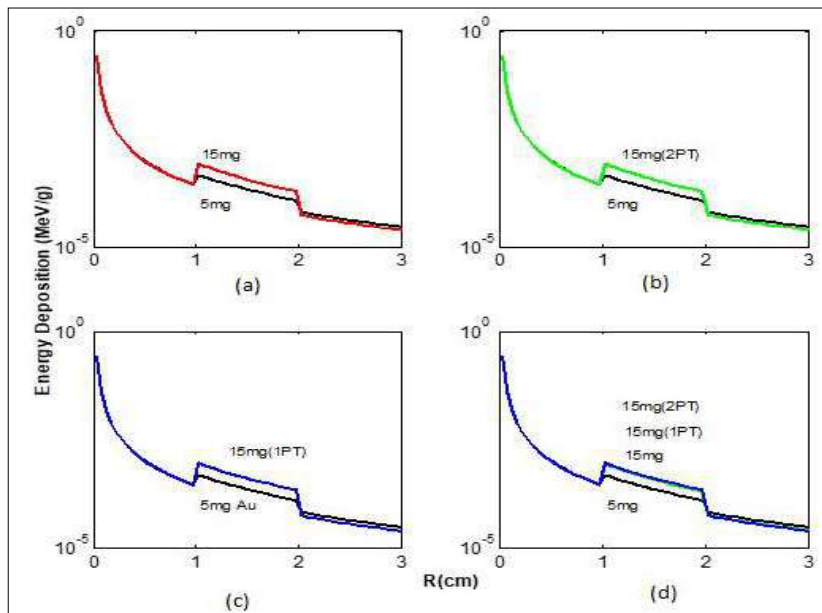


Figure 4: Energy deposition (MeV/g) vs. distance for photon energy 40 keV: (a) two independent MC simulations; (b) 5 mg simulation compared with 2nd order perturbation theory estimate for 15 mg perturbed case; (c) 5 mg simulation compared with 1st order perturbation theory estimate for 15 mg perturbed case; (d) all four cases

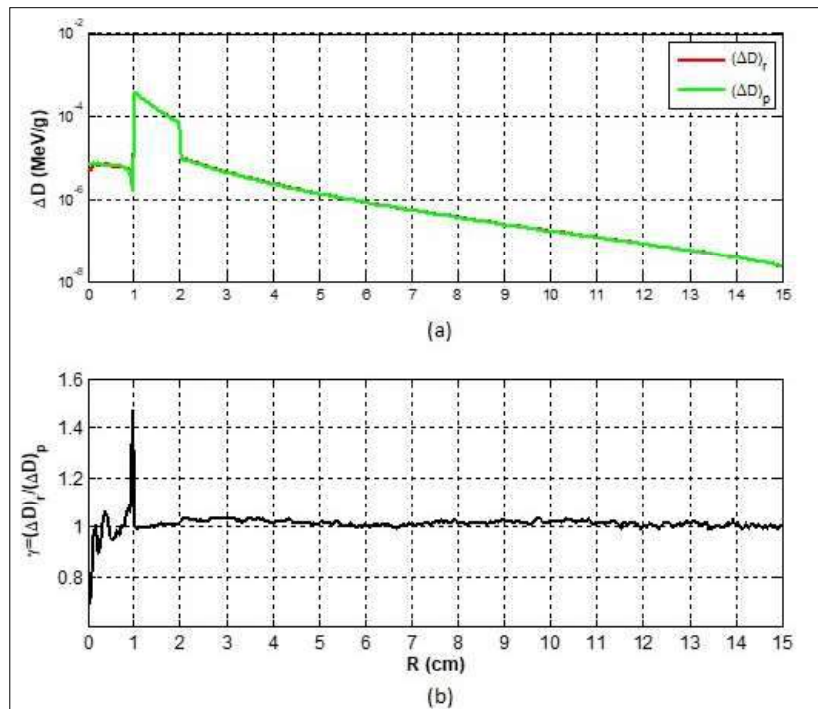


Figure 5: Energy deposition (MeV/g) vs. distance for photon energy 40 keV: (a) differences from independent re-runs $(\Delta D)_r$ and differences based on perturbation estimate $(\Delta D)_p$; (b) ratio of differences γ

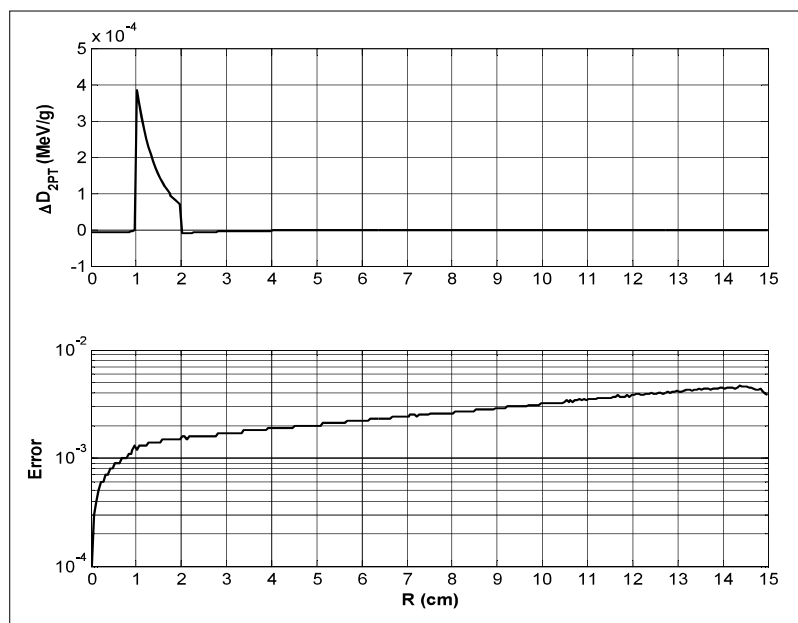


Figure 6: Differences in energy deposition (MeV/g) vs. distance for photon energy 40 keV: (a) differences based on 2nd order perturbation estimate $(\Delta D)_{2PT}$; (b) standard errors in estimates of $(\Delta D)_p$

$$\gamma \equiv \frac{D^{new} - D^{ref}}{D_p^{new} - D_p^{ref}} \quad \dots(3)$$

A further test of the reliability of the results is given in Figure 6 which shows the magnitude of the second-order perturbation estimate and the errors R for which the 68% confidence limit of a result is where is the estimate of the change in estimated dose from 2nd order MC perturbation sampling, increasing from 10^{-4} to $\sim 5 \times 10^{-3}$ at the outer edge of the sphere.

CONCLUSIONS

In this work, the dose enhancement by injecting gold in solutions was estimated as a function of source energy and solution concentration. The important photon interaction for materials with high atomic number (Z) is the photoelectric effect for which the cross-section varies as $\mu_{PE} \sim \frac{\rho Z^3}{E^3}$ (where μ_{PE} is photoelectric attenuation coefficient) so that low energy and high- Z are desirable for dose enhancement which is localized to the tumour due to the short range of photoelectrons and Auger electrons in the surrounding medium which for electrons of energy 0.1 MeV is ~ 100 microns in water and ~ 15 microns in gold so that the effect of gold will require thin layers (of the order of λ) to utilize the energy of photoelectrons in water. At this energy, the photoabsorptions were estimated to be $\sim 13.5\%$ of all interactions.

Computational efficiency in MC simulation for estimating small changes in parameters has been demonstrated using a perturbation feature of MC simulation, thereby greatly reducing the computational effort to perform simulations in brachytherapy, extending its applicability to full-scale heterogeneity sensitivity studies pertinent to the modelling of nanoparticles in implanted solutions.

Important conclusions from this research were: (i) MCNP dose estimates were found to be in acceptable agreement with PENELOPE and GEANT in spite of artifacts such as cut-offs in electron transport (Archambault & Mainegra-Hing, 2015), (ii) dose increases with energy of a source, (iii) dose enhancement, for a given concentration, decreases with source energy, and (iv) MC perturbation theory is valid and useful, due to enhanced computational efficiency, for the practically important range of material density in solutions of gold and water, assumed homogeneously mixed.

Conflict of interest

Authors declare that they have no conflict of interest.

REFERENCES

- Allison J. *et al.* (2006). Geant4 developments and applications. *IEEE Transactions on Nuclear Science* **53**(1): 270–278. DOI: <https://doi.org/10.1109/TNS.2006.869826>
- Almansa J.F., Guerrero R., Al-Dweri F.M.O., Anguiano M. & Lallena A.M. (2006). Dose distribution in water for monoenergetic photon point sources in the energy range of interest in brachytherapy: Monte Carlo simulations with PENELOPE and GEANT4. *Nuclear Instruments and Methods in Physics Research B* **254**: 219–230.
- Archambault J.P. & Mainegra-Hing E. (2015). Comparison between EGSnrc, Geant4, MCNP5 and Penelope for mono-energetic electron beams. *Physics in Medicine and Biology* **60**(13): 4951–4962. DOI: <https://doi.org/10.1088/0031-9155/60/13/4951>
- Asadi S., Vaez-zadeh M., Masoudi S.F., Rahmani F., Knaup C. & Meigooni A.S. (2015). Gold nanoparticle-based brachytherapy enhancement in choroidal melanoma using a full Monte Carlo model of the human eye. *Journal of Applied Clinical Medical Physics* **16**(5): 344–357. DOI: <https://doi.org/10.1120/jacmp.v16i5.5568>
- Bahreyni Toossi M.T., Ghorbani M., Mehrpouyan M., Akbari F., Sobhkhiz Sabet L. & Soleimani Meigooni A. (2012). A Monte Carlo study on tissue dose enhancement in brachytherapy: a comparison between gadolinium and gold nanoparticles. *Australasian Physical and Engineering Sciences in Medicine* **35**(2): 177–185. DOI: <https://doi.org/10.1007/s13246-012-0143-3>
- Banoqitah E. & Djouider F. (2016). Dose distribution and dose enhancement by using gadolinium nanoparticles implant in brain tumor in stereotactic brachytherapy. *Radiation Physics and Chemistry* **127**: 68–71. DOI: <https://doi.org/10.1016/j.radphyschem.2016.06.002>
- Brivio D., Nguyen P.L., Sajo E., Ngwa W. & Zygmanski P. (2017). A Monte Carlo study of I-125 prostate brachytherapy with gold nanoparticles: dose enhancement with simultaneous rectal dose sparing via radiation shielding. *Physics in Medicine and Biology* **62**(5): 1935–1948. DOI: <https://doi.org/10.1088/1361-6560/aa5bc7>
- Chatterjee D.K., Wolfe T., Lee J., Brown A.P., Singh P.K., Bhattarai S.R., Diagaradjane P. & Krishnan S. (2013). Convergence of nanotechnology with radiation therapy-insights and implications for clinical translation. *Translational cancer research* **2**(4): 256–268. DOI: <https://doi.org/10.3978/j.issn.2218-676X.2013.08.10>
- Common Cancer Types. National Cancer Institute. Available at <https://www.cancer.gov/types/common-cancers>
- Gray T., Mayer K., Kirby N. & Team T.G. (2019). Computational

- assessment of radiation dose enhancement and secondary electron production for variable sizes and concentrations of gold nanospheres in a tumor using MCNP6.2. APS March Meeting. Abstract id. P23.006. Available at <https://ui.adsabs.harvard.edu/abs/2019APS..MARP23006G>
- Jabbari K. (2011). Review of fast Monte Carlo codes for dose calculation in radiation therapy treatment planning. *Journal of Medical Signals and Sensors* **1**(1): 73–86.
- Jain S., Hirst D.G. & O'Sullivan J.M. (2012). Gold nanoparticles as novel agents for cancer therapy. *The British Journal of Radiology* **85**(1010): 101–113.
DOI: <https://doi.org/10.1259/bjr/59448833>
- Jangjoo A.G., Ghiasi H. & Mesbahi A. (2019). A Monte Carlo study on the radio-sensitization effect of gold nanoparticles in brachytherapy of prostate by ¹⁰³Pd seeds. *Polish Journal of Medical Physics and Engineering* **25**(2): 87–92.
DOI: <https://doi.org/10.2478/pjmpe-2019-0012>
- Kalos M.H. & Whitlock P.A. (2008). *Monte Carlo Methods*. Wiley-Blackwell, USA.
- Koivunoro H., Siiskonen T., Kotiluoto P., Auterinen I., Hippeläinen E. & Savolainen S. (2012). Accuracy of the electron transport in mcnp5 and its suitability for ionization chamber response simulations: A comparison with the EGSNRC and PENELOPE codes. *Medical Physics* **39**(3): 1335–1344.
DOI: <https://doi.org/10.1118/1.3685446>
- Koreshi Z.U. & Lewins J.D. (1990). Two-group Monte Carlo perturbation theory and applications in fixed-source problems. *Progress in Nuclear Energy* **24**(1–3): 27–38.
DOI: [https://doi.org/10.1016/0149-1970\(90\)90020-6](https://doi.org/10.1016/0149-1970(90)90020-6)
- Lechtman E., Chattopadhyay N., Cai Z., Mashouf S., Reilly R. & Pignol J.P. (2011). Implications on clinical scenario of gold nanoparticle radiosensitization in regard to photon energy, nanoparticle size, concentration and location. *Physics in Medicine and Biology* **56**(15): 4631–4647.
DOI: <https://doi.org/10.1088/0031-9155/56/15/001>
- Lechtman E., Mashouf S., Chattopadhyay N., Keller B.M., Lai P., Cai Z., Reilly R.M. & Pignol J.P. (2013). A Monte Carlo-based model of gold nanoparticle radio sensitization accounting for increased radiobiological effectiveness. *Physics in Medicine and Biology* **58**(10) 3075–3087.
DOI: <https://doi.org/10.1088/0031-9155/58/10/3075>
- Luxton G. & Jozsef G. (1999). Radial dose distribution, dose to water and dose rate constant for monoenergetic photon point sources from 10 keV to 2 MeV: EGS4 Monte Carlo model calculation. *Medical Physics* **26**(12): 2531–2538.
DOI: <https://doi.org/10.1118/1.598790>
- Mesbahi A., Jamali F. & Garehaghaji N. (2013). Effect of photon beam energy, gold nanoparticle size and concentration on the dose enhancement in radiation therapy. *BioImpacts:BI* **3**(1): 29–35.
DOI: <https://doi.org/10.5681/bi.2013.002>
- Mobit P.N., Nguyen A., Packianathan S., He R. & Yang C.C. (2016). Dosimetric comparison of brachytherapy sources for high dose-rate treatment of endometrial cancer: ¹⁹²Ir, ⁶⁰Co and an electronic brachytherapy source. *British Journal of Radiology* **89**(1059).
DOI: <https://doi.org/10.1259/bjr.20150449>
- Neves L.P., Santos W.S., Gorski R., Perini A.P., Maia A.F., Caldas L.V.E. & Orengo G. (2014). Dosimetric study of a brachytherapy treatment of esophagus with Brazilian ¹⁹²Ir sources using an anthropomorphic phantom. *Radiation Physics and Chemistry* **104**: 240–243.
DOI: <https://doi.org/10.1016/j.radphyschem.2013.11.029>
- Perez-Calatayud J., Ballester F., Das R.K., Dewerd L.A., Ibbott G.S., Meigooni A.S., Ouhib Z., Rivard M.J., Sloboda R.S. & Williamson J.F. (2012). Dose calculation for photon-emitting brachytherapy sources with average energy higher than 50 keV: Report of the AAPM and ESTRO. *Medical Physics* **39**(5): 2904–2929.
DOI: <https://doi.org/10.1118/1.3703892>
- Pisansky T.M., Gold D.G., Furutani K.M., Macdonald O.K., McLaren R.H. Mynderse L.A, Wilson T.M., Hebl J.R. & Choo R. (2008). High-dose-rate brachytherapy for localized prostate cancer. *Mayo Clinic Proceedings* **83**(12): 1364.
- Radioisotopes in Medicine. Nuclear Medicine - World Nuclear Association. Available at <http://www.world-nuclear.org/information-library/non-power-nuclear-applications/radioisotopes-research/radioisotopes-in-medicine.aspx>
- Rief H. (1984). Generalized Monte Carlo perturbation algorithms for correlated sampling and a second-order Taylor series approach. *Annals of Nuclear Energy* **11**(9):455–476.
DOI: [https://doi.org/10.1016/0306-4549\(84\)90064-1](https://doi.org/10.1016/0306-4549(84)90064-1)
- Safigholi H. & Song W.Y. (2018). Macroscopic and Microscopic dose enhancement factor (def) for tumor diffusion with gold nanoparticles (gnps) using Monte Carlo simulations: ¹⁰³ Pd, ¹²⁵ I, and electronic brachytherapy (ebt) sources. *Brachytherapy* **17**(4): S32–S33.
DOI: <https://doi.org/10.1016/j.brachy.2018.04.044>
- Salvat F., Fernández-Varea J.M. & Sempau J. (2006). PENELOPE2008: a code system for monte carlo simulation of electron and photon transport. Available at <http://www.oecd-nea.org/lists/penelope.html>
- Saw C. B. (2013). Brachytherapy: High Dose Rate (HDR) Implants. In: Encyclopedia of Radiation Oncology (L. W. Brady & T. E. Yaeger (eds.)). Springer, Berlin, Heidelberg.
DOI: https://doi.org/10.1007/978-3-540-85516-3_143
- Seco J. (2016). *Monte Carlo Techniques in Radiation Therapy*: CRC Press, USA.
- Šídlová V. & Trojek T. (2010). Testing Monte Carlo computer codes for simulations of electron transport in matter. *Applied Radiation and Isotopes* **68**(4–5): 961–964.
DOI: <https://doi.org/10.1016/j.apradiso.2009.12.019>
- Team X.-M.C. (2008). *MCNP- A General MC N-Particle Transport Code*, Version 5. 836.
- Worldwide Cancer Data. World Cancer Research Fund. American Institute for Cancer Research. Available at <https://www.wcrf.org/dietandcancer/cancer-trends/worldwide-cancer-data>
- Yu P.C., Nien H.H., Tung C.J., Lee H.Y., Lee C.C., Wu C.J. & Chao T.C. (2017). CT-based MCNPX dose calculations for gynecology brachytherapy employing a Henschke applicator. *Radiation Physics and Chemistry* **140**: 392–397.
DOI: <https://doi.org/10.1016/j.radphyschem.2017.03.044>

RESEARCH ARTICLE

Recognition of handwritten characters using deep convolution neural network

S Arivazhagan¹, M Arun^{1*} and D Rathina²

¹ Department of Electronics and Communication Engineering, Mepco Schlenk Engineering College, Sivakasi, India.

² Department of Electronics and Communication Engineering, Renganayagi Varatharaj College of Engineering, Sivakasi, India.

Submitted: 24 March 2020; Revised: 18 January 2021; Accepted: 23 April 2021


Abstract: Character recognition is a very interesting technique in the field of pattern recognition. Specifically, handwritten character recognition is gaining the attention of researchers as it is necessary for historical documents, archives, or mass digitization of hand-filled forms. The correct classification of handwritten characters is really a challenging task due to its variability in the writing styles of an individual at different times and among different individuals such as size, shape, speed of writing and thickness of characters, etc. To solve this challenging task, the features extracted from the characters should be suitable for the variability of the characters. In this research work, Deep Convolution Neural Network (DCNN) has been used instead of hand-crafted features from the handwritten characters, to automatically learn the best features for this task. The proposed DCNN framework is trained and tested on the Chars74K handwritten dataset in all the aspects of handwritten numbers and handwritten English alphabets with various training and testing proportions and various subproblems. The recognition rate for the proposed DCNN provides better results when compared with the other schemes. The recognition rates for 62 classes in the Chars74K dataset with 50:50, 70:30 and 80:20 train test ratio is 88.05 %, 89.21 % and 90.32 %, respectively.

Keywords: Character recognition, Chars74K, CNN, deep learning, handwritten characters.

INTRODUCTION

The human brain can store trillions of bytes of information. With time, the memory in human brain gets

faded, so, written information is very important for the memory retrieval process. The handwritten information is very useful in both private (letters, notes, addresses, reminders, lists, diaries, etc.) and official correspondence (bank cheques, tax forms, admission forms, historical documents, etc.). Hence, there is a dire need to digitize all these paper documents, enabling people to easily search for necessary information and get access to the important sources of knowledge written in papers. To digitize these documents, the image of handwritten text is captured using a digital camera, pre-processed, segmented into individual characters and finally are recognized by a classifier. This entire process is known as Handwritten Character Recognition (HCR), which interprets the handwritten characters in digitized form which can be used for applications such as document verification, digital library, reading bank deposit slips, cheque interpretation, data entry of application, loan, and tax forms. HCR contributes to the advancement of automation process by reducing the human work (Attigeri, 2018). In the field of Pattern Recognition, HCR is a challenging part due to its un-deterministic characteristics. The handwritten characters differ in size and style from person to person and they differ in the same person due to ageing factor. HCR is of two types depending on the handwritten input source, namely, online handwritten character recognition and offline handwritten character recognition. Online handwritten character recognition is the process of interpreting the

* Corresponding author (m_arun@outlook.com;  <https://orcid.org/0000-0002-7860-8230>)



This article is published under the Creative Commons CC-BY-ND License (<http://creativecommons.org/licenses/by-nd/4.0/>). This license permits use, distribution and reproduction, commercial and non-commercial, provided that the original work is properly cited and is not changed in anyway.

handwritten characters as it is written on the touch screen by a digital pen. Here, recognizing the characters involves finding the position of the pen tip movements and the up/down pen strokes. The information is extracted from the strokes and the structures of the handwritten character, and the character is recognized instantly. Offline character recognition is a process of interpreting the handwritten characters from the scanned image of the handwritten document. The handwritten character in the image is subjected to feature extraction based on shape, orientation, and other transformable features. The offline HCR is quite complex than the online HCR because the information of pen tip movement is not available. The only way to recognize offline handwritten images is to extract the features which are more suitable for character recognition. In this research work, we have studied the effect of Deep Convolution Neural Network (DCNN) in the field of HCR.

Many researchers have worked on character recognition for the past few decades. The performance for character recognition using the multi-layer perceptron classifier is compared with the convolutional neural network (Driss *et al.*, 2017). Handwritten digits recognition by convolutional neural networks and with traditional features extraction (Hu invariant moments, Fourier descriptors, projections histograms, horizontal cell projections, local line fitting and zoning) and classification techniques (k-NN, Mahalanobis distance and support vector machines) is done and compared (Enriquez *et al.*, 2019). A novel feature extraction method known as Deep Contextual Stroke Pooling (DCSP) has been introduced for Scene Character Recognition (Zhang *et al.*, 2018). An adaptive deep Q-learning strategy for handwritten digit recognition was proposed by Qiao *et al.* (2018). This Q-learning strategy merges the feature extracting capability of deep learning and the decision-making of reinforcement learning to form a deep belief network. A new data augmentation method and directional feature maps using CNNs have been introduced for handwritten Chinese character recognition (Qu *et al.*, 2018).

CNN architecture for outputting the arbitrary length symbol streams from the handwritten text was presented by Ptucha *et al.* (2019). A new method for combining position embeddings with residual networks (ResNets) and bidirectional long short-term memory (BiLSTM) networks for unconstrained offline handwritten word recognition was proposed by Wu *et al.* (2019). A

feature extraction technique using non-redundant Stockwell transform for handwritten digit recognition of Odia language was introduced (Dash *et al.*, 2015). Another transformed domain feature extraction using Slantlet coefficients is also proposed by the same researchers. A DIGI-Net CNN for recognizing digits, which has the ability to learn common features from three different formats (handwritten, natural images, printed font) was designed (Madakannu & Selvaraj, 2019). A shared-hidden-layer deep convolutional neural network (SHL-CNN) for image character recognition for different languages was designed (Bai *et al.*, 2014). A convolutional network for handwritten character recognition based on subspace method was designed by Gatto *et al.* (2017). A machine learning model for recognizing handwritten characters on form document based on CNN for feature extraction and support vector machines (SVM) for classification was proposed (Darmatasia, 2017). A method called DropSample, a new training method for enhancing the deep convolutional neural networks for large-scale unconstrained handwritten Chinese character recognition was introduced by Yang *et al.* (2016). Recently, Sinhala handwritten character recognition was done by convolutional neural networks (Mariyathas *et al.*, 2020). Considering the popularity of the Convolutional Neural Network, in this research work, a new DCNN architecture is proposed for recognizing the handwritten characters rather than using famous architectures like ResNet, VGGNet and GoogleNet, etc. because of their computational complexity and memory requirement. Also, the proposed architecture is a full sparse convolutional, as it does not have any fully connected layers except the output layer.

METHODOLOGY

The handwritten dataset should have diverse writing styles by numerous authors in order to design a good character recognition model. This research work used the Chars74K dataset (<http://www.ee.surrey.ac.uk/CVSSP/demos/chars74k/>) for recognizing the individual handwritten characters. This dataset has handwritten images which are drawn using a tablet PC. It consists of 3410 handwritten images, which includes 62 classes (0-9, A-Z, a-z); each class consists of 55 images. Apart from the handwritten characters, the dataset also has 7705 natural images and 62992 images of synthetic fonts used in the computer, making the total number of images in the dataset as 74000 (74K). The sample handwritten images from the Chars74K dataset are shown in the Figure 1.



Figure 1: Sample handwritten images of the chars 74K image dataset

is the pre-processing stage. The pre-processing stage in this research work is a two-step process. The first step in the pre-processing stage is the binarization, which converts the RGB image to a binary image. As it is simple to process the low-level colour, the input image is binarized by means of the Otsu algorithm (Haseena & Clara, 2017). The second process in the pre-processing stage is to get the interested portion from the dataset image. The handwritten character images in the Chars74k dataset have a wide background area more than the Region of Interest (ROI). The bounding box approach is used to extract the ROI from the handwritten character images. The excess background is removed based on the connectivity of the binary image. The image is cropped based on the bounding box and the ROI is obtained.

The block diagram of the proposed method is shown in the Figure 2. The first block in the proposed methodology

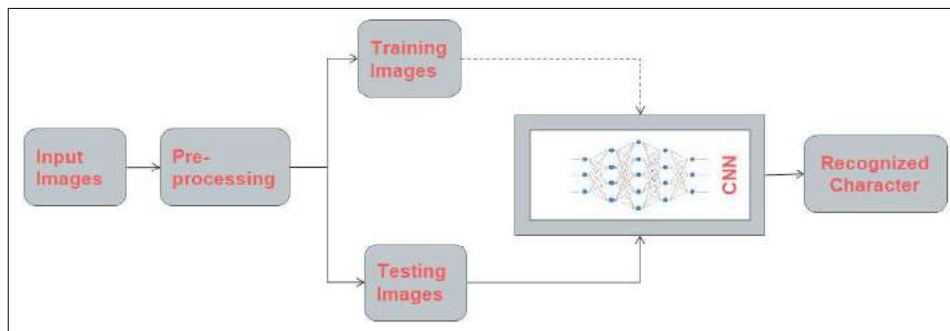


Figure 2: Block diagram of proposed methodology

After the pre-processing stage, the images were split into different train and test ratios such as 80:20, 70:30 and 50:50. Then the images are trained and tested using the proposed DCNN architecture. The proposed DCNN

architecture has seven (07) stages of consecutive hidden layers between the input layer and the fully connected layer. The architecture of the proposed DCNN is shown in Figure 3.

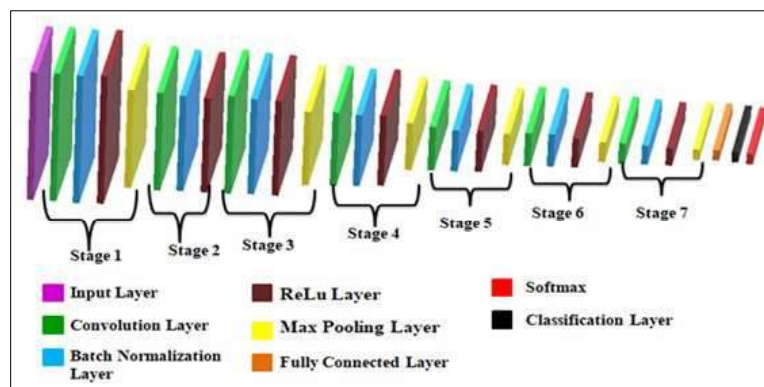


Figure 3: Architecture of proposed deep convolution neural network

The proposed DCNN architecture has 7 hidden layers, which are the convolution layers, along with batch normalization and activation functions (ReLU). Between every hidden layer, there is a pooling operation, which takes place except in the 2nd hidden layer.

Convolution layer is the heart of the CNNs. They are responsible for the automatic learning of the features from the given input image. This layer applies the filter to the input to create a feature map that encapsulates the occurrence of the detected features in the input. The filters in the neural networks are handcrafted, but the idea of CNN is to learn the filters during the training stage in the context of a specific application. The convolution operation is shown in Figure 4.

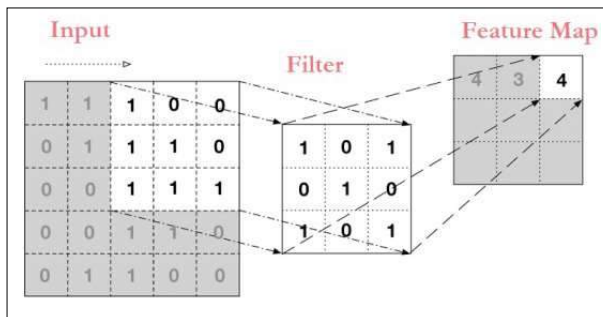


Figure 4: Convolution operation in convolution neural network

The size of the feature map after the convolution operation is given by equation 1.

$$O_f = \left\lfloor \frac{I+2P-F_c}{S} \right\rfloor + 1 \quad \dots (1)$$

where O_f is the size of the feature map, I is the size of the input to the convolution layer, P and S stands for length of the padding and stride and F_c is the size of the convolution filter.

Training deep neural networks is a challenging task. The CNN is updated layer-by-layer backward during the back propagation from the output to the input using the estimate of error that assumes the weights in the layers prior to the current layer are fixed. As all layers are getting updated simultaneously during an update, the update procedure will be trying to chase a moving target. Batch normalization is the technique to coordinate the update of multiple layers in the CNN. The

batch normalization can be applied after or before the activation function. For ReLU activation function, it is identified that batch normalization should be used before the activation function. Batch normalization provides a well-designed way of re-parameterizing any deep network. The re-parameterization drastically reduces the problem of coordinating updates across many layers. Standardizing the activations of the prior layer makes spread and distribution of inputs of the subsequent layer does not change during the weight update, at least not dramatically. This effects stabilizing and speeding-up the training process of deep neural networks.

Activation functions are really important in a Convolution Neural Network (CNN) to identify the non-linear complex functional mappings between the input and output. If the activation function has not been added, the CNN would simply be a linear regression model of polynomial function of one degree. Therefore, the hidden layers in the CNNs are added with an activation function such as tanh, ReLU or sigmoid, etc. In this research work, we have used ReLU as the activation function as it avoids and rectifies vanishing gradient problem. The only limitation of this ReLU activation function is that it can be used only in the hidden layers. Therefore, we have used Softmax activation function in the output layer as we are dealing with a multiclass classification problem.

A limitation of the feature map output of convolution layer is that the feature maps trace the accurate location of features in the input making the feature map translation variant. Therefore, small movements in the location of the feature in the input will result in a different feature map. To avoid this situation, pooling layer is introduced for down-sampling. A pooling layer is added mostly after the convolution layer. Even though more pooling operations are available, in this research work we have used Max Pooling in the DCNN. We have added 6 pooling layers between the 7 hidden layers and randomly eliminated a pooling layer between the 2nd and 3rd hidden layer.

After the sequence of 7 stages, the fully connected output layer is stacked to the DCNN. Neurons present in this layer are connected to all the activations of hidden layers in the architecture. This layer flattens the two-dimensional vectors into one-dimensional features. The final output from this layer consists of $N \times 1$ dimensions, where N denotes the number of classes. Then the decision-making action is taken by the Softmax layer. Table 1 specifies the parameters of the proposed DCNN in every layer.

Table 1: Parameters of the proposed DCNN architecture in every layer

Layer	Filter size	No. of feature maps	Input size	Output size
1-Conv	3 × 3	128	64 × 64	64 × 64
MaxPooling	2 × 2	128	64 × 64	32 × 32
2-Conv	3 × 3	128	32 × 32	32 × 32
3- Conv	3 × 3	128	32 × 32	32 × 32
MaxPooling	2 × 2	128	32 × 32	16 × 16
4-Conv	3 × 3	128	16 × 16	16 × 16
MaxPooling	2 × 2	128	16 × 16	8 × 8
5-Conv	3 × 3	128	8 × 8	8 × 8
MaxPooling	2 × 2	128	8 × 8	4 × 4
6-Conv	3 × 3	128	4 × 4	4 × 4
MaxPooling	2 × 2	128	4 × 4	2 × 2
7-Conv	3 × 3	128	2 × 2	2 × 2
MaxPooling	2 × 2	128	2 × 2	1 × 1

The training process involves the back propagation technique, which adjusts the weight value depending on the previous trained validation. The back propagation does the optimization process, which involves forward pass, loss function, background pass and weight update. The forward pass is used to interchange the input and the output values. The loss function, which is used for the optimization is mean square error (MSE) between the predicted and the target one. The backward pass is defined by the weight update value that gives the least loss measure.

RESULTS AND DISCUSSION

The entire research work was done on the Chars74K handwritten dataset using the proposed DCNN architecture, and was carried out by MATLAB R2018a software in an Intel core i5 Processor @3.2 GHz with 64 bit OS.

First the experiment was carried out for finding the optimum number of epochs. The experiment was done on the handwritten characters of the Chars74K dataset with different train and test ratios. Also, the experiment was carried out as 4 different subproblems. The first subproblem considers only the numerals of the dataset (10 class problem). The numerals 0–9 is considered

and only 550 images out of 3410 images were used. The second subproblem considers only the uppercase alphabets (A-Z), making it a 26-class problem. The third subproblem considers only the lowercase alphabets (a-z), making it as another 26-class problem. Finally, all the alphanumeric handwritten characters (0-9, A-Z, a-z) were considered, and made into a 62-class recognition problem. The experiment was carried out for 80:20, 70:30 and 50:50 train test ratios for different epochs and the recognition rates are tabulated in Table 2.

It is evident from Table 2 that 20 epochs give the best recognition rate. When the number of epochs increased, we observed the problem of overfit; also, the computational time is increased with the increase of the epochs. Therefore, further experimentation is carried out with 20 epochs. Now the experiment was done to find the optimum filter size for the convolution layer. Filter size is also an important factor for extracting the features. Most of the best features are usually local in nature, so a convolution filter capturing the local features will make sense. To get the useful feature of the image, a single filter slides all over the height and width of the image. In this research work, it is decided to keep the filter sizes common across all the seven hidden convolution layers. To find the optimum filter size, the experiment was carried out with several filter sizes such as 3×3, 5×5, 7×7, 9×9 and its recognition rate is tabulated in Table 2.

Table 2: Recognition rates for different epochs using the proposed DCNN

No. of epochs	Train test ratio (%)	Recognition rate (%)			
		Numerals (0-9)	Uppercase alphabets (A-Z)	Lowercase alphabets (A-Z)	Alphanumeric (0-9, A-Z, a-z)
20	50:50	98.52	98.72	94.02	88.05
	70:30	100	99.04	96.15	89.21
	80:20	100	97.90	93.36	90.32
50	50:50	98.52	98.01	92.88	87.69
	70:30	99.38	98.56	94.95	88.91
	80:20	70	98.95	93.71	89.15
100	50:50	97.41	98.43	93.30	87.22
	70:30	98.75	97.60	93.75	87.30
	80:20	76.36	96.85	94.41	88.56

Table 3: Recognition rates for different filter sizes using the proposed DCNN

Filter size	Train test ratio (%)	Recognition rate (%)			
		Numerals (0-9)	Uppercase alphabets (A-Z)	Lowercase alphabets (A-Z)	Alphanumeric (0-9, A-Z, a-z)
3 × 3	50–50%	98.52	98.72	94.02	88.05
	70–30%	100	99.04	96.15	89.21
	80–20%	100	97.90	93.36	90.32
5 × 5	50–50%	99.63	96.44	92.17	85.90
	70–30%	96.88	95.91	93.75	87.90
	80–20%	99.09	98.60	96.15	88.56
7 × 7	50–50%	94.81	96.44	90.17	84.11
	70–30%	100	95.67	92.55	85.08
	80–20%	100	95.45	94.06	88.71
9 × 9	50–50%	94.81	96.44	88.46	82.20
	70–30%	95	95.91	93.51	85.99
	80–20%	98.18	96.85	92.31	85.45

While using different filter sizes, the padding was adjusted so that it does not affect the dimensions of the architecture described in Table 1. For the filter sizes 3×3, 5×5, 7×7 and 9×9, the padding sizes used are 1, 2, 3, and 4, respectively. Again, the same four subproblems were carried out using different filter sizes with adjusted padding. The recognition rate for the different filter sizes for the subproblems is listed in Table 3.

It is not an easy task to pick the optimum filter size from Table 3. For an example, 5×5 filter size is better than 3×3 filter size for 50:50 train test ratio in numeral subproblem. But for other test ratios, 3×3 filter size performs better. The same was observed with lowercase alphabets also. Filter sizes 7×7 and 9×9 provided more or less comparable results among each other. But for the subproblem of recognizing the alphanumeric (62 class)

characters, without any doubt, the filter size 3×3 performs better. Therefore, it was observed that lower filter size extracts more local features than the higher filter size. In larger filter size, it was observed that weight sharing is poor compared to the smaller filter size because of the padding size. Further experiments were carried out using the filter size 3×3 .

Learning rate, learning rate schedule, L2 regularization parameter, learning rate drop factor, drop period and batch size are the parameters, which are fixed as per the values given in Table 4.

Table 4: Fixed values of the options for the proposed DCNN

S. no.	Options	Value
	Learning rate	0.001
	Learning rate schedule	piecewise
	L2 regularization parameter	0.0001
	Learn rate drop factor	0.1
	Drop period	8 epochs
	Batch size	4

Learning rate (Brownlee, 2019) is defined as the amount that the weights are updated during training. The learning rate is a tuneable parameter that has a small positive value, often in the range between 0.0 and 1.0. It is cited as a positive scalar determining the size of the step. During training phase of the DCNN, the back propagation of error estimates the amount of error for which the weights of a node in the network are responsible. Instead of updating the weight with the full amount, it is scaled by the learning rate. For example, if the learning rate is 0.001, it means that weights in the network are updated by 0.1% of the estimated weighted error whenever the weights are updated. Similarly, large weights in a DCNN lead to a more complex network that has overfitting. Penalizing the DCNN based on the size of the network weights during training can reduce overfitting, so that an L1 or L2 vector norm penalty is added to the optimization of the network to encourage smaller weights (Brownlee, 2018)

The pictorial representation of the confusion matrix for the recognition of the alpha numeric (62 classes) of the proposed DCNN with 20 epochs, 3×3 filter size, 0.001 as learning rate and 0.0001 as L2 regularization parameter is shown in Figure 5.

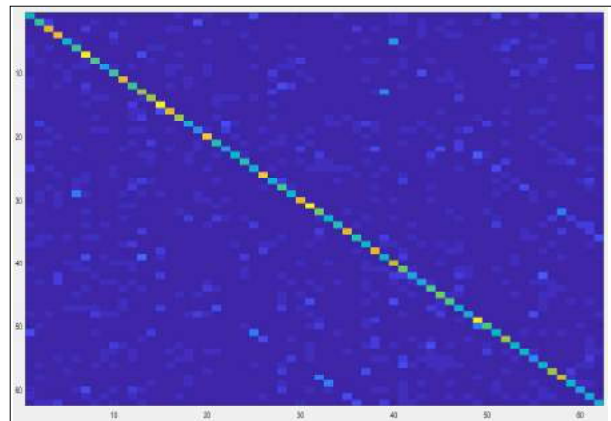


Figure 5: The pictorial plot of the confusion matrix

From the pictorial plot, it is noted that 37 % of the testing images of numeric character 0 is wrongly predicted as the uppercase alphabet ‘O’, and 14 % of the numeric character 0 is wrongly predicted as the lowercase alphabet ‘o’. Only 48 % test images of numeric character 0 is predicted as numeric zero. Another 1 % is predicted as other character than ‘O’ or ‘o’. In similar manner, only 62 % lower case alphabet ‘o’ is correctly predicted. Therefore, to resolve this problem, a different subproblem (36 class problem considering case insensitiveness in alphabets and numerals) was formulated and the training was done with the above DCNN architecture. Now, the experimentation is done in a case insensitive method and the recognition rate is tabulated in the Table 5.

Table 5: Recognition rate for the case insensitive problem using the proposed DCNN

Train test ratio (%)	Recognition rate (%)	
	Alphabets (case insensitive) + numerals (A-Z & a-z)	Alphabets (case insensitive) + numerals (A-Z & a-z, 0-9)
50:50	94.55	90.53
70:30	94.99	94.20
80:20	95.97	94.43

The recognition of the model improves when we consider case insensitiveness, as ‘O’ and ‘o’ have the same features. The system could now train wisely with

the features automatically learnt by the proposed DCNN architecture. The recognition rate of the handwritten character recognition (62 class problem) of the proposed DCNN is compared with other available methods in Table 6. The aggregation table shows that the proposed DCNN architecture performs well compared with the other schemes. From the table, we also inferred that the machine-tuned features have better recognition results than man-tuned features.

Table 6: Recognition rate comparison of state-of-art methods on the Chars74K dataset with 62 classes

State-of-art methods	Recognition rate (%)
GoogleNet (Soomro et al., 2017)	88.89
Alex Net (Soomro et al., 2017)	77.77
Multiscale HoG Features (Newell & Griffin, 2011)	80.00
ConvNet (Sundaresan & Lin, 2015)	71.69
Proposed DCNN architecture	90.32

CONCLUSION

A deep convolution neural network (DCNN) was designed for classifying handwritten characters and the proposed DCNN architecture achieved better recognition rate compared with the state-of-art methods. Detailed experimentation was conducted for tuning the parameter of the filter size and found that smaller filter size would give a better recognition rate. It was observed that the smaller filter size provides useful features, and it is computationally effective. The recognition of handwritten characters using the proposed DCNN architecture is well suitable for the Chars74K dataset. Therefore, this model can be used for digitizing bank deposit slips, cheque interpretations, and data entry of applications, loan and tax forms when combined with a good segmentation method.

Conflict of interest

The authors declare that there is no conflict of interest.

REFERENCES

- Attigeri S. (2018). Neural network based handwritten character recognition system. *International Journal of Engineering and Computer Science* 7(3): 23761–23768. DOI: <https://doi.org/10.18535/ijecs/v7i3.18>
- Bai J., Chen Z., Feng B. & Xu B. (2014). Image character recognition using deep convolutional neural network learned from different languages, *Proceedings of 2014 IEEE International Conference on Image Processing (ICIP)*, October 27–30, Paris, France, pp. 2560–2564.
- Brownlee J. (2018). Use weight regularization to reduce overfitting of deep learning models. Available at <https://machinelearningmastery.com/weight-regularization-to-reduce-overfitting-of-deep-learning-models/>
- Brownlee J. (2019). How to configure the learning rate when training deep learning neural networks. Available at <https://machinelearningmastery.com/learning-rate-for-deep-learning-neural-networks/>
- Darmatasia & Fanany M.I. (2017). Handwriting recognition on form document using convolutional neural network and support vector machines (CNN-SVM), *2017 5th International Conference on Information and Communication Technology (ICoICT)*, Malacca City, pp. 1–6. DOI: <https://doi.org/10.1109/ICoICT.2017.8074699>
- Dash K.S., Puhan N.B. & Panda G. (2015). Handwritten numeral recognition using non-redundant Stockwell transform and bio-inspired optimal zoning. *IET Image Processing* 9(10): 874–882. DOI : <https://doi.org/10.1049/iet-ipr.2015.0146>
- Driss S.B., Soua M., Kachouri R. & Akil M. (2017). A comparison study between MLP and convolutional neural network models for character recognition, *Proceedings of SPIE 10223, Real-Time Image and Video Processing 2017*: 1022306. DOI: <https://doi.org/10.1117/12.2262589>
- Enriquez E.A., Gordillo N., Bergasa L.M., Romera E. & Hu'elamo C.G. (2019). Convolutional neural network vs traditional methods for offline recognition of handwritten digits. In: *Advances in Physical Agents. WAF 2018. Advances in Intelligent Systems and Computing* (eds. R.F. Pizán, Á.G. Olaya, M.S. Lorente, J.I. Martínez, A.L. Espino), volume 855. Springer, Switzerland. DOI: https://doi.org/10.1007/978-3-319-99885-5_7
- Gatto B.B., Santos E.M. dos & Fukui K. (2017). Subspace-based convolutional network for handwritten character recognition, *2017 14th IAPR International Conference on Document Analysis and Recognition (ICDAR)*, Kyoto, Japan, pp. 1044–1049. DOI: <https://doi.org/10.1109/ICDAR.2017.173>
- Haseena M. & Clara A.R. (2017). A review on an efficient iterative thinning algorithm. *International Journal of Innovative Research in Science, Engineering and Technology* 6(11): 541–548.
- Madakannu A. & Selvaraj A. (2020). DIGI-Net: a deep convolutional neural network for multi-format digit recognition. *Neural Computing and Applications* 32: 11373–11383. DOI: <https://doi.org/10.1007/s00521-019-04632-9>
- Mariyathas J., Shanmuganathan V. & Kuhaneswaran B. (2020). Sinhala handwritten character recognition using convolutional neural network, *5th International Conference*

- on *Information Technology Research (ICITR)*, Moratuwa, Sri Lanka, pp. 1–6.
DOI: <https://doi.org/10.1109/ICITR51448.2020.9310914>
- Newell A.J. & Griffin L.D. (2011). Multiscale histogram of oriented gradient descriptors for robust character recognition, *2011 International Conference on Document Analysis and Recognition*, Beijing, China, pp. 1085–1089.
DOI: <https://doi.org/10.1109/ICDAR.2011.219>
- Ptucha R., Such F.P., Pillai S., Brockler F., Singh V. & Hutkowski P. (2019). Intelligent character recognition using fully convolutional neural networks. *Pattern Recognition* **88**: 604–613.
DOI: <https://doi.org/10.1016/j.patcog.2018.12.017>
- Qiao J., Wang G., Li W. & Chen M. (2018). An adaptive deep Q-learning strategy for handwritten digit recognition. *Neural Networks* **107**: 61–71.
DOI: <https://doi.org/10.1016/j.neunet.2018.02.010>
- Qu X., Wang W., Lu K. & Zhou J. (2018). Data augmentation and directional feature maps extraction for in-air handwritten Chinese character recognition based on convolutional neural network. *Pattern Recognition Letters* **111**: 9–15.
DOI: <https://doi.org/10.1016/j.patrec.2018.04.001>
- Soomro M., Farooq M.A. & Raza R.H. (2017). Performance evaluation of advanced deep learning architectures for offline handwritten character recognition, *2017 International Conference on Frontiers of Information Technology (FIT)*, Islamabad, Pakistan, pp. 362–367.
DOI: <https://doi.org/10.1109/FIT.2017.00071>
- Sundaresan V. & Lin J. (2015). Recognizing handwritten digits and characters. Available at http://cs231n.stanford.edu/reports/2015/pdfs/vishnu_final.pdf
- Wu X., Chen Q., You J. & Xiao Y. (2019). Unconstrained offline handwritten word recognition by position embedding integrated ResNets Model. *IEEE Signal Processing Letters* **26**(4): 597–601.
DOI: <https://doi.org/10.1109/LSP.2019.2895967>
- Yang W., Jin L., Tao D., Xie Z. & Feng Z. (2016). DropSample: a new training method to enhance deep convolutional neural networks for large-scale unconstrained handwritten Chinese character recognition. *Pattern Recognition* **58**: 190–203.
DOI: <https://doi.org/10.1016/j.patcog.2016.04.007>
- Zhang Z., Wang H., Liu S. & Xiao B. (2018). Deep contextual stroke pooling for scene character recognition. *IEEE Access* **6**: 6454–6463.
DOI: <https://doi.org/10.1109/ACCESS.2018.2817342>

RESEARCH ARTICLE

Mechanical and barrier properties of flexible packaging materials after the flexo printing process

P Balaban¹, D Viduka², V Ristic³, M Maksin⁴, V Radic⁵, R Vladislavjevic², M Vulic², M Josimovic⁶ and NZ Radivojevic^{7*}

¹ Department of Mechanical Engineering, Higher Education Technical School of Professional Studies, Novi Sad, Serbia.

² Department of Economics, Faculty of Economics and Engineering Management in Novi Sad, University Business Academy in Novi Sad, Serbia.

³ MIANU-IRASA International Research Academy of Science and Art, University Singidunum, University Metropolitan, Belgrade, Serbia.

⁴ Institute of Architecture and Urban / Spatial Planning of Serbia, University of Belgrade, Serbia.

⁵ Department of Management, College of Business Economics and Entrepreneurship, Belgrade, Serbia.

⁶ Department of Industrial Engineering/Engineering Management, Faculty of Technical Science, University of Novi Sad, Serbia.

⁷ Department of Economics, Applied Management and Entrepreneurship, Academy at Applied Studies, Kragujevac, Serbia.

Submitted: 05 November 2020; Revised: 20 April 2021; Accepted: 21 May 2021

Abstract: In the flexo printing process, flexible food packaging materials are exposed to various effects (solvents, temperature, transport devices, etc.), that impact the quality of food packaging materials. Although, literature is available on the impact of these factors on the quality of food packaging, there are very few papers examining the impact of the flexo printing process on food packaging materials. Therefore, the aim of this paper is to examine if there are any changes occurring in tensile strength, elongation before tearing and gas permeability after the flexographic printing process regarding the selected flexible packaging materials – oriented polypropylene (OPP) and coated paper/polyethylene (PAP/PE). The measurement of tensile strength and elongation before tearing was carried out according to SRPS G.S2.734, and the measurement of gas permeability according to Lussy Method - DIN 53380. The results presented in this paper show that the tensile strength and elongation in both foil samples increased after the printing process (a higher increase of strength is determined in the PAP/PE foil). The exception is the PAP/PE sample, where increased permeability of N₂ was observed. The reason for such results could be due to different surface characteristics of the tested materials since the process of ink absorption is different. Surface tension tests were conducted by applying measurements of the contact angle. The results show that the process of flexo printing did not change the functional properties of the packaging.

Keywords: Elongation before tearing, flexible packaging materials, flexo printing process, gas permeability, surface tension, tensile strength.

INTRODUCTION

For many years, flexible packaging has been the most rapidly growing segment of the packaging industry (Selke & Culter, 2016). The food industry has been the largest end-user of flexible packaging, and in 2020, it held a 70% share of the global flexible packaging market (Flexible Packaging Market, 2021). The global flexible packaging market is estimated at 31.5 million tonnes in 2021, with an annual average growth of 3.3% (Smithers, 2021).

Flexible packaging includes bags, sacks and bags of various shapes, as well as wrappers made of foil, which, when filled and closed, get a flexible shape (Ebnesajjad, 2012).

Of all flexible packaging materials, particularly polymer mono-materials and polymer-based multilayer

* Corresponding author (radivojevic034@gmail.com;  <https://orcid.org/0000-0002-6137-4431>)



This article is published under the Creative Commons CC-BY-ND License (<http://creativecommons.org/licenses/by-nd/4.0/>). This license permits use, distribution and reproduction, commercial and non-commercial, provided that the original work is properly cited and is not changed in anyway.

materials), are extensively used in the packaging industry and have a wide application in food packaging (Palić *et al.*, 2019; Żołek-Tryznowska *et al.*, 2020). The reason for that is having good properties such as low cost, low weight, tolerability with content (especially foodstuff), appropriate barrier, mechanical and optical properties, as well as suitability for processing by printing and packaging machines (Perić-Maretić *et al.*, 2004; ShaguftaIshteyaq *et al.*, 2019).

Among other characteristics of flexible packaging foils, tensile strength, elongation and permeability, are the key performance requirements and have a significant place within the general characteristics of printed packaging products made of polymeric materials (Ebnesajjad, 2013).

Barrier properties of polymers are low permeation by light, oxygen, moisture, CO₂, aroma, or fat (Desnica *et al.*, 2015). These characteristics are very important because the contact between atmospheric gases and food products can lead to biochemical or physical reactions that can affect the food quality (Fotić *et al.*, 2017). Packaging materials have different barrier properties to gases. Packaging materials are characterized by the property of porosity or permeability. Porosity is a characteristic of paper where the diffusion of gases occurs physically by the transition of molecules between the interpores of the material. Permeability is a physico-chemical process where the passage of gas molecules is done by the influence of chemical affinity or solubility. The molecules absorb on the surface of the material, then diffuse in the direction of the concentration gradient through the foil, and then desorb on the other side.

Tensile strength and elongation are important mechanical properties of foil. These parameters show the suitability of the material for manufacturing during the entire technological process (printing, lamination, packing), as well as resistance during transport, handling and storage. Insufficient strength can lead to cracking of the material and seizing production (Izdebska & Thomas, 2015). Also, just as with other thermoplastic materials, the resistance to elongation of OPP film decreases as the temperature increases (Flexographic Technical Association, 1999).

The packaging should be able to withstand the operations of further production and processing, handling, transport and distribution of food in it (Balaban-Djurđjević, 2006; Izdebska *et al.*, 2015; Marangoni *et al.*, 2020). In previous research conducted by Hertlein (1997); Rubino *et al.* (2001); Mrkić *et al.* (2007), and Siracusa (2012), it

has been found that processes of production, handling, packaging and printing can affect some characteristics of flexible packaging materials, primarily barrier properties. For example, the absorption of vapours or liquids from the environment can cause a decrease in mechanical properties (Siracusa, 2012; Sangroniz *et al.*, 2019). It has been found that the mechanical stress of the folds causes changes in the properties of the barrier, both monofilm and laminate. In general, the largest change in gas permeability with an increased stress cycle was observed in the film having a metalized layer in the structure (Hertlein, 1997; Mrkić *et al.*, 2007; Siracusa, 2012).

The main characteristics of unprinted packaging foils are more or less researched and known (Dunn, 2015), and much data on these characteristics are given by the manufacturer of packaging foils to potential buyers. The material datasheet can be a useful tool for assessing the attributes of material in a stable state (Dunno, 2017), but is usually limited in terms of material performance due to, e.g. heat treatment (Ašonja *et al.*, 2013; Han *et al.*, 2018). These and other phenomena can have a negative impact on the performance and shelf life of products packaged in this material (Dunno, 2017).

Flexographic printing is one of the most widely used procedures for printing flexible packaging today (Bolanča *et al.*, 2015). Flexo printing is a technique of direct rotary printing that uses printing plates made of rubber or photopolymer material. Printing plates are mounted on the printing cylinder and inked by the anilox that transfers fast-drying printing ink. It is possible to print on almost all substrates (absorbent and non-absorbent) (Izdebska & Thomas, 2015).

In flexographic printing, changes can occur primarily in the printing machine during the printing process, due to the direct action of machine elements, primarily printing and transport devices and solvents on the foil, or the indirect effect of energy through the medium (in the case of devices for drying printed foils) or the energy field (e.g., in the corona process) (Balaban-Đurđević, 2006; Gosh, 2015).

In addition to examining the change of the mechanical and barrier characteristics, the influence of ink acceptance on the printed material was also investigated. One of the factors that significantly affect the quality of the flexo print is wetting of the ink on the substrate, as well as wetting of the ink on ink. Factors that affect the wetting are surface tension of the ink and surface energy of the

substrate. These two factors must remain in a certain ratio in order to avoid poor ink acceptance on the substrate or the ink on the ink (Izdebska & Thomas, 2015; Aydemir *et al.*, 2020). In this paper, the calculation of the surface tension of the tested materials is performed through contact angle measurements.

In practice, as well as in the literature, the question of whether to what extent and why the stated characteristics change in the printing process is often neglected (or only assessments of a qualitative nature are given).

In order to give a solution to the issue, the aim of this study was to examine whether the mechanical and barrier characteristics of flexible packaging foils remain the same after the flexographic printing process and thus determine whether there are quantitative changes that may affect their characteristics. The samples were taken from the industrial flexo printing process.

Packaging materials that were selected for testing are in the production program of one domestic printing facility: monomaterial-oriented polypropylene (OPP) and multilayer foil-coated paper/polyethylene (PAP/PE).

METHODOLOGY

Flexo printing machine

In general, flexo printing machines consist of four aggregates, which can be with various variations. These are unwinding and rewinding devices, printing and drying devices and devices for transporting and guiding foils. Particularly, important for this work are the phases with a direct interaction between the work process and the printing material (foil) (Balaban-Đurđev, 2006). These are primarily devices for printing, transport and drying of printed foils.

The most important part of the printing machine is the device for dyeing or colour transfer. This colour transfer is done with an anilox roll that transfers a precise amount of ink onto the printing plate. The volume of the

ink transferred to the printing plate is determined by the number and size of engraved cells on the surface of the anilox roll. The doctor blades remove the excess ink.

In the process of guiding the foil strip through the printing machine, complex physical operations occur, the consequence of which is the appearance of stress and elongation of the foil. Changes in these characteristics of the foil during printing process is mostly due to the action of temperature and tensile forces, that affect the print quality or the appearance of deviations in the colour register, the length of repetition and the creation of folds in the printing foil.

The drying of printed foils has a significant impact on the quality of printing. At elevated drying temperatures (approx. 100–115 °C), changes in the properties of the foils are possible (excessive elongation of the foil can occur and thus cause the web tension to be incorrect). The possible influence on the tested characteristics of the films is due to intercooling.

Flexo printing predominantly uses solvents of the evaporation range below 100 °C. The drying time of the ink depends on the evaporation temperature of the solvent, on the speed of the foil, the heat input and the turbulence of the air. The time in which the printed ink must dry without problems occurring in the next printing device (e.g., problems with ink trapping) is measured in fractions of a second. On such a short distance between individual printing devices, approx. 80–85% of the solvent from the ink must be removed, and the remaining part is eliminated during the final drying in the channel. The materials referred to in this paper are printed on a 'flexotechnic' machine with six dyeing units and a maximum print speed of 140 m/min. The positioning of the inking unit was mechanical.

Printing machine parameters during printing are shown in Table 1. Printing was done in industrial conditions, and the machine parameters, including the anilox roller, were adjusted according to the sample that was printed because the parameters of anilox rollers

Table 1: Printing machine settings during printing

Printing machine	Speed (m/min)	Anilox rolls (lines/cm)	Ink transfer (cm ³ /m ²)	Anilox cell angle (for all colours in CMYK)	Drying effect	Printing pressure
Flexotechnic	100–140	200	5	45°	intermediate drying 30%, final drying 90%	Manually adjusted

depend on the type of the printed image. Screen ruling in this experiment was 200 L/cm, which is mostly used for printing halftone images (Izdebska & Thomas, 2015). The ink capacity of the anilox roller in the experiment was 5 cm³/m². Solvent printing flexo inks based on nitrocellulose, with a viscosity of 15–20 seconds, were used.

Printing materials

In the production of polymer films, macromolecules in a melt are arranged randomly and in a ‘relaxed’ state in all three directions, homogeneously, such as in cast or blown films. The distribution of macromolecules in a melt is always isotropic. If the film stretches at an elevated temperature in a certain direction, the macromolecules will be under tension. If such a film cools to room temperature, the stresses and positions of the macromolecules freeze, and the macromolecules are fixed in their new dimension. The dimensions of such a film are constant even if heated for a long time at an elevated temperature (Gosh, 2015).

Oriented films are obtained by stretching previously produced films in one (longitudinal) direction or in both (longitudinal and transverse) directions. This process improves the quality characteristics of the produced films. Compared to non-oriented, oriented films, which increase the tensile strength and elongation at break in the direction of stretching, more transparent and higher smoothness films are obtained, and to some extent, the barrier characteristics for gases and water vapour are improved. In biaxially oriented films, the macromolecules are stretched in the longitudinal and transverse directions (the ratios of stretching are adjustable).

In this paper, polyethylene (PE) does not appear as a monofoil but as a component of a multilayer PAP/PE foil, made by extrusion process with a slightly coated paper surface. Coating and roughness tolerances are not controlled. For the examination of the characteristics of the foils in this study, samples of unprinted foils were used followed by the examination of the printed foils.

The properties of tested OPP and PAP/PE foil were:

- Oriented polypropylene film (OPP) with a thickness of 20 μm, and unit weight of 18.20 g/m²,
- Multilayer material with a coated paper as a layer and polyethylene as an inner layer (PAP/PE) which is in contact with the product, with a thickness of 72 μm and unit weight of 69.25 g/m² (paper 47.85 g; polyethylene 21.40 g).

Surface tension

In the case of non-polar materials that include the tested polypropylene, the surface of the foil to be printed is pre-treated in order to increase the polarity of the surface. This surface treatment of the foil (mainly by the corona process through electrical discharge) achieves the effect of surface oxidation, and the existing non-polar structure is converted into polar groups (Aydemir *et al.*, 2021). This significantly improves the print quality, adhesion and chemical affinity, which are a condition for the optimal process of printing, laminating and coating (Aydemir *et al.*, 2021).

The foils tested in the study come to the printing facility after pre-processed by the corona process and therefore, not additionally processed (by the corona process) before printing.

In flexo printing houses, the usual surface tension measurement is performed using a liquid with known surface tension. The surface tension of the foil then corresponds to the surface tension of the test liquid. With this method, it is only possible to determine the interval in which the surface tension of the foil is located, which is usually 2 mN/m. Using this test, as well as the test with a special pen with a surface tension of 38 mN/m (normally used in operating conditions), it is only possible to approximately determine the surface tension.

The surface tension of solids can only be measured indirectly. The most common method is based on the measurement of the contact angle. The determination of the surface tension of solids is based on the fact that the shape of a drop of a liquid on a solid body depends on the surface tension of the materials in contact. The surface tension calculation is based on the Young-Dupre equation, where σ_s = surface free energy, σ_{sl} = interfacial tension between the liquid and solid, σ_l = surface tension of the liquid (Krüss Application Report, 2014):

$$\sigma_s = \sigma_{sl} + \sigma_l \cdot \cos\theta \quad \dots(1)$$

The contact angle θ and the surface tension of the liquid σ_l are measurable. The quantities σ_s and σ_{sl} cannot be determined experimentally. However, the surface of a solid body can be indirectly characterised by measuring or calculating the size of the contact angle. The problem is solved with the help of Fowkes’ theoretical setting, which defines the surface tension of a solid (σ_s) and a liquid (σ_l) as the sum of the dispersive (non-polar) - σ_d and polar part - σ_p :

$$\sigma_l = \sigma_l^p + \sigma_l^d \quad \dots(2)$$

$$\sigma_s = \sigma_s^p + \sigma_s^d \quad \dots(3)$$

The Owens, Wendt, Rabel and Kaelble (OWRK) is a method that uses the values of contact angle of two test liquids with a known polar and dispersive part. It is a standard method for calculating the surface free energy of a solid from the contact angle with several liquids (Aydemir *et al.*, 2019). In this way, the surface free energy is divided into polar and non-polar parts.

By combining or arranging the equations of Young, Owens, Wendt and Rabel, the equation is as follows:

$$\frac{1 + \cos\theta}{2} \cdot \frac{\sigma_l}{\sqrt{\sigma_l^d}} = \sqrt{\sigma_s^p} \cdot \sqrt{\frac{\sigma_l^p}{\sigma_l^d}} + \sqrt{\sigma_s^d} \quad \dots(4)$$

This expression represents the equation of the straight line:

$$y = ax + b \quad \dots(5)$$

Where,

$$x = \sqrt{\frac{\sigma_l - \sigma_l^d}{\sigma_l^d}} = \sqrt{\frac{\sigma_l^p}{\sigma_l^d}} \quad y = \frac{1 + \cos\theta}{2} \cdot \frac{\sigma_l}{\sqrt{\sigma_l^d}}$$

$$a = \sqrt{\sigma_s^p} \quad b = \sqrt{\sigma_s^d} \quad \dots(6)$$

If the values of the total surface tension (σ_l) and of the polar and dispersion part (σ_l^p and σ_l^d) are known for different liquids with which the test is performed, as well as the corresponding contact angles of the droplet. Then, using the above expressions, the line can be determined (by linear regression), on which the values can be read directly.

The coefficient of line a and section b is calculated according to the following equations:

$$a = \frac{\sum x_i \cdot y_i - \frac{\sum x_i \cdot \sum y_i}{n}}{\sum (x_i)^2 - \frac{(\sum x_i)^2}{n}} \quad \dots(7)$$

$$b = \frac{\sum x_i \cdot (\sum x_i \cdot y_i) - (\sum y_i) \cdot (\sum x_i^2)}{(\sum x_i)^2 - n \cdot (\sum x_i^2)} \quad \dots(8)$$

x_i, y_i - the coordinates of the points calculated for the individual test fluids according to the above equations.

According to the above equations (Owens & Wendt, 1969),

$$\sigma_s^p = a^2 \text{ (polar part)} \quad \dots(9)$$

$$\sigma_s^d = b^2 \text{ (polar part)} \quad \dots(10)$$

$$\sigma_s = \sigma_s^p + \sigma_s^d \text{ (total surface tension)} \quad \dots(11)$$

The calculation of the surface tension of the foils in this paper was performed using the sessile drop method based on the values of the measured contact angles using the DSA 25 device from Krüss with the integrated image processing (Software Zur Tropfenkonturanalyse, 2012). The principle of measuring the contact angle is based on the fact that a drop of the test liquid is dosed on the sample. The drop is recorded with a camera, and the video is analysed. Based on the mean values of five measured contact angles and known surface tension of the test liquids, the total surface tension of the films has been calculated.

Tensile strength and elongation

Tensile strength and elongation before tearing were determined by the method of SRPS G.S2.734. Both materials were tested on an Instron machine (Instron Universal Testing Instrument, Model No 4301). Samples of packaging materials were cut into dimensions 200 mm × 15 mm. The initial distance of the clamps was 100 mm, and the crosshead speed was 400 mm/min. The tensile strength is calculated according to the formula:

$$\bar{\sigma}_B = \frac{F_B}{A} \text{ [N/mm}^2\text{]} \quad \dots(12)$$

- F_B - value of the breaking force [N]
- $A = b \cdot d$ - the smallest initial cross-sectional area of the foil, mm²
- b - 15mm, foil width
- d - foil thickness, mm

The relative elongation at break (ε) is the ratio of the absolute elongation of the foil sample ($l_2 - l_1$) and its length before testing (l_1):

$$\varepsilon = \frac{l_2 - l_1}{l_1} \cdot 100 \text{ [%]} \quad \dots(13)$$

l_2 - the length of the foil sample at the moment of tearing

The values of tensile strength and elongation are expressed as the mean value of five individual measurements in both the longitudinal and transverse directions. Standard deviation and coefficient of variation are also given. In the case of combined foils, such as the tested foil PAP50 / PE20, the strength of their individual components is different. Hence the increase in strength of this film after printing is expressed with a tearing force of N/15 mm (15 mm-foil width).

Gas permeability

Measurement of gas permeability was performed by the Lussy method according to DIN 53380, on a Lyssy GPM-200 apparatus, with the corresponding Gasokuro Kogyo GC-320 gas chromatography and Hewlett-Packard 3396 A integrator (Lyssy, 1984).

Gas permeability was determined isostatically in a chamber divided by the sample of the tested packaging into two units. In a one chamber, there was pure helium, and in the other, a mixture of gases: oxygen, carbon dioxide, nitrogen (1:1:1). The pressure on both sides of the film was identical (0.2 bar). During the analysis, it gradually came to the saturation of helium, depending on the permeability of the packaging material. The concentration of measured gases in the helium chamber was detected in a chromatogram with an integrator. The retention time is given with the area under the peak, is a function of time, and it represents the amount of permeate from the mixture. The air permeability is calculated on the basis of the known constituent of individual gases in the air. The results of the obtained gas permeability are expressed in units of $\text{cm}^3 \text{ m}^{-2} \text{ d}^{-1}$ at a pressure difference of 1 bar.

RESULTS AND DISCUSSION

Surface tension

In order to calculate the surface free energy (SFE) of a solid, using the OWRK method, it is necessary to have at least two liquids with known disperse and polar parts, wherein at least one of the liquids must have a polar part greater than 0 (this choice is made in order to better determine the polar and dispersed fractions), (Kruess Application Report, 2014). The list of the most common measuring liquids can be found in (Kopczyńska & Ehrenstein, 2017).

The surface tension components of the fluids used for calculation are found in Table 2.

Table 2: The surface tension components (mN/m) of the fluids used for characterisation of the tested materials

Liquid	σ_i (mN/m)	σ_i^d (mN/m)	σ_i^p (mN/m)
Water	73.0	26.0	46.8
Ethylene glycol	47.7	26.4	21.3
1,4 – dioxane	33.0	33.0	0.0

Table 3 shows the measured contact angles and the calculated values of the total (σ) and polar (σ_p) parts of the tested materials. The surface tension of solvent-based inks (that are used for printing the tested samples) ranges from 20 to 30 mN (Aydemir *et al.*, 2021). According to some studies, the surface energy of polymeric materials should be 10 mN/m higher than the surface tension of the ink, although in some studies, this is not decisive (Aydemir *et al.*, 2021). Untreated polymeric materials have non-porous surface, hydrophobic characteristics and show a low value of surface energy and low polarity. In order to achieve adequate ink reception, the required surface energy of plastic materials on a printing press should be greater than 42 mN /m (Morsy *et al.*, 2006; Brandt, 2015). As it can be seen from the results in the table, the calculated surface tension is slightly lower than the recommended. The reason for this may be that during the storage surface, free energy decreases (Izdebska & Thomas, 2015). Therefore, corona treatment is recommended just before printing.

Table 3: Measured contact angles and surface tension of the tested materials

Specimen	PAP/PE	OPP
Contact angle	Θ [°]	Θ [°]
Water	80.5	77.2
Ethylene glycol	54.4	46.9
1,4 - dioxane	28.37	30.5
σ	33.85	35.6
σ_p	4.8	6.58

Using this method, the surface tension of the polar and non-polar parts of the test materials can be determined. The greater the similarity between liquid and solid material in terms of its polar and dispersed proportions, the better the wetting must be. In general, for good wetting, the surface free energy and its polar interactive component must be increased.

The results presented show a slightly higher polar component of the OPP sample (Kopczynska & Ehrenstein, 2017). However, in order to determine whether the cause of sorptive behaviour is energy (contact angle) or geometry (capillarity/porosity) in the examined paper sample, it would be necessary to do Washburn measurements (Zilles, 2000). It can also be seen from the results that the coated paper showed a higher value for contact angle with water, indicating that it has a hydrophobic nature. It also has a lower polar fraction value.

Tensile strength and elongation

Measurements have shown that the tensile strength and elongation before tearing of the OPP and PAP/PE foil increase after the printing process (Tables 4 and 5). When it comes to the OPP foil, the results show that this increase is 3.48% longitudinally, 5.84% transversely, and for the PAP/PE foil, the increase is 6.80% longitudinally and 8.55% transversely.

The results show a higher increase in tensile strength after printing on the PAP/PE foils compared to the OPP foils. The reason could be different surface characteristics of the tested materials and, therefore, different ink transfer. In general, ink transfer takes place in three steps: contact and wetting between the substrate and the ink, immobilisation of part of the ink layer and ink splitting (Thorman, 2018). The interaction between the ink and polymeric materials is a very complex process that depends on the physical and chemical properties of both the ink and the substrate. When applying solvent-based ink, a solid film of ink is created by evaporating the solvent at room or slightly elevated temperatures.

The combination of coating, paper/polyethylene material has a cellulose-based surface. In general, the penetration of liquids into porous materials is regulated by two main properties of the system: geometry (capillarity/ porosity) and energy (contact angle) (Zilles, 2000). It is generally accepted that liquid absorption into porous networks can depend on wetting, liquid properties and the pore structure. Namely, cellulose fibres in contact with water and cause structural change (Aydemir, 2019). The reason for the increase of the values of tensile strength and elongation could be a stronger penetration of the binder from the ink and fixation in the capillary structure of the paper part of the foil during drying, due to PAP/PE porous structure. However, due to the fact that porosity is not measured in this study additional tests should be done.

Whether the above explanation also applies to other flexible packaging materials could not be reliably assessed by this investigation. However, this may be the reason for the stated, although slightly smaller, increase in the tensile strength of the tested OPP foils.

The results of the elongation before tearing off of the foils show that the PAP/PE foils have a negligible stretching potential, longitudinally 2.65% before printing, and 2.95% after printing and transversely 9.63% before printing and 6.24% after printing. The tensile strength is higher in the longitudinal direction and the elongation in the transverse direction, which is a consequence of the orientation of the cellulose fibres in the paper.

For the OPP films, the relative elongation was 33.40% longitudinally before printing and 27.94% after printing, and transversely 121.09% before printing and 127.05% after printing. The test results obtained for oriented PP films are in accordance with the theoretical explanation of the relationship between their mechanical characteristics in the longitudinal and transverse directions. The film had a higher tensile strength in the longitudinal direction and less elongation in the transverse direction, and the same behaviour was shown after the printing process. The elongation property is especially important in polymeric films that show properties of viscoelastic behaviour (Izdebska & Thomas, 2015) because under unchanged load, the material is constantly elongated. It does not return to its original length but remains elongated. If the printed film stretches permanently after passing through the printing device due to excessive stress, e.g. in the winding device and/or due to overheating in the drying device, then, in the end, the repetition length may be longer than the format length, which can affect the print quality.

However, according to some literature sources (Schröder, 2012), more attention should be paid to the starting point of the tensile test in the measuring range of the so-called secant modulus at an elongation of 1–2%. The linear-elastic, as well as linear-viscoelastic area are especially important because it is in these areas with mild deformations (e.g., 1–2%) that the foil is loaded. For printing and packaging machines, the deformation by stretching the foil is less than 1% (Schröder, 2012).

The first assumption that the printing process, solvent, and drying temperature could cause a decrease in mechanical properties of the tested packaging material was not confirmed by these tests.

Table 4: Tensile strength and elongation of unprinted and printed OPP foils

No	Longitudinal				Transverse			
	Unprinted	Printed	Unprinted	Printed	Unprinted	Printed	Unprinted	Printed
	F_B [N]		ϵ [%]		F_B [N]		ϵ [%]	
1	74.71	82.52	32.28	31.54	36.86	43.6	126.53	129.12
2	80.92	78.36	33.28	38.70	38.04	43.9	127.56	130.16
3	83.37	84.56	32.54	47.41	42.80	40.9	119.91	105.17
4	81.48	91.78	35.34	37.42	41.22	38.6	106.78	110.08
5	84.03	81.38	33.58	29.70	39.80	43.3	124.67	150.70
\bar{x}	80.90	83.72	33.40	36.95	39.74	42.06	121.09	125.05
s	3.70	5.032	2.16	6.973	2.376	2.268	8.52	18.165
Kv [%]	4.57	6.01	6.47	18.87	5.98	5.39	7.00	14.52
$\bar{\sigma}_B$ [N/mm ²]	273.67	279.10		132.47	140.47			

Table 5: Tensile strength and elongation of unprinted and printed PAP/PE foils

No	Longitudinal				Transverse			
	Unprinted	Printed	Unprinted	Printed	Unprinted	Printed	Unprinted	Printed
	F_B [N]		ϵ [%]		F_B [N]		ϵ [%]	
1	51.83	53.70	2.54	2.66	24.33	26.56	9.13	6.92
2	54.90	59.55	2.91	2.71	25.02	26.34	9.63	5.81
3	53.25	56.68	2.57	3.00	24.36	26.07	9.55	6.24
4	50.74	56.72	2.67	2.92	24.75	28.41	9.45	5.93
5	52.26	54.25	2.59	3.47	25.45	27.12	10.38	6.32
\bar{x}	52.60	56.18	2.65	2.95	24.78	26.90	9.63	6.24
s	.57	2.33	0.15	0.11	0.447	0.99	0.46	0.43
Kv [%]	3.00	4.15	5.66	3.73	1.80	3.65	4.79	6.92

Gas permeability

The results of gas barrier characteristics of the unprinted and printed OPP and the PAP/PE foils are presented in Figures 1 and 2, respectively.

By comparing the mean measured values of the permeability of the unprinted and printed samples of OPP, a decrease in the permeability of the foils after printing was noticed. In the case of CO₂, this reduction is 9.54%, for O₂ 18.02%, for N₂ 15.03% and 16.66% for air. In the case of tested PAP/PE foils, the permeability after printing is even higher in some gases: CO₂ - permeability reduced by 47.38 %, O₂ - permeability reduced by

20.64% and air - permeability reduced by 5.93%. The measurements showed an increase in permeability only for N₂ by 5.43%.

The results obtained can be compared only with available data by Rubino *et al.* (2001) and Yahya and Khalifa (2016) (Table 6).

Research done by Rubino *et al.* (2001) concluded that permeation could be influenced by the type, but not simply by the presence of printing ink on the film, and that barrier properties imparted by the film coatings were more important in oxygen transmission than the presence or type of the ink.

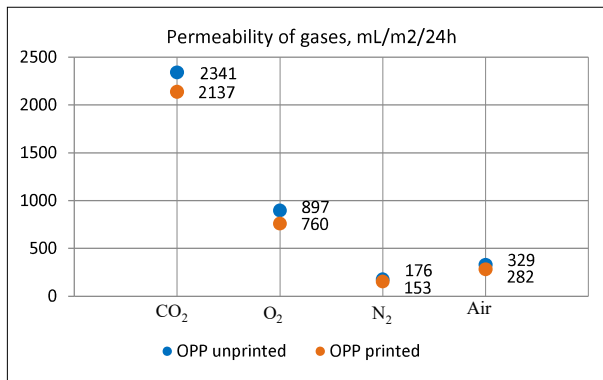


Figure 1: Gas barrier characteristics of unprinted and printed OPP foils

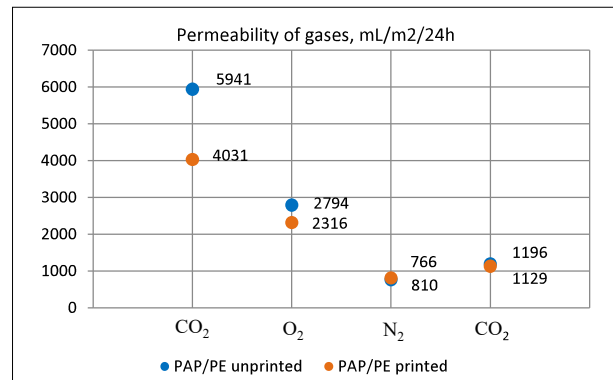


Figure 2: Gas barrier characteristics of unprinted and printed PAP/PE foils

Table 6: Comparison of research results of other authors

Authors	Material	Ink layer applica-tion	Measurement tech-nique	Results
Rubino <i>et al.</i> (2001)	1.OPP film, 25 µm 2.OPP film, 22 µm two-side coated	Laboratory condi-tions, two different inks	Oxygen Transmis-sion Rate (OTR), with Ox-Tran 2/20 analyser	On uncoated OPP film, which is printed with one type of ink, the OTR decreased. On coated OPP film, the oxygen barrier was improved.
Yahya & Kha-lifa, (2016)	BOPP film, 20 µm	Industrial condi-tions, rotogravure press	Oxygen transmis-sion rate (OTR) ac-cording to ASTM D3985	OTR increased

The explanation for a higher permeability reduction in the tested printed PAP/PE foils compared to the printed OPP foils could be similar to the increased tensile strength after printing. The material made from paper and polyethylene, due to its structure, is more susceptible to colour penetration during the drying process of the printed foil. In this process, one part of the binder from the ink penetrates into the surface structure of the foil and solidifies in it, which fills the micropores. Another part forms a layer of ink tied to the surface of the foil. Both cases could contribute to the reduction of permeability in relation to the permeability of the foil before printing, but the first case is primary for a larger decrease in permeability in the PAP/PE foil.

A research done by Bohlin (2013) on the porous structure of pigment coatings on paperboard revealed that a more porous coating structure increases ink penetration. However, to verify this statement in this

paper, measurement of porosity of the tested materials should be done.

In another research done by Aydemir *et al.* (2019), an explanation for the increase of the tested characteristics after the printing process can also be found. In this work, the surface energy on matte and glossy coated papers were examined after printing with offset printing ink. It was found that on both papers, the surface energy decreased, although more on the glossy coated papers. The reason for that was that paper fibres absorb the liquid phase of the ink (because of the capillarity action), become saturated with liquids and thus become hydrophobic, which increases the contact angle. That is, wettability decreases.

It should be emphasised that these tests are not to determine the absolute values of permeability of the tested foils and their comparison but to compare the change in permeability after the printing process.

CONCLUSION

In this paper, it has been analysed whether changes in the mechanical and barrier characteristics of the two flexible packaging materials (OPP and PAP/PE) occur after the flexographic printing process in industrial conditions. In order to get a clear idea of the interaction between the tested substrates and the ink, the surface energies of the substrates were also obtained by measuring the contact angle via the OWRK method.

In both the tested flexible materials (OPP and PAP/PE), there was an increase in tensile strength and elongation of the foils after printing. The results show a higher increase in strength after printing on PAP/PE foils compared to OPP foils. As the coated paper is more porous than the polymer foil, the reason for this could be a stronger penetration of the binder from the ink and fixation in the capillary structure of the paper part during drying. However, for further clarifications of the sorptive behaviour on porous materials, it would be necessary to make additional measurements (e.g., the capillarity and porosity).

The permeability of the foils in both foil samples decreased after printing. The reason for the higher reduction of permeability in the tested printed PAP/PE foils compared to the printed OPP foils, especially for CO₂ and O₂ gases, could be the same as for the increase in tensile strength (different surface structure of the material and consequently different ways of ink transfer during drying).

The research has shown that the printing process has an impact on changing certain characteristics of the film, but without a significant effect on the functional properties of packaging. Since the foils were tested as used in production and with tolerances given by the manufacturer, the reliability of the results after printing should be respected within these tolerances.

For more reliable results and assessment of the impact of flexo printing on the functional properties of flexible packaging materials, additional research should be done with other flexible materials and inks as well as with a defined amount of transferred inks.

REFERENCES

- Aydemir C., Altay B.N. & Akyol M. (2021). Surface analysis of polymer films for wettability and ink adhesion. *Color Research and Application* **46**: 489–499. DOI: <https://doi.org/10.1002/col.22579>
- Aydemir C., Karademir, A., Imamoglu S., Nazli Altay B., Fleming P. & Tutak D. (2019). Investigation of the evolution of hydrophobicity and wettability of paper in multi-color printing process. *Cellulose Chemistry and Technology* **53**(7–8): 787–794. DOI: <https://doi.org/0.35812/CelluloseChemTechnol.2019.53.77>
- Ašonja A., Adamović Ž. & Jevtić N. (2013). Analysis of reliability of cardan shafts based on condition diagnostics of bearing assembly in cardan joints. *Journal Metalurgia International* **18**(4): 216–221.
- Balaban-Đurđev P. (2006). Influence of flexo printing process on characteristics of polymer packaging foils. *Masters Thesis*, Faculty of Technical Sciences, University of Novi Sad, Serbia.
- Bohlin E. (2013). Surface and porous structure of pigment coatings-Interactions with flexographic ink and effects on print quality. *Dissertation*, Karlstad University Studies, Sweden.
- Bolanča S., Majnarić, I. & Golubović K. (2015) Packaging printing today. *Acta Graphica* **26**(4): 27–33.
- Brandt N. (2015). Geeignete Testmethoden zur Charakterisierung von Flexodrucksubstraten für eine verbesserte Druckfarbenhaftung und Bedruckbarkeit. *PTS-Forschungsbericht IGF 69 EBR*.
- Desnica E., Ašonja A., Mikić D. & Stojanović B. (2015). Reliability of model of bearing assembly on an agricultural of Cardan shaft. *Journal of the Balkan Tribological Association* **21**(1): 38–48.
- Dunn T. (2015). *Manufacturing Flexible Packaging*. Elsevier, Netherlands.
- Dunno K. (2017). Effects of transportation hazards on high barrier flexible packaging films. *Journal of Applied Packaging Research* **9**(1): 1–7.
- Ebnesajjad S. (2013). *Plastic Films in Food Packaging*, pp. 53. Elsevier, Netherlands. DOI: <https://doi.org/10.1016/C2012-0-00246-3>
- Flexible Packaging Market - Global Outlook and Forecast 2021–2026 (2021). Available at <https://www.arizton.com/market-reports/flexible-packaging-market-industry-report>, accessed 1 April 2021.
- Flexographic Technical Association (1999). *Flexography, Principles & Practices*, volume 1, 5th edition, pp. 19. Foundation of Flexographic Technical Association, USA.
- Fotie G., Rampazzo R., Ortenzi M.A., Checchia S., Fessas D. & Piergiovanni L. (2017). The effect of moisture on cellulose nanocrystals intended as a high gas barrier coating on flexible packaging materials. *Polymers* **9**: 415. DOI: <https://doi.org/10.3390/polym9090415>
- Gosh A. (2015). *Technology of Polymer Packaging*, pp. 47. Carl Hanser Verlag, Munich, Germany. DOI: <https://doi.org/10.3139/9781569905777>
- Han J.-W., Ruiz-Garcia L. & Qian J.P. (2018). Food packaging: a comprehensive review and future trends. *Comprehensive Reviews in Food Science and Food Safety* **17**(4): 860–877. DOI: <https://doi.org/10.1111/1541-4337.12343>
- Hertlein J. (1997). Untersuchung über Veränderung der Barriereigenschaften metallisierter Kunststofffolien

- beim maschinellen Verarbeiten. *Dissertation*. Technical University of Munich, Germany. (In German)
- Izdebska J. & Thomas S. (2015). *Printing on Polymers, Fundamentals and Applications*. Elsevier, Netherlands.
- Kopczynska A. & Ehrenstein G W. (2017). Oberflächen spannung von Kunststoffen. Messmethoden am LKT. Friedrich-Alexander-Universität Erlangen-Nürnberg. Available at <https://www.lkt.tf.fau.de/files/2017/06/Oberflaechenspannung.pdf>, accessed 5 April 2021.
- Krüss Application Report (2014). Warum Testintin nicht die ganze Wahrheit über die freie Oberflächenenergie sagen. Available at <https://www.kruss-scientific.com/de-DE/know-how/applikationsberichte/ar272-warum-testintin-nicht-die-ganze-wahrheit-ueber-die-freie-oberflaechenenergie-sagen>
- LYSSY A. (1984). *Analytical Gas Permeability Tester GPM-200, Operation Manual*, pp. 1–24.
- Izdebska J., Tryznowska Z. & Swietonski A. (2015). Correlation between plastic film properties and flexographic prints quality. *Journal of Graphic Engineering and Design* **6**(2): 19–25.
- Marangoni Junior L., De Oliveira L.M., Balardin H.D.F., Cristianini M., Padula M. & Anjos C.A.R. (2020). Influence of high-pressure processing on morphological, thermal and mechanical properties of retort and metallized flexible packaging. *Journal of Food Engineering* **273**: 109812. DOI: <https://doi.org/10.1016/j.jfoodeng.2019.109812>
- Morsy F.A., Elsayad S.Y., Bakry A. & Eid M.A. (2006). Surface properties and printability of polypropylene film treated by an air dielectric barrier discharge plasma. *Surface Coatings International Part B: Coatings Transactions* **89**: 49–55. DOI: <https://doi.org/10.1007/BF02699614>
- Mrkić S., Galić K. & Ivanković M. (2007). Effect of temperature and mechanical stress on barrier properties of polymeric films used for food packaging. *Journal of Plastic Film and Sheeting* **23**(3): 239–256. DOI: <https://doi.org/10.1177/8756087907086102>
- Owens D.K. & Wendt R.C. (1969). Estimation of the surface free energy of polymers. *Journal of Applied Polymer Science* **13**(18): 1741–1747.
- Palić N., Slavković V., Jovanović Ž., Živić F. & Grujović N. (2019). Mechanical behaviour of small load bearing structures fabricated by 3D printing. *Applied Engineering Letters* **4**(3): 88–92. DOI: <https://doi.org/10.18485/aeletters.2019.4.3.2>
- Perić-Maretić K., Bates I. & Modrić D. (2014). Comparison of colorimetric values of prints made with cyan ink on different polymer materials. *Procedia Engineering* **69**: 1556–1561. DOI: <https://doi.org/10.1016/j.proeng.2014.03.155>
- Rubino M., Tung A.M., Yada S. & Britt I.J. (2001). Permeation of oxygen, water vapor, and limonene through printed and unprinted biaxially oriented polypropylene films. *Journal of Agricultural and Food Chemistry* **49**(6): 3041–3045. DOI: <https://doi.org/10.1021/jf001427s>
- Sangroniz A., Zhu J., Tang X., Etxeberria A., Chen E.Y.X. & Sardon H. (2019). Packaging materials with desired mechanical and barrier properties and full chemical recyclability. *Nature Communications* **10**: 3559. DOI: <https://doi.org/10.1038/s41467-019-11525-x>
- Schröder K. (2012). Spezifikationen für folienverpackungen teil 4: dynamische folienprüfungen, *Inno-Letter*. Available at https://expertenecke1.rssing.com/chan-14308869/all_p1.html
- ShaguftaIshteyaq A., Asiameelam, Omm-e-hany & Syed J.M. (2019). Physical properties and biodegradable study of metallized and non-metallized polypropylene (pp) films: a comparative research. *Advances in Biotechnology & Microbiology* **12**(3): 555838. DOI: <https://doi.org/10.19080/AIBM.2019.12.555838>
- Selke E.M.S. & Culter J. (2016). *Plastics Packaging*, 3rd edition, Hanser Publishers, Munich, Germany.
- Siracusa V. (2012). Food packaging permeability behaviour: a report. *International Journal of Polymer Science* **2012**: 30202. DOI: <https://doi.org/10.1155/2012/302029>
- Smithers (2021). Flexible packaging market to grow at 3.4% across 2021–2026. Available at <https://www.smithers.com/resources/2021/feb/flexible-packaging-market-grow-3-4-to-2026>, accessed 2 April 2021.
- Software zur Tropfenkonturanalyse (2012). Benutzerhandbuch Teil 1 u. 2, Krüss GmbH, Hamburg, Germany. (in German)
- Thorman S. (2018). Where did the ink go? The effect of liquid absorption on ink distribution in flexography. *PhD thesis*, Karlstad University Studies, Sweden. DOI: <https://doi.org/10.31803/tg-20190226231838>
- Yahya I. & Khalifa M. (2016). Effect of the printing remedies and lamination techniques on barrier properties ‘WVTR and OTR value’ for polypropylene film. *EC Nutrition* **5**(2): 1089–1099.
- Zilles J.U. (2000). Wettabilities and surface tensions of different paper types. *KRÜSS Application/Technical Notes* **2001**: 1–6.
- Żolek-Tryznowska Z., Rombel M., Petriaszwili G., Dedijer S. & Kašiković N. (2020). Influence of Some Flexographic Printing Process Conditions on the Optical Density and Tonal Value Increase of Overprinted Plastic Films. *Coatings* **10**: 816. DOI: <https://doi.org/10.3390/coatings10090816>

RESEARCH ARTICLE

Effect of priming with neem seed extract on seeds of four traditional rice varieties of Sri Lanka; Kaluheenati, Kurulurthuda, Madathawalu and Maa-wee

MO Galappaththi*, KMGG Jayasuriya and NS Gama-Arachchige

Department of Botany, Faculty of Science, University of Peradeniya, Peradeniya.

Submitted: 14 December 2020; Revised: 20 April 2021; Accepted: 25 June 2021

Abstract: With the concern for environmentally friendly agriculture, demand for traditional rice varieties in Sri Lanka has been increased. Farmers claim that the seed germination in traditional rice varieties in Sri Lanka is remarkably low. Considering the reported benefits of neem in enhancing the germination, priming of rice seeds with distilled water and neem seed extracts (100, 50 and 25% strength) for 0, 24, 48, and 72 hours was used to enhance the performances in seed germination of four selected traditional rice varieties. Primed seeds were dried under ambient conditions until initial weight was achieved. Seed germination was tested at ambient laboratory conditions (~27 °C). Seed vigour was evaluated by measuring the root, and shoot lengths and seedling emergence in glasshouse conditions. Four replicates of 100 seeds were used in each treatment. Arcsine transformed data were analysed using one-way ANOVA. Germination percentages of un-primed seeds of Kaluheenati, Kurulurthuda, Maa-wee and Madathawalu were 62, 32, 24, and 20%, respectively, while seedling emergence of the same were 65, 10, 12 and 40%, respectively. Half strength neem priming (50%) for 24 hours and 24 hours pre-soaking significantly improved seed germination (83%) and seedling emergence (83%) of Kaluheenati, while quarter strength neem priming for 72 hours and 24 hours pre-soaking improved germination (64%) and seedling emergence (25%) of Kurulurthuda. Quarter strength neem priming for 48 hours, and 48 hours pre-soaking was effective in improving the germination (49%) and seedling emergence (30%) of Maa-wee, while priming with 100% neem extract for 72 hours and 48 hours pre-soaking improved the germination (55%) and seedling emergence (53%) of Madathawalu. Root and shoot lengths were higher in seedlings of neem primed seeds. Thus, priming with neem seed extracts can be recommended to

improve the performance in seed germination of studied rice varieties.

Keywords: Germination, neem priming, seed vigour.

INTRODUCTION

Rice is one of the most important staple foods in the world. Nevertheless, more than 90% of the world's rice is grown and consumed by Asian people (IRRI, 2020). As 60% of the world's population lives in Asia, rice could be considered as the world's most important food. Rice provides 50% of the dietary calorie supply for ~5 billion Asians (Muthayya *et al.*, 2014). Rice is cultivated in every continent except in Antarctica (Muthayya *et al.*, 2014). Moreover, rice is planted on about 148 million hectares annually, or on 11% of the world's cultivated land (Khush, 1997). Annually > 715 million tons of paddy rice is produced globally (FAO, 2013) showing its significance as a global crop. In Sri Lanka, rice was grown in 1,040,954 ha of land in the year 2018, while the production was 3,929,831 tons. However, only 1.22% of the rice grown lands has been devoted to produce traditional rice varieties of Sri Lanka (Department of Agriculture, 2019).

Traditional rice varieties that have been used by Sri Lankan farmers are with low yields. Thus, rice improvement programs in Sri Lanka have attempted to

* Corresponding author (mogalappaththi91@gmail.com;  <https://orcid.org/0000-0002-6640-5284>)



This article is published under the Creative Commons CC-BY-ND License (<http://creativecommons.org/licenses/by-nd/4.0/>). This license permits use, distribution and reproduction, commercial and non-commercial, provided that the original work is properly cited and is not changed in anyway.

develop new rice varieties with higher yields. Most of these new varieties heavily dependent on agrochemicals (Rajapakse *et al.*, 2000). Nevertheless, the introduction of these new rice varieties caused the extinction of many traditional rice varieties from the field (Rajapakse *et al.*, 2000; Kennedy & Burlingame, 2003). Usage of extensive levels of agrochemicals is a significant problem as it has created many health and ecological problems. Most agrochemicals used in rice cultivation are not environmentally friendly (Bambaradeniya & Amarasinghe, 2003). These agrochemicals cause many human health problems (Weeraratne, 1983; Bandara *et al.*, 2008; 2010; Jayasumana *et al.*, 2014). Especially, with the emergence of chronic kidney disease with unknown aetiology, a new debate has been initiated in the country on the use of agrochemicals.

In the light of the current debate on health issues, organic farming, as well as traditional rice varieties were promoted as many of the traditional rice varieties are claimed to have health benefits (Dharmasena, 2010). Traditional rice varieties contain variety of chemicals with antioxidant properties. Thus, consumption of traditional rice varieties gives health benefits such as reducing the risk of non-infective diseases (Samaranayake *et al.*, 2017). Therefore currently, these traditional varieties have a good market value especially if they were produced organically (Wickramasinghe & Noda, 2008; Suriyagoda *et al.*, 2011).

However, low germinability and storability of seeds of the traditional rice varieties is a drawback in popularizing these varieties (*Personal communication with the organic farming community*). Thus, the current research was initiated on the request of the organic farming community to address the low germinability and storability issue of traditional rice varieties of Sri Lanka. In the current study, effect of priming on seed quality of four traditional rice varieties; Maa-wee, Kaluheenati, Kuruluthuda and Madthawalu were studied. No information was available on the improvement of seed quality of these rice varieties in scientific literature. However, few studies were conducted to reveal the medicinal (Samaranayake *et al.*, 2017) and physical (Ranawake *et al.*, 2013; Rebeira *et al.*, 2014) properties of these rice varieties.

Seed priming was used in this research to improve the seed quality of the selected species. Seed priming is a controlled hydration of seeds to initiate the molecular level process towards germination. Hydration is ceased prior to radicle emergence (Bradford & Bewley, 2002). Priming improves seed performance specially under stress conditions, inducing the rapid establishment of

vigorous rice seedlings (Tilahun *et al.*, 2013). Moreover, it improves the germination rate, growth of seedlings, and reduces the time to start germination (Drew & Dearman, 1993). Several seed priming methods are used to improve seed quality (Nawaz *et al.*, 2013); hydro-priming (use of water), osmopriming (use of solutions with low osmotic potentials), matrix priming (use of solid matrix; Harris *et al.*, 2002), nutrient priming (use of solutions with micronutrients; Johnson *et al.*, 2005) and hormonal priming (use of solutions with plant growth regulators; Ghobadi *et al.*, 2012).

Neem has been used as pesticide and as a treatment for many fungal and bacterial diseases in crops (Girish & Bhat, 2008). Isolated chemicals as well as neem seed extract have shown antibacterial (Coventry & Allan, 2001; Biswas *et al.*, 2002), antifungal (Achimu & Schlosser, 1992; Coventry & Allan, 2001; Biswas *et al.*, 2002; Wang *et al.*, 2010) and anti-viral (Biswas *et al.*, 2002) properties. Further, neem seed extract has been reported to have significant antioxidant activity (Nahak & Sahu, 2011; Revathi & Thambidurai, 2019). Free radicle damage and pathogenic effects are the main factors reducing quality of seeds during storage (Copeland and McDonald, 2001). Thus, we hypothesized that antimicrobial and antioxidant effects of neem seed extract would improve the seed quality of traditional rice seeds. Furthermore, if neem seed extract is effective in improving seed quality it could be used as an organic treatment. Thus, the main objective of our study was to improve the seed quality of four selected traditional rice varieties in Sri Lanka with priming treatments using different concentrations of commercially available neem seed extract.

Four traditional rice varieties were used for the study. Three varieties (Madathawalu, Kaluhenati and Kuruluthuda) are cultivated in both Yala and Maha seasons whilst the other variety (Maa-Wee) is grown only in the Maha season (Ginigaddara, 2018). Kaluhenati and Madathawalu take 3 ½ months from sowing to harvest, while Kuruluthuda takes 4 months. In contrast, Maa-Wee require 5-6 months to get mature. Generally, Maa-Wee have a strong root system and healthy tillers. It is popular in Ratnapura, Kalutara, Galle, Matara and Gampaha districts (*Personal communications with farmers*). Madathawalu is suitable for muddy rice fields and cultivated in all districts. However, this variety is recommended by the Department of Agriculture for acidic soils. Kuruluthuda is better for flooded and high saline fields. Kaluhenati is suitable for puddled muddy lands and perform well in dry zone conditions (Ginigaddara, 2018).

METHODOLOGY

Seed materials

Seeds of the four studied rice varieties were obtained from HELA SAHAL Ayurvedic Seed Suppliers Pvt. Ltd., Kottawa, Sri Lanka on 4th of January 2017. Seeds were stored in polysac bags (710 × 480 mm² with 60 GSM thicknesses) until used for experiments. Seeds were from Maha cultivation season (cultivation season from September to March) 2016/2017 and were stored for only < 2 weeks by the supplier under ambient temperature conditions in gunny bags. Visually healthy seeds were selected for the field and laboratory experiments. Experiments were initiated within a week from the date of purchase. Field and laboratory experiments were conducted in the Department of Botany, University of Peradeniya. Experiments were initiated within 3 months from 6 January 2017 to April 2017.

Initial information for seed priming

Seed moisture content

Ten replicates of 10 seeds each from each variety were taken randomly and the seed samples were crushed separately using motor and pestle. Fresh weights of these crushed samples were measured using an analytical balance to the nearest 0.0001 g and were oven dried at 121°C for 3 h. Seed samples were reweighed, and moisture content was calculated in fresh mass basis (Fischer, 2007).

Imbibition of seeds

This experiment was conducted to evaluate the imbibition pattern of seeds to determine the suitable priming time. Four replicates of 20 seeds from each variety were weighed using a digital chemical balance to nearest 0.001 g. The seed samples were immersed in 30 ml of distilled water in beakers with aluminium foil lids and incubated at 25 °C. Seed samples were retrieved after 2, 4, 6, 8, 24, 48 and 72 h, surface blotted, reweighed and returned to the beakers. Imbibition curves were prepared.

Initial seed germination

Three samples containing three replicates of twenty seeds from each rice variety was taken randomly and incubated on tissue papers moistened with distilled water in 9 cm diameter Petri dish. One samples of each variety were

incubated at 25 °C in a temperature-controlled incubator [Model- MGC- 450BP, Company- Qualitron (Pvt) Ltd., Rajagiriya], at 35 °C in a temperature-controlled incubator [Model- MGC- 250P, Company- Qualitron (Pvt) Ltd., Rajagiriya] and the other at the ambient room temperature conditions. Samples were watered every day with distilled water and germinated seeds were counted for two weeks. Germination rate and the percentage were calculated.

Effect of seed priming on seed quality

Hydro-priming

Four replicates of 100 seeds from each variety were used for each priming treatment. Seed samples were weighed and immersed in 100 mL of distilled water in a 250 mL beaker. Seed samples were kept in distilled water for 0, 24, 48 and 72 h separately and were retrieved and reweighed. Then the seed samples were air dried until they came to their initial weight.

After the priming treatments, the vigour of the primed seeds was determined using the seedling growth test. Further, seed germination under laboratory conditions and seedling emergence under plant house conditions in rice field soils were studied after four pre-soaking treatments, i.e., 0 (no soaking), 24, 48 and 72 h soaking in distilled water as practiced by the traditional farmers.

Seed germination under the laboratory conditions

Hydro primed seed samples (from each priming treatment) and a non-primed sample from each species were incubated on manila papers moistened with distilled water. Manila papers with seeds were rolled and kept for germination under room temperature. Seeds were observed for germination after 7 d. The same experiment was conducted at 25 and 35 °C in temperature-controlled incubators.

Seed vigour test

Seed vigour of the primed seed samples were determined using the seedling growth criteria (Hampton & TeKrony, 1995). Twenty-five seedlings from each replicate of each sample mentioned above were selected randomly and were placed on a black coloured cloth and photographed. Root length and shoot length of the seedlings were measured using the images with the aid of Image J software.

Seedling emergence under the plant house conditions

Four replicates containing 100 primed (from each priming treatments separately) and non-primed seed samples of each species were pre-soaked in distilled water as explained above and incubated on moistened paddy field soil in separate 30 × 45 cm² plastic trays at ambient plant house temperature conditions. Trays were watered every day for 7 d. Emerged seedlings were counted after 7 d. This experiment was conducted using only the best distilled water priming treatment and the best neem priming treatment as identified from seed germination and from seed vigour tests. Thus, the experiment was initiated two weeks after the initiation of the seed germination and seed vigour tests.

Seed priming with neem seed extract

Commercially available neem seed extract (Kohomba Saraya, 322/7, Negombo road, Kurunegala) was used, as neem seeds were not available at the time of initiation of the experiment. This commercially available neem seed extract is 100% natural as verified by the producers. According to the producer, neem seed extract has been prepared by crushing 5 kg of neem seeds and mixing with 10 L of water. This mixture has been kept overnight (12 h) and filtered. The filtrate was made up to 100 L by adding water.

Three samples containing four replicates with 100 seeds in each were selected randomly from each study rice variety and weighed with a digital chemical balance to the nearest 0.001 g. Seed samples were immersed in 100 mL of three different neem extract concentrations prepared (50 mL of neem solution mixed with 1 L of distilled water - full strength, 25 mL of neem solution mixed with 1 L of distilled water - half strength and 12.5 mL of neem solution mixed with 1 L of distilled water - quarter strength) from the commercially available neem seed solution.

Seed samples were allowed to imbibe neem solutions for 24, 48 and 72 h, after which seed samples were reweighed and air-dried until they came to their initial weight. Neem primed seeds samples were subjected to pre-soaking treatments as mentioned in hydro-priming. Then, seed germination at laboratory conditions, seed vigour, and seedling emergence under plant house conditions were studied as explained above. Different treatment combinations of priming and pre-soaking are depicted in figure 1.

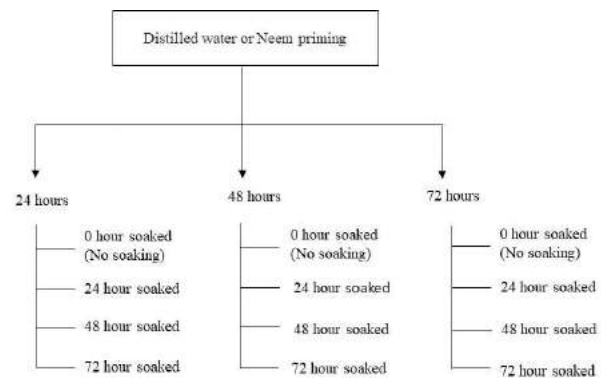


Figure 1: Flow diagram depicting different hydro-priming and Neem-priming treatments and different pre-soaking treatments conducted in the research

Analysis of data

Arc-sine transformed germination percentage data, shoot and root length data and conductivity data were analysed using one-way and two-way ANOVA procedures. All the data were statistically analysed using Minitab 17 statistical software. All the graphs were drawn for non-transformed data using Sigma Plot 10.0 software.

RESULTS AND DISCUSSION

Initial information for seed priming

Seed moisture

Dry weights of studied rice varieties were between 1.72–2.33 g. Seed moisture contents of four traditional rice varieties were between 13–15% (Table 1).

Table 1: Average (\pm SD: standard deviation) seed moisture content of the four rice varieties studied

Variety	Moisture content (%)
Maa-wee	13.7 \pm 0.6
Kaluheenati	13.8 \pm 0.8
Kuruluthuda	14.6 \pm 1.7
Madathawalu	14.5 \pm 1.3

Imbibition of seeds

Seeds of all the rice varieties increased in mass during the imbibition (Figure 2). Even after 72 hours of imbibition none of the seeds of different varieties reached the lag phase of seed germination.

Seed germination

Seeds with Kaluheenati germinated to ~ 80% at 25 °C and at ambient laboratory temperature conditions (Figure 3). Seeds of Madathawalu, Kuruluthuda and Maa-Wee germinated to ~60, 70 and 50%, respectively at these temperatures. However, at 35 °C, seeds of all the tested varieties germinated to < 20%.

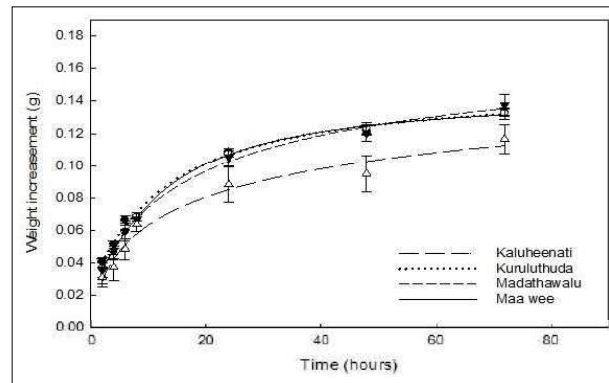


Figure 2: Variations of the seed weigh of rice varieties studied during imbibition with distilled water at ambient temperature conditions. Error bars \pm SD

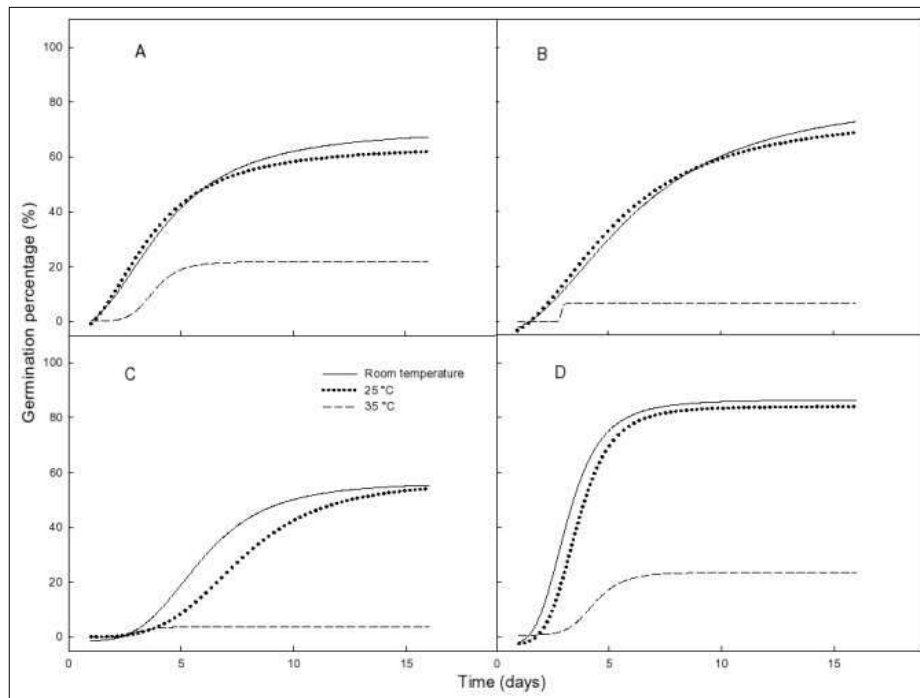


Figure 3: Cumulative germination of Madathawalu (A); Kuruluthuda (B); Maa-wee (C); and Kaluheenati (D) seeds at different temperature regimes (ambient laboratory temperature, and at 25 and 35 °C). Logistic 4-parameter curves were fitted to the germination percentage data to prepare the cumulative germination curves

Seeds of these four rice varieties, except Kaluheenati, had germination percentage <70% within 7 days at all the temperatures tested. The remaining seeds were soft and rotted within a short period. Low initial germination indicated that the initial quality of seeds of these four

varieties was low. Further, observed low germination percentages of seeds in studied varieties confirmed the claims of the traditional rice-growing farmers that seeds of traditional varieties had lower germinability. Even though the seeds were stored < 2 weeks by the supplier

and <1 week prior to the initiation of the experiments, seeds of Kuruluthuda, Maa-wee and Madathawalu had lost the germinability. Moreover, according to the results, seeds of all the varieties had low germination at 35 °C and thus we concluded that 35 °C is not favourable for seed germination of the traditional rice varieties that were tested. However, it is strange to see thermo-inhibition of rice germination at a temperature like 35 °C, as rice is a crop mainly cultivated in the tropical-subtropical regions of the world (Krishnan *et al.*, 2011). Several researchers have shown that the temperature requirement of rice seeds for germination depends on the rice variety (Tanida, 1996; Krishnan *et al.*, 2011).

Preliminary imbibition experiments showed that seeds of all the studied rice varieties would not have attained the lag phase (Bewley, 1997) of seed germination within 72 hours of the study period. Thus, we used seed priming treatments 24-, 48- and 72-hours duration in all the priming experiments conducted during the research.

Effect of priming on the quality of seeds of the study varieties

Seed germination at laboratory conditions

Kaluheenati: Non-primed Kaluheenati seeds germinated to 63% within 7 days, while most of the priming treatments

improved the germination percentage. However, the significantly highest germination percentage was observed in seeds primed for 24 hours with distilled water subjected to 24 hours pre-soaking treatment (86%) and 24 hours priming with a half strength of neem extract subjected to 24 hours pre-soaking treatment (85%, $F = 5.6$, $p < 0.01$, Table 2).

Kuruluthuda: Non-primed Kuruluthuda seeds reached only 32% cumulative germination within 7 days. However, significantly higher germination percentage was observed after 72 hours priming of seeds in distilled water followed with no pre-soaking treatment (55%), 72 hours priming of seed in half strength neem extract with no pre-soaking treatment (57%), 72 hours priming of seed in half strength neem extract followed by 48 hours soaking treatment (56%) and 72 hours priming of seed in quarter strength neem extract followed by 24 hours soaking treatment (64%, $F = 7.31$, $p < 0.01$; Table 2).

Maa-wee: Germination percentage of Maa-wee (unprimed 25% within 7 days) has significantly increased by many priming treatments. The highest germination was recorded after priming with quarter strength neem extract for 48 hours + 48 hours soaking (49%) (Table 2). Germination percentage after these priming treatments are significantly higher than the control ($F = 11.4$, $p < 0.01$).

Table 2: Average (\pm SD) germination percentage of Kaluheenati, Kuruluthuda, Maa-wee and Madathawalu seeds after different priming treatments. Germination percentage in bold are significantly different from the germination percentage of the control

Treatment	Average (\pm SD) of germination percentage			
	Kaluheenati	Kuruluthuda	Maa-wee	Madathawalu
no prime (no soak)	62.5 \pm 1.4	32.4 \pm 1.5	24.5 \pm 2.9	20.0 \pm 0.4
dw-24-0	72.3 \pm 1.7	50.0 \pm 0.8	22.2 \pm 2.2	37.2 \pm 1.3
dw-24-24	74.5 \pm 1.2	50.2 \pm 0.6	19.0 \pm 1.4	33.5 \pm 1.6
dw-24-48	79.8 \pm 1.9	50.1 \pm 3.2	24.5 \pm 2.7	37.2 \pm 2.5
dw-24-72	84.8 \pm 1.6	50.3 \pm 3.0	28.5 \pm 1.5	34.7 \pm 0.7
dw-48-0	75.8 \pm 1.3	50.0 \pm 1.8	29.5 \pm 3.0	46.2 \pm 2.7
dw-48-24	76.8 \pm 0.9	38.0 \pm 2.7	19.7 \pm 2.2	45.7 \pm 3.2
dw-48-48	79.3 \pm 1.2	50.5 \pm 1.4	25.2 \pm 3.3	54.2 \pm 2.0
dw-48-72	78.0 \pm 0.7	51.0 \pm 1.5	24.0 \pm 3.3	45.7 \pm 5.2
dw-72-0	77.8 \pm 3.1	55.5 \pm 1.1	27.5 \pm 2.6	42.5 \pm 2.1
dw-72-24	79.2 \pm 1.0	50.0 \pm 1.0	23.7 \pm 1.6	43.7 \pm 3.3
dw-72-48	78.3 \pm 1.5	49.0 \pm 1.2	32.5 \pm 3.2	41.7 \pm 2.4
dw-72-72	77.0 \pm 1.3	50.0 \pm 1.3	40.5 \pm 2.9	47.3 \pm 3.0

Continued on page 531 -

- Continued from page 530

Treatment	Average (\pm SD) of germination percentage			
	Kaluheenati	Kuruluthuda	Maa-wee	Madathawalu
neem 1-24-24	81.8 \pm 2.5	43.7 \pm 1.1	30.7 \pm 1.3	39.5 \pm 1.7
neem 1-24-48	79.5 \pm 0.9	46.7 \pm 2.0	28.7 \pm 2.5	41.5 \pm 1.1
neem 1-24-72	81.0 \pm 2.1	47.5 \pm 1.1	30.0 \pm 3.8	44.7 \pm 2.0
neem 1-48-0	81.5 \pm 1.9	49.5 \pm 2.1	28.5 \pm 2.1	42.0 \pm 1.4
neem 1-48-24	83.8 \pm 1.0	49.0 \pm 2.1	34.0 \pm 3.1	40.0 \pm 2.2
neem 1-48-48	81.5 \pm 2.5	51.0 \pm 2.7	28.7 \pm 2.2	38.5 \pm 5.3
neem 1-48-72	78.0 \pm 1.6	45.3 \pm 2.6	33.2 \pm 1.3	39.2 \pm 1.4
neem 1-72-0	81.3 \pm 1.4	43.0 \pm 2.7	30.2 \pm 3.8	38.2 \pm 3.1
neem 1-72-24	81.3 \pm 2.5	44.5 \pm 1.3	31.7 \pm 2.5	39.6 \pm 3.8
neem 1-72-48	78.8 \pm 1.7	46.5 \pm 1.4	28.0 \pm 2.0	55.0 \pm 2.6
neem 1-72-72	76.5 \pm 2.1	45.0 \pm 2.0	37.7 \pm 2.6	39.2 \pm 3.1
neem 1/2-24-0	79.8 \pm 2.3	48.5 \pm 1.7	35.2 \pm 2.5	45.5 \pm 2.0
neem 1/2-24-24	85.5 \pm 2.2	45.0 \pm 2.4	40.7 \pm 2.4	43.0 \pm 3.1
neem 1/2-24-48	79.3 \pm 1.1	45.7 \pm 1.3	32.7 \pm 1.6	39.9 \pm 0.6
neem 1/2-24-72	78.9 \pm 1.4	43.5 \pm 2.6	38.2 \pm 1.7	41.3 \pm 1.2
neem 1/2-48-0	79.0 \pm 2.5	52.7 \pm 1.3	23.7 \pm 1.4	47.7 \pm 2.8
neem 1/2-48-24	83.3 \pm 0.4	45.7 \pm 2.7	20.5 \pm 2.0	39.2 \pm 2.2
neem 1/2-48-48	78.0 \pm 2.4	51.0 \pm 2.2	21.0 \pm 1.5	42.5 \pm 0.2
neem 1/2-48-72	74.4 \pm 0.9	52.7 \pm 1.8	28.0 \pm 2.2	45.2 \pm 2.2
neem 1/2-72-0	74.0 \pm 0.5	56.5 \pm 2.7	36.0 \pm 0.9	37.7 \pm 2.1
neem 1/2-72-24	77.5 \pm 1.0	50.5 \pm 3.4	34.0 \pm 2.5	37.2 \pm 1.6
neem 1/2-72-48	76.3 \pm 1.9	55.7 \pm 1.4	38.0 \pm 1.6	39.0 \pm 0.9
neem 1/2-72-72	76.8 \pm 1.3	52.0 \pm 0.9	40.5 \pm 2.7	39.3 \pm 2.2
neem 1/4-24-0	76.7 \pm 2.2	50.2 \pm 1.0	40.2 \pm 1.8	39.5 \pm 2.2
neem 1/4-24-24	80.7 \pm 0.6	47.7 \pm 1.4	41.2 \pm 1.7	35.5 \pm 3.2
neem 1/4-24-48	74.4 \pm 2.4	46.0 \pm 3.3	40.7 \pm 2.6	37.5 \pm 4.3
neem 1/4-24-72	75.0 \pm 1.4	48.7 \pm 4.0	37.5 \pm 2.1	37.2 \pm 3.3
neem 1/4-48-0	79.0 \pm 2.7	48.2 \pm 1.7	44.5 \pm 1.8	38.5 \pm 1.6
neem 1/4-48-24	78.5 \pm 1.3	47.0 \pm 2.1	44.7 \pm 0.7	36.7 \pm 2.2
neem 1/4-48-48	76.1 \pm 1.7	49.0 \pm 1.0	48.7 \pm 1.8	38.7 \pm 0.6
neem 1/4-48-72	74.7 \pm 2.4	49.2 \pm 1.3	40.0 \pm 1.2	39.0 \pm 1.5
neem 1/4-72-0	73.9 \pm 0.8	45.0 \pm 1.9	36.5 \pm 1.5	39.9 \pm 2.0
neem 1/4-72-24	75.5 \pm 1.7	63.7 \pm 3.9	37.5 \pm 1.5	43.0 \pm 2.7
neem 1/4-72-48	70.3 \pm 1.7	57.0 \pm 2.4	35.7 \pm 1.8	40.7 \pm 0.8
neem 1/4-72-72	72.5 \pm 1.2	51.0 \pm 1.4	41.7 \pm 2.5	39.7 \pm 2.2

*Treatment = priming agent-priming time (h)-pre-soaking time (h). dw = distilled water. neem 1, 1/2, 1/4 = neem extract full strength, half strength, quarter strength

Madathawalu: Cumulative germination of non-primed Madathawalu seeds (20% within 7 days) was improved by all the priming treatments (Table 2). However, significantly higher cumulative germination percentage

was observed in seeds after priming with full strength Neem extract for 72 hours + 48 hours soaking (55%) and priming with distilled water for 48 hours + 48 hours soaking (54%). (F = 3.85, p < 0.01).

Seed vigour of primed seeds

Kaluheenati: Root length (121.3 mm) of the seedlings developed from seeds primed in ½ strength neem extract for 24 hours + 24 hours soaking were higher than those developed from non-primed and non-soaked seeds (86.8 mm), and those developed from seeds subjected to other priming and pre-soaking treatments (F = 90.4, p < 0.001, Figure 4). Shoot length followed a similar trend (F = 17.5, p < 0.001).

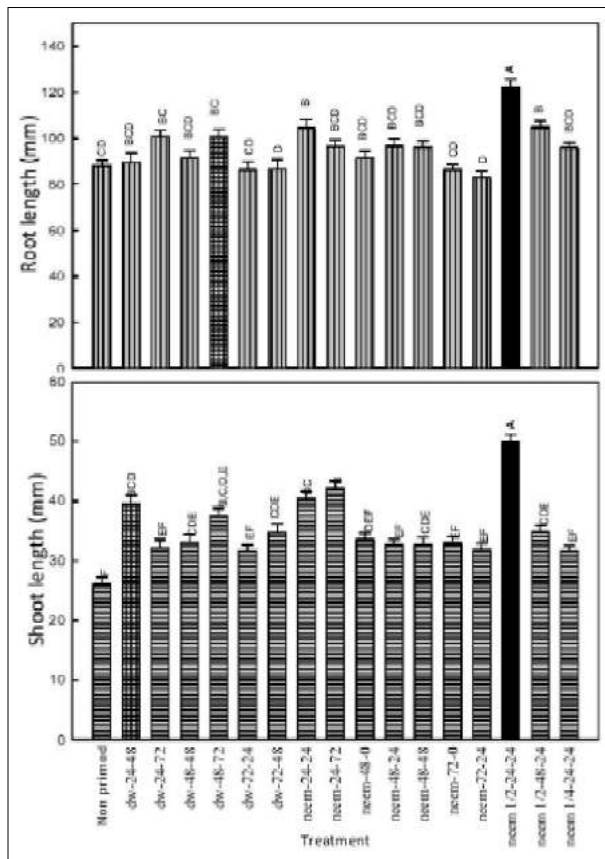


Figure 4: Mean of root (A) and shoot (B) lengths of Kaluheenati seedlings developed from seeds subjected to different priming and pre-soaking treatments. Different upper-case letters indicate significant differences between treatments. Error bars mean + SD. Only results of treatments that resulted in > 70 mm root and >25 mm shoot length are shown in the figure.

Kuruluthuda: Seedlings with significantly higher root lengths (F = 12.1, p < 0.001) were produced by seeds primed with ¼ strength neem extract for 24 hours + 0 hours soaking, than those developed from non-primed

and non-soaked seeds (Figure 5). Same trend was observed in shoot length data (F = 27.8, p < 0.001).

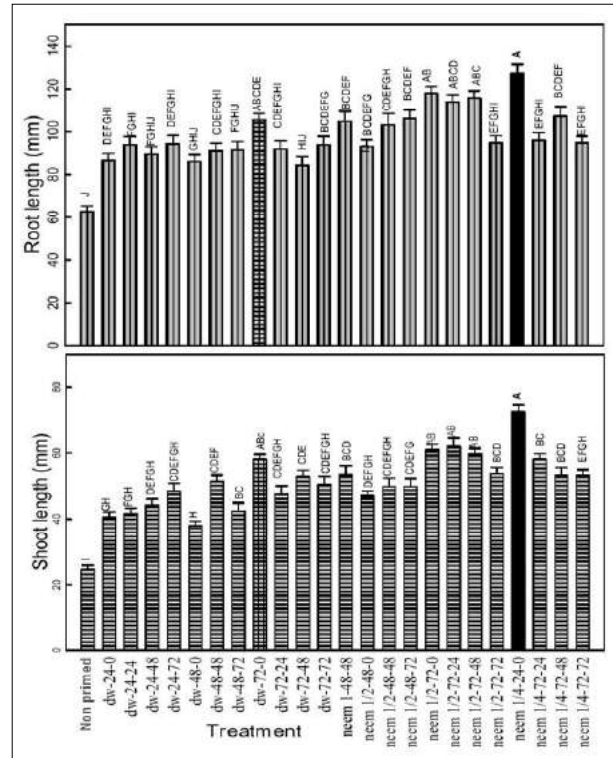


Figure 5: Mean of root (A) and shoot (B) lengths of Kuruluthuda seedlings developed from seeds subjected to different priming and pre-soaking treatments. Different upper-case letters indicate significant differences between treatments. Error bars mean ± SD. Only results of treatments that resulted in > 60 mm root length and >20 mm shoot length are shown in the figure.

Maa-wee: Root (F = 17.7, p < 0.005) and shoot lengths (F = 33.4, p < 0.005) of seedlings developed from seeds primed in quarter strength neem for 48 hours + 48 hours soaking were significantly higher than those developed from non-primed and non-soaked seeds and those developed from seeds subjected to other priming and pre-soaking treatments (Figure 6).

Madathawalu: Root lengths of seedlings developed from seeds primed with full strength neem extract for 72 hours + 48 hours soaking, and with full strength neem extract for 48 hours + 0 hours soaking were significantly higher than non-primed and non-soaked seeds (63 mm) and those developed from the seeds subjected to other priming and

soaking treatments ($F = 9.1$, $p < 0.005$, Figure 7). Shoot length (70.4 mm) of seedlings developed from seeds primed in full strength neem extract for 72 hours + 48

hours soaking was significantly higher ($F = 4.90$, $p < 0.005$) than those of non-primed and non-soaked seeds (32.4 mm).

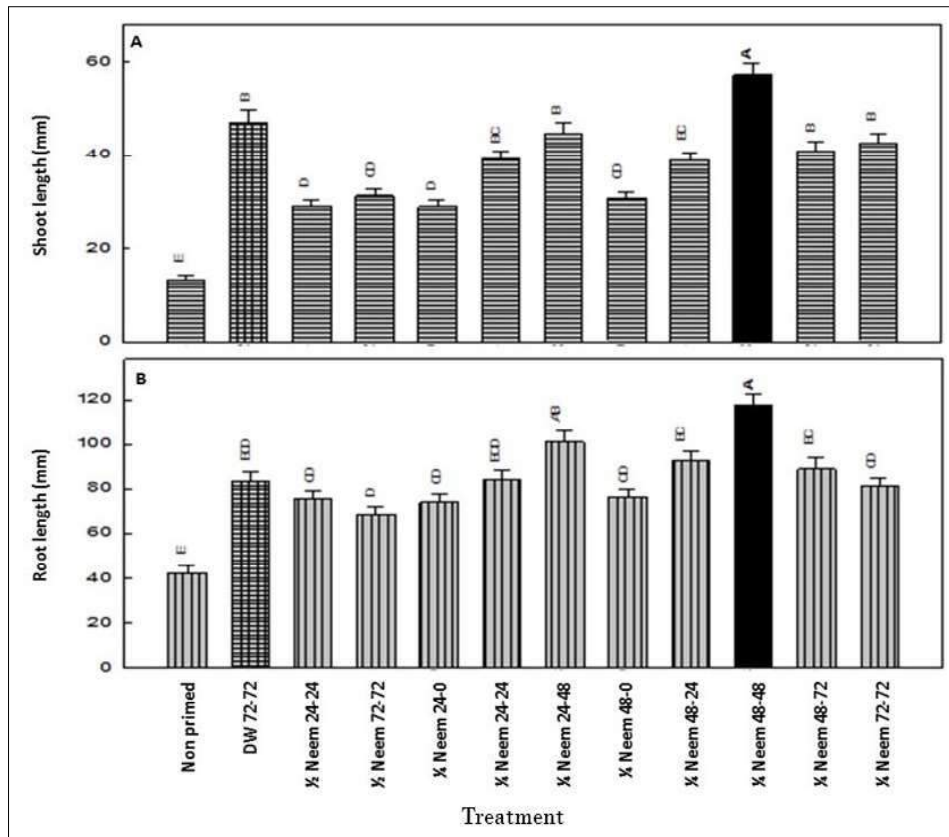


Figure 6: Mean of root (A) and shoot (B) lengths of Maa-wee seedlings developed from seeds subjected to different priming and soaking treatments. Different upper-case letters indicate significant differences between treatments. Error bars mean \pm SD. Only results of treatments that resulted in > 60 mm root and > 20 mm shoot length were shown in the figure.

Effect of priming on seedling emergence under plant house conditions

Kaluheenati

The seedling emergence percentage of non-primed seeds (65%) improved, significantly after priming with distilled water or neem extract (Figure 8A). However, the seedling emergence percentage of seeds primed in half strength neem extract for 72 hours followed by 24 hours soaking was significantly ($F = 28.9$, $p < 0.01$) higher than that of all the other treatments (82.5%).

Kuruluthuda

Percentage seedling emergence of non-primed Kuruluthuda seeds (10%) improved significantly ($F = 76.4$, $p < 0.01$) by distilled water (72 hours) or neem (quarter strength for 72 hours) priming (25%, Figure 8B).

Maa-wee

Seedling emergence of non-primed Maa-wee seeds was very low (12%, Figure 8C). However, when seeds were primed with quarter neem extract for 48 hours, seedling

emergence percentage (28%) was significantly improved ($F = 212.5, p < 0.01$).

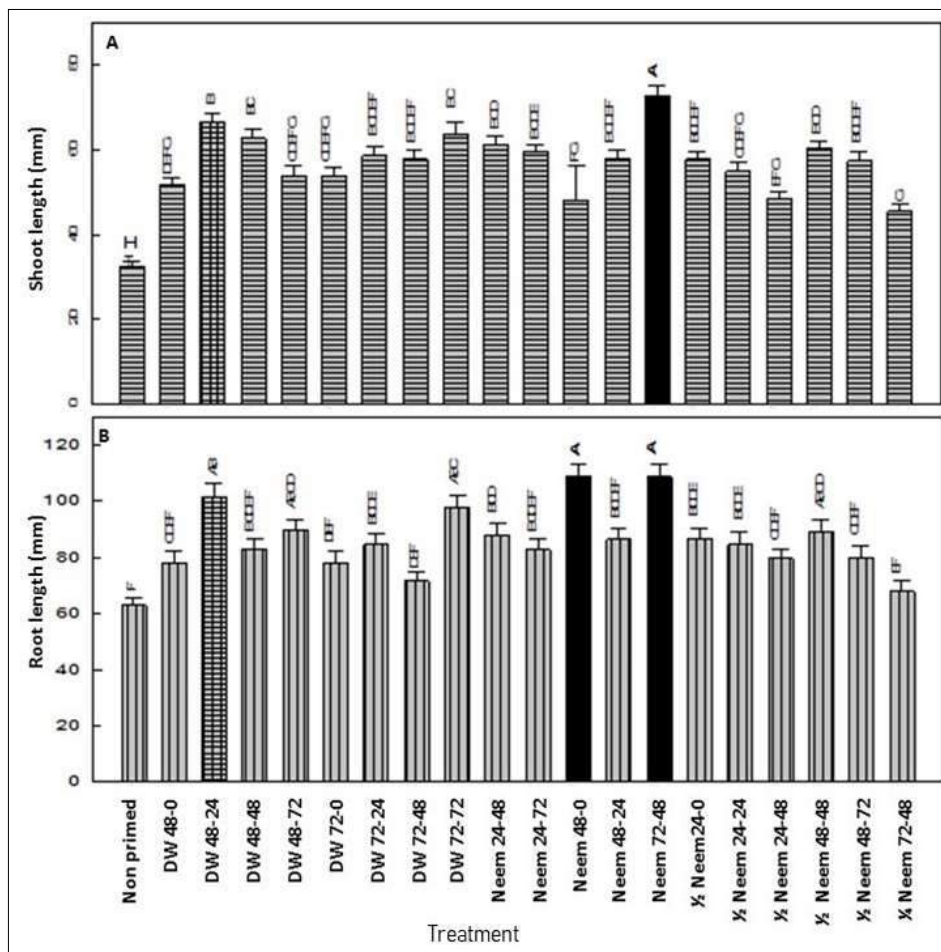


Figure 7: Mean root (A) and shoot (B) lengths of Madathawalu seedlings developed from seeds subjected to different priming and soaking treatments. Different upper-case letters indicate significant differences between treatments. Error bars \pm SD. Only results of treatments that resulted in > 70 mm root and > 30 mm shoot length are shown in the figure.

Madathawalu

Seedling emergence percentage of non-primed Madathawalu seeds was $\sim 40\%$. When seeds were primed with full strength Neem extract for 72 hours, seedling emergence percentage has significantly ($F = 29.9, p < 0.01$) increased to 54% (Figure 8D).

Non-primed Kaluheenati seeds had $\sim 60\%$ germinability. Among hydro-priming treatments, distilled water priming for 24 hours+ 72 hours pre-soaking treatment resulted the highest germinability, while among

neem priming treatments half strength neem extract priming for 24 hours+ 24 hours pre-soaking resulted the highest germinability. Neem priming treatment has improved the germination percentage of Kaluheenati seeds to about 85% . This percentage germinability was significantly higher than that of the hydro-primed seeds too. Further, the highest root and shoot length were observed after seeds were subjected to $1/2$ strength neem extract priming for 24 hours + 24-hour pre-soaking. Under glasshouse conditions, half strength neem extract priming for 24 hours+ 24 hours- pre-soaking treatment resulted the highest seedling emergence too. Therefore,

half strength neem extract priming for 24 hours + 24 hours pre-soaking could be recommended as the best treatment to improve seed quality of Kaluheenati.

Kuruluthuda had a very low initial germination ~35%. When seed germination percentage was considered, the best hydro-priming treatment was distilled water priming for 24 hours with no pre-soaking and the best neem priming treatments were quarter strength neem priming for 72 hours + 24 hours pre-soaking and half strength neem priming for 72 hours with no pre-soaking treatments. Neem priming treatments have improved the seed germinability significantly to ~ 65%. However, no significant difference was observed between distilled water priming for 24 hours with that of the two neem priming treatments. However, the highest root and shoot length were observed in seedlings of seeds primed with quarter strength neem extract for 72 hours + 24 hours pre-soaking treatment. However, quarter strength neem extract priming for 72 hours + 24 hours pre-soaking treatment as well as distilled water priming for 24 hours with no pre-soaking treatment has increased the seedling emergence over that of non-primed or primed with other treatments. Further, there was no significant difference

between seedling emergences of these two treatments. When all the germination parameters were considered, half strength neem extract priming for 72 hours + 24 hours pre-soaking was the best treatment for Kuruluthuda.

Maa-wee also had a low initial germinability (~25%). Distilled water priming for 72 hours+ 72 hours pre-soaking treatment was the best hydro-priming treatment that resulted the highest germinability. However, there were several neem priming treatments which improved the germinability of seeds of Maa-wee. Nevertheless, the germination percentage of seeds within seven days of this variety was always < 50% indicating the initial low quality of the seeds. Although neem priming has significantly increased the shoot and root lengths of seedlings, there were no significant differences between the shoot and root lengths of seedlings of neem primed seed with that of distilled water primed once. However, quarter strength neem extracts priming for 48 hours+ 48 hours pre-soaking treatment resulted in significantly the highest seedling emergence percentage. Therefore, it revealed that the best treatment to improve seed quality of Maa-wee is the quarter strength neem extract priming for 48 hours+ 48 hours pre-soaking treatments.

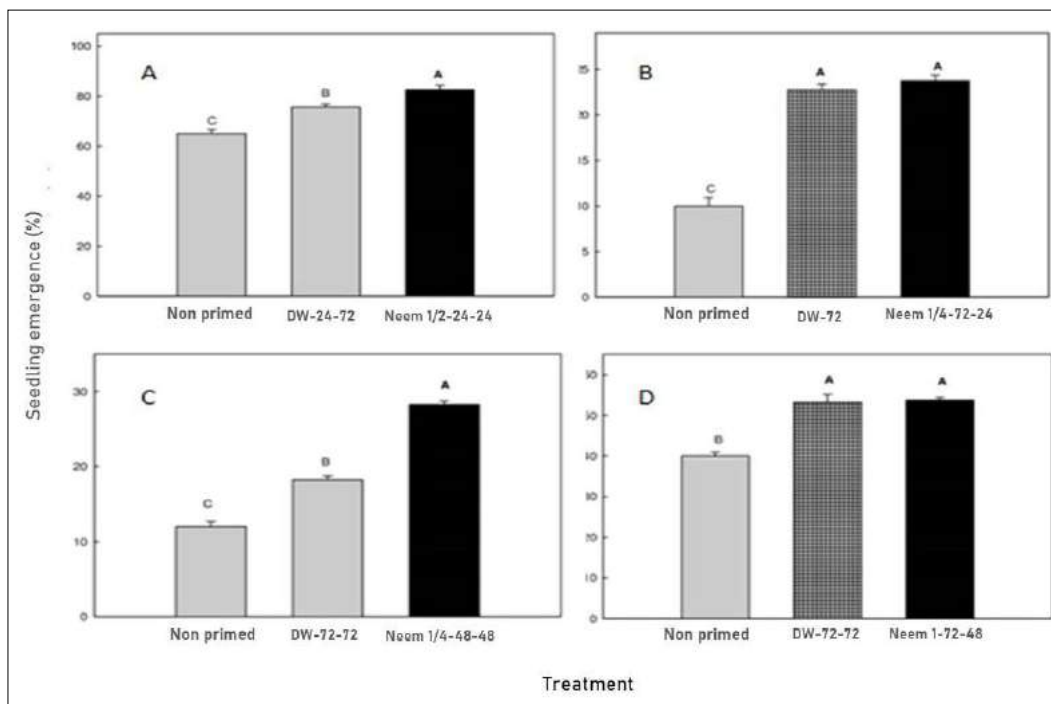


Figure 8: Seedling emergence of primed and non-primed seeds of (A) Kaluheenati, (B) Kuruluthuda, (C) Maa-wee and of (D) Madathawalu sown on rice field soil in ambient plant house conditions. Different uppercase letters indicate significant differences between treatments. Error bars mean \pm SD.

Madathawalu had initial germination of ~20%. Distilled water priming for 48 hours + 48 hours pre-soaking treatment was the best hydro-priming treatment for Madathawalu to increase the seed germinability. Whereas full strength neem priming for 72 hours + 48 hours pre-soaking resulted the highest germinability among neem priming treatments. These treatments have significantly improved the germinability of Madathawalu seeds to about 55% but with no significant differences of germinability between the best hydro-priming and neem priming treatments. However, seed vigour (as determined with the shoot and root length) of seeds with full strength neem priming for 72 hours + 48 hours pre-soaking was significantly higher than that of the seeds hydro-primed for 48 hours + pre-soaking for 48 hours. Thus, full strength neem seed extract priming for 72 hours + pre-soaking for 48 hours could be considered as the best treatment for Madathawalu. However, there is no significant difference between seedling emergences of seed primed with full strength neem extract for 72 hours + 48 hours pre-soaking and that of 72 hours hydro-priming + 72 hours pre-soaking.

The results of the priming experiments revealed that neem priming has a higher ability than water priming to improve seed quality of Kaluheenati, Kuruluthuda, Maa-wee and Madathawalu. There could be basically three reasons for reduced seed quality: imbibition stress during germination, antioxidant stress and pathogenic activity. During imbibition, if water enters to seeds without a control, it could cause reactive oxygen species (ROS) accumulation ((Liu *et al.*, 2007, Paparella *et al.*, 2015). ROS could damage cellular components (Paparella *et al.*, 2015). The reasons for the increment of seed quality (seed germination and seed vigour) with distilled water may be that it reduces imbibition stress. Neem extract has a lower water potential than distilled water. Therefore, it controls (reduces) water uptake. It could limit ROS formation and thereby reduce cellular damages and oxidative injuries. Further, neem seed extracts show antioxidant properties (Nahak & Sahu, 2011; Revathi & Thambidurai, 2019) and may reduce the effect of ROS during germination. Moreover, the anti-microbial activity of neem seed extract (Biswas *et al.*, 2002) may reduce the pathogenic activities in the seed during germination. These may be the reasons for seed quality improvement shown after neem priming in our experiments. However, a detailed study has to be conducted to determine the mode of action of the neem seed extract during seed priming.

No studies on seed germination/vigour tests have been reported on the studied four rice varieties. However, several studies have been conducted to determine the

effects of hydro-priming, dehydration priming and osmo-priming (by NaCl and KH_2PO_4) on germination of rice seeds. Galappaththi *et al.* (2020) have reported that hydro-priming for 72 hours significantly improve the seed germination, vigour and emergence of two traditional rice varieties; Suwadal and Batapola-el. Illangakoon *et al.* (2016) have showed that seed hydro-priming has improved the survival of both traditional and newly developed varieties under anaerobic conditions. They further reported that, hydro-primed seeds showed increased synthesis of soluble sugars, starch degradation and α amylase activity compared to non-primed seeds under anaerobic conditions. They suggested that these enhanced activities are the modes by which hydro-priming enhanced seed quality. Islam *et al.* (2012) have reported that CaCl_2 was the best osmo-priming agent. Priming using CaCl_2 enhanced all germination parameters of BRRI dhan41 rice variety in Bangladesh. Seeds of BRRI dhan41, when treated with NaCl, showed the highest germination percentage, germination energy, germination speed. However, vigour index was found to be highest in BRRI dhan40 when it was treated with KCl. BRRI dhan41 produced the largest root when seeds were treated with NaCl. BRRI dhan40 and BINA dhan7 produced the highest shoot length at the controlled and CaCl_2 treated seed, respectively. Esmeili and Heidarzade, (2012) have found that the osmo-priming mainly with PEG could improve seed germination and seedling development parameters of many rice genotypes.

Heretofore, neem priming has not been used to improve seed quality of any species. Our experiments showed the high potential of neem priming in the improvement of seed quality of traditional rice varieties. This finding is especially important as neem can be used as an organic agrochemical in organic farming. Thus, our experiments provide a solution to a basic problem of low seed quality faced by organic farmers who produce organic traditional rice.

According to the results obtained from our experiments, it revealed that hydro priming and neem priming are promising methods to enhance seed quality of all four traditional rice varieties studied. Priming treatments increase seed germinability, seed vigour and seedling emergence. Neem priming gives a more significant improvement of all these seed parameters thus, neem priming is more promising than hydropriming in improving seed quality of traditional rice varieties. However, it is necessary to determine how the antioxidant activity and other properties of neem affect the seed quality of rice.

CONCLUSIONS

Neem-priming treatment improved the seed quality (germination and vigour) of Kaluheenati, Kuruluthuda, Maa-wee and Madathawalu rice varieties. For Kaluheenati, the best results were obtained by half strength neem extract priming for 24 hours +24 hours water pre-soaking. For Kuruluthuda quarter strength neem extract priming for 72 hours + 24 hours water pre-soaking, for Maa-wee quarter strength neem extract priming for 48 hours +48 hours water pre-soaking and for Madathawalu full strength neem extract priming for 72 hours + 48 hours water pre-soaking, gave the best results.

REFERENCES

- Achimu P. & Schlosser E. (1992). Effect of neem extracts against *Plasmopara viticola*, *Practise Oriented Results on Use and Production of Neem Ingredients* (ed. H. Kleeborg), pp. 99–109. Druck & Graphic, Giessen, Germany.
- Alabi O. & Olorunju P.E. (2004). Evaluation of neem seed extract, black soap and cow dung for the control of groundnut leaf spot at Samaru, Nigeria. *Archives of Phytopathology and Plant Protection* **37**: 123–127. DOI: <https://doi.org/10.1080/0323540042000203921>
- Bambaradeniya C.N.B. & Amerasinghe F.P. (2003). Biodiversity associated with the rice field agroecosystem in Asian countries: A brief review. *Working Paper 63*. International Water Management Institute, Colombo.
- Bandara J.M.R.S., Senevirathna D.M.A.N., Dassanayake D.M.R.S.B., Herath V., Bandara J.M.R.P., Abeysekera T. & Rajapaksha K.H. (2008). Chronic renal failure among farm families in cascade irrigation systems in Sri Lanka associated with elevated dietary cadmium levels in rice and freshwater fish (Tilapia). *Environmental Geochemistry and Health* **30**(5): 465–478. DOI: <https://doi.org/10.1007/s10653-007-9129-6>
- Bandara J.M.R.S., Wijewardena H.V.P., Liyanage J., Upul M.A. & Bandara J.M.U.A. (2010). Chronic renal failure in Sri Lanka caused by elevated dietary cadmium: Trojan horse of the green revolution. *Toxicology Letters* **198**(1): 33–39. DOI: <https://doi.org/10.1016/j.toxlet.2010.04.016>
- Bewley J.D. (1997). Seed germination and dormancy. *The Plant Cell* **9**(7): 1055–1066.
- Biswas K., Chattopadhyay I. & Banerjee R.K. (2002) Biological activities and medicinal properties of neem (*Azadirachta indica*). *Current Science* **82**: 1336–1345.
- Bradford K.I. & Bewley J.D. (2002). Seeds: biology, technology and role in agriculture. In: *Plants, Genes and Crop Biotechnology* (eds. M.J. Chrispeels & D.E. Sadava), pp. 210–239, 2nd edition, Jones & Barlett. Boston, MA, USA
- Copeland L.O. & McDonald M. (2001). *Principals of Seed Science and Technology*. Springer Nature Publications, Switzerland.
- Coventry E. & Allan E.J. (2001). Microbiological and chemical analysis of neem (*Azadirachta indica*) extracts: new data on antimicrobial activity. *Phytoparasitica* **29**: 441–449. DOI: <https://doi.org/10.1007/BF02981863>
- Department of Agriculture (2019). *Agricultural Statistics*, volume 16. Socio Economic and Planning Centre, Department of Agriculture, Peradeniya.
- Dharmasena P.B. (2010) Traditional rice farming in Sri Lanka, *Economic Review* **36**: 48–53.
- Drew R. L. K. & Dearman J. (1993). Effect of osmotic priming on germination characteristics of celeriac (*Apiumgraveolens* L. var. *rapaceum*). *Seed Science and Technology* **21**(2): 411–415.
- Esmeli M. & Heidarzade A. (2012). Osmopriming enhance the seeds emergence and seedling parameters of two rice cultivars (*Oryza sativa*) under tough condition. *International Journal of Agricultural Crop Science* **4**(5): 247–250.
- Food and Agricultural Organisation (FAO). 2013. FAOSTAT Database. Food and Agricultural Organization, Rome, Italy.
- Fischer K. (2007). Methods of moisture testing. In: *ISTA Handbook on Moisture Determination* (eds. H. Nijenstein, J. Nydam & R. Don). International Seed Testing Association, Switzerland.
- Galappaththi M.O., Jayasuriya K.M.G.G. & Gama-Arachchige N.S. (2020). Storage and hydro-priming treatments to improve the seed quality of two traditional rice varieties; Batapola-el and Suwendal, from Sri Lanka. *Oryza-An international Journal on Rice* **57**(1): 25–35. DOI <https://doi.org/10.35709/ory.2020.57.1.3>
- Ghobadi M., Abnavi M.S., Honarmand S.J., Ghobadi M.E. & Mohammadi G.R. (2012). Effect of hormonal priming (GA3) and osmopriming on behavior of seed germination in wheat (*Triticum aestivum* L.). *Journal of Agricultural Science* **4**(9): 244. DOI: <https://doi.org/10.5539/jas.v4n9p244>
- Ginigaddara G.A.S. (2018). *Traditional Rice Varieties in Sri Lanka*. Rajarata University of Sri Lanka, Mihinthale, Sri Lanka. Available at http://www.rjt.ac.lk/agri/agri_onlinematerials/agricultural_systems/Traditional%20rice%20varieties%20GAS%20Ginigaddara.pdf
- Girish K. & Bhat S.S. (2008). Neem, a green treasure. *Electronic Journal of Biology* **4**: 102–111.
- Hampton J.G. & TeKrony D.M. (1995). *Handbook of Vigour Testing Methods*, 3rd edition. International Seed Testing Association, Switzerland.
- Harris D., Tripathi R.S. & Joshi A. (2002). On-farm seed priming to improve crop establishment and yield in dry direct-seeded rice. In: *Direct seeding: Research Strategies and Opportunities*, pp. 231–240. International Research Institute, Manila, Philippines.
- Illangakoon T.K., Ella E.S., Ismail A.M., Marambe B., Keerthisena R.S.K., Bentota A.P. & Kulatunge S. (2016). Impact of variety and seed priming on anaerobic germination-tolerance of rice (*Oryza sativa* L.) varieties in Sri Lanka. *Tropical Agricultural Research* **28**: 26–37. DOI: <https://doi.org/10.4038/tar.v28i1.8181>

- International Rice Research Institute (IRRI) (2021). *World Rice Statistics 2020*. International Rice Research Institute, Los Banos, Philippines. Available at <http://irri.org/index.php?option=comk2&view=item&id=9081&Itemid=100481&lang=en>. Accessed 09 April 2020.
- Islam R., Mukherjee A. & Hossin M. (2012). Effect of osmopriming on rice seed germination and seedling growth. *Journal of the Bangladesh Agricultural University* **10**(1): 15–20.
DOI: <https://doi.org/10.3329/jbau.v10i1.12013>
- Jayasumana C., Gunatilaka S. & Senanayake P. (2014). Glyphosate, hard water and nephrotoxic metals: are they the culprits behind the epidemics of chronic kidney disease of unknown etiology in Sri Lanka. *International Journal of Environmental Research and Public Health* **11**(2): 2125–2147.
DOI: <https://doi.org/10.3390/ijerph110202125>
- Johnson S.E., Lauren J.G., Welch R.M. & Duxbury J.M. (2005). A comparison of the effects of micronutrient seed priming and soil fertilization on the mineral nutrition of chickpea (*Cicer arietinum*), lentil (*Lens culinaris*), rice (*Oryza sativa*) and wheat (*Triticum aestivum*) in Nepal. *Experimental Agriculture* **41**: 427–448.
DOI: <https://doi.org/10.1017/S0014479705002851>
- Kennedy G. & Burlingame B. (2003). Analysis of food composition data on rice from a plant genetic resource perspective. *Food Chemistry* **80**(4): 589–596.
DOI: [https://doi.org/10.1016/S0308-8146\(02\)00507-1](https://doi.org/10.1016/S0308-8146(02)00507-1)
- Khush G.S. (1997). Origin, dispersal, cultivation and variation of rice. *Oryza: From Molecule to Plant* **35**(1): 25–34.
DOI: <https://doi.org/10.1023/A:1005810616885>
- Krishnan P., Ramakrishnan B., Reddy K.R. & Reddy V.R. (2011). High temperature effects on rice growth, yield, and grain quality. In: *Advances in Agronomy* (ed. D.L. Sparks), pp. 87–206, volume 111, Academic Press, Burlington, Canada.
DOI: <https://doi.org/10.1016/B978-0-12-387689-8.00004-7>
- Liu X., Xing D., Li L. & Zhang L. (2007). Rapid determination of seed vigor based on the level of superoxide generation during early imbibition. *Photochemical & Photobiological Sciences* **6**(7): 767–774.
DOI: <https://doi.org/10.1039/b704337f>
- Muthayya S., Sugimoto J.D., Montgomery S. & Maberly F. (2014). An overview of global rice production, supply, trade and consumption. *Annals of the New York Academy of Sciences* **1324**: 7–14.
DOI: <https://doi.org/10.1111/nyas.12540>
- Nahak G. & Sahu R. (2011). Evaluation of antioxidant activity of flower and seed oil of *Azadirachta indica* A. juss. *Journal of Applied and Natural Science* **3**: 78–81.
DOI: <https://doi.org/10.31018/jans.v3i1.158>
- Nawaz J., Hussain M., Jabbar A., Nadeem G.A., Sajid M., Subtain M. & Shabbir I. (2013). Seed priming techniques. *International Journal of Agriculture Crop Science* **6**(20): 1373–1381.
- Paparella S., Araújo S.S., Rossi G., Wijayasinghe M., Carbonera D. & Balestrazzi A. (2015). Seed priming: state of the art and new perspectives. *Plant Cell Reports* **34**(8): 1281–1293.
DOI: <https://doi.org/10.1007/s00299-015-1784-y>
- Rajapakse R.M.T., Sandanayake C.A. & Pathinayake B.D. (2000) Footprints in rice variety improvement and its impact on rice production in Sri Lanka. *Annual Symposium of the Department of Agriculture*, Department of Agriculture, Sri Lanka **2**: 423–433.
- Ranawake A.L., Amarasinghe U.G.S. & Dahanayake N. (2013). Agronomic characters of some traditional rice (*Oryza sativa* L.) cultivars in Sri Lanka. *Journal of the University of Ruhuna* **1**(1): 3–9.
DOI: <https://doi.org/10.4038/jur.v1i1.6150>
- Rebeira S.P., Wickramasinghe H.A.M., Samarasinghe W.L.G. & Prashantha B.D.R. (2014). Diversity of grain quality characteristics of traditional rice (*Oryza sativa* L.) varieties in Sri Lanka. *Tropical Agricultural Research* **25**(4): 570–578.
DOI: <https://doi.org/10.4038/tar.v25i4.8062>
- Revathi T. & Thambidurai S. (2019). Cytotoxic, antioxidant and antibacterial activities of copper oxide incorporated chitosan-neem seed biocomposites. *International Journal of Biological Macromolecules* **139**: 867–878.
DOI: <https://doi.org/10.1016/j.ijbiomac.2019.07.214>
- Samaranayake M.D.W., Yathursan S., Abeysekera W.K.S.M. & Herath H.M.T. (2017). Nutritional and antioxidant properties of selected traditional rice (*Oryza sativa* L.) varieties of Sri Lanka. *Sri Lankan Journal of Biology* **2**(2): 25–35.
DOI: <https://doi.org/10.4038/slj.v2i2.10>
- Schmutterer H. (1990). Properties and potential of natural pesticides from the neem tree, *Azadirachta indica*. *Annual Review of Entomology* **35**(1): 271–297.
DOI: <https://doi.org/10.1146/annurev.en.35.010190.001415>
- Suriyagoda L.D.B., Thilakarathne R.M.M.S., Nissanka S.P. & Samita S. (2011). Morphological variation in selected rice (*Oryza sativa* L.) germplasm of Sri Lanka. *Journal of the National Science Foundation of Sri Lanka* **39**(2): 129–137.
DOI: <https://doi.org/10.4038/jnsfsr.v39i2.3173>
- Tanida M. (1996). Catalase activity of rice seed embryo and its relation to germination rate at a low temperature. *Breeding Science* **46**(1): 23–27.
DOI: <https://doi.org/10.1270/jsbbs1951.46.23>
- Tilahun-Tadesse F., Nigussie-Dechassa R., Bayu W. & Gebeyehu S. (2013). Effect of hydro-priming and pre-germinating rice seed on the yield and terminal moisture stress mitigation of rain-fed lowland rice. *Agriculture, Forestry and Fisheries* **2**(2): 89–97.
DOI: <https://doi.org/10.11648/j.aff.20130202.15>
- Wang J., Li J., Cao J. & Jiang W. (2010). Antifungal activities of neem (*Azadirachta indica*) seed kernel extracts on postharvest diseases in fruits. *African Journal of Microbiology Research* **4**: 1100–1104.
- Weeraratne C.S. (1983). Pesticides, an overview with particular reference to Sri Lanka. *Economic Review* **8**: 4–12.
- Wickramasinghe H.A.M. & Noda T. (2008). Physicochemical properties of starches from Sri Lankan rice varieties. *Food Science and Technology Research* **14**(1)
DOI: <https://doi.org/10.3136/fstr.14.49>

RESEARCH ARTICLE

Numerical prediction of early age concrete temperature via 3D finite difference simulation

MP Dissanayaka and HD Yapa*

Department of Civil Engineering, Faculty of Engineering, University of Peradeniya, Peradeniya.

Submitted: 17 November 2020; Revised: 17 June 2021; Accepted: 03 August 2021

Abstract: Cement hydration is an exothermic reaction. It leads to increase in temperature and creates temperature gradients inside concrete structures during early ages. Extremes of such scenarios cause cracking of concrete and, therefore, affect the structural integrity and durability. Hence, prediction of temperature development of the concrete interior is vital in order to identify appropriate temperature control mitigation measures. However, it remains a challenge because, on the one hand, the governing thermal equations do not have closed-form solutions, and on the other hand, the thermal behaviour of concrete is influenced by numerous factors, including heat evolution, heat conduction/convection, boundary conditions, etc. One possible solution is to implement numerical modelling via finite element (FE) or finite difference (FD) approaches. Amongst the two approaches, the former has a better simulating capacity to deal with complex problems, whereas the latter is relatively simple and less expensive. In this light, this research expanded an existing 2-dimensional FD temperature prediction tool towards a 3-dimensional (3D) model in view of enhancing the prediction accuracy of the 2D version. The 3D model was validated for three distinct experiments, and the prediction accuracy was found to be notable where the maximum temperature prediction offset was below 2.2%. Then, the significance of using 3D FD temperature modelling for cube shape concrete structures and for pipe-cooled concrete structures was highlighted.

Keywords: 3D modelling, concrete temperature, finite difference.

INTRODUCTION

The hydration of cement is an exothermic reaction. Consequently, internal temperature development is a major concern prevailing with mass concrete construction. High temperature is undesirable for concrete due to a number of reasons. On the one hand, temperature beyond 70 °C could be a cause of delayed ettringite formation (Taylor *et al.*, 2001), and on the other, concrete has low thermal conductivity, and it dissipates heat to the environment at the boundaries. Consequently, the heat generation leads to internal temperature gradients which could cause undesirable cracking effects (Neville, 2011). For instance, the temperature gradient limit applicable for concrete with gravel aggregate is about 20 °C (Bamforth, 2007). Also, in externally restrained structures, the drop of temperature during the cooling phase introduces tensile stresses that lead to undesirable cracking (Bamforth, 2007). It is therefore vital to take appropriate measures to control temperature development in concrete. Several temperature controlling methods are practised by the construction industry. The traditional methods include the use of low-heat concrete, use of pre-cooling methods (e.g., use of chilled water), and application of appropriate curing. The use of water-cooled pipes (Myers *et al.*, 2009; Li *et al.*, 2012) and air-

* Corresponding author (hdy@pdn.ac.lk;  <https://orcid.org/0000-0002-7213-5276>)



cooled pipes (Azenha *et al.*, 2014) are relatively modern options applicable for temperature control of concrete.

The temperature development of concrete depends on many factors, including heat evolution of concrete, time, thermal conductivity, convection at the boundaries, and boundary conditions (Ballim, 2004). The heat transfer inside the concrete involves a number of inter-related mechanisms where none of which has a closed-form solution. Hence, accurate temperature prediction is complex, and consequently, the identification of the appropriate temperature controlling requirement is always a challenge (Ballim, 2004). In this context, numerical approaches of Finite Element (FE) and Finite Difference (FD) methods have been effectively used as a temperature prediction tool for concrete structures (Ballim, 2004; Bobko *et al.*, 2015; Dissanayake *et al.*, 2017). The FE method is a complex approach, but it can be used to model sophisticated problems, including irregular geometry, diverse boundary conditions, construction patterns, etc. However, commercially available FE software packages are usually expensive (Bobko *et al.*, 2015). In contrast, the applicability of the FD method is limited to regular shape structures, whereas it is relatively a less complex formulation (Ballim, 2004). Hence, the FD method also occupies a unique demand amongst the concrete temperature modelling options. Numerous successful investigations that explored 2-dimensional (2D) FD concrete temperature modelling are found in the literature (Ballim, 2004; Bobko *et al.*, 2015; Yikici & Chen, 2015). However, an extension of the FD approach towards 3-dimensional (3D) modelling has seldom been investigated in spite of the 3D predictions that should necessarily be more precise than the 2D results, particularly for structures with heat flow across all three directions. Also, if the modelling of pipe-cooling systems is to be facilitated, necessarily the use of 3D simulation is vital. In this context, as an expansion of the commonly used 2-dimensional (2D) FD concrete temperature modelling, this research explored the use of 3-dimensional (3D) FD modelling to predict the temperature in concrete structures.

METHODOLOGY

A literature survey was conducted to explore the application of the FD approach to predict the temperature development in concrete. Based on the existing 2D models, the formulation was extended to a 3D FD formulation. The 3D model was then validated on available experimental results and subsequently was utilised on parametric studies to identify the contexts

where 3D simulation is significant. Also, the potential of the 3D model to simulate pipe-cooled concrete systems was assessed. These steps of the methodology are further elaborated in the following sections.

Temperature prediction model development

Heat flow relations

Conduction of heat across a mass can be expressed in the Fourier equation form by,

$$q = -kA \frac{\partial T}{\partial x} \quad \dots(01)$$

where q is the heat transfer rate, k is the thermal conductivity, A is the cross-sectional area, and $\frac{\partial T}{\partial x}$ is the temperature gradient in the direction of the heat flow (Holman, 1986). The minus sign indicates that the heat flow is in the direction of temperature reduction.

Considering the energy balance in a body where a heat source exists, the expression for one-dimensional heat flow can be obtained in the form of,

$$\frac{\partial}{\partial x} \left(k \frac{\partial T}{\partial x} \right) + Q' = \rho c \frac{\partial T}{\partial t} \quad \dots(02)$$

where Q' is the rate of heat generated per unit volume, ρ is the density of the material, c is the specific heat capacity of the material, and $\frac{\partial T}{\partial t}$ is the rate of change of temperature (Holman, 1986). It is, therefore, possible to extend equation 2 to obtain the 3D heat flow as,

$$k \left(\frac{\partial^2 T}{\partial x^2} + \frac{\partial^2 T}{\partial y^2} + \frac{\partial^2 T}{\partial z^2} \right) + Q' = \rho c \frac{\partial T}{\partial t} \quad \dots(03)$$

where x , y , z are the coordinates at a particular point in the structure. It is assumed here that the thermal conductivity in each direction is similar.

Development of finite difference (FD) equations

The FD method gives a point-wise solution to the governing differential equations by using a finite set of points (Patini, 2011). Ballim (2004) developed an FD model, which is a 2D solution for the Fourier equation for heat flow in solid bodies. By extending his work via equation 3, this study developed FD equations for seven distinct nodal positions, as shown in Figure 1 (a) for a cubical (3D) concrete block. These equations are expressed in equations 4 to 12.

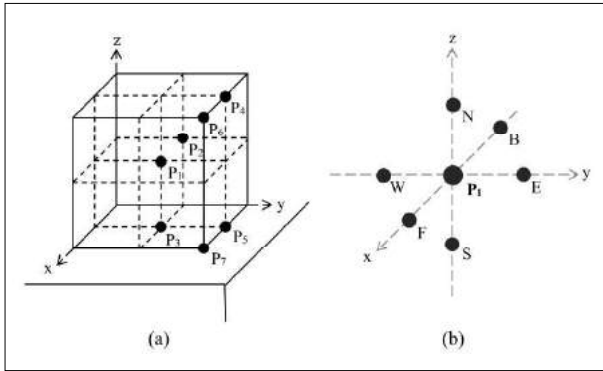


Figure 1: (a) Nodal locations and (b) nodal arrangement for an internal node

For an internal node P1 [shown in Figures 1 (a) and (b)], the 3D FD equation can be formulated to be:

$$T_{P_1}^{n+1} = \frac{Q^n \delta t}{\rho c} + T_{P_1}^n (1 - 6F_0) + F_0 (T_N^n + T_E^n + T_S^n + T_W^n + T_F^n + T_B^n) \quad \dots(4)$$

subjected to $\delta t \leq \frac{\rho c \Delta^2}{6k}$

Here $T_{P_1}^{n+1}$ is the temperature at node P₁ in the (n + 1)th time interval (similar notation is applicable to all the other nodal positions), Q^n is the rate of internal heat evolution in the nth time interval, δt is the time-step interval used in the FD analysis and F_0 is the Fourier number, which is defined as,

$$F_0 = \frac{k \delta t}{\rho c \Delta^2} \quad \dots(5)$$

where $\Delta = \Delta_x = \Delta_y = \Delta_z$ is the nodal distance. Also, $T_N, T_E, T_S, T_W, T_F, T_B$ are the temperatures of the nodes to the north, east, south, west, front, and back of node P₁ during this particular time interval [see Figure 1 (b)].

Similarly, the FD equation for an exposed surface node P₂ is,

$$T_{P_2}^{n+1} = \frac{Q^n \delta t}{\rho c} + T_{P_2}^n (1 - F_0(6 + 2B_i)) + F_0 (T_N^n + T_E^n + T_S^n + T_W^n + 2T_F^n + 2B_i T_A^n) \quad \dots(6)$$

subjected to $\delta t \leq \frac{\rho c \Delta^2}{(6k + 2h\Delta)}$

where T_A is the ambient temperature and B_i is the Biot number, which is defined as,

$$B_i = \frac{h\Delta}{k} \quad \dots(7)$$

where h is the heat transfer coefficient.

The bottom surface node FD equation is,

$$T_{P_3}^{n+1} = \frac{Q^n \delta t}{\rho c} + T_{P_3}^n \left(1 - F_0 \left(6 + 2 \frac{k_R}{k}\right)\right) + F_0 (T_E^n + T_W^n + T_F^n + T_B^n + 2T_N^n + 2 \frac{k_R}{k} T_R^n) \quad \dots(8)$$

subjected to $\delta t \leq \frac{\rho c \Delta^2}{(6k + 2k_R)}$

where k_R is the thermal conductivity of the base material (rock) and T_R is the base temperature.

The FD equation for an exposed edge node P₄ is,

$$T_{P_4}^{n+1} = \frac{Q^n \delta t}{\rho c} + T_{P_4}^n (1 - F_0(6 + 4B_i)) + F_0 (T_F^n + T_B^n + 2T_S^n + 2T_W^n + 4B_i T_A^n) \quad \dots(9)$$

subjected to $\delta t \leq \frac{\rho c \Delta^2}{(6k + 4h\Delta)}$

The FD equation for a bottom edge node P₅ is,

$$T_{P_5}^{n+1} = \frac{Q^n \delta t}{\rho c} + T_{P_5}^n \left(1 - F_0 \left(6 + 2B_i + 2 \frac{k_R}{k}\right)\right) + F_0 (T_F^n + T_B^n + 2T_N^n + 2T_W^n + 2B_i T_A^n + 2 \frac{k_R}{k} T_R^n) \quad \dots(10)$$

subjected to $\delta t \leq \frac{\rho c \Delta^2}{(6k + 2h\Delta + 2k_R)}$

The top corner node P₆ FD equation is,

$$T_{P_6}^{n+1} = \frac{Q^n \delta t}{\rho c} + T_{P_6}^n (1 - 6F_0(1 + B_i)) + 2F_0 (T_S^n + T_W^n + T_B^n + 3B_i T_A^n) \quad \dots(11)$$

subjected to $\delta t \leq \frac{\rho c \Delta^2}{6(k+h\Delta)}$ and, that for a bottom corner node P_7 is,

$$T_{P_7}^{n+1} = \frac{Q_n \delta t}{\rho c} + T_{P_7}^n \left(1 - F_0 \left(6 + 4B_i + 2 \frac{k_R}{k} \right) \right) + 2F_0 \left(T_N^n + T_W^n + T_B^n + \frac{k_R}{k} T_R^n + 2B_i T_A^n \right) \quad \dots(12)$$

$$\text{subjected to } \delta t \leq \frac{\rho c \Delta^2}{(6k+4h\Delta+2k_R)}$$

Determination of internal heat evolution

Several options are available to estimate the internal heat evolution of concrete. The use of analytical models is one such possibility (Bamfoth, 2007), where the concrete composition is usually the main parameter in such models. Matharaarachchi *et al.* (2012) showed the potential of using a more detailed analytical model that was based on the composition of the cement constituents for obtaining highly accurate temperature predictions for concrete structures. Nevertheless, the use of calorimeter test results is deemed to be a more accurate option to quantify the internal heat evolution of concrete (Riding *et al.*, 2006), hence it was opted in the current study. This test can be conducted either in the adiabatic or semi-adiabatic condition—in the latter case, heat loss compensation is to be carried out in order to obtain the adiabatic behaviour. Details of calorimeter tests and heat loss compensation methods can be found elsewhere (Ng *et al.*, 2008; Wasala & Yapa, 2017).

In the Fourier equation, the term Q' is used to account for the rate of heat evolution, and it is determined by differentiating the total heat with respect to time, which is called the time-based heat rate (Ballim, 2004). This can be expressed by,

$$Q' = \frac{dQ}{dT} \quad \dots(13)$$

where,

$$Q = mc\delta T \quad \dots(14)$$

and m is the mass of the sample, c is the concrete specific heat, and δT is the change in temperature of the sample over the time period. The extent and the rate of cement hydration depend on the absolute temperature under which the reaction takes place. The temperature of hardening concrete varies from point to point, and therefore, each point has a unique time-temperature

profile (Ballim, 2004). To address this phenomenon, the time component in the heat relations is to be incorporated with maturity where the maturity based heat rate is given by,

$$Q'_M = \frac{dQ}{dM} \quad \dots(15)$$

where, M is the maturity time. Accordingly, the time-based heat rate becomes to the form of,

$$Q' = Q'_M \frac{dM}{dt} \quad \dots(16)$$

Amongst commonly used maturity functions, the Arrhenius function provides a good basis to determine maturity-based heat rate (Ballim & Graham, 2003). It details the maturity of concrete cured at any temperature to be an equivalent maturity time (t_{20}) of concrete cured at 20 °C, and is expressed as,

$$t_{20} = \sum_{i=1}^n \exp \left[\left(\frac{E}{R} \right) \left(\frac{1}{293} - \frac{1}{273+0.5(T_i - T_{i-1})} \right) \right] (t_i - t_{i-1}) \quad \dots(17)$$

where E is the activation energy parameter, R is the universal gas constant (8.31 J/mol °C), and T_i is the temperature (in °C) at the end of the i^{th} time interval t_i . It is of note that E is governed by the material, and Soutsos *et al.* (2017) report that it could be in the range of 30–50 kJ/mol for OPC based concrete.

Temperature prediction algorithm development

The MATLAB software was used for programming the FD model. Using the FD solutions of the Fourier equation for 3D heat flow for distinct nodal locations, an algorithm was formulated to model structural and boundary configurations for a given concrete structure.

The inputs for the algorithm were nodal distance (Δ), time interval t_i , number of cycles to be run (n), density (ρ), specific heat capacity (c), and thermal conductivity (k) of concrete, thermal conductivity (k_R) and temperature (T_R) of the base material, heat transfer coefficients (convection) before and after formwork striking ($h_{plywood}$ and h_{air}), formwork striking time (t_s), ambient temperature variation (T_a), concrete placing temperature (T_p), and adiabatic temperature profile for the concrete mix. As the major output, the temperature profile with respect to time at any nodal location within the concrete block could be obtained. Based on the findings of Ballim (2004) on optimum levels of the nodal distance (Δ) and time interval (δT), these two input parameters were maintained at 100 mm and 30 min, respectively. It is

noted that a FE approach might use a similar size for the concrete mesh whilst the time step could be considerably lower than that (Tahershima & Tikalshy, 2017).

FD Model validation

Experimental data selection

The 3D prediction model was applied to three distinct experiments reported in the literature (Nanayakkara & Wannigama, 2003; Ballim, 2004; Madupushpa *et al.*, 2017) in order to verify the potential of the model for different block sizes, concrete mixes, environmental conditions, and boundary conditions. For instance, these experiments cover: concrete dimensions of 350 mm to

1200 mm, cement content of 220 kg/m³ to 493 kg/m³, ambient temperatures of 16–30 °C. Table 1 shows the width (*w*), height (*h*), length (*l*) of each experimental block and the cement content. Table 2 and Table 3 tabulate the thermal properties and the other parameters used in the analysis. These parameters were identified based on the information available from each literature source. In case of the absence of direct information, the thermal parameters were estimated with the guidelines in Bamforth (2007).

In the Ballim (2004) experiment, the temperature was monitored in a 700 × 1000 × 700 mm cuboid. The two opposite 700 × 1000 mm surfaces were insulated using 20 mm thick styrofoam panels in addition to the 18 mm

Table 1: Experimental data

Experiment	<i>w</i> (mm)	<i>h</i> (mm)	<i>l</i> (mm)	Cement content (kg/m ³)
Ballim (2004)	700	700	1000	220
Nanayakkara & Wannigama (2003)	1000	1200	1200	400
Madupushpa <i>et al.</i> (2017)	350	700	1000	493

Table 2: Concrete parameters used for the model verification

Experiment	ρ (kg/m ³)	<i>c</i> (J/g °C)	<i>k</i> (W/m °C)	<i>T</i> ₀ (°C)
Ballim (2004)	2400	1.23	3.5	17
Nanayakkara & Wannigama (2003)	2366	1.38	2.7	32
Madupushpa <i>et al.</i> (2017)	2349	1.13	2.5	27.5

Table 3: Other parameters used for the model verification

Experiment	<i>k</i> _R (W/m °C)	<i>T</i> _R (°C)	<i>h</i> _{plywood} (W/m ² °C)	<i>h</i> _{air} (W/m ² °C)	<i>T</i> _a (°C)
Ballim (2004)	1.2	18	2* or 5	30	16 - 21
Nanayakkara & Wannigama (2003)	1.2	30	2* or 8	14	30
Madupushpa <i>et al.</i> (2017)	1.2	29	6.5	23	29

*Heat transfer coefficient for sides insulated from polystyrene

thick form board (in order to facilitate 2D heat flow). In the Nanayakkara and Wannigama (2003) experiment, a cuboid of 1000 × 1200 × 1200 mm was insulated with 12 mm thick plywood formwork and additionally, the two 1000 × 1200 mm ends were insulated using 25 mm polystyrene panels. A concrete block with similar dimensions to the Ballim (2004) experiment was used in the Madupushpa *et al.* (2017) experiment, and 12 mm plywood formwork was used for all four vertical surfaces. In their experiment, there was a second block cast on top

of the first block after 18 hours from the initial concrete placing (however this second cast was not considered in the current FD modelling).

Figure 2 shows the adiabatic temperature profiles (starting from the initial temperature) used for the analysis of the three experiments. It is of note that, for the FD modelling of the experiment in Nanayakkara and Wannigama (2003), the exact adiabatic detail was not available; hence an adiabatic temperature profile suitable

for the concrete mix was chosen from the data in Wasala and Yapa (2017).

Parametric study

In order to identify the attributes of the 3D prediction model, a parametric study was conducted to compare

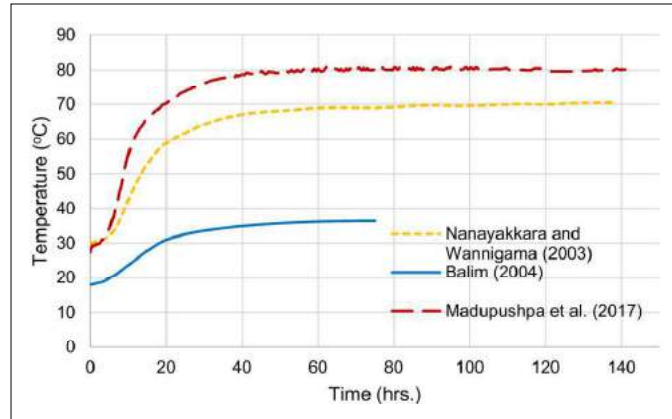


Figure 2: Adiabatic temperature profiles

2D and 3D FD temperature predictions for two distinct applications shown in Figure 3. Here, 1 m high ($z = 1$ m) and 1 m wide ($y = 1$ m) concrete block was considered where the length (l) to width (w) ratio (l/w) was varied at 1 and 2. This selection was made presuming 3D modelling to be more accurate for the $l/w = 1$ scenario, in which the heat flow in the 3rd direction (along the length, x direction) could be considerable.

Temperature simulation of pipe-cooled concrete

Another exclusive potential of 3D numerical modelling is the temperature simulation possibility of pipe-cooled

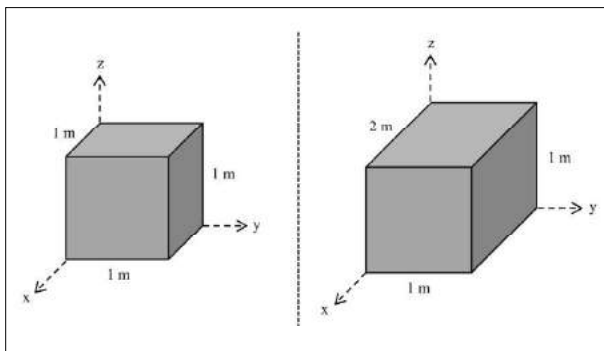


Figure 3: Concrete block dimensions

concrete systems. Generally, the pipe systems do not have regular/symmetric layouts, so, application of 2D modelling for such a scenario is problematic. It is noted that the finite element (FE) simulation potential for the pipe-cooled concrete systems has been extensively explored (Myers *et al.*, 2009; Liu *et al.*, 2015; Zhong *et al.*,

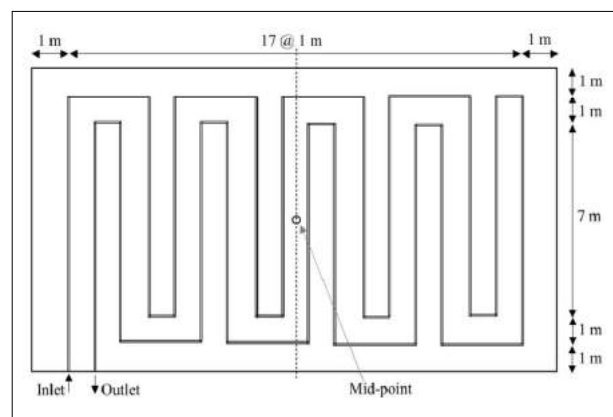


Figure 4: Pipe network arrangement (Kim *et al.*, 2001)

2017). In order to observe the possibility of extending the current 3D FD algorithm towards such systems, a brief attempt was made to model the temperature behaviour of the pipe-cooled concrete unit found in Kim *et al.* (2001). In that investigation, 11 m x 22 m x 2 m concrete footing, which comprised a pipe cooling system at the mid-plane, was cast on a 6 m high rock foundation. Figure 4 shows the pipe network at the mid-plane (at 1 m height) of the footing. The key parameters of the experiment are tabulated in Table 4.

The 3D FD algorithm was extended to incorporate the pipe-cooling system along with the suggestions found in Kim *et al.* (2001). Basically, the nodes in the FD formulation that are along the pipeline represented both concrete and the water pipe where the amount of heat that transfers from the concrete to the water at node (m,n) was formulated as,

Table 4: Experimental properties

Initial concrete temperature (°C)	31
Adiabatic temperature profile	$47[1 - e^{-1.3(t-0.1)}]$
Concrete thermal conductivity (W/m °C)	2.21
Coefficient of convection to atmosphere (W/m ² °C)	10.5
Water volume (m ³ /h)	1.08
Water velocity (m/s)	0.6
Inlet temperature (°C)	25
Thermal conductivity of water (W/m °C)	0.644
Specific heat of water (kJ/kg °C)	4.2
Pipe diameter (mm)	25.4

$$h_w \pi D (T_{c_{m,n}} - T_{w_{m,n}}) \frac{1}{V} \quad \dots(18)$$

where, h_w is the heat transfer coefficient of water, D is the pipe diameter, $T_{c_{m,n}}$ is the concrete temperature at node (m,n) , $T_{w_{m,n}}$ is the water temperature at node (m,n) , and V is the volume of concrete. The governing differential equation for a node that represents both concrete and water then becomes,

$$k \left(\frac{\partial^2 T}{\partial x^2} + \frac{\partial^2 T}{\partial y^2} + \frac{\partial^2 T}{\partial z^2} \right) + \frac{\partial q}{\partial t} = \rho C_p \frac{\partial T}{\partial t} + h_w (\pi D d) (T_{c_{m,n}} - T_{w_{m,n}}) \frac{1}{V} \quad \dots(19)$$

whilst the other concrete nodes are represented from equation (3).

The heat transfer coefficient of water was approximated by Kim *et al.* (2001) as,

$$h_w = 4.75u + 43 \quad \dots(20)$$

where u is the water velocity. Here, h_w is in kcal/m² hr °C, and u is in cm/s, which is valid for $20 \leq u \leq 60$ cm/s. Kim *et al.* (2001) further showed that the temperature of node $(m,n+1)$ of water could be found from,

$$T_{w_{m,n+1}} = \frac{(C_1 - C_2) T_{w_{m,n}} + C_2 T_{c_{m,n}}}{C_1} \quad \dots(21)$$

where,

$$C_1 = Q_w \rho_w C_w \quad \dots(22)$$

and,

$$C_2 = h_w \pi D \Delta \quad \dots(23)$$

Here Q_w is the flow rate, ρ_w is the density of water, C_w is the specific heat capacity of water, Δ is the nodal distance.

RESULTS AND DISCUSSION

Validation results

The FD predictions and the experimental results pertaining to the temperature profile at the centre of each block were compared to verify the prediction model potential. Figures 5(a) to (c) illustrate the comparison of experimental and predicted temperature profiles for each experiment. Table 5 summarizes the comparison for the peak temperature and the corresponding time.

As highlighted in Figures 5(a)–(c), the temperature profiles were predicted with reasonable accuracy. The slight prediction discrepancy noted over the temperature descending branch of the Madupushpa *et al.* (2017) experiment could be possibly due to the secondary cast, which was not incorporated into the prediction model. Table 5 indicates that the maximum deviation for the peak temperature prediction was 2.2 %, and the maximum deviation for the time of reaching the peak temperature was 15 %. Since the peak temperature has more significance than the timing, this prediction accuracy can be deemed satisfactory. Interestingly, Tahershima and Tikalshy (2017) showed that the level of prediction accuracy in their FE element approach in terms of peak temperature and its time were 0.2 % and 9.6 %, respectively. Hence, the potential of the FD approach was, in fact, fairly close to the FE potential. The FD simulations were of cause associated some approximate level of thermal parameters, and hence, there is still room for further

improving the FD prediction accuracy. Furthermore, the incorporation of time-dependent behaviour of the key

parameters (e.g. thermal conductivity) may also improve the prediction precision.

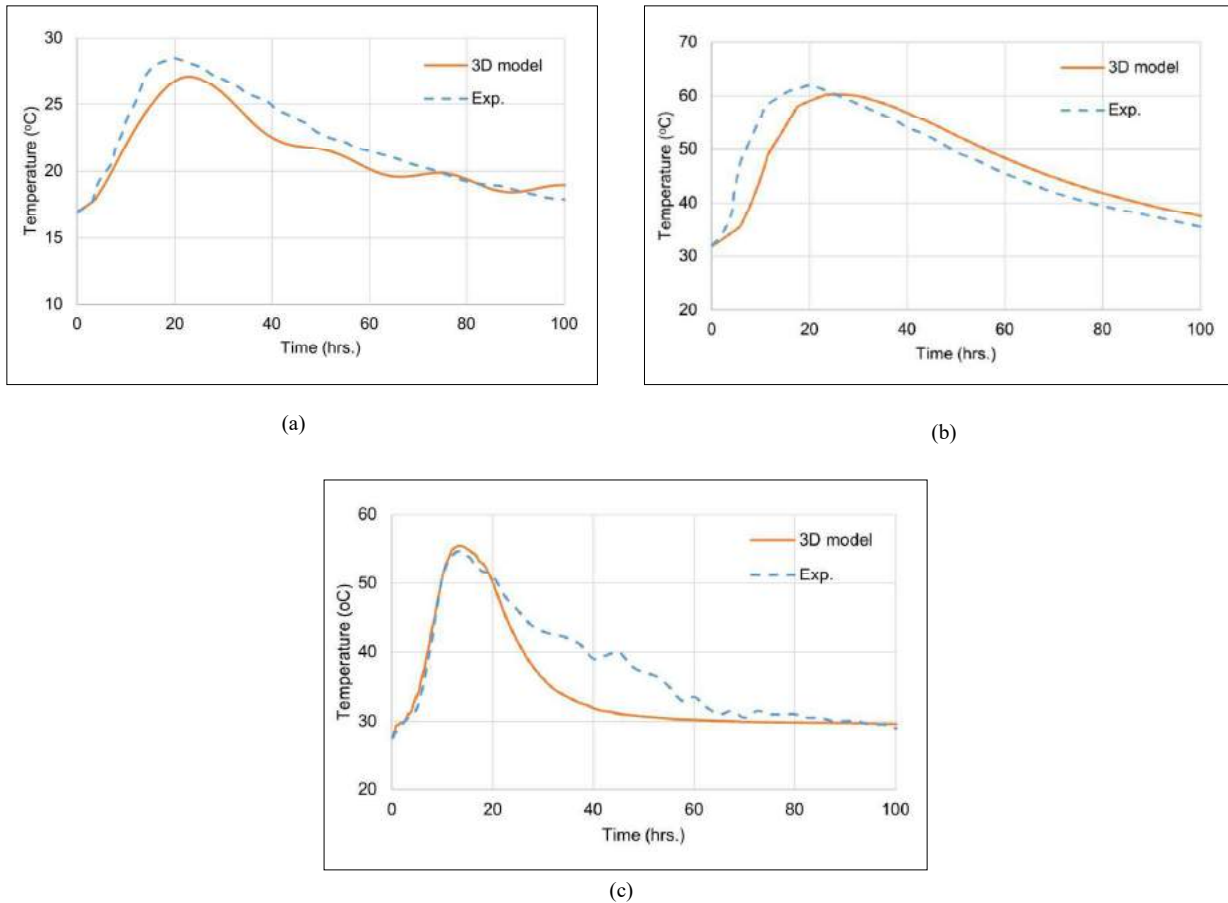


Figure 5: Center node temperature variation: (a) Ballim (2004); (b) Nanayakkara and Wannigama (2003); (c) Madupushpa *et al.* (2017)

Table 5: Validation results

Experiment	Validation results		FD prediction (deviation %)	
	Peak temperature (°C)	Time (hours)	Peak temperature (°C)	Time (hours)
Ballim (2004)	28	20	27.1 (1.9%)	23 (15%)
Nanayakkara & Wannigama (2003)	62	20	60.3 (2.2%)	25.25 (11%)
Madupushpa <i>et al.</i> (2017)	54.5	12.5	55.5 (1.4%)	13.5 (8%)

Parametric study results

Figures 6 and 7 compare the predicted 2D and 3D temperature profiles for the central point of these two scenarios, respectively. It is noted that for the 2D

predictions, 1 m × 1 m central vertical cross section was considered to be the heat flowing cross section for each analysis. The inputs for the algorithm were: $\Delta = 100$ mm, $\rho = 2349$ kg/m³, $c = 1.13$ J/g °C, $k = 2.5$ W/m °C, $k_R = 1.2$ W/m °C, $T_R = 29$ °C, $h_{plywood} = 6.5$ W/m² °C,

$h_{air} = 23 \text{ W/m}^2 \text{ }^\circ\text{C}$, $t_s = 18 \text{ hours}$, $T_a = 29 \text{ }^\circ\text{C}$ and $T_0 = 30 \text{ }^\circ\text{C}$. The adiabatic temperature profile found in the Madupushpa *et al.* (2017) investigation was used to represent concrete with a cement content of about 500 kg/m^3 .

As shown in Figure 6, for the length/ width ratio of one ($l/w = 1$), a difference of about $1 \text{ }^\circ\text{C}$ between the 2D and 3D predictions for the maximum temperatures was observed. Also, a significant prediction discrepancy was observed along the descending branch. In contrast, Figure 7 shows that the two predictions were almost similar for the cuboid ($l/w = 2$) application. As expected, when $l/w = 1$, the heat flow in all three directions is significant in contrast to the $l/w = 2$ condition, where the heat flow along the length (x) is less significant. It is therefore, reasonable to expect the 2D model to make over predictions for the $l/w = 1$ case. Despite the discrepancy for the maximum temperature prediction is not found large, considerable prediction disparity along the descending branch of the 2D model could be

a concern in terms of assessing temperature differentials across the mass, and this fact will be elaborated in the following section.

As a further extension of the parametric study, the 2D and 3D temperature predictions at 20 hours (when peak temperature occurs) along the central width (parallel to y -axis in Figure 3) and the central length (parallel to x -axis in Figure 3) of each concrete block were compared. Figure 8 shows those predictions for the $l/w = 1$ block. It is found that, as previously observed, $1 \text{ }^\circ\text{C}$ prediction discrepancy at the middle of the block diminishes towards the block edges along the width of the block. Despite the 2D model assuming the temperature along the length to be uniform, the 3D prediction shown in Figure 8 depicts that it actually varies significantly towards the edges.

Figures 9 and 10 compare 2D and 3D temperature predictions along the width and length for the cuboid ($l/w = 2$) case, respectively. As previously highlighted, it is shown in Figure 9 that both types of predictions along the width were almost similar. Yet again, along the length

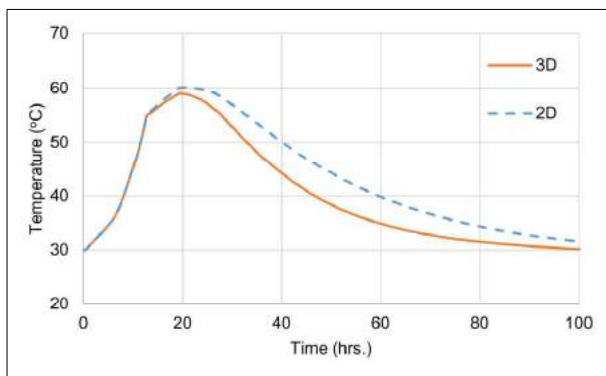


Figure 6: Temperature profiles for the cube ($l/w = 1$) unit

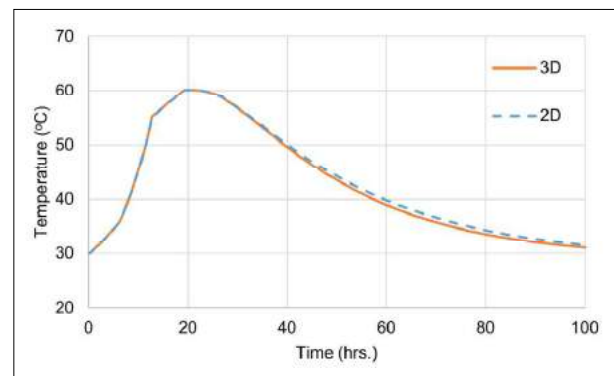


Figure 7: Temperature profiles for the cuboid ($l/w = 2$) unit

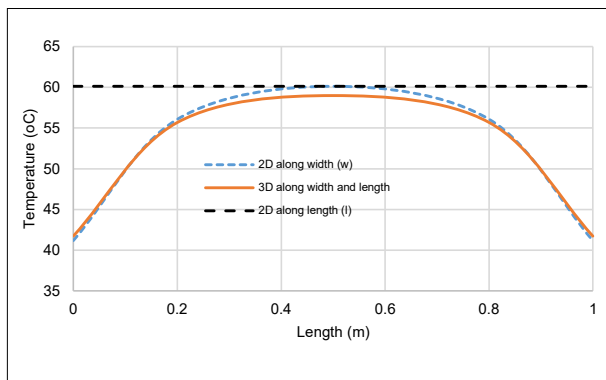


Figure 8: Temperature profiles at the peak temperature (at 20 hrs) of the cube ($l/w = 1$) unit

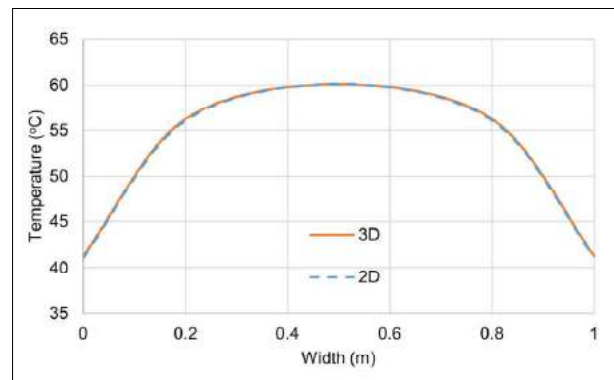


Figure 9: Temperature profiles along the width at peak temperature of the cuboid ($l/w = 2$) unit

(x -direction), the 2D approach assumes it to be constant, whereas the 3D profile follows the actual behaviour, see Figure 10. It is however of note that, along the length, the temperature persists to be stable for a longer length in the $l/w = 2$ block than in the $l/w = 1$ block.

Figure 11 depicts a comparison of 2D and 3D temperature predictions along the width of the $l/w = 1$ block at 50 hours (in the post-peak region). In contrast to the behaviour illustrated in Figure 8, it is noted that the discrepancy between the two types of predictions in the post-peak behaviour is much considerable. As observed in adiabatic vs. semi-adiabatic temperature behaviours for concrete (Ng *et al.*, 2008), during the ascending branch, heat generation dominates, whereas in the descending branch, heat dissipation dominates. Since the heat generation is mostly uniform across the concrete mass whereas the heat dissipation is vastly governed by

the location, in view of concrete temperature modelling, simulation of heat dissipation could be the challenge. For these reasons, it is fair to expect a larger prediction disparity in the post-peak temperature region between the 2D and 3D prediction models. In view of assessing the temperature differential across the mass (to check thermal cracking issues), such prediction inaccuracies in the 2D model could result in over-conservative warnings. Figure 12 depicts the computed temperature difference for each type of simulation, where it clearly highlights the overprediction level of the 2D FE based temperature differential during the post-peak region.

Thus, the parametric analysis highlights the significance of applying a 3D approach for FD based temperature modelling for concrete structures when the structure is of cube shape and when the temperature gradients are to be assessed accurately.

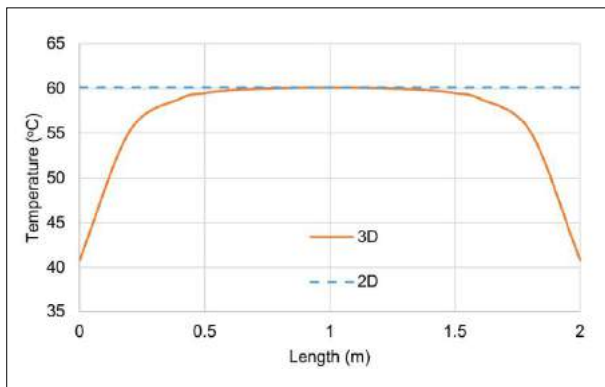


Figure 10: Temperature profiles along length at peak temperature for the cuboid ($l/w = 2$) unit

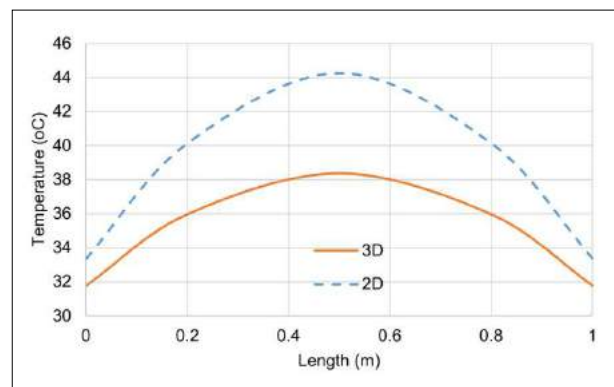


Figure 11: Temperature profiles along length after 50 hours for the cube ($l/w = 1$) unit

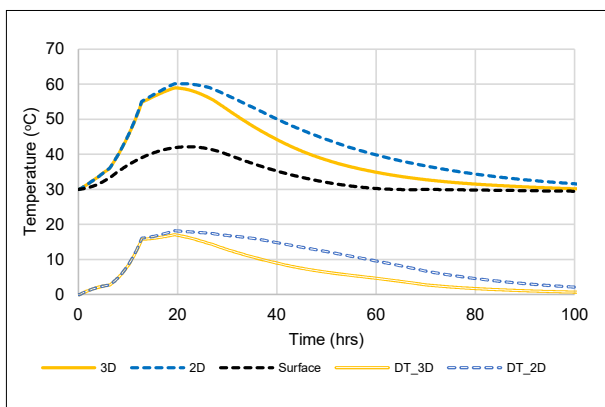


Figure 12: Temperature rise and differential for the cube ($l/w = 1$) unit

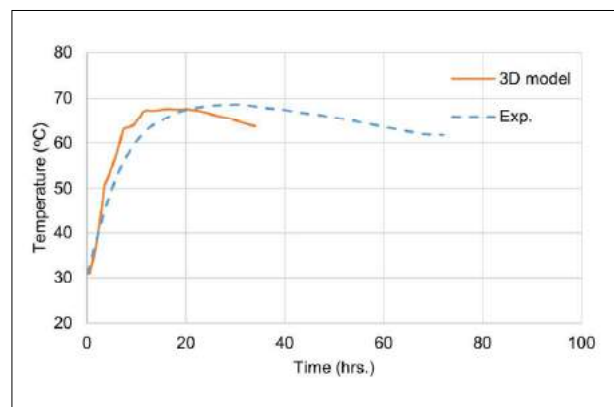


Figure 13: Centre node temperature variation

Pipe-cooled concrete simulation results

Figure 13 compares the 3D FD modelling results with the experimental prediction of Kim *et al.* (2001) for the centre node of the concrete block. As depicted, the experimental maximum temperature at the centre node was about 68.6 °C, whereas the predicted maximum was about 67.6 °C; hence the deviation was below 1.4%. However, there is a considerable discrepancy between the experimental and predicted result in terms of the time to reach a maximum temperature where the deviation was about 33.3%. It has to be noted that during the validation step in the current study, the predicted time was ahead of the actual. However, in this case, it is vice-versa. Hence, the rate of heat absorption by the water has not accurately been captured by the current FD version, and therefore, further tuning up of the model is necessary. Such improvement of the 3D FD model is identified as a matter for future work.

CONCLUSIONS

An existing 2D Finite Difference (FD) model was extended into the 3D form in order to expand its capacity to predict the early age temperature profile of concrete. The potential of the developed 3D tool was verified for three distinct experiments found in the literature. The prediction accuracy was impressive, and the maximum deviation for the peak temperature and the pertaining time predictions were less than 2.2% and 15%, respectively. In addition, a parametric study highlighted the significance of using 3D temperature modelling in contrast to using 2D modelling for cube shape structures where the heat flow in all three (x,y,z) directions is significant. The applicability of the 3D approach to model concrete masses that comprise internal pipe cooling networks was also investigated and need further improvements.

Conflicts of interest

The authors declare that there is no conflict of interest.

REFERENCES

- Azenha M., Lameiras R., Sousa C. & Barros J. (2014). Application of air cooled pipes for reduction of early age cracking risk in a massive RC wall. *Engineering Structures* **62–63**(15): 148–163.
DOI: <https://doi.org/10.1016/j.engstruct.2014.01.018>
- Ballim Y. (2004). A numerical model and associated calorimeter for predicting temperature profiles in mass concrete. *Cement and Concrete Composites* **26**: 695–703.
DOI: [https://doi.org/10.1016/S0958-9465\(03\)00093-3](https://doi.org/10.1016/S0958-9465(03)00093-3)
- Ballim Y. & Graham P.C. (2003). A maturity approach to the rate of heat evolution in concrete. *Magazine of Concrete Research* **55**(3): 249–256.
DOI: <https://doi.org/10.1680/mac.55.3.249.37571>
- Bamforth P.B. (2007). *Early-Age Thermal Crack Control in Concrete*. CIRIA, London, UK.
- Bobko C.P., Zadeh V.Z. & Seracino R. (2015). Improved Schmidt method for predicting temperature development in mass concrete. *ACI Materials Journal* **112**(4): 579–586.
DOI: <https://doi.org/10.14359/51687454>
- Dissanayake D.M.M.P., Dissanayake D.M.M. & Yapa H.D. (2017). Numerical modelling of temperature development in concrete comprising pipe-cooling networks. *Proceedings of the 8th International Conference on Structural Engineering and Construction Management*, Kandy, Sri Lanka, pp. 18–27.
- Holman J.P. (1986). *Heat Transfer*. International Student Edition. McGraw-Hill Book Company, Singapore.
- Kim J.K., Kim K.H. & Yang J.K. (2001). Thermal analysis of hydration heat in concrete structures with pipe-cooling system. *Computers and Structures* **79**: 163–171.
DOI: [https://doi.org/10.1016/S0045-7949\(00\)00128-0](https://doi.org/10.1016/S0045-7949(00)00128-0)
- Liu X., Zhang C., Chang X., Zhou W., Cheng Y. & Duan Y. (2015). Precise simulation analysis of the thermal field in mass concrete with a pipe water cooling system. *Applied Thermal Engineering* **78**(5): 449–459.
DOI: <https://doi.org/10.1016/j.applthermaleng.2014.12.050>
- Madupushpa K.D., Kahatapitiya N.K.S.S. & Yapa H.D. (2017). Numerical prediction of concrete temperature. *Proceedings of the 5th International Symposium on Advances in Civil and Environmental Engineering Practices for Sustainable Development*, Sri Lanka, pp. 347–354.
- Mataaraarachchi A.I.G.K., Nanayakkara S.M.A. & Asamoto S. (2012). Control of thermal cracking in concrete water retaining structures, *Proceedings of the Second Annual Sessions*, Society of Structural Engineers Sri Lanka, Colombo.
- Myers T.G., Fowkes N.D. & Ballim Y. (2009). Modeling the cooling of concrete by piped water. *Journal of Engineering Mechanics* **135**(12): 1375–1383.
DOI: [https://doi.org/10.1061/\(ASCE\)EM.1943-7889.0000046](https://doi.org/10.1061/(ASCE)EM.1943-7889.0000046)
- Nanayakkara S.M.A. & Wannigama W.R.K. (2003). Experimental investigations on temperature rise due to heat of hydration. *Annual transaction of Institution of Engineers*, Sri Lanka, pp. 9–15.
- Neville A.M. (2011). *Properties of Concrete*, 5th Edition. Pearson Education Ltd., Harlow, UK.
- Ng P.L., Ng I.Y. & Kwan A.K. (2008). Heat loss compensation in semi-adiabatic curing test of concrete. *ACI Materials Journal* **105**(1): 52–61.
DOI: <https://doi.org/10.14359/19207>
- Patini A. (2011). Numerical analysis of temperature development in concrete at an early age. *MSc thesis*. University of Witwatersrand, Johannesburg, South Africa.
- Riding K.A., Poole J.L., Schindler A.K., Juenger M.C. & Folliard K.J. (2006). Evaluation of temperature prediction methods for mass concrete members. *ACI Materials*

- Journal* **103**(5): 357–365.
DOI: <https://doi.org/10.14359/18158>
- Soutsos M., Hatzitheodorou A., Kwasny J. & Kanavaris F. (2017). Effect of temperature on the strength development of mortar mixes with GGBS and fly Ash. *Magazine of Concrete Research* **69**(15): 787–801.
DOI: <https://doi.org/10.1680/jmacr.16.00268>
- Tahersima M & Tikalsky P. (2017). Finite element modeling of hydration heat in a concrete slab-on-grade floor with limestone blended cement. *Construction and Building Materials* **154**: 44–50.
DOI: <https://doi.org/10.1016/j.conbuildmat.2017.07.176>
- Taylor H.F.W., Famy C. & Scrivener K.L. (2001). Delayed ettringite formation. *Cement and Concrete Research* **31**(5): 683–693.
DOI: [https://doi.org/10.1016/S0008-8846\(01\)00466-5](https://doi.org/10.1016/S0008-8846(01)00466-5)
- Wasala W.M.T.D. & Yapa H.D. (2017). Prediction of temperature development in concrete using semi-adiabatic temperature measurements. *Engineer: Journal of the Institution of Engineers, Sri Lanka* **50**(3): 1– 8.
DOI: <https://doi.org/10.4038/engineer.v50i3.7261>
- Yang J., Hu Y., Zuo Z., Jin F. & Li Q. (2012). Thermal analysis of mass concrete embedded with double-layer staggered heterogeneous cooling water pipes. *Applied Thermal Engineering* **35**: 145– 156.
DOI: <https://doi.org/10.1016/j.applthermaleng.2011.10.016>
- Yikici T.A. & Chen H. (2015). Numerical prediction model for temperature development in mass concrete structures. *Journal of the Transportation Research Board* **2508**(1): 102–110.
DOI: <https://doi.org/10.3141/2508-13>
- Zhong R., Hou G. & Qiang S. (2017). An improved composite element method for the simulation of temperature field in massive concrete with embedded cooling pipe. *Applied Thermal Engineering* **124**: 1409– 1417.
DOI: <https://doi.org/10.1016/j.applthermaleng.2017.06.124>

RESEARCH ARTICLE

Acaricide resistance in the spinose ear tick, *Otobius megnini* (Acari: Argasidae) infesting racehorses in Sri Lanka

GCP Diyes^{1,2}, KMUJ Bandara¹, RS Rajakaruna^{*1} and SHPP Karunaratne¹

¹ Department of Zoology, Faculty of Science, University of Peradeniya, Peradeniya.

² Department of Biology, University of Saskatchewan, 112 Science Place, Saskatoon, SK S7N 5E2, Canada.

Submitted: 24 November 2020; Revised: 11 May 2021; Accepted: 03 August 2021

Abstract: The spinose ear tick *Otobius megnini* is a causative agent of otoacariasis in horses and jockeys in the Nuwara Eliya racecourses. The present study aimed at investigating the status of acaricide resistance and underlying mechanisms in this tick species under laboratory conditions. Live ticks collected from the ear canal of horses were used to establish a laboratory colony. Larval bioassays were carried out with an organophosphate (malathion), pyrethroids (flumethrin and permethrin), and an organochlorine (DDT) using Larval Packet Tests (LPT). The LC₅₀ (24 h) values for malathion, flumethrin, permethrin and DDT were recorded as 0.11%, 0.0003%, 0.008% and 0.124%, respectively, and the respective values for LC₉₀ were 0.722%, 0.004%, 0.300% and 3.049%. Biochemical assays revealed that the mean specific activity levels of esterase, glutathione S-transferases (GSTs), and monooxygenase amounts were $0.064 \pm 0.008 \mu\text{mol min}^{-1} \text{mg}^{-1}$, $0.104 \pm 0.050 \mu\text{mol min}^{-1} \text{mg}^{-1}$, and 0.068 ± 0.020 equivalent units of cytochrome P450, respectively. The percentage remaining activity of the propoxur-inhibited Acetylcholinesterase (AChE) was $33.88 \pm 13.60\%$. Our data indicated that the *O. megnini* population of Nuwara Eliya, Sri Lanka was most susceptible to flumethrin and showed resistance to DDT. Development of resistance to malathion through increased activity of esterase and insensitive AChEs was evident. Since the activities of monooxygenases and GSTs were not enhanced, permethrin and DDT resistance may have developed through target site insensitivity.

Keywords: Biochemical assays, DDT, ectoparasiticide, flumethrin, malathion, permethrin.

INTRODUCTION

The spinose ear tick *Otobius megnini* (Acari: Argasidae) is a nidicolous soft tick whose immature stages (larvae and nymphs) parasitize domestic animals and occasionally humans causing otoacariasis. *Otobius megnini* has four developmental stages in its life cycle: egg, larva, nymph and adult (male/female) and completes its life cycle on a single host with larvae and nymphs parasitizing for several days to months (Nava *et al.*, 2009; Diyes & Rajakaruna, 2017). The unfed larvae are highly active, and it is the only life stage that participates in a host-seeking activity. Following attachment, larvae feed for 8–13 days before moulting to nymphs and these nymphs continue feeding for another 17–37 days. After that, fully engorged nymphs detach and moult to non-feeding adults on the ground. After successful mating, females lay eggs in a refuge. The life cycle of *O. megnini* stretches over 51 to 901 days (Diyes & Rajakaruna, 2017). The life cycle duration strongly depends on the prevailing temperature and relative humidity. The presence of the tick inside the ear canal causes severe pain and irritation and can lead to toxic conditions, eardrum perforation, muscle spasms, and otitis (Madigan *et al.*, 1995; Estrada-Peña & Jongejan, 1999). Additionally, disease-causing agents such as *Coxiella burnetii* (Desjardins *et al.*, 2018),

* Corresponding author (rupikar@pdn.ac.lk;  <https://orcid.org/0000-0001-7939-947X>)



This article is published under the Creative Commons CC-BY-ND License (<http://creativecommons.org/licenses/by-nd/4.0/>). This license permits use, distribution and reproduction, commercial and non-commercial, provided that the original work is properly cited and is not changed in anyway.

Borrelia burgdorferi (Fivaz et al., 1991) and *Babesia* (Diyes et al., 2018) have been detected in blood meal analysis of *O. megnini*.

In Sri Lanka, this tick species appears to have a limited distribution. To date, there are no records on *O. megnini* infestations in any domesticated animals except the horses and jockeys in the Nuwara Eliya racecourses. However, the dynamic nature of the life cycle with high population stability has enabled *O. megnini* to become an invasive tick species in the Nuwara Eliya racecourse. Controlling *O. megnini* using acaricides is not very common due to its presence in the ear canal of the horse. Current control practices used to manage *O. megnini* infestations include regular cleaning of the ear canals of the horses and frequent renewal of the sawdust inside the stables. However, effective complete control of *O. megnini* infestations is hard. Consequently, alternative control strategies, including vaccines and, synthetic and botanical acaricides are essential.

The application of synthetic acaricides such as carbamates, organophosphates, synthetic pyrethroids, formamidines, macrocyclic lactones and pyrazoles have played a pivotal role in controlling ticks worldwide (Lovis et al., 2011). However, the long-term use of these compounds has resulted in the development of acaricide resistance, thereby reducing the effectiveness (Graf et al., 2004). Therefore, constant monitoring of the level of susceptibility of pests to these chemicals is required to control the spread of any acquired resistance (Graf et al., 2004). However, to the best of our knowledge, there were no previously published reports on the susceptibility of *O. megnini*. Therefore, it is important to collect baseline data on the level of acaricide susceptibility of *O. megnini*.

In both insects and acarines, elevated enzymatic activity and target site insensitivity are the two major metabolic resistance mechanisms to insecticides (Karunaratne et al., 2018). The high enzymatic activity involves variations in insecticide metabolizing enzymes, i.e., esterases, glutathione-S-transferases (GSTs) and monooxygenases, which metabolize the acaricide before reaching the target site. However, target site insensitivity is the inability of mutated target sites to recognize the acaricide. Recently, Bandara and Karunaratne (2017) reported that DDT and malathion resistance in the cattle tick *Rhipicephalus microplus* from Sri Lanka was caused by both elevated esterase activity and insensitive target sites. Here, we determined the status of acaricide susceptibility of *O. megnini* larvae against four commonly used acaricides: malathion, flumethrin, permethrin, and DDT. The activity of acaricide metabolizing enzymes,

and the insensitivity of the organophosphate and carbamate target site to acetylcholinesterase were also investigated to understand the potential mechanism of resistance.

METHODOLOGY

Tick collection and rearing

Live specimens of *O. megnini* were collected from 14 stabled thoroughbred horses in a racecourse in Nuwara Eliya (GPS: 6.9628 N 80.7692 E). Immediately after collecting the ticks, they were transferred to a laboratory facility where they were weighed and separated according to life stage. Fully engorged nymphs weighing over 60 mg were used to establish the laboratory tick colony. Nymphs were not fed after the collection because female ticks do not require an additional blood-meal to produce eggs (Diyes & Rajakaruna, 2017). Tick rearing chambers were prepared according to Sonenshine (1993) and were maintained at $28 \pm 2^\circ \text{C}$ under 96% relative humidity (RH) until nymphs molted into adults. New horse-blood-fed nymphs were introduced biweekly to the tick-rearing chambers to maintain a high genetic diversity in the colony.

In total, 100 engorged females, weighing from 60 to 120 mg, were used in this study. Each female was transferred into a separate slot of a 30-well plastic grid plate. Multiple plates were used to house all the females. After that, males were introduced to each female. Plates containing mating pairs were placed in a glass chamber kept in darkness and maintained at $28 \pm 2^\circ \text{C}$ under 96% RH until oviposition. The eggs obtained from multiple females were mixed, subdivided into groups of 150 and then transferred into Eppendorf® tubes with perforated caps. Eggs, and later larvae, were maintained under the same conditions as those of females. Tubes were monitored daily for any fungal or mite infestations and were changed whenever contamination was observed. The tick colonies were maintained between September 2014 and March 2015. Larvae at the age of 14 to 21 days were used for all the bioassays.

Acaricide bioassays

A total of 8,408 larvae of *O. megnini* were subjected to acaricide bioassays. Acaricide bioassays were conducted using four technical grade acaricides, i.e., organochlorine (DDT), organophosphate (malathion) and two pyrethroids (permethrin and flumethrin) (Sigma Chemicals, UK) using the experimental protocol described by Larval Packet Test (LPT) (FAO, 2004). As there were no

recommended dosages by FAO for soft ticks, the dosage recommended for hard ticks was used (Bandara & Karunaratne, 2017). Acaricide solutions with different concentrations were prepared using olive oil:acetone (1:2; analytical grade) as the solvent. All concentrations used ranged from 10^{-6} to 10%. These concentrations (v/v for malathion and w/v for DDT, flumethrin and permethrin) were determined using published dose-response data for ticks (Bandara & Karunaratne, 2017; Miller *et al.*, 1999) and by conducting preliminary studies. An aliquot of 0.7 mL from each dilution was evenly distributed on a Whatman No.1 filter paper (7.5 cm × 9.0 cm) (Miller *et al.*, 1999) and the control received the solvent alone. Acaricide impregnated papers were wrapped individually in aluminium foil and stored at 4° C until the larvae reached 14–21 days old (FAO, 2004). They were used within a month after preparation, and each paper was used in a maximum of two trials/replicates (WHO, 2016) as follows. An acaricide impregnated paper was folded along the middle line with the impregnated surface inside and two bulldog clips were fixed on two opening sides, making a packet (FAO, 2004). Tick larvae (150 larvae) were inserted into the packet with the aid of a fine brush through the remaining open side and a third bulldog clip was used to seal the opening end. The packets were kept in separate humidity chambers with a temperature of 27–28° C, and 85–95% RH. Mortality was recorded after 24 h after exposure to the treatment. Larvae that did not show a response to a needle touch were considered dead. A hand lens was used to confirm the response, whenever necessary. According to FAO (2004), if the mortalities of the controls were less than 5% of the mortalities of the treated, sample mortalities can be directly used for analyses without correction. However, if control mortalities were between 5–10%, the mortalities of the treated sample must be adjusted using Abbott's formula (FAO, 2004). Since there were no mortalities observed in the controls, the mortalities of the treated samples were processed normally. All the acaricide bioassays were performed in triplicate.

Statistical analysis

Mortality values were plotted against acaricide concentrations to obtain log concentration-probit regression lines using Sigma Plot software (version 10.0). For each tested acaricide, lethal concentrations that kill 50% (LC_{50}) and 90% (LC_{90}) of the packet population, confidence intervals (CI) of 95% and the slope of the regression line (through regression analysis) were determined. A Chi-square test was used to evaluate the goodness of fit of the linear regression

to log concentration-probit transformed data. Resistance discriminating dosages were not available for *O. megnini*. Therefore, we adopted a method similar to Bandara and Karunaratne (2017) to evaluate the current resistance/susceptibility status of *O. megnini* larvae. Here, the discriminating dosages available for *Rhipicephalus microplus* (Acari, Ixodidae) (FAO, 2004) were used to assess the susceptibility/resistance status of the *O. megnini* population: susceptible (98–100% mortality), possible resistant (90–97.9% mortality) and resistant (< 90% of mortality) (WHO, 2016). Discriminating dosages given for anopheline mosquitoes (WHO, 2016) were also used to evaluate the susceptibility/resistance status due to the absence of discriminating dosages for *O. megnini* or other ticks.

Biochemical assays

All the biochemical assays were carried out according to the procedures recommended by WHO (1998a) with slight modifications. Randomly selected *O. megnini* larvae were subjected to total protein, esterase, glutathione S-transferase (GST), monooxygenase and acetylcholinesterase assays in two replicates. Larvae were homogenized in groups of 25 individuals in 150 μ L ice-cold distilled water. An aliquot of 50 μ L was taken for the two replicates of AChE assay and the rest was centrifuged at 13,000 rpm for 2 min. The supernatant was used for esterase, GST, monooxygenase and protein assays (WHO, 1998a). This whole experiment was repeated 21 times. The average values from 21 homogenates (total number of larvae = 25 × 21) were used for the analysis. The results of the following biochemical assays are expressed as mean ± SD.

Acetylcholinesterase assay

Two 25 μ L aliquots of crude homogenate were added to two consecutive microtiter plate wells. The membrane-bound AChE in the mosquito homogenate was solubilized by adding 145 μ L of 1% (v/v) Triton X-100 in 0.1 M phosphate buffer (pH 7.8). Ten microliters of the substrate solution dithobis-2 nitrobenzoic acid (DTNB) in phosphate buffer (pH 7.0) was added to each aliquot. To one replicate, 25 μ L of acetylthiocholine iodide (ASChI) and propoxur solution (10 mL of 0.01 M ASChI 20 μ L of 0.1 M propoxur in acetone) were added. To the other replicate, 25 μ L of 0.01 M ASChI alone was added. The plate was read at 405 nm for 5 min. Results were expressed as the percentage remaining activity in the inhibited fraction and was compared with the control (uninhibited) activity (WHO, 1998b).

Glutathione-S-transferase assay

To prepare the working solution, 0.5 mL of 63 mM I-chloro-2,4-dinitro benzene (CDNB) in methanol and, 9.5 mL of 10 mM reduced glutathione (GSH) in 100 mM phosphate buffer (pH 6.5) were mixed. Ten microliters of each insect homogenate was mixed with 200 μ L of freshly prepared GSH/CDNB working solution in a microtiter plate well. The enzyme reaction rate was measured at 340 nm at 12 s intervals for 5 min. An extinction coefficient of 5.76 mM^{-1} (corrected for the path length of 0.6 cm) was used to convert the absorbance values to moles product. Thus, the GST activity per individual was reported as CDNB conjugated $\mu\text{mol product min}^{-1}\text{mg}^{-1}$ protein (Karunaratne & Hemingway, 1996).

Carboxylesterase assay

A stock solution of 100 mM *p*-nitrophenyl acetate (*p*NPA) was prepared in acetone. The working solution of *p*NPA (1 mM) was prepared freshly for each assay by adding 50 μ L of 100 mM *p*NPA stock solution into 5 mL of 50 mM phosphate buffer (pH 7.4). Ten microliters of each homogenate were mixed with 200 μ L of the 1 mM *p*NPA working solution in a microliter plate well. The reaction rate was read immediately at 12s intervals at 405 nm for 2 min at 21 °C. An extinction coefficient of 6.53 mM^{-1} (correlated for the path length of 0.6 cm) was used to convert the absorbance values to moles product. The *p*NPA activity per individual was reported as $\mu\text{mol product min}^{-1}\text{mg}^{-1}$ protein.

Cytochrome P450 monooxygenase assay

Twenty microliters of each insect homogenate were mixed with 80 μ L of potassium phosphate buffer (pH 7.2) + 200 μ L of 6.3 mM tetramethylbenzidine (TMBZ) working solution [0.01 g TMBZ dissolved in 5 mL methanol and then in 15 mL of sodium acetate buffer (pH 5.0) + 25 μ L of 3% H_2O_2 solution] in a microtiter plate well. After 2 h of incubation at room temperature, the plate was read at 630 nm as an endpoint assay. This assay does not measure the monooxygenase activity but titrates the amount of heme in the mosquito homogenate. Since heme is present in the active site of the monooxygenases, the amount of heme corresponds to the amount of monooxygenases present. Using a standard curve of cytochrome C, an estimate of the amount of monooxygenases present was obtained and expressed as equivalent units of cytochrome P450.

Protein assay

To obtain specific activities of enzymes, protein concentrations of the tick homogenates were determined by BIO-RAD protein determination kit, using bovine serum albumin as the standard protein. Ten microliters of homogenate were mixed with 300 μ L of BIO-RAD working solution (prepared according to the instructions of the manufacturer), and the absorbance was read at 630 as an endpoint assay after a 5-minute incubation at room temperature.

RESULTS AND DISCUSSION

Dose-response mortalities against DDT, malathion, flumethrin and permethrin are summarized in Table 1 and the log concentration-probit mortalities are shown in Figures 1–4. No larval mortalities were detected in untreated controls. LC_{50} and LC_{90} (24 hours exposure) values along with 95% confident intervals (CI) are listed in Table 2. Ninety-five percent CI values were narrow at LC_{50} and LC_{90} levels in all graphs except for malathion and DDT at the LC_{90} level, where they were much wider. Except for permethrin, χ^2 values for the

Table 1: Percentage mortalities of *Otobius megnini* for malathion, flumethrin, permethrin and DDT as determined by Larval Packet Test (LPT) bioassays (FAO, 2004)

Acaricide concentration (%)	Mean (%) mortality			
	Malathion	Flumethrin	Permethrin	DDT
0.00001	*	7.29	*	*
0.0001	12.28	7.89	7.65	1.77
0.0005	27.91	*	16.22	*
0.00075	*	*	17.53	*
0.001	18.31	81.50	22.81	3.56
0.005	22.68	*	47.92	*
0.01	62.92	98.74	53.43	4.70
0.05	*	99.62	*	*
0.1	63.86	99.62	100	11.30
0.5	50.00	100	*	*
1	97.78	*	*	59.77
2	*	*	*	93.97
5	*	*	*	99.46
7	*	*	*	100

* Not tested

goodness-of-fit estimations were high and significant (Table 2). The regression coefficient was highest for permethrin and similar for the other three acaricides (Table 2). Since discriminating dosages of acaricides are not available for *O. megnini* in the literature, the resistance of *O. megnini* was measured using the established discriminating dosages for the Australian and Yeerongpilly strains of *Rhipicephalus microplus* (FAO, 2004) and anopheline mosquitoes (WHO, 2016). Although a direct determination of resistance cannot be made using discriminating dosages specified for other species, a comparison was attempted in order to obtain a rough estimation (Figures 1 to 4 and Table 2). According to anopheline discriminating dosages, the *O. megnini* population had possible resistant genes for malathion (2.93% survivals), permethrin (5.38%) and DDT (8.0%). With Australian *R. microplus* discriminating dosages, *O. megnini* population was susceptible to flumethrin

(0.05% survivals) but resistant to DDT (13.77% survivals). However, *O. megnini* population was resistant to flumethrin when the discriminating dosage of the Ceremonially strain of *R. microplus* was considered (10.79% survivals) (Table 2). It is important to develop separate discriminating dosages for *O. megnini* using a laboratory-maintained susceptible strain to obtain accurate results. S-shaped mortality curve in Figure 5 indicates the heterogenic response (i.e. both susceptible and resistant) of the *O. megnini* population to DDT (FAO, 2004). The mean specific activity levels of esterases and GSTs, and the amount of monooxygenases obtained from the biochemical assays were $0.064 \pm 0.008 \mu\text{mol min}^{-1} \text{mg}^{-1}$, $0.104 \pm 0.05 \mu\text{mol min}^{-1} \text{mg}^{-1}$ and 0.068 ± 0.02 equivalent units of cytochrome P450, respectively. The percentage remaining activity of the target site AChE, after propoxur inhibition was 33.88 ± 13.6 .

Table 2: LC₅₀ and LC₉₀ values for malathion, flumethrin, permethrin, and DDT as determined by Larval Packet Test (LPT) acaricide bioassays (FAO, 2004) for the Sri Lankan population of *Otobius megnini*

Acaricide	Slope	SE	LC ₅₀ (%) (95% CI)	LC ₉₀ (%) (95% CI)	χ^2 (df)	R ²	DD (%)	R (%)	Resistance status**
Malathion (n=1741)	8.87	13.30	0.011 (0.048–0.002)	0.722 (60.284–0.113)	28.11* (7)	0.84	5 ^a	2.93	Possible resistant
Flumethrin (n=2567)	7.56	10.14	0.0003 (0.001–0.0001)	0.004 (0.015–0.001)	18.19* (5)	0.73	0.01 ^{b1} 0.0036 ^{b2}	0.05 10.79	Susceptible Resistant
Permethrin (n=2087)	10.88	2.60	0.008 (0.0132–0.0049)	0.300 (1.2112–0.111)	1.18 (5)	0.95	0.75 ^a	5.38	Possible resistant
DDT (n=2013)	9.42	19.40	0.124 (2.852–0.013)	3.049 (1703.73–0.291)	51.53* (6)	0.77	4 ^a 2 ^{b1}	8.00 13.77	Possible resistant Resistant

N = total number of individuals used; SE = standard error; LC = lethal concentration; CI = confident intervals; χ^2 = goodness of fit (Log concentration-probit transformed data); R² = regression coefficient; DD = discriminating dosage; R = resistance percentage; * = p < 0.05

^a = discriminating dosage for anopheline mosquitos (WHO, 2016)

^b = discriminating dosage for ^{b1}Australian and ^{b2}Yeerongpilly strains of *Rhipicephalus microplus* (FAO, 2004).

**Resistance status was determined as susceptible (98–100 % mortality), possible resistant (90–97.9 % mortality) and resistant (< 90 % mortality) (WHO, 2016)

This study reports the first evidence of the development of acaricide resistance in spinose ear ticks, which infest the horses in the world. Resistance status was assessed using the larval packet test described by Stone and Haydock (1962) and later adopted and recommended by the Food and Agriculture Organization (FAO, 2004). This is a low cost straightforward method, which has been widely used to assess the resistance levels in hard and soft ticks, including *R. microplus*, *R. sanguineus*,

Hyalomma anatolicum and *Ornithodoros savignyi* (Miller *et al.*, 2001; Ahmed *et al.*, 2007; Lovis *et al.*, 2011; Shyma *et al.*, 2012; Bandara & Karunaratne, 2017). Ahmed *et al.* (2007) executed the same larval packet test for the soft tick *O. savignyi* but did not provide a discriminative dosage. Recently, Surbhi *et al.* (2018) used an adult immersion test for resistance trials in *O. savignyi* but results from this technique were difficult to compare with LPT results.

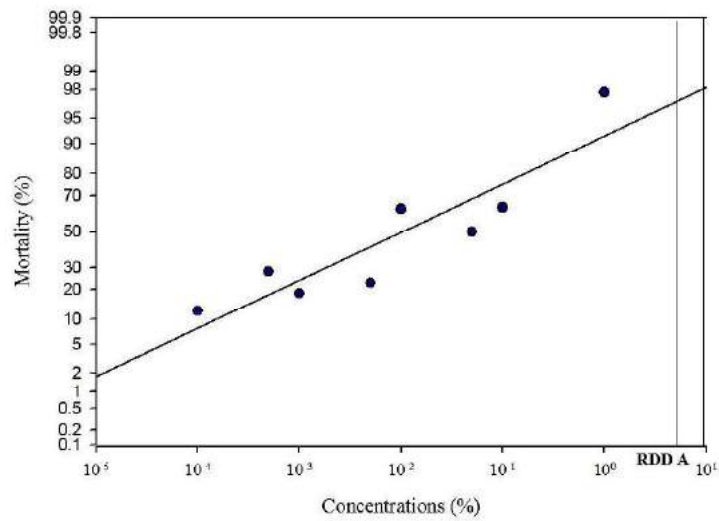


Figure 1: Log concentration-probit mortality of *Otobius megnini* for malathion as determined by the Larval Packet Test (LPT). The RDD A line indicates the resistance discriminating dosage (5%) for anopheline mosquitos (WHO, 2016).

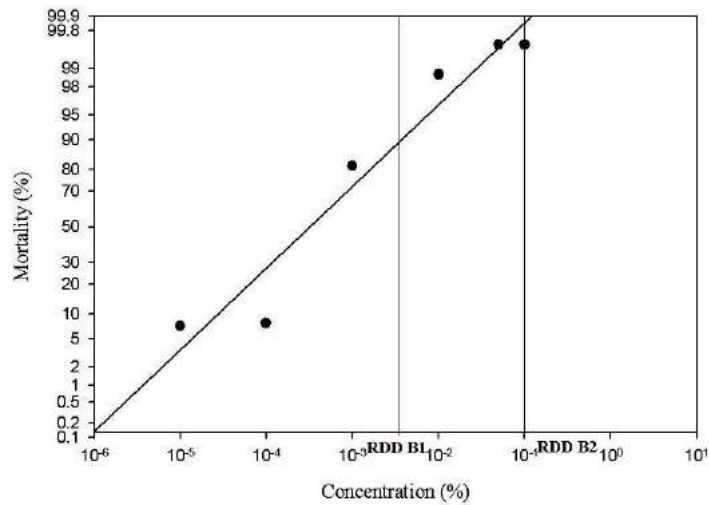


Figure 2: Log concentration-probit mortality of *Otobius megnini* for flumethrin as determined by the Larval Packet Test (LPT). The RDD B1 and RDD B2 lines indicate the resistance discriminating doseages for Australian (0.0036%) and Yeerongpilly strains (0.01%) of *Rhipicephalus microplus*, respectively (FAO, 2004).

The discriminative dosage is generally assessed by doubling the mean LC_{99.9} for a particular acaricide derived from a susceptible population (WHO, 2016). Susceptible strains of ticks are usually maintained under optimal conditions within laboratories for generations. Since this

is the first study carried out in Sri Lanka for *O. megnini*, a reliable susceptible-haplotype could not be found during the investigation. Since data for a susceptible *O. megnini* population were lacking, discriminating dosages available for hard tick *R. microplus* (FAO, 2004) were

used to assess the acaricide susceptibility of *O. megnini*. The presence of resistance was seen only against DDT. Two Sri Lankan populations of *R. microplus* have shown LC₅₀ values of 0.04% and 0.03% for malathion, 0.002% and 0.001% for permethrin, 3.68% and 0.21%

for DDT, respectively (Bandara & Karunaratne, 2017). In comparison to Bandara and Karunaratne (2017), the present study showed that the tested *O. megnini* population has a similar LC₅₀ value for malathion, a higher value for permethrin and a lower value for DDT.

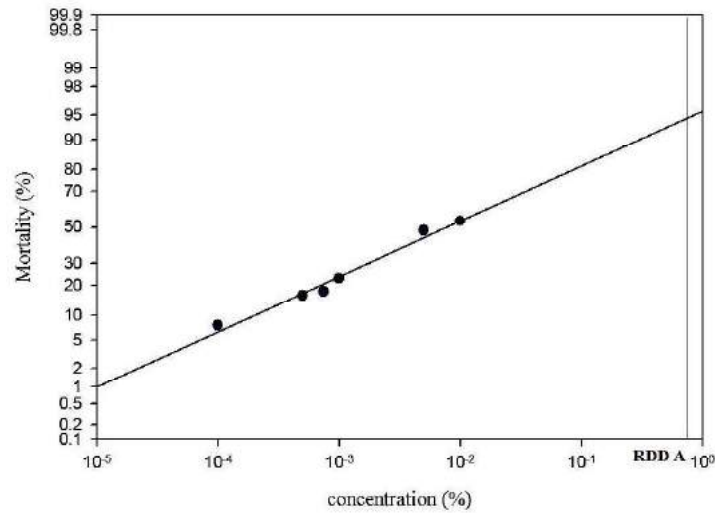


Figure 3: Log concentration-probit mortality of *Otobius megnini* for permethrin as determined by the Larval Packet Test (LPT). The RDD A line indicates the resistance discriminating dosage (0.75%) for anopheline mosquitos (WHO, 2016).

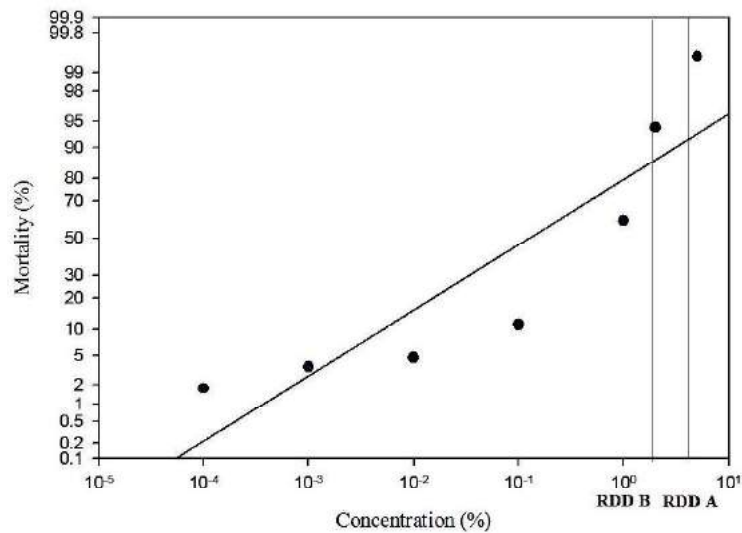


Figure 4: Log concentration-probit mortality of *Otobius megnini* for DDT as determined by the Larval Packet Test (LPT). The RDD A and RDDB lines indicate the resistant discriminating dosages for anopheline mosquitos (4%) and *Rhipicephalus microplus* (2%), respectively (FAO, 2004; WHO, 2016).

However, mortality outcomes must be analysed carefully and interpreted cautiously when comparing data across different species as there are several species-specific

interfering factors, including rate of acaricide/ insecticide absorption and physiology of the organism, which can contribute to the mortality rate.

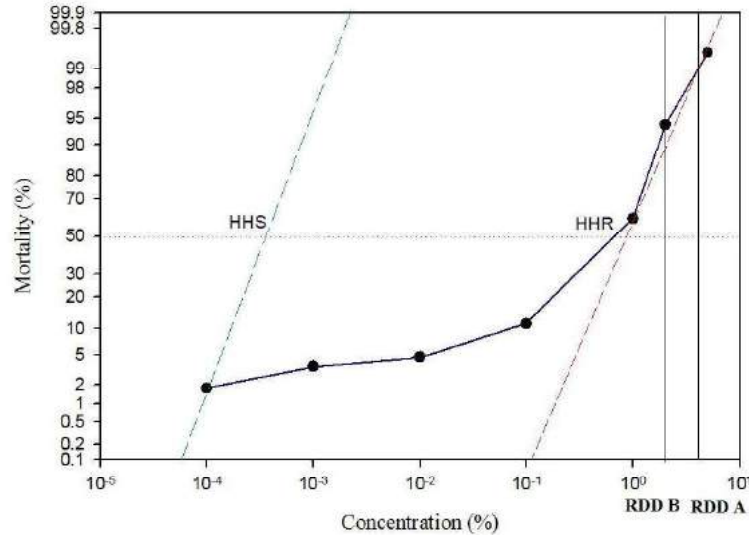


Figure 5: Line and scatter plot for the mortality response of *O. megnini* to DDT as determined by the Larval Packet Test (LPT). The RDD A and RDD B lines indicate the resistant discriminating dosages for anopheline mosquitos (4%) (WHO, 2013) and *R. microplus* (2%) (FAO, 2004), respectively. The two parallel broken lines represent hypothetical homogeneously susceptible (HHS) and hypothetical homogeneously resistant (HHR) populations.

Log concentration-probit mortality of DDT for the *O. megnini* population did not fit into a linear regression line indicating heterogeneous response for DDT (WHO, 2016; Karunaratne *et al.*, 2018). The high slope in the regression line with low LC_{50} and LC_{90} values indicated that the population was homozygous susceptible for flumethrin. However, there are no previous studies for *O. megnini* for comparison.

In Sri Lanka, DDT was extensively used in agriculture and to control malaria vectors for more than three decades (Kondradsen *et al.*, 2000) until it was replaced by malathion in the mid-1970s due to the development of resistance in *Anopheles* mosquitos (Kondradsen *et al.*, 2000). The use of organophosphates was legally limited to the health sector and carbamate was limited to the agricultural sector as a strategy to prevent resistance development. In the 1990s, pyrethroids were introduced to both agriculture and health sectors to control insect pests/vectors. Presently, pyrethroids are widely utilized in tick control programs in the country (personal communication

with veterinarians). The results of our study showed the presence of resistance for DDT of *O. megnini* despite the absence of DDT usage for more than four decades. It has been reported that intensive use of DDT in antimalarial and agricultural programs within the country from 1946 to 1977 has caused irreversible DDT resistance in almost all arthropod species including mosquitoes, bedbugs, ticks and agricultural pests (Damayanthi & Karunaratne, 2005; Karunaratne *et al.*, 2007, 2013; Perera *et al.*, 2008; Bandara & Karunaratne, 2017). This may be due to the selection of the same molecular mechanism initially developed to provide DDT resistance to *O. megnini* using insecticides. Alternatively, the evolved resistance mechanisms for other molecules may also be capable of causing DDT resistance in *O. megnini* (Bandara & Karunaratne, 2017).

Metabolic resistance based on GSTs is the major mechanism of DDT resistance (Hemingway *et al.*, 2004; Karunaratne *et al.*, 2018). Susceptible populations of the mosquitoes *Anopheles gambiae* and *Culex*

quinquefasciatus had GST specific activities of 0.42 ± 0.06 and $0.34 \pm 0.007 \mu\text{mol min}^{-1} \text{mg}^{-1}$, respectively, which was higher than the observed specific activity of *O. megnini* ($0.104 \pm 0.007 \mu\text{mol min}^{-1} \text{mg}^{-1}$) tested in the present study. Bandara and Karunaratne (2017) reported 0.38 and $0.13 \mu\text{mol min}^{-1} \text{mg}^{-1}$ for Sri Lankan *R. microplus*. Therefore, it appears that GSTs are not responsible for the observed high DDT tolerance of *O. megnini*. The presence of mutations in the DDT target site, which is the voltage-gated sodium channel (VGSC) on the nerve membranes, may provide this resistance by making the target site insensitive to DDT. Although the pyrethroids share this target site, mutations of VGSC gene which provide DDT resistance does not necessarily provide resistance to pyrethroids (Hemingway *et al.*, 2004).

Increased esterase activity is a well-known mechanism for protecting organophosphates and carbamates as they are rich with ester bonds (Karunaratne *et al.*, 2018). The *O. megnini* population showed an esterase activity of $0.06 \pm 0.01 \mu\text{mol min}^{-1} \text{mg}^{-1}$, which is higher than that of a susceptible population ($0.02 \pm 0.007 \mu\text{mol min}^{-1} \text{mg}^{-1}$) but lower than that of a resistant population ($0.92 \pm 0.08 \mu\text{mol min}^{-1} \text{mg}^{-1}$) of the mosquito *Culex quinquefasciatus* (Karunaratne & Hemingway, 1996). Two *R. microplus* tick populations with esterase-based resistance had 0.09 ± 0.02 and $0.08 \pm 0.04 \mu\text{mol min}^{-1} \text{mg}^{-1}$ esterase activities (Bandara & Karunaratne, 2017). Esterases of *O. megnini* population may therefore play a role in the development of resistance against organophosphates similar to the malathion. The results of AChE assay can be used to distinguish susceptible homozygous (< 30% remaining activity), heterozygous (30–70% remaining activity), and resistant homozygous (> 70% remaining activity) populations for altered or insensitive AChE mechanisms (WHO, 1998b). Accordingly, the *O. megnini* population has slightly more than 30% remaining activity indicating that the resistant alleles have been introduced in the population, expressing altered AChE mechanism, which in turn act in OP resistance.

Monooxygenases are an essential and diverse family of heme-containing enzymes which unitize as a resistance mechanism against pyrethroids (Karunaratne *et al.*, 2018). A discriminating amount of 0.35 equivalent units of cytochrome P450 was introduced to enhance monooxygenase activity. The introduced amount of cytochrome P450 was based on the monooxygenase amounts given for susceptible *An. culicifacies* and *An. subpictus* by Perera *et al.* (2008). The Sri Lankan cattle tick *R. microplus* had 0.14 and 0.34 equivalent units

of cytochrome P450 as monooxygenase amounts from two populations (Bandara & Karunaratne, 2017). Since the studied *O. megnini* population had a lower amount of monooxygenase activity (0.068 ± 0.02 equivalent units of cytochrome P450), it can be inferred that this mechanism is absent in *O. megnini* population and does not support pyrethroid resistance.

The incidence of acaricide resistance is highest in one-host ticks with short life cycles such as *R. microplus* compared to multi-host ticks (Wharton & Roulston 1970; Shyma *et al.*, 2013). This is because one-host ticks spend a more significant period of their life cycle on the same host under constant exposure to chemical acaricide/insecticides (Kiffner *et al.*, 2011; Leger *et al.*, 2013). Although most soft ticks have multi-host feeding patterns with shorter parasitic periods, *O. megnini* has a one-host life cycle with a high degree of host and feeding site predilection (Sonenshine, 1993).

CONCLUSION

Otobius megnini collected from racehorses from Nuwara Eliya, Sri Lanka, are susceptible to flumethrin and resistant to DDT. The development of organophosphate resistance through enhanced activity of esterases and altered target site AChE were evident. Future research is needed to generate more information on the persistence of acaricide resistance in *O. megnini*.

Conflict of interest

The authors declare that they have no competing interests

Acknowledgements

Authors thank USDA-ARS Knipling-Bushland U.S. Livestock Insects Research Laboratory, Kerrville, TX 78028, USA for the instructions on preparing acaricide impregnated papers, and the management of the racecourse in Nuwara Eliya, T.D.B. Lenadora, W.M.N. Wanninayake and Shantha Bandara for their support in tick collection. Laboratory assistance from Nalaka Nugapola and financial assistance from the National Research Council, Sri Lanka (grant11-44) are gratefully acknowledged.

REFERENCES

- Ahmed M.I., Shinggu P.A. & Basu A.K. (2007). Susceptibility of the soft tick *Ornithodoros savignyi* to different classes of acaricides. *Nigerian Journal of Parasitology* **24**(1):

- 179–184.
DOI: <https://doi.org/10.4314/njpar.v24i1.37824>
- Bandara K.J. & Karunaratne S.H.P.P. (2017). Mechanisms of acaricide resistance in the cattle tick *Rhipicephalus (Boophilus) microplus* in Sri Lanka. *Pesticide Biochemistry and Physiology* **139**: 68–72.
DOI: <https://doi.org/10.1016/j.pestbp.2017.05.002>
- Damayanthi B.T. & Karunaratne S.H.P.P. (2005). Biochemical characterization of insecticide resistance in insect pests of vegetables and predatory ladybird beetles. *Journal of the National Science Foundation of Sri Lanka* **33**(2): 115–122.
DOI: <https://doi.org/10.4038/jnsfsr.v33i2.2341>
- Desjardins I. et al. (11 authors) (2018). Seroprevalence of horses to *Coxiella burnetii* in an Q fever endemic area. *Veterinary Microbiology* **215**: 49–56.
DOI: <https://doi.org/10.1016/j.vetmic.2017.11.012>
- Diyes G.C.P. & Rajakaruna R.S. (2017). Life cycle of Spinose ear tick, *Otobius megnini* (Acari: Argasidae) infesting the race horses in Nuwara Eliya, Sri Lanka. *Acta Tropica* **166**: 164–176.
DOI: <https://doi.org/10.1016/j.actatropica.2016.11.026>
- Diyes G.C.P., Rajapaksha R.P.V.J. & Rajakaruna R.S. (2018). Molecular evidence of *Babesia* infections in spinose ear tick, *Otobius megnini* infesting stabled horses in Nuwara Eliya racecourse. *Ceylon Journal of Science* **47**(4): 405–409.
DOI: <https://doi.org/10.4038/cjs.v47i4.7559>
- Estrada-Peña A. & Jongejan F. (1999). Ticks feeding on humans: a review of records on human-biting Ixodoidea with special reference to pathogen transmission. *Experimental and Applied Acarology* **23**: 685–715.
DOI: <https://doi.org/10.1023/a:1006241108739>
- FAO (2004). *Guidelines for Resistance Management and Integrated Parasite Control in Ruminants*. Module 1-Ticks: Acaricide resistance: Diagnosis, Management and prevention, pp. 4–55. Animal Product and Health Division, Food and Agriculture Organization, Rome, Italy.
- Fivaz B.H., Botha P. & Cairns L.M. (1991). A putative outbreak of equine Lyme borreliosis in Natal. *Journal of the South African Veterinary Association* **61**: 128–129.
- Graf J.F., Gogolewski R., Leach-Bing N., Sabatini G.A., Molento M.B., Bordin E.L. & Arantes G.J. (2004). Tick control: an industry point of view. *Parasitology* **129**: s427–s442.
DOI: <https://doi.org/10.1017/s0031182004006079>
- Hemingway J., Hawkes N.J., McCarroll L. & Ranson H. (2004). The molecular basis of insecticide resistance in mosquitoes. *Insect Biochemistry and Molecular Biology* **34**(7): 653–665.
DOI: <https://doi.org/10.1016/j.ibmb.2004.03.018>
- Karunaratne S.H.P.P. & Hemingway J. (1996). Different insecticides select multiple carboxylesterase isoenzymes and different resistance levels from a single population of *Culex quinquefasciatus*. *Pesticide Biochemistry and Physiology* **54**: 4–11.
DOI: <https://doi.org/10.1006/pest.1996.0003>
- Karunaratne S.H.P.P., Damayanthi B.T., Fareena M.H.J., Imbuldeniya V. & Hemingway J. (2007). Insecticide resistance in the tropical bedbug *Cimex hemipterus*. *Pesticide Biochemistry and Physiology* **88**: 102–107.
DOI: <https://doi.org/10.1016/j.pestbp.2006.09.006>
- Karunaratne S.H.P.P., Weeraratne T.C., Perera M.D.B. & Surendran S.N. (2013). Insecticide resistance and efficacy of space spraying and larviciding in the control of dengue vectors *Aedes aegypti* and *Aedes albopictus* in Sri Lanka. *Pesticide Biochemistry and Physiology* **107**: 98–105.
DOI: <https://doi.org/10.1016/j.pestbp.2013.05.011>
- Karunaratne S.H.P.P., De Silva W.A.P.P., Weeraratne T.C. & Surendran S.N. (2018). Insecticide resistance in mosquitoes: Development, mechanisms and monitoring. *Ceylon Journal of Science* **47**(4): 299–309.
DOI: <https://doi.org/10.4038/cjs.v47i4.7547>
- Kiffner C., Vor T., Hagedorn P., Niedrig M. & Ruhe F. (2011). Factors affecting patterns of tick parasitism on forest rodents in tick-borne encephalitis risk areas, Germany. *Journal of Parasitology Research* **108**: 323–335.
DOI: <https://doi.org/10.1007/s00436-010-2065-x>
- Konradsen F., Amerasinghe F.P., van der Hoek W. & Amerasinghe P.H. (2000). *Malaria in Sri Lanka: Current Knowledge on Transmission and Control*. International Water Management Institute.
- Leger E., Vourch G., Vial L., Chevillon C. & McCoy K.D. (2013). Changing distributions of ticks: causes and consequences. *Experimental and Applied Acarology* **59**: 219–244.
DOI: <https://doi.org/10.1007/s10493-012-9615-0>
- Lovis L., Perret J.L., Bouvier J., Fellay J.M., Kaminsky R., Betscharta B. & Sager H. (2011). A new in vitro test to evaluate the resistance level against acaricides of the cattle tick, *Rhipicephalus (Boophilus) microplus*. *Veterinary Parasitology* **182**: 269–280.
DOI: <https://doi.org/10.1016/j.vetpar.2011.06.004>
- Madigan J.E., Valberg S.J., Ragle C. & Moody J.L. (1995). Muscle spasms associated with ear tick (*Otobius megnini*) infestations in five horses. *Journal of the American Veterinary Medical Association* **207**: 74–76.
- Miller R.J., George J.E., Guerrero F., Carpenter L. & Welch J.B. (2001). Characterization of acaricide resistance in *Rhipicephalus sanguineus* (Latreille) (Acari: Ixodidae) collected from the Corozal army veterinary quarantine center, Panama. *Journal of Medical Entomology* **38**(2): 298–302.
DOI: <https://doi.org/10.1603/0022-2585-38.2.298>
- Miller R.J., Davey R.J. & George J.E. (1999). Characterization of pyrethroid resistance and susceptibility to coumaphos in Mexican *Boophilus microplus* (Acari: Ixodidae). *Journal of Medical Entomology* **36**(5): 533–538.
DOI: <https://doi.org/10.1093/jmedent/36.5.533>
- Nava S., Guglielmone A.A. & Mangold A.J. (2009). An overview of systematics and evolution of ticks. *Frontiers in Bioscience* **14**(8): 2857–2877.
DOI: <https://doi.org/10.2741/3418>
- Perera M.D.B., Hemingway J. & Karunaratne S.P. (2008). Multiple insecticide resistance mechanisms involving metabolic changes and insensitive target sites selected in anopheline vectors of malaria in Sri Lanka. *Malaria*

- Journal* 7(1): 168.
DOI: <https://doi.org/10.1186/1475-2875-7-168>
- Shyma K.P., Kumar S., Sangwan A.K., Sharma A.K., Nagar G., Ray D.D. & Ghosh S. (2013). Acaricide resistance status of *Rhipicephalus (Boophilus) microplus* and *Hyalomma anatolicum* collected from Haryana. *Indian Journal of Animal Sciences* 83(6): 591–594.
DOI: <https://doi.org/10.1007/s10493-016-0046-1>
- Shyma K.P., Kumar S., Sharma A.K., Ray D.D. & Ghosh S. (2012). Acaricide resistance status in Indian isolates of *Hyalomma anatolicum*. *Experimental and Applied Acarology* 58(4): 471–481.
DOI: <https://doi.org/10.1007/s10493-012-9592-3>
- Sonenshine D.E. (1993). *Biology of Ticks*. 2. Oxford University Press, New York, USA.
- Stone B. F. & Haydock. K.P. (1962). A method for measuring the acaricide-susceptibility of the cattle tick *Boophilus microplus* (Canestrini). *Bulletin of Entomological Research* 53: 563–578.
DOI: <https://doi.org/10.1017/s000748530004832x>
- Surbhi Gupta S., Sangwan A.K. & Sangwan N. (2018). Determination of efficacy of commercial acaricides against *Ornithodoros savignyi* ticks collected from Haryana. *Journal of Entomology and Zoology Studies* 6: 237–239.
- Wharton R.H. & Roulston W.J. (1970). Resistance of ticks to chemicals. *Annual Review of Entomology* 5: 381–403.
DOI: <https://doi.org/10.1146/annurev.en.15.010170.002121>
- WHO (1998a). Test procedures for insecticide resistance monitoring in malaria vectors, bio efficacy and persistence of insecticides on treated surfaces. World Health Organization, Geneva, Switzerland.
- WHO (1998b). Techniques to detect insecticide resistance mechanisms (field and laboratory manual). World Health Organization, Geneva, Switzerland.
- WHO (2016). Test procedures for insecticide resistance monitoring in malaria vector mosquitoes. World Health Organization, Geneva, Switzerland.

RESEARCH ARTICLE

Production and characterization of β -galactosidase from the fungus *Thielaviopsis ethacetica* Went.

DMS Dissanayaka¹, SNT De Silva^{2*}, DPSTG Attanayaka¹ and EMM Vimukthi¹

¹ Department of Biotechnology, Faculty of Agriculture and Plantation Management, Wayamba University of Sri Lanka, Makandura, Gonawila.

² Department of Material and NanoScience Technology, Faculty of Technology, Wayamba University of Sri Lanka, Kuliypitiya.

Submitted: 14 December 2020; Revised: 24 May 2021; Accepted: 03 August 2021

Abstract: β -galactosidase (EC 3.2.1.23) is an industrially important enzyme. It can catalyse two different types of reactions, namely lactose hydrolysis and transgalactosylation. β -galactosidase enzyme production by *Thielaviopsis ethacetica*, was investigated and the enzyme was partially purified and characterized in the present study. Qualitative assay for the pre β -galactosidase activity indicated the formation of water insoluble blue-green colour, dichloro-dibromo-indigo zone towards the edges of the fungal colony after a 72-hour incubation period. Quantitative assay recorded a maximum enzyme activity of 0.599 U/mL at 72 hours. The enzyme was partially purified from the crude enzyme using ammonium sulphate precipitation and dialysis. Fraction 40-60 % (fraction 2) had the highest specific enzymes activity of 1.65 U/mg with 8.68 purification fold and 28.3 % recovery. SDS-PAGE analysis of fraction 2 resulted three separate protein bands above 40 kDa. The protein band corresponding to 50 kDa molecular weight was confirmed as β -galactosidase. The optimum temperature and pH for the enzyme was at 60 °C and 7.0, respectively. The present study reveals the fungal strain *Thielaviopsis ethacetica* with β -galactosidase activity. To our knowledge this is the first report about β -galactosidase activity of the strain *T. ethacetica*. This investigation suggests the potential use of this species in industrial applications.

Keywords: β -galactosidase, industrial enzyme, MALDI/MS, starch hydrolysis, *Thielaviopsis ethacetica*.

INTRODUCTION

β -galactosidase (EC 3. 2. 1. 23), also known as β -D-galactohydrolase, β -D-galactoside galactohydrolase,

galactosyltransferase or lactase is an enzyme that has a wide range of applications in the industrial sector. It catalyses two different reactions in organisms: the hydrolyzation of lactose into glucose and galactose (Akcan, 2011), and transgalactosylation reaction which synthesizes important prebiotics such as lactulose and galacto-oligosaccharides (GOS) (Lu *et al.*, 2009). These prebiotics have numerous health benefits and thus β -galactosidase has high demand in both food (Mahoney & Adamchuk, 1980; Jokar & Karbassi, 2009; Princely *et al.*, 2013; Klein *et al.*, 2016; Saqib *et al.*, 2017) and dairy industries (He *et al.*, 2007; Pal *et al.*, 2013; Erich *et al.*, 2015).

β -galactosidases are widely distributed in different biological systems, e.g. microorganisms, plants such as almonds, peaches, apricots, and animal tissues such as brain and placenta (Kayukawa *et al.*, 2020). β -galactosidases are members of the family of hydrolases that belongs to the group of saccharide-converting enzymes. Properties, activity and the structure of the enzyme such as position of the active site, molecular weight of the enzyme, length of the amino acid chain, thermal and pH stability vary with the sources from which the enzyme is obtained (Zhou & Chen, 2001). Therefore, source of the enzyme can be selected according to one's choice, depending on reaction conditions. Among all the natural sources, production of the enzyme is focused on microorganisms as they have the ability to grow on low-cost substrates. Moreover, compared to plants and

* Corresponding author (nimalides@wyb.ac.lk;  <https://orcid.org/0000-0002-4481-4247>)



This article is published under the Creative Commons CC-BY-ND License (<http://creativecommons.org/licenses/by-nd/4.0/>). This license permits use, distribution and reproduction, commercial and non-commercial, provided that the original work is properly cited and is not changed in anyway.

animal sources, higher yields can be obtained while minimizing the cost of production (Santos *et al.*, 1998). Microorganisms including yeast, fungi, bacteria and actinomycetes have been exploited for β -galactosidase production (Zadow, 1992; Fernandez, 1999; Bhanwar & Ganguli, 2014; Panesar *et al.*, 2016; Xu *et al.*, 2019). Among these microorganisms special attention is still paid to fungal sources as their enzymes are thermostable. Since the enzyme is extracellular, additional cost for the extraction is very low. Furthermore, fungi give higher yields, and their enzymes show broad stability profiles. Therefore, the commercially available β -galactosidases have been mainly obtained from fungi: yeast and moulds. The most important sources are *Aspergillus* and *Kluyveromyces* species including *A. oryzae*, *K. lactis*, *K. marxianus* and *K. fragilis* (Zhou & Chen, 2001; Roy & Gupta, 2003; Johnson & Echavarrri-Erasun, 2011; Maccaferri *et al.*, 2012; Martarello *et al.*, 2019). As the demand is high, finding new fungal source for the production of the enzyme is of current interest.

The objective of the present study was the optimisation of production, partial purification and characterisation of β -galactosidase secreted by *Thielaviopsis ethacetica*.

METHODOLOGY

The microorganism and culture conditions

Fungal strain *Thielaviopsis ethacetica* has been previously isolated from the topsoil and identified to exhibit alpha-amylase activity (Dissanayaka *et al.*, 2019). The internal transcribed spacer (ITS) sequences have been deposited in the GenBank/NCBI (Accession no; MG062870.1). The fungus was stored in potato dextrose agar (PDA) slants for long term storage and subcultures were prepared once a month throughout the study period. After reviving on PDA supplemented with tetracycline, spores were picked up using a sterile moistened loop and streaked on to 2 % sterile agar plates and incubated at 26 °C for 18 h. Germinated spores were transferred aseptically onto fresh PDA plates to get a single spore culture.

Qualitative assay for the pre β -galactosidase activity

To observe the pre β -galactosidase activity, 6 mm diameter disc of mycelium cut from the growing edge of fungal colonies were transferred aseptically onto YpSs agar plates (2% agar, 0.4% yeast extract, 0.05% $\text{MgSO}_4 \cdot 7\text{H}_2\text{O}$, 0.1% KH_2PO_4 and 1.5% soluble starch), supplemented with 80 $\mu\text{g}/\text{mL}$ X-gal (5-bromo-4-chloro-

3-indolyl- β -D-galactoside) (Sigma). The plates were incubated at 32 °C for 72 h and the observations were made at every 24-hour intervals. In the presence of β -galactosidase enzyme, X-Gal would be cleaved at the β -1-4 bond between galactose and the 5-bromo-4-chloro-3-indolyl part of X-Gal producing a blue-green colour formation in culture plates.

Determining the time for optimal enzyme production

Pre-inoculum was prepared in 50 mL of fermentation medium comprising 2% soluble starch, 0.5% yeast extract, 0.03% MgSO_4 , 0.03% CaCl_2 and 0.7% KH_2PO_4 at pH 4. Sterile medium was inoculated with 3 agar plugs of profusely growing fungi (6 mm diameter) and incubated at room temperature with shaking at 120 rpm. After 96 hours of incubation, 5 mL of homogenized pre-inoculum (5×10^4 – 6×10^4 spore/mL) was carefully withdrawn and added to 50 mL of the fermentation medium.

Fermentation medium was incubated at 32 °C for 72 h in a rotary shaker at 120 rpm (Dissanayaka *et al.*, 2019). β -galactosidase activity and total protein concentration was measured at 12-hour intervals by removing 150 μL from the fermentation medium. All assays were carried out in triplicate.

β -galactosidase enzyme assay

β -galactosidase activity on soluble starch was assayed by using o-nitrophenol-galactopyranoside (o-NPG) (Miller, 1972).

Appropriately diluted 0.15 mL crude enzyme was mixed with 0.6 mL of substrate solution. 1 mM o-NPG was prepared in 0.1 M sodium phosphate buffer at pH 7.0. The reaction mixture was incubated at 40 °C for 30 min. The reaction was terminated by adding 1 mL of 1 M Na_2CO_3 . The concentration of o-nitrophenol (oNP) released from o-NPG was determined by measuring the absorbance at 420 nm by UV spectrophotometer using the standard calibration curve (Soydan, 2006; Konsoula & Liakopoulou-Kyriakides, 2007). For enzyme blank, 0.15 mL of sample was mixed with 0.6 mL of buffer and 1 mL of 1 M Na_2CO_3 . For substrate blank, 0.15 mL of buffer was mixed with 0.6 mL of substrate solution and 1 mL of 1 M Na_2CO_3 . Mean absorbance value of the triplicates was taken to calculate the unit enzyme activity. One unit of β -galactosidase activity was defined as the amount of enzyme required to release 1 μmol o-nitrophenol per minute under assay conditions (Soydan, 2006, Konsoula & Liakopoulou-Kyriakides, 2007).

Total protein content assay

Total protein concentration was assayed in triplicate using Qubit 3 Invitrogen™ Qubit™ 3.0 Fluorometer according to the given instructions in Qubit assay kit (Invitrogen™).

Partial purification of the β-galactosidase enzyme

Five hundred millilitres from the submerged fermentation medium containing 2% soluble starch were inoculated with the fungal strain *Thielaviopsis ethacetica* and incubated at 32 °C for 72 h. After the incubation, culture medium was centrifuged at 6000 rpm for 15 min at 40 °C and the supernatant was subjected to gradient ammonium sulphate fractionation. The supernatant was brought into 40% (Fraction 1) saturation followed by 60% (Fraction 2), 80% (Fraction 3), and 100% (Fraction 4). Ammonium sulphate was gradually added into the medium while stirring continuously using a magnetic stirrer (Wingfield, 2001). Saturated protein samples were then centrifuged at 12000 rpm for 15 min, at 40 °C and the protein pellets were recovered. Before the dialysis, each pellet was dissolved in a minimum volume of 0.1 M phosphate buffer at pH 7 separately. Dialysis was accompanied by continuous stirring over 24 hours at 40 °C against the same buffer and the buffer was changed intermittently. Finally, all the fractions were assayed for enzyme activity and total protein concentration.

Investigation the effect of temperature on β-galactosidase activity

To find the effect of temperature and pH on β-galactosidase activity, Fraction 2 (40–60%) with the highest enzyme activity was collected and used. The effect of temperature was evaluated at 20, 37, 40, 60 and 80 °C by incubating the reaction mixture for 30 min. β-galactosidase enzyme activity was determined as previously described.

Investigation of the effect of pH on β-galactosidase activity

The effect of pH on enzyme activity was evaluated by adjusting the pH of the substrate at 4, 5, 6, 7, and 8. The reaction mixture was incubated at 60 °C for 30 min under specific pH value and enzyme activity was determined as previously described.

Determination of the molecular weight of *Thielaviopsis ethacetica* β-galactosidase

Partially purified protein fraction 2 with the highest enzyme activity was freeze-dried (CHRIST Alpha 1-2

LDplus, Germany) and 1 mg of lyophilized protein sample was dissolved in an appropriate volume of sample buffer (Laemmli, 1970). To separate proteins in the sample, 10 % sodium dodecyl sulfate polyacrylamide gel (SDS-PAGE) stained with Coomassie Brilliant Blue R-250 was used. To determine the molecular weight of the protein, a broad range molecular weight protein marker ranging from 10–100 kDa was used.

Protein identification using mass spectrometry peptide sequencing (MALDI/MS) method

Molecular weight of many fungal β-galactosidases lies around 40–75 kDa. Therefore, three separated protein bands representing more than 40 kDa were used for MALDI/MS identification. Immediate gel surface around these three bands were carefully separated and stored in an appropriate amount of sterilized distilled water. Three protein samples were sent to ALPHALYSE, Denmark for protein identification using Bruker Autoflex Speed MALDI TOF/TOF instrument. The resulted spectra were searched against available protein databases from UniProtKB using the Mascot software.

RESULTS AND DISCUSSION

Qualitative assay for the pre β-galactosidase activity

Although X-Gal is a commonly associated colourimetric method with lac operon in *E. coli*, the applicability of X-Gal for the detection of fungal β-galactosidase is still under assessment. In the present study, it has been attempted to determine the presence of an active fungal β-galactosidase in culture plates containing X-Gal. IPTG was not added to the culture plates as an inducer. After a 72-hour incubation period, a blue-green colour zone formation was observed towards the edges of the fungal colony. A similar finding has been reported by Fischer *et al.* (1995a), Soydan (2006), and Kishore and Kayastha (2012) with fungal β-galactosidase enzyme. This method will be a great advantage during the early screening procedures when the number of testing samples are high.

β-galactosidase enzyme assay

Thielaviopsis ethacetica containing fermentation medium gave a prominent peak for β-galactosidase enzyme activity during the 3rd day of the incubation. During the first 24 hours protein concentration gradually increased and then peaked at 48 hours (184.2 µg/mL), where β-galactosidase enzyme activity remained in lower points until 36 h. After 36 hours, enzyme activity

gradually increased reaching its maximum at 72 hours giving 0.599 U/mL maxima with a simultaneous drop in protein content to 67 µg/mL (Figure 1). After 72 hours, enzyme activity remained static where the protein concentration started to increase. Static enzyme activity may probably be due to the denaturation of protein resulted from unfavourable culture conditions during the latter part of the incubation period. Moreover, due to the depletion of initial substrate concentration, newly synthesised mycelia may be secreting other proteins extracellularly to degrade substrates other than starch, resulting in an increased protein concentration after 72 hours.

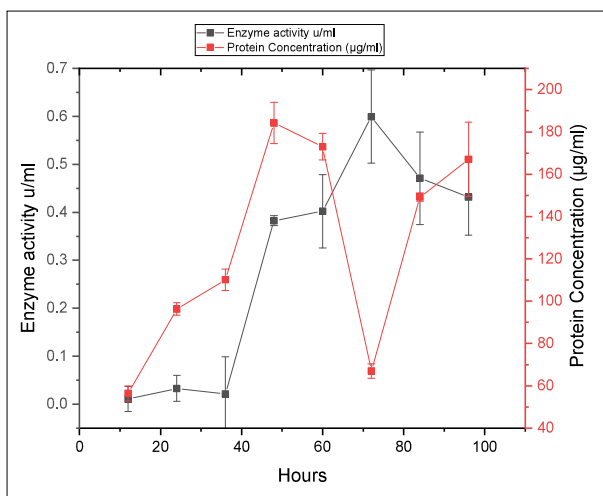


Figure 1: Total protein content and enzyme activity against incubation time. Error bars represents standard deviation

Optimum β -galactosidase enzyme activity was observed at 72 hours incubation period. Therefore, the

extraction of β -galactosidase from *T. ethacetica* was fixed to 72 hours of incubation period. Late secretion of β -galactosidase enzyme was observed in many other organisms; for example, *Bacillus* sp., *Rhizomucor* sp. and *Aspergillus* sp. (Shaikh et al., 1997; Akcan, 2011; Martarello et al., 2019). Quantitative determination of the β -galactosidase activity is commonly accomplished by using colourimetric method. β -galactosidase is capable of catalysing substrates with b-D-galactopyranoside residues like o-nitrophenol-galactopyranoside (o-NPG). During the hydrolysing process it can form galactose and o-nitrophenol (oNP) with a yellow colour. oNP is capable of absorbing light at 420 nm, therefore the colour intensity can be used to detect β -galactosidase activity of complex biological systems (Miller, 1972).

The present study used starch as the substrate, instead of well-known β -galactosidase substrates containing b-D-galactopyranoside moiety or lactose. The results suggest that one of the intermediate or an end product such as maltose or malto dextrin produced during the starch hydrolysis may act as the substrate for β -galactosidase enzyme production. Konsoula and Liakopoulou-Kyriakides (2007) reported that there can be about 1.5 fold increment of β -galactosidase enzyme activity when using soluble starch as the fermentation medium instead of lactose under the co-production culture conditions of alpha-amylase enzyme. Further, it has been reported that the enzyme production is induced in the presence of yeast extract (Konsoula & Liakopoulou-Kyriakides, 2007). Nitrogen dependency and carbon independency of β -galactosidase have opened many arguments among the scientific community and still there is no strong conclusion regarding its substrate specificity (Lind et al., 1989; Fischer et al., 1995; Konsoula & Liakopouloukyriakides, 2007).

Table 1: Enzyme activity and total protein content of ammonium sulphate fractions

Ammonium sulphate percentage	Total enzyme activity (u/mL)	Total protein content (mg)	Specific activity (u/mg)	Purification fold	Recovery (%)
Crude	8.75	45	0.19	1	100
0–40%	1.15	1.83	0.63	3.31	13.1
40–60%	2.475**	1.5	1.65	8.68	28.3
60–80%	1.776	1.25	1.42	7.47	20.3
80–100%	0.860	0.84	1.02	5.37	9.8

0 – 40% (fraction 1); 40–60 % (fraction 2); 60–80 % (fraction 3); 80–100 % (fraction 4)

**Indicates the highest enzyme activity for fraction 2

Partial purification of the β-galactosidase enzyme

During the partial purification of β-galactosidase, initially, the culture supernatant was saturated with ammonium sulphate from 0–40% (Fraction 1), 40–60% (Fraction 2), 60–80% (Fraction 3) and 80–100% (Fraction 4). Out of the four fractions, fraction 2 had the highest specific enzymes activity of 1.65 U/mg with an 8.68 purification fold and 28.28% recovery (Table 1). Therefore, Fraction 2 was selected for further assay.

Effect of temperature on β-galactosidase activity

Under the defined assay conditions maximum temperature for β-galactosidase enzyme activity was determined at temperatures ranging from 20–80°C. The optimum temperature for maximum *T. ethacetica* β-galactosidase activity was found to be around 60 °C (Figure 2). Many researchers have reported an optimum temperature around 60 °C for *Aspergillus oryzae*, *A. niger*, *A. carbonarius*, *A. fonsecaeus*, *Rhizomucor* sp., *Mucor* sp. and *Fusarium* sp. (Sorensen & Crisan, 1974; Park *et al.*, 1979; Gonzalez & Monsan, 1991; Shaikh *et al.*, 1997; O’Connell & Walsh, 2008; Martarello *et al.*, 2019).

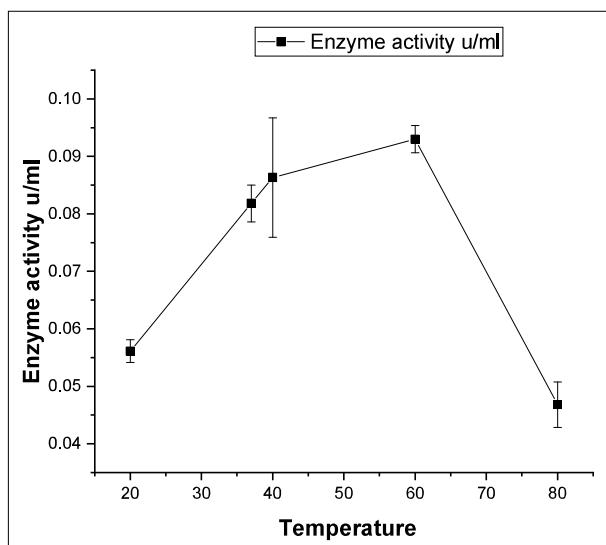


Figure 2: Variation of activity of purified enzyme from fraction 2 with temperature at pH 7.0. Error bars represent standard deviation

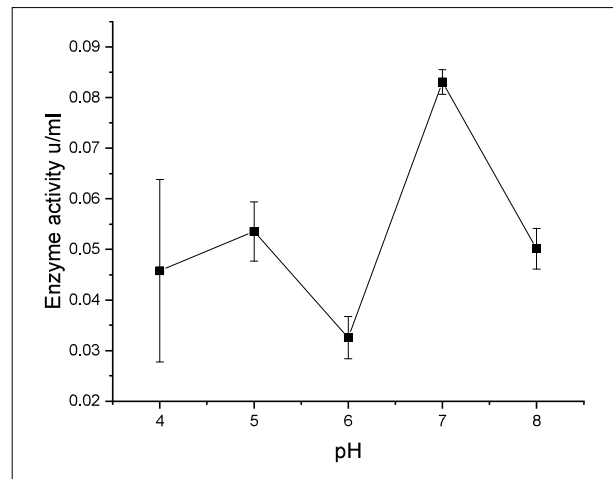


Figure 3: Variation of activity of partially purified enzyme from fraction 2 with pH at 60 °C. Error Bars represent standard deviation

Effect of pH on β-galactosidase activity

Thielaviopsis ethacetica exhibited two prominent enzyme activity peaks for β-galactosidases at distinct pH values. The highest activity peak with 0.083 U/mL was observed at pH 7 and slightly lower second peak of 0.054 U/mL at pH 5 (Figure 3).

These results show similarities to the observations made by Fisher *et al.* (1995) for *Thermomyces* sp. In the literature it is reported that most fungal β-galactosidase showed high activity in two pH ranges from 3–5 and 6–7. Borglum and Sternberg (1972), Cardoso *et al.* (2017), Gekas and Lopez-Leiva (1985), Niu *et al.* (2017), and O’Connell and Walsh (2008) reported that most of the *Aspergillus* and *Mucor* species exhibited enhanced enzyme activity under low pH values. On the other hand, Đfrij and Ögel (2002), Fischer *et al.* (1995), Martarello *et al.* (2019) and Matioli *et al.* (2001) reported that the highest enzyme activity was near neutral pH with *Aspergillus*, *Thermomyces* and *Kluyveromyces* species. However, due to having two enzyme activity peaks in the acidic and neutral pH ranges, the present strain can give an additional advantage for use in industry. Considering the acid stability nature of the enzyme, it can be useful in the pharmaceutical industry, while its activity near neutral pH values can be useful in the dairy industry.

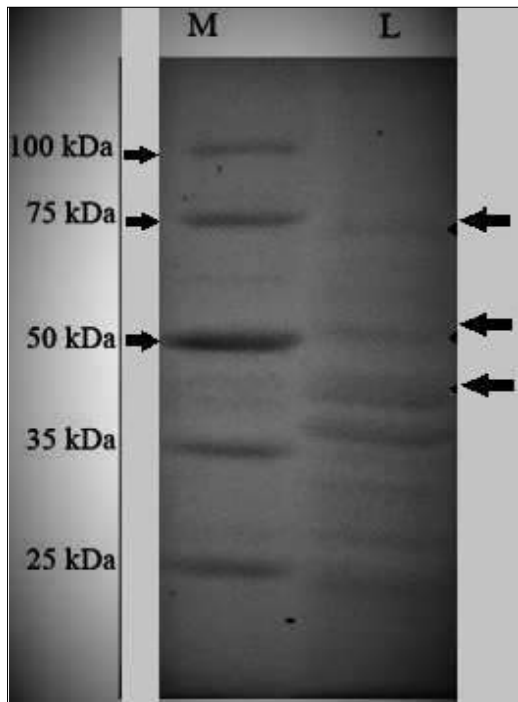


Figure 4: Image of SDS-PAGE (fraction 2). Arrows indicate three protein bands used for MALDI/MS identification. (M) molecular marker; (L) protein profile of the *T. ethacetica*

Determination of the molecular weight of *T. ethacetica* β -galactosidase

Partially purified lyophilised fraction 2 was run with a marker protein in SDS-PAGE. The resulted gel image is given in Figure 4. Three protein bands designated by arrows were used for MALDI-MS/MS identification. MALDI-MS/MS analysis involved 15 partially sequenced peptides and identity searching against UniProtKB using Mascot software. The protein band corresponded to 50 kDa molecular weight was matched to *E. coli* β -galactosidase with 729 Mascot score value (> 95% confidence level). Identified peptides corresponding to *E. coli* β -galactosidase are shown in Figure 5 with 25% sequence coverage. MALDI/MS peptide mapping and sequencing permit the identification of peptide sequences in a mixture especially when it is difficult to obtain one single pure protein. During the SDS-PAGE, Coomassie Brilliant Blue R-250 was used for staining to minimize the interference during mass spectrometry. According to available data on the molecular weight summary report on β -galactosidase, its molecular weight can range from 12 kDa to 270 kDa depending on the species from which it has been isolated. β -galactosidase isolated from *Thermomyces* and *Thermotoganaaphthophila* species had molecular weights between 75–80 kDa (Fischer *et al.*, 1995) and 70 kDa (Kong *et al.*, 2014), respectively, whereas the enzyme

1	MTMITDSLAV VLQPRDWENF GVTQLNRLAA HPPFASWRNS BEARTDRFSQ
51	QIRSLNGEWR FAWFFAPEAV PFSWLECDLP EADTVVVPNS WQMHHGYDAFI
101	YTNVTYPITV NPPFFVPTENF TSCYSLTFNV DESWLQEGQT R.IIFDGVNSA
151	FHLWCNGRWV GYGQDSRLPS EFDLSAFLRA GKNRLAVMVL RWSDDGTYLED
201	QDMWRMGGIF RDVSLHLKPT TQISDFHIVAT RFNDDFSGRAV LEAEVQMCCE
251	LRDYLRVTVS LWQGETQVAS GTAPFGGEII DERGGYADRV TLRNLNENFK
301	LWSAEIPNLY RAVVELHTAD GTLLIEAEACD VGFREVRLEN GLLLLLNGKFL
351	LIRGVNRHEH HPLHGQVMDE QTMVQDILLM KQNNFNAVRC SHYPNHPLWY
401	TLCDRYGLYV VDEANIETHG MVEFMNRLTDD PRWLPAMSER VTRMVQRDRN
451	HPSVLIWGLC NESCHGANHD ALYRWIKQVD FGRFVQYDCC GADTTATDII
501	CPMYAR VDED QFFPAVPKWS IKKWLSPGGE TRPLILCEYA HAMGNSLGGF
551	AKYWQAPROY PRLQGGFVWD WVDQSLIKYD ENGNPWSAYG GDFGDTPNDR
601	QFCMNGLVFA DRTPHPALTE AKHQQQFFQF RLSGQTIEVT SEYLFRRHSDN
651	ELLHWMVALD GKPLASGEVP LDVAPQGGQL IELPELPQPE SAGQLWLTVR
701	VVQPNATAWS EAGHISAWQQ WRLAENLSVT LPAASHAIPH LTTSEMDFCI
751	ELGNKRWQFN RQSGFLSQMW IGDKKQLLTP LRDQFTRAPL DNDIGVSEAT
801	RIDFNWVVER WKAAGHYQAE AALLQCTADT LADAVLITTA HAWQHQQKTL
851	FISRKTYRID GSGQMAITVD VEVASDTPHP ARIGLNCQLA QVAERVNWLG
901	LGEQENYPDR LTAACFDRWD LPLSDMYTEY VFSENGLRG GTRELNYGPH
951	QWRGDFQFNI SRYSQQQLME TSHRHLLHAE EGTWLNIDGF HMGISGDDSW

Figure 5: Partial amino acid sequences of protein band correspond 50 kDa molecular weight of *T. ethacetica* matched to *E. coli* β -galactosidase enzyme. Mapped peptides are shown in bold. 729 Mascot score value (> 95% confidence level).

of *Aspergillus* species reported to have a molecular weight range of 27–126 kDa (Tanaka *et al.*, 1975; Park *et al.*, 1979; Gonzalez & Monsan, 1991; Saad, 2004; Todorova-Balvay *et al.*, 2006). Considering the results of the protein sequencing analysis of the present study, it is indicated that majority of the starch hydrolase at 72 hours represent β -galactosidase enzyme.

CONCLUSION

The present study identified a fungal strain *Thielaviopsis ethacetica* with β -galactosidase activity and to the best of our knowledge this is the first report on β -galactosidase activity by *T. ethacetica*. Enzyme activity at high temperature, pH preference and substrate independency make the β -galactosidase produced by this strain suitable for industrial applications. Further, we emphasize the co-production ability of alpha amylase and β -galactosidase under starch fermentation medium, which can be readily substituted with low-cost substrates such as rice bran, banana peel and cassava starch (Dissanayaka *et al.*, 2019). During the initial stages of growth, *T. ethacetica* secretes extracellular alpha-amylase to the medium and involves starch hydrolysing process. Subsequently, it begins and continues to secrete β -galactosidase up to its death phase. Fungal strains having such beneficial enzyme production characteristics would have a significant impact on industrial-scale applications. Therefore, new opportunities exist for further research on enzyme production abilities of *T. ethacetica* and optimization of such capabilities to fulfil the industrial demands on starch processing.

Conflict of interest statement

The authors declare that they have no known competing financial interests or personal relationships that could have appeared to influence the work reported in this paper.

Acknowledgement

Authors wish to gratefully acknowledge the financial assistance provided by the National Science Foundation of Sri Lanka (NSF grant Number RG/2016/BT/01).

REFERENCES

Akcan N. (2011). High level production of extracellular β -galactosidase from *Bacillus licheniformis* ATCC 12759 in submerged fermentation. *African Journal of Microbiology Research* **5**(26): 4615–4621.
DOI: <https://doi.org/10.5897/AJMR11.716>

Bhanwar S. & Ganguli A. (2014). Alpha-amylase and β -galactosidase production on potato starch waste by *Lactococcus lactis* subsp *lactis* isolated from pickled yam. *Journal of Acientific and Industrial Research* **73**(5): 324–330.

Borglum G.B. & Sternberg M.Z. (1972). Properties of a fungal lactase. *Journal of Food Science* **37**: 619–623.

Cardoso B.B., Silvério S.C., Abrunhosa L., Teixeira J.A. & Rodrigues L.R. (2017). β -galactosidase from *Aspergillus lacticoffeatus*: A promising biocatalyst for the synthesis of novel prebiotics. *International Journal of Food Microbiology* **257**: 67–74.
DOI: <https://doi.org/10.1016/j.ijfoodmicro.2017.06.013>

Đfrij Đ.H. & Ögel Z. (2002). Production of neutral and alkaline proteases by the thermophilic fungus *Scytalidium thermophilum*, grown on microcrystalline cellulose. *Biotechnology Letters* **24**: 1107–1110.

Dissanayaka D.M.S., De Silva S.N.T., Attanayaka D.P.S.T.G., Kurera M.J.M.S. & Fernando C.A.N. (2019). Characterization of alpha amylase producing *Thielaviopsis ethacetica* and its raw starch hydrolyzing ability on different agricultural substrates. *Microbiology and Biotechnology Letters* **47**(3) : 412–422.
DOI: <https://doi.org/10.4014/mb.1812.12002>

Erich S., Kuschel B., Schwarz T., Ewert J., Bohmer N., Niehaus F., Eck J., Lutz-Wahl S., Stressler T. & Fischer L. (2015). Novel high-performance metagenome β -galactosidases for lactose hydrolysis in the dairy industry. *Journal of Biotechnology* **210**: 27–37.
DOI: <https://doi.org/10.1016/j.jbiotec.2015.06.411>

Fernandez M. (1999). Duplication of the β -galactosidase gene in some *Lactobacillus plantarum* strains. *International Journal of Food Microbiology* **48**(2): 113–123.
DOI: [https://doi.org/10.1016/S0168-1605\(99\)00031-8](https://doi.org/10.1016/S0168-1605(99)00031-8)

Fischer L., Scheckermann C. & Wagner F. (1995). Purification and characterization of a thermotolerant β -galactosidase from *Thermomyces lanuginosus*. *Applied and Environmental Microbiology* **61**(4): 1497–1501.
DOI: <https://doi.org/10.1128/AEM.61.4.1497-1501.1995>

Gekas V. & Lopez-Leiva M. (1985). Hydrolysis of lactose: a literature review. *Process Biochemistry* **20**: 2–11.

Gonzalez R.R. & Monsan P. (1991). Purification and some characteristics of β -galactosidase from *Aspergillus fonsecaeus*. *Enzyme and Microbial Technology* **13**: 349–352.

He T., Priebe M.G., Zhong Y., Huang C., Harmsen H.J.M., Raangs G.C., Antoine J.M., Welling G.W. & Yonk R.J. (2007). Effects of yogurt and bifidobacteria supplementation on the colonic microbiota in lactose-intolerant subjects. *Journal of Applied Microbiology* **104**(2): 595–604.
DOI: <https://doi.org/10.1111/j.1365-2672.2007.03579.x>

Johnson E.A. & Echavarri-Erasun C. (2011). Yeast biotechnology. In: *The Yeasts* (eds. C.P. Kurtzman, J.W. Fell & T. Boekhout), 5th edition, pp. 21–44. Elsevier, Netherlands.
DOI: <https://doi.org/10.1016/B978-0-444-52149-1.00003-3>

Jokar A. & Karbassi A. (2009). Determination of proper conditions for the production of crude β -galactosidase

- using *Lactobacillus delbrueckii* ssp. *Bulgaricus*. *Journal of Agricultural Science and Technology* **11**(3): 301–308.
- Kayukawa C.T.M., Oliveira M.A.S., Kaspchak E., Sanchuki H.B.S., Igarashi-Mafra L. & Mafra M.R. (2020). Quillaja bark saponin effects on *Kluyveromyces lactis* β -galactosidase activity and structure. *Food Chemistry* **303**: 125388.
DOI: <https://doi.org/10.1016/j.foodchem.2019.125388>
- Kishore D. & Kayastha A.M. (2012). A β -galactosidase from chick pea (*Cicer arietinum*) seeds: Its purification, biochemical properties and industrial applications. *Food Chemistry* **134**(2): 1113–1122.
DOI: <https://doi.org/10.1016/j.foodchem.2012.03.032>
- Klein M.P., Hackenhaar C.R., Lorenzoni A.S.G., Rodrigues R.C., Costa M.H., Ninow J.L. & Hertz P.F. (2016). Chitosan crosslinked with genipin as support matrix for application in food process: Support characterization and β -D-galactosidase immobilization. *Carbohydrate Polymers* **137**: 184–190.
DOI: <https://doi.org/10.1016/j.carbpol.2015.10.069>
- Kong F., Yeging W., Shugui C., Renjun G. & Guigui X. (2014). Cloning, purification and characterization of a thermostable β -galactosidase from *Thermotoga naphthophila* RUK-10. *Process Biochemistry* **49**: 775–782.
- Konsoula Z. & Liakopoulou-Kyriakides M. (2007). Co-production of α -amylase and β -galactosidase by *Bacillus subtilis* in complex organic substrates. *Bioresource Technology* **98**(1): 150–157.
DOI: <https://doi.org/10.1016/j.biortech.2005.11.001>
- Laemmli U.K. (1970). Cleavage of structural proteins during the assembly of the head of bacteriophage T4. *Nature* **227**: 680–685.
- Lind D.L., Daniel R.M., Cowan D.A. & Morgan H.W. (1989). β -Galactosidase from a strain of the anaerobic thermophile, *Thermoanaerobacter*. *Enzyme and Microbial Technology* **11**(3): 180–186.
DOI: [https://doi.org/10.1016/0141-0229\(89\)90079-3](https://doi.org/10.1016/0141-0229(89)90079-3)
- Lu L., Xiao M., Li Z., Li Y. & Wang F. (2009). A novel transglycosylating β -galactosidase from *Enterobacter cloacae* B5. *Process Biochemistry* **44**(2): 232–236.
DOI: <https://doi.org/10.1016/j.procbio.2008.10.010>
- Maccaferri S., Klinder A., Brigidi P., Cavina P. & Costabile A. (2012). Potential probiotic *Kluyveromyces marxianus* B0399 modulates the immune response in CaCO-2 cells and peripheral blood mononuclear cells and impacts the human gut microbiota in an in vitro colonic model system. *Applied and Environmental Microbiology* **78**(4): 956–964.
DOI: <https://doi.org/10.1128/AEM.06385-11>
- Mahoney R.R. & Adamchuk C. (1980). Effect of milk constituents on the hydrolysis of lactose by lactase from *Kluyveromyces fragilis*. *Journal of Food Science* **45**(4): 962–964.
DOI: <https://doi.org/10.1111/j.1365-2621.1980.tb07487.x>
- Martarello R.D., Cunha, L., Cardoso S.L., de Freitas M.M., Silveira D., Fonseca-Bazzo Y.M., de Mello M.H., Filho E.X.F. & Magalhaes P.O. (2019). Optimization and partial purification of β -galactosidase production by *Aspergillus niger* isolated from Brazilian soils using soybean residue. *AMB Express* **9**: Article number 81 (2019).
DOI: <https://doi.org/10.1186/s13568-019-0805-6>
- Matioli G., Farias de Moraes F. & Maria Zanin G. (2001). Hydrolysis of lactose by β -galactosidase from *Kluyveromyces fragilis*: characterization of the enzyme. *Maringá* **23**: 655–659.
- Miller J.H. (1972). *Experiments in Molecular Genetics: Assay of β -Galactosidase*, pp. 352–355. CSH Laboratory Press, Cold Spring Harbor, USA.
- Niu D., Tian X., Mchunu N.P., Jia C., Singh S., Liu X., Prior B.A. & Lu F. (2017). Biochemical characterization of three *Aspergillus niger* β -galactosidases. *Electronic Journal of Biotechnology* **27**: 37–43.
DOI: <https://doi.org/10.1016/j.ejbt.2017.03.001>
- O'Connell S. & Walsh G. (2008). Application relevant studies of fungal β -galactosidases with potential application in the alleviation of lactose intolerance. *Applied Biochemistry and Biotechnology* **149**(2): 129–138.
DOI: <https://doi.org/10.1007/s12010-007-8098-7>
- Pal A., Melita L., M. & Khanum F. (2013). Extraction, purification and thermodynamic characterization of almond (*Amygdalus communis*) β -galactosidase for the preparation of delactosed milk. *Food Technology and Biotechnology* **51**(1): 53–61.
- Panesar P.S., Kaur R. & Singh R.S. (2016). Isolation and screening of fungal strains for β - isolation and screening of fungal strains for β -galactosidase production. *International Journal of Nutrition and Food Engineering* **10**(7): 400–404.
- Park Y.K., Santi M.S.S. & Pastore G.M. (1979). Production and characterization of β -galactosidase from *Aspergillus oryzae*. *Journal of Food Science* **44**(1): 100–103.
DOI: <https://doi.org/10.1111/j.1365-2621.1979.tb10016.x>
- Princely E.G., Basha S., Kirubakaran J. & Dhanaraju M.D. (2013). Biochemical characterization, partial purification, and production of an intracellular β -galactosidase from *Streptococcus thermophilus* grown in whey. *Pelagia Research Library European Journal of Experimental Biology* **3**(2): 242–251.
- Roy I. & Gupta M.N. (2003). Lactose hydrolysis by lactozym immobilized on cellulose beads in batch and fluidized bed modes. *Process Biochemistry* **39**: 325–332.
DOI: [https://doi.org/10.1016/S0032-9592\(03\)00086-4](https://doi.org/10.1016/S0032-9592(03)00086-4)
- Saad R.R. (2004). Purification and some properties of β -galactosidase from *Aspergillus japonicus*. *Annals of Microbiology* **54**(3): 299–306.
- Santos F.A.P., Huber J.T., Theurer C.B., Swingle R.S., Simas J.M., Chen K.H. & Yu P. (1998). Milk yield and composition of lactating cows fed steam-flaked sorghum and graded concentrations of ruminally degradable protein. *Journal of Dairy Science* **81**(1): 215–220.
DOI: [https://doi.org/10.3168/jds.S0022-0302\(98\)75568-7](https://doi.org/10.3168/jds.S0022-0302(98)75568-7)
- Saqib S., Akram A., Halim S.A. & Tassadug R. (2017). Sources of β -galactosidase and its applications in food industry. *3 Biotech* **7**(1): 79.
DOI: <https://doi.org/10.1007/s13205-017-0645-5>

- Shaikh S.A., Khire J.M. & Khan M.A. (1997). Production of β -galactosidase from thermophilic fungus *Rhizomucor* sp. *Journal of Industrial Microbiology and Bacteriology* **19**(4): 239–245.
DOI: <https://doi.org/10.1038/sj.jim.2900452>
- Sorensen S.G. & Crisan E.V. (1974). Thermostable lactase from thermophilic fungi. *Journal of Food Science* **39**(6): 1184–1187.
DOI: <https://doi.org/10.1111/j.1365-2621.1974.tb07349.x>
- Soydan M. (2006). Production of thermosatable β -galactosidase from thermophilic fungi for use in low lactose milk production. *MSc thesis*. Middle East Technical University, Ankara, Turkey.
- Tanaka T., Kagamiishi A., Kiuchi A. & Horiuchi T. (1975). Purification and properties of β -galactosidase from *Aspergillus oryzae*. *The Journal of Biochemistry* **77**(1): 241–247.
DOI: <https://doi.org/10.1093/oxfordjournals.jbchem.a130713>
- Todorova-Balvay D., Stoilova I., Gargova S. & Vijaylakshmi M.A. (2006). An efficient two step purification and molecular characterization of β -galactosidases from *Aspergillus oryzae*. *Journal of Molecular Recognition* **19**(4): 299–304.
DOI: <https://doi.org/10.1002/jmr.788>
- Wingfield P.T. (2001). Protein precipitation using ammonium sulfate. *Current Protocols in Protein Science* **80**: 6.1.1–6.1.35.
DOI: <https://doi.org/10.1002/0471140864.ps0601s80>
- Xu X., Fan X., Fan C., Qin X., Liu B., Nie C., Sun N., Yao Q., Zhang Y. & Zhang W. (2019). Production optimization of an active β -galactosidase of *Bifidobacterium animalis* in heterologous expression systems. *BioMed Research International* **2019**: 1–10.
DOI: <https://doi.org/10.1155/2019/8010635>
- Zadow J.G. (1992). Lactose hydrolysis. In: *Whey and Lactose Processing* (ed. J.G. Zadow), pp 361. Elsevier Applied Sciences, London and New York.
- Zhou Q.Z. & Chen X.D. (2001). Effects of temperature and pH on the catalytic activity of the immobilized β -galactosidase from *Kluyveromyces lactis*. *Biochemical Engineering Journal* **9**(1): 33–40.
DOI: [https://doi.org/10.1016/S1369-703X\(01\)00118-8](https://doi.org/10.1016/S1369-703X(01)00118-8)

RESEARCH ARTICLE

A new foliar disease of *Ficus religiosa* caused by *Diaporthe acutispora*, identified using molecular phylogeny based multigene DNA sequence analyses

N Adikaram^{1*}, S Maharachchikumbura², ISK Vithanage³, D Yakandawala³ and L Jayasinghe¹

¹ National Institute of Fundamental Studies, Hantana Road, Kandy.

² School of Life Science and Technology, University of Electronic Science and Technology of China, Chengdu, 611731, China.

³ Department of Botany, Faculty of Science, University of Peradeniya, Peradeniya.

Submitted: 11 January 2021; Revised: 20 April 2021; Accepted: 25 June 2021

Abstract: *Ficus religiosa* is a large tree, native to India, and considered to have religious significance and found invariably in Buddhist shrines. The manuscript reports a new foliar disease, named as ‘*Diaporthe* leaf disease’ (DLD) in *F. religiosa*. DLD was first observed in a Buddhist temple in Colombo, Sri Lanka, in 2012 and now spread over some other parts of the island. Causal organism was identified as *Diaporthe acutispora*, based on combined ITS, TUB and TEF phylogenetic analysis. Koch’s postulates were fulfilled, confirming that *D. acutispora* was the pathogen, producing symptoms originally observed in *F. religiosa* leaves. Initial infections occur in younger but fully expanded leaves, producing darkened, 1.0-1.5 cm segments of the mid-rib or primary/secondary veins. Peripheral tissues around the darkened mid-rib/vein became necrotic with large, circular and chlorotic zones. The most striking symptom was the appearance of clusters of numerous, shiny, blackish and spherical to irregular conidiomata (pycnidial) over the leaf surface and along the affected mid-rib/veins of senescing leaves. Infected leaves, younger or mature, tended to roll upwards showing desiccation probably due to blockage of water movement through infected mid-rib/veins. Considering the potentially devastating nature of the DLD, and that the disease has already spread over to parts of the country, findings in the present work will be significant in terms of disease diagnosis and management. Accurate identification of the pathogen is a prerequisite to determine the epidemiology and, effective disease management strategies. This is the first report of DLD in *F. religiosa* anywhere in the world.

Keywords: β -tubulin, *Diaporthe*, sacred fig, translation elongation factor.

INTRODUCTION

Ficus religiosa Linn. (Family Moraceae) is a large tree native to India that is thought to have religious significance and is always found in Buddhist shrines, hence the names Sacred Fig or Sacred ‘Bo’ in Nepal, Sri Lanka, South-eastern China, and Indochina (Corner, 1981). *Ficus religiosa* is a dry season-deciduous or semi-evergreen tree growing up to 30 meters tall without aerial roots from the branches. The tree is considered to have a religious significance in three major religions that originated in the Indian subcontinent, Hinduism, Buddhism and Jainism. *Ficus religiosa* is known to have a very long lifespan. A sprig of the tree, under which the Gautama Buddha attained enlightenment, was brought to Sri Lanka in the year 288 B.C. It has survived up to the present day by means of its ability to supplant the ageing trunk with new shoots and this tree, in Anuradhapura (North Central Province), is acclaimed as one of the oldest in the historical record (Corner, 1981).

Leaves are cordate shaped and spirally arranged; the new leaves are pink in colour. The leaf lamina has

* Corresponding author (nimal.ad@nifs.ac.lk;  <https://orcid.org/0000-0001-8570-1241>)



This article is published under the Creative Commons CC-BY-ND License (<http://creativecommons.org/licenses/by-nd/4.0/>). This license permits use, distribution and reproduction, commercial and non-commercial, provided that the original work is properly cited and is not changed in anyway.

a truncate base, caudate-acuminate with a distinctive extended drip tip, 25–90 mm long. The petiole is 35–130 cm, mostly longer than leaf lamina (Corner, 1981). The tree is also known to have been used in traditional medicine to treat various health complications (Kumar *et al.*, 2018).

Ficus religiosa is affected by several fungal diseases of which the leaf spot disease caused by *Glomerella cingulata* is the most common in Sri Lanka (Abeygunawardhane, 1969). A leaf blotch caused by a *Botryosphaeria* species was also reported (Maharachchikumbura & Adikaram, 2009).

A leaf blight disease was reported in *F. religiosa* from Jaipur, India, and the causal agent was identified as *Phyllosticta* sp. (Sharma *et al.*, 2011). Another leaf spot disease was reported from Lahore, Pakistan, caused by *Curvularia aerea* (Nayab & Akhtar, 2016). Brown root disease caused by *Phellinus noxius* is responsible for the mysterious death of individual trees (Abeygunawardhane, 1969).

Diaporthe (syn. *Phomopsis*) species are well-known as pathogens, endophytes or saprobes on a range of economically important crops, ornamentals and forest trees (Udayanga *et al.*, 2011). Species of *Diaporthe* cause various diseases on a range of plant hosts including some economically important hosts worldwide (Gomes *et al.*, 2013). The genus is placed in the family Diaporthaceae, order Diaporthales, in the class Sordariomycetes (Maharachchikumbura *et al.*, 2016). Morphological characters are not always suitable for species definition because of their plasticity and overlap between different species (Santos & Phillips, 2009).

Literature surveys have established no previous records of a leaf disease from *F. religiosa* with symptoms and causal agents similar to those of the disease reported in the present study, in Sri Lanka or elsewhere. Therefore, the leaf disease that the present study reports was taken as a new and unknown disease. The objectives of the study were to study and record the symptomatology, isolate and identify the causal agent of the disease using morphological characteristics and multigene DNA sequence analyses and determine phylogeny. Koch's postulates were performed to test if the fungus isolated could be consistently isolated from all symptomatic leaves, the pathogenicity of the fungus and, its ability to produce symptoms that were originally shown by the disease, on re-inoculation.

METHODOLOGY

Diseased specimens

Leaves of *F. religiosa* showing DLD symptoms were collected from trees located in several places from Colombo (Western Province) in 2012, when the disease was first encountered. Since then, diseased leaves were sampled from Danthure, Peradeniya and Hantana (Kandy District, Central Province). The diseased leaves were first examined and photographed in the field in every sampling, and the observations were recorded. Leaves at different stages of symptom development were collected in separate polythene bags and delivered to the Plant Pathology laboratory at the Department of Botany, the University of Peradeniya for further examination.

Examination of diseased specimens and isolation of the pathogen

Leaves showing DLD symptoms were first examined visually for external symptoms. Surface scrapings were taken from lesions and transverse sections cut through diseased tissues were examined under the light microscope (Olympus BX53 with Olympus DP72 digital camera), and the observations were recorded. The fungus was isolated from diseased tissues on leaves at different stages of symptom development. Small (0.5 × 0.5 cm²) segments cut from the advancing margin of necrotic lesions on leaf lamina, necrotic areas of the mid-rib, lateral veins, and petioles were surface sterilized by immersing in 2% sodium hypochlorite (Clorox[®] USA) for 2 min (Indrakeerthi & Adikaram, 1995). After placing on a sterilized filter paper to remove excess liquid the segments were transferred aseptically onto Potato Dextrose Agar (PDA) medium supplemented with tetracycline (10 mg/L) to suppress bacterial growth. The plates were incubated at 25±3°C for one week, and the colonies that emerged from diseased tissue were examined under a light microscope and sub-cultured on a fresh PDA medium.

Preparation of mono-conidial cultures

Mono-conidial cultures of the isolate were prepared using the procedure described by Johnston & Booth (1983). The plates were incubated for seven days at 28–30°C, and the isolates were sub-cultured on PDA to be used in morphological and molecular studies.

Morphological studies

The colony morphology viz. colony colour, texture, pigmentation underneath, the presence or absence of concentric rings and sectoring etc., was studied using two weeks-old cultures. Conidial morphology was also studied taking 4–5 wks ancient cultures. A drop (20 μ L) of a conidia suspension, prepared as described previously, was mounted on a clean slide. The conidial characteristics, the shape and colour of conidia, presence of septa etc., were observed under the microscope and photographed and recorded. The dimensions of 50 randomly selected conidia were measured in μ m with a graticule connected to an eyepiece of a light microscope. The average length and breadth were calculated and presented with their range.

For morphological studies, the conidiomata obtained from 4–5 wks old cultures and diseased tissues on senescing or fallen leaves were mounted on slides and after crushing by gently tapping over the coverslip, the structures were examined under the light microscope. The conidiomata, conidiogenous cells and conidia were photographed, the dimensions of conidia were measured and averaged.

DNA extraction, PCR amplification and sequencing

DNA was extracted using a Wizard® genomic DNA purification kit (Promega Corporation, USA) and a modified protocol (Doyle & Doyle, 1987; Lee & Taylor, 1990).

Three gene regions, internal transcribed spacer (ITS), partial β -tubulin (TUB) and partial translation elongation factor 1-alpha (TEF) were amplified using primer pair ITS1 and ITS4, BT2a and BT2b, and EF1-728F and EF1-986R, respectively (White *et al.*, 1990; Glass & Donaldson, 1995; Carbone & Kohn, 1999). PCR reactions were performed using Applied Biosystems Veriti 96-well thermal cycler (9902, Singapore). Amplification reactions had a total reaction volume of 40 μ L, which was composed of 1 \times PCR buffer (Promega Corporation, USA), 5.6% DMSO (v/v), 40 μ M dNTPs (Promega Corporation, USA), 0.2 μ M of each forward and reverse primers, 0.25 U of GoTaq™ *Taq* DNA polymerase (Promega Corporation, USA), sterilized water and 10 ng of genomic DNA. For ITS and TUB regions, 1.5 mM of MgCl₂ was used, and for the TEF region, two mM MgCl₂ was used. PCR cycling conditions were; an initial denaturation for 3 min at 94 °C, followed by 40 cycles

of denaturation at 94 °C for 30 s; annealing for 1 min at 58 °C for ITS, 55 °C for TEF and TUB, and elongation at 72 °C for 1 min; and final extension step at 72 °C for 3 min. Amplicons were sequenced at MacroGen Inc. (Seoul, South Korea) and the Department of Molecular Biology, Faculty of Science, University of Peradeniya, Sri Lanka. DNASTAR Lasergene SeqMan Pro v. 8.1.3 was used to gain consensus sequences from sequences generated from forward and reverse primers, and these were deposited in GenBank (Table 1).

Phylogenetic analysis

A preliminary species identification of the isolate was made through a BLASTn search conducted with each locus at the NCBI (<http://blast.ncbi.nlm.nih.gov>). The sequences produced in this study with more than 98% similarity with reference sequences for *Diaporthe* were chosen for phylogenetic analysis (Table 1). Multiple sequences were aligned with MEGA v.7.0.26 (Kumar *et al.*, 2016) and edited manually. The maximum likelihood (ML) analysis was conducted using RAxML v8.2.10 (Stamatakis, 2014) performed on the CIPRES Science Gateway server (Miller *et al.*, 2012) and using the GTRGAMMA model. Branch support values were determined using the rapid bootstrapping algorithm with 1000 replicates. The phylogenetic tree was visualised in FigTree v. 1.4.0 (Rambaut, 2014) and edited Adobe Illustrator.

Koch's postulates

Diseased *Ficus* leaves were examined and symptoms were recorded. The pathogen isolated was grown in pure culture. Uniform-sized saplings of *F. religiosa* devoid of blemishes or any disease symptoms were used for artificial inoculation. Drops (20 μ L) of conidia from a suspension (1×10^6 conidia/mL) were applied onto the mid-rib and two lateral veins on the upper surface of the leaf lamina. Six replicate leaves in three plants were used for inoculation and another three leaves were treated with drops of sterile distilled water as controls. Inoculated and control leaves were kept covered with perforated polythene bags at 28–30°C, and after 24 h, the polythene bags were taken off. Inoculated leaves were examined regularly. Symptoms, when appeared, were described and compared with those of the original diseased leaves. The pathogen was re-isolated from the symptomatic leaves on PDA. The isolate's colony and asexual reproductive morphology were compared with those of the original isolate used for inoculation.

RESULTS AND DISCUSSION

This disease was first encountered in June 2012 in a *F. religiosa* tree, at a temple in Kalubowila area, Colombo (Western Province), Sri Lanka and a few months later in another temple in Danthure, Kandy District (Central Province). Following this, *F. religiosa* trees showing similar leaf symptoms were found in temples, wayside trees, etc. in villages in Kandy area and within the premises of the University of Peradeniya. *Diaporthe* species generally produce alpha- and beta-conidia in pycnidia in large numbers, which can also persist under adverse conditions. Splash dispersal of conidia during rain is an effective method for the spread of the fungus (Linders *et al.*, 1996) serving as a source of inoculum for new infections. The fungus also survives in plant debris (Panwar *et al.*, 1970). *Diaporthe* species have been introduced into new areas as endophytes or latent pathogens together with plant produce (Torres *et al.*, 2016). Production of conidia in large numbers and splash dispersal during rain (Linders *et al.*, 1996) coupled with warm and humid conditions conducive to infection facilitate the spread of the disease posing a major threat to *F. religiosa* trees in the country.

Disease symptoms

Disease symptoms appear mainly in the foliage of *F. religiosa*. Leaf symptoms were slightly variable among trees, or with the location where the *F. religiosa* is grown. Disease symptoms first appeared in younger but fully expanded leaves as browning of 1–1.5 cm long segments on the mid-rib, secondary or tertiary vein, which were surrounded by circular to oval-shaped chlorotic areas of about 1–2 cm diameter in the leaf lamina which gradually enlarged in size (Figure 1).

A small area of leaf lamina immediately outside the browned mid-rib or vein became necrotic but most of the peripheral tissue remained chlorotic. In all affected leaves a portion of 2–4 cm of the mid-rib/vein was infected and turned blackish brown colour. The necrotic area originated around from the vein gradually expanded laterally towards one or both sides of the mid-rib/vein, covering an area of 2–3 cm diameter on either side of the leaf lamina to form a prominent necrotic zone with an irregular margin. A necrotic zone on one side of the affected mid-rib/vein was the most common (Figure 1). Occasionally, two or more infected areas in closer proximity coalesced to form larger lesions. The younger leaves and those with badly infected mid-rib/veins tended to roll upwards often during the daytime

showing desiccation probably due to blockage of water transport along affected mid-rib/vein. In addition, the petiole is often angled downwards giving an appearance of epinasty. This could result in rolling leaves upwards, a symptom commonly shown by certain infected leaves.

As the disease progressed, widespread necrosis could be observed in the leaf lamina. In the senescing leaves, numerous black, small, raised, round or oval-shaped clusters of scattered conidiomata were seen crowded along the mid-rib, lateral secondary and tertiary veins. Small, circular to oval-shaped isolated necrotic patches were also observed along the petiole. The segments of the mid-rib and secondary veins in infected leaves become necrotic leading to dysfunction of vascular tissues within leaves, which could cause devastating effects on the entire tree.

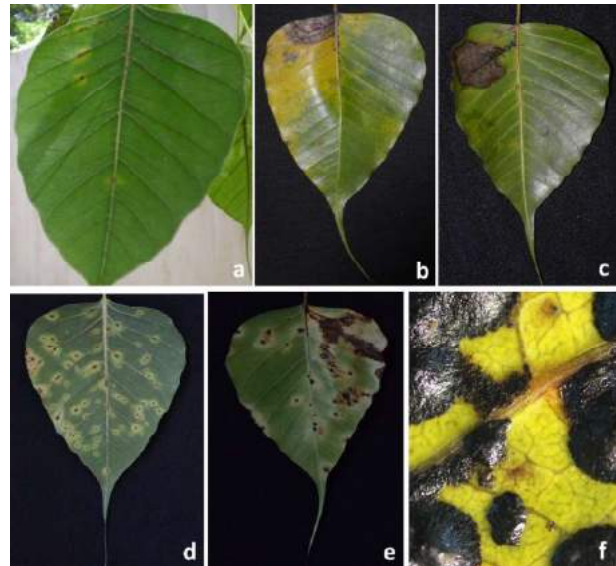


Figure 1: *Diaporthe* leaf disease in *F. religiosa*: (a) initial symptoms on fully-expanded leaf showing browning of smaller discrete segments of the vein surrounded by chlorotic area with a diffused margin; (b) a mature leaf with a large necrotic lesion bordered between two primary veins, developed towards one half from the infected mid-rib; (c) darkened, necrotic lesion at an advanced stage with black conidiomata formed on infected secondary and tertiary veins; (d) slightly different symptoms appeared in leaves in a *F. religiosa* tree with tiny necrotic lesion in the centre surrounded by somewhat larger, diffused chlorotic zone; (e) an advanced stage of the disease with irregular, dark brown and extensive necrotic lesions formed by coalescence of adjacent individual lesions.

In some trees, the initial symptoms appeared as bright yellow, up to 2 cm diameter circular areas surrounding a small circular necrotic area, always covering a segment of the mid-rib or the lateral vein. In older lesions, a greyish, irregular patch developed by expansion of the central necrotic area covering the mid-rib/lateral vein. In some leaves only a single lesion appeared and in others a few or numerous isolated, infected areas could be seen scattered over the leaf lamina. Although the disease's symptomatology is slightly variable among trees, the darkening of the mid-rib or the vein, secondary or tertiary, is a common symptom constantly associated with the disease. This is a striking symptom that could be conveniently used to diagnose the disease (Figure 1).

Pathogen morphology

Three isolates of the pathogen were obtained in the study. The isolate D2 used for morphological and molecular studies was slow growing on PDA. It produced a whitish colony initially and after about ten days, took a characteristic yellow colour with conidiomata appearing black scattered and mostly at the margins (Figure 2a) of concentric rings. Pigmentation began with the edges of the concentric rings which eventually spread all over the plate. The mycelium appeared sparse with concentric rings having irregular peripheral margins. The reverse

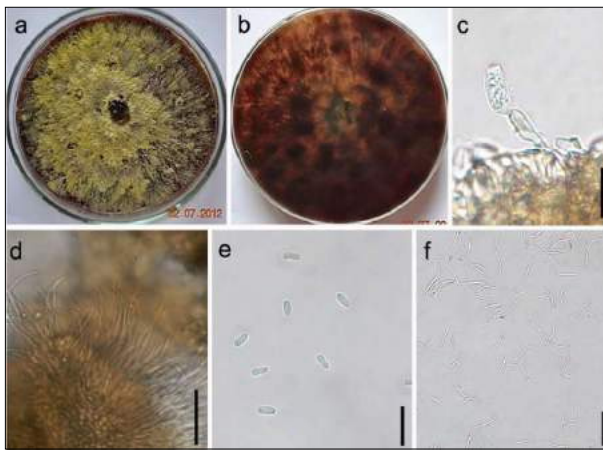


Figure 2: *Diaporthe acutispora* (isolate D2). Growth on PDA (a) from above; (b) from below; (c) alpha conidiogenous cells; (d) beta conidiogenous cells; (e) alpha and beta conidia, and (f) beta conidia (scale bars c–f = 20 μ M)

was white colour at initially and turned orange brownish later (Figure 2b).

Conidiomata were pycnidial, globose to irregular, black colour, thick-walled and shiny, varying in size, abundant, isolated or grouped, opening by apical ostiole, isolated or merged into smaller or larger clusters, 100–550 μ M in diameter; conidiophores cylindrical to obclavate, hyaline, simple or branched, 9–35 \times 2–3 μ M. Two types of conidia were observed, alpha and beta conidia. Alpha conidia were hyaline, unicellular and fusiform to ellipsoid in shape (Figure 2e), biguttulate, 7–12 \times 2–3 μ M. Beta conidia were single-celled, hyaline, elongated, filiform and thin with a slight curvature at the centre (Figure 2f), 8–23 \times 1–2 μ M.

Molecular identification of the pathogen - phylogenetic analyses

The alignment contained 47 (Table 1) isolates and the tree was rooted to *Diaporthe corylina* (CBS 121124). The final alignment contained a total of 1,316 characters (ITS: 1-509, TUB: 510-951, TEF:952-1,316) used for the phylogenetic analyses, including alignment gaps. The RAxML analysis of the combined dataset yielded a best scoring tree with a final ML optimization likelihood value of -12417.118871 (Figure 3). The phylogenetic tree that resulted from the ML analysis is given in Figure 3. The bootstrap support values above 50% are given at the nodes. The species name is followed by the strain accession numbers, and the newly introduced strain is in red.

Based on combined ITS, TUB and TEF phylogenetic analysis, the isolate D2 clustered with the isolates of *Diaporthe acutispora* (including the type CGMCC 3.18285). The causative agent was identified as *Diaporthe acutispora* Y.H. Gao & L. Cai. *Diaporthe acutispora* was first isolated from *Coffea* sp. as an endophyte and described in 2017 (Gao *et al.*, 2017). Only the asexual morph of *D. acutispora* is known and the sexual morph is not described. The species has also been isolated from *Camellia sasanqua* as an endophyte (Dissanayake *et al.*, 2017; Gao *et al.*, 2017). *Diaporthe acutispora*, being a relatively new species (Gao *et al.*, 2017), not much is known about the species as a plant pathogen or its host range. However, *Diaporthe* species are widely known as important plant pathogens (Dissanayake *et al.*, 2017).

Table 1: Sequence data used for phylogenetic analysis. The newly introduced strain is in red.

Taxon	Isolate	GenBank accessions		
		ITS	TUB	TEF
<i>Diaporthe acutispora</i>	LC6160	KX986763	KX999194	KX999154
<i>Diaporthe acutispora</i>	CGMCC 3.18285	NR_152466	KX999195	KX999155
<i>Diaporthe acutispora</i>	LC6142	KX986762	KX999193	KX999153
<i>Diaporthe acutispora</i>	D2	MW255638	MW276072	MW276073
<i>Diaporthe anacardiae</i>	CBS 720.97	NR_111841	KC343992	KC343750
<i>Diaporthe aseana</i>	MFLUCC 12-0299	NR_154920	KT459432	KT459448
<i>Diaporthe aspalathi</i>	CBS 117169	NR_165951	KC344004	KC343762
<i>Diaporthe baccae</i>	CBS 136972	NR_152458	MF418509	KJ160597
<i>Diaporthe biconispora</i>	ZJUD62	KJ490597	KJ490418	KJ490476
<i>Diaporthe canthi</i>	CBS 132533	NR_111758	KC843230	KC843120
<i>Diaporthe caulivora</i>	CBS 127268	NG_064239	KC344013	KC343771
<i>Diaporthe chamaeropsis</i>	CBS 454.81	KC343048	KC344016	KC343774
<i>Diaporthe cinerascens</i>	CBS 719.96	KC343050	KC344018	KC343776
<i>Diaporthe crotalariae</i>	CBS 162.33	MH855395	KC344024	KC343782
<i>Diaporthe cytosporella</i>	FAU461	MN899309	KC843221	-
<i>Diaporthe dorycnii</i>	MFLUCC 17-1015	NR_152505	KY964099	KY964171
<i>Diaporthe elaeagni</i>	CBS 504.72	KC343064	KC344032	KC343790
<i>Diaporthe elaeagni-glabrae</i>	LC4802	KX986779	KX999212	KX999171
<i>Diaporthe eugeniae</i>	CBS 444.82	KC343098	KC344066	KC343824
<i>Diaporthe foeniculaceae</i>	CBS 111553	NR_145303	KC344069	KC343827
<i>Diaporthe hickoriae</i>	CBS 145.26	MH854869	KC344086	KC343844
<i>Diaporthe hongkongensis</i>	CBS 115448	NR_111848	KC344087	KC343845
<i>Diaporthe incomplete</i>	LC6754	KX986794	KX999226	KX999186
<i>Diaporthe inconspicua</i>	CBS 133813	NR_111849	KC344091	KC343849
<i>Diaporthe isoberliniae</i>	CPC 22549	KJ869133	KJ869245	-
<i>Diaporthe litchicola</i>	BRIP 54900	NR_147521	KF170925	JX862539
<i>Diaporthe lithocarpus</i>	CGMCC 3.15175	NR_147524	KF576311	KC153095
<i>Diaporthe macintoshii</i>	BRIP 55064	NR_147539	KJ197269	KJ197251
<i>Diaporthe maytenicola</i>	CPC 21896	NR_137826	KF777250	-
<i>Diaporthe multiguttulata</i>	ZJUD98	NR_158389	KJ490454	KJ490512
<i>Diaporthe oncostoma</i>	CBS 589.78	KC343162	KC344130	KC343888
<i>Diaporthe osmanthusis</i>	GUCC9165	MK303388	MK502091	MK480610
<i>Diaporthe parapterocarpi</i>	CPC 22729	KJ869138	KJ869248	-
<i>Diaporthe pseudomangiferae</i>	CBS 101339	NR_111858	KC344149	KC343907
<i>Diaporthe psoraleae</i>	CPC 21634	KF777158	KF777251	KF777245
<i>Diaporthe psoraleae-pinnatae</i>	CPC 21638	NR_137827	KF777252	-
<i>Diaporthe ravennica</i>	MFLUCC 15-0479	KU900335	KX432254	KX365197
<i>Diaporthe rhoina</i>	CBS 146.27	KC343189	KC344157	KC343915
<i>Diaporthe saccarata</i>	CBS 116311	NR_120260	KC344158	KC343916
<i>Diaporthe stictica</i>	CBS 370.54	KC343212	KC344180	KC343938
<i>Diaporthe undulata</i>	LC6624	KX986798	KX999230	KX999190
<i>Diaporthe vawdreyi</i>	BRIP 57887	NG_059129	KR936128	KR936129

Continued on page 579 -

- continued from page 578

Taxon	Isolate	GenBank accessions		
		ITS	TUB	TEF
<i>Diaporthe velutina</i>	LC4421	KX986790	KX999223	KX999182
<i>Diaporthe woodii</i>	CBS 558.93	KC343244	KC344212	KC343970
<i>Diaporthe xishuangbanica</i>	LC6707	KX986783	KX999216	KX999175
<i>Diaporthella corylina</i>	CBS 121124	KC343004	KC343972	KC343730

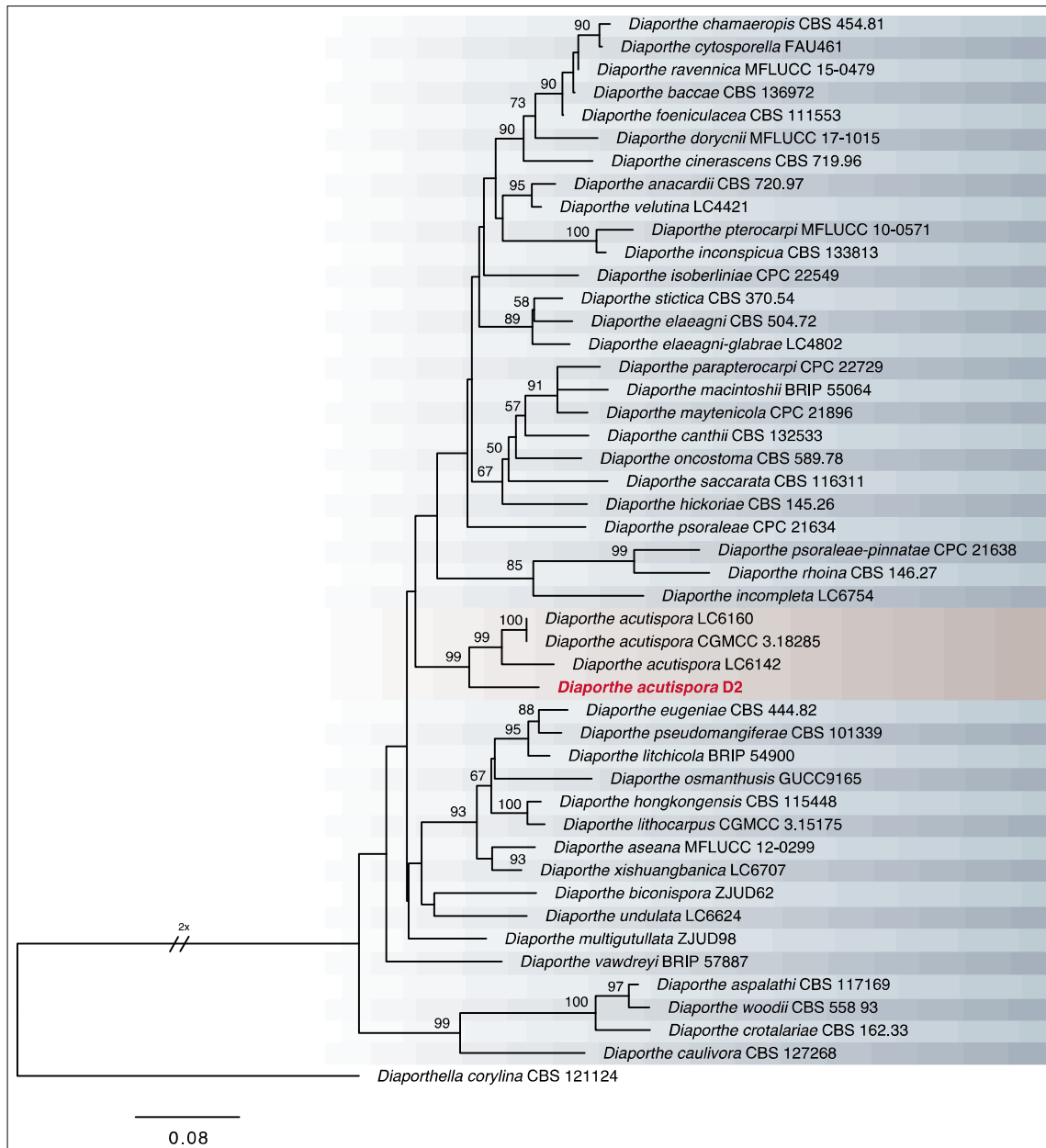


Figure 3: Maximum likelihood tree resulting from a RAxML analysis of the combined (ITS, TUB and TEF) alignment of the analysed *Diaporthe* species. The bootstrap support values above 50% are given at the nodes. The species name is followed by the strain accession numbers, and the newly introduced strain is in red.



Figure 4: Browned mid-rib and secondary veins with extended necrosis of the leaf lamina of *F. religiosa* following artificial inoculation with conidia of *D. acutispora*.

Koch's postulates

The fungus could be repeatedly isolated from diseased leaves and grown on pure culture, indicating its consistent presence. Healthy leaves of *F. religiosa* artificially inoculated with *D. acutispora* showed darkening of the mid-rib and lateral veins, the most consistent symptom observed in the disease (Figure 4). The inoculation also resulted in a dark brown extensive necrosis bordered by already darkened mid-rib and lateral secondary veins 7–14 days after inoculation. There were no symptoms observed in the control plants. Cultural and morphological characteristics of conidia of the fungus obtained from re-isolation were similar to those of the fungus used for inoculation.

Species of *Diaporthe* are known as important plant pathogens, endophytes, or saprobes (Udayanga et al., 2011). They have host ranges, including cultivated crops, trees, and ornamentals (Rossman et al., 2007). Some *Diaporthe* species are responsible for severe die-back, cankers, leaf spots, blights, decay or wilts on different plant hosts of which some are economically important (Gomes et al., 2013).

Ficus religiosa in Sri Lanka is highly susceptible to *D. acutispora* infection, and once infected, often producing disease symptoms in the entire foliage. *Diaporthe* Leaf Disease could incur considerable damage to the foliage of *F. religiosa*, including the mid-rib and secondary veins interfering with water movement within the leaf leading to potentially devastating consequences. The outcome of the present study could contribute significantly towards diagnosis of the disease, including identification of the causal organism accurately and management which are

crucial to understand epidemiology and, prerequisites for developing effective disease management strategies.

Cultural practices such as burning of plant debris (i.e. fallen leaves) or burying them by deep ploughing (Singh, 1987) may reduce disease incidence. Tebuconazole-based fungicide (250 g/L) diluted (5 mL in 10 L) and tested *in vitro* showed 100% inhibition of mycelial growth (*Komala Vithanage, Unpublished data*).

CONCLUSIONS AND RECOMMENDATIONS

The disease, named as *Diaporthe* Leaf Disease (DLD), was new to *F. religiosa*.

The disease is caused by a fungus *Diaporthe acutispora*, identified using cultural and reproductive morphology, DNA sequence analyses, and phylogeny.

The symptoms varied slightly among *F. religiosa* trees, but the darkening of the mid-rib or the vein within the lesion remained a constant characteristic of the disease.

The symptoms described with colour images in the article would conveniently assist diagnosis of the disease.

This is also the first record of *D. acutispora* in Sri Lanka.

Acknowledgements

Authors gratefully acknowledge Lakshika Manawadu for maintaining fungal cultures and Eranga Yakandawala for preparing photo plates.

Conflict of interest statement

All the authors disclose that there is no conflict of interest.

REFERENCES

- Abeygunawardhane D.V.W. (1969). *Diseases of Cultivated Plants in Ceylon*, pp. 240. The Colombo Apothecaries Ltd., Colombo.
- Carbone I. & Kohn L. M. (1999). A method for designing primer sets for speciation studies in filamentous ascomycetes. *Mycologia* **91**(3): 553–556.
DOI: <https://doi.org/10.1080/00275514.1999.12061051>
- Corner E.J.H. (1981). Moraceae. In: *A Revised Handbook to the Flora of Ceylon*, volume III (eds. M.D. Dassanayake & F.R. Fosberg). pp. 213–292. Amerind Publishing Co. Pvt. Ltd., New Delhi, India.
- Dissanayake A.J., Phillips A.J.L., Hyde K.D., Yan J.Y. & Li

- X.H. (2017). The current status of species in *Diaporthe*. *Mycosphere* **8**(5): 1106–1156.
DOI: <https://doi.org/10.5943/mycosphere/8/5/5>
- Doyle J.J. & Doyle J.L. (1987). A rapid DNA isolation procedure for small quantities of fresh leaf tissue. *Phytochemical Bulletin* **19**: 11–15.
- Gao Y., Liu F., Duan W., Crous P.W. & Cai L. (2017). *Diaporthe* is paraphyletic. *IMA Fungus* **1**(1): 153–187.
DOI: <https://doi.org/10.5598/ima fungus.2017.08.01.11>
- Glass N. & Donaldson G. (1995). Development of primer sets designed for use with PCR to amplify conserved genes from filamentous ascomycetes. *Applied Environmental Microbiology* **61**: 1323–1330.
DOI: <https://doi.org/10.1128/aem.61.4.1323-1330.1995>
- Gomes R.R., Glienke C., Videira S.I.R., Lombard L., Groenewald J.Z. & Crous P.W. (2013). *Diaporthe*: a genus of endophytic, saprobic and plant pathogenic fungi. *Personia* **31**: 1–41.
DOI: <https://doi.org/10.3767/003158513X666844>
- Huang F., Udayanga D., Wang X., Hou X., Mei X., Fu Y., Hyde K.D. & Li H. (2015). Endophytic *Diaporthe* associated with *Citrus*: A phylogenetic reassessment with seven new species from China. *Fungal Biology* **119**: 331–347.
DOI: <https://doi.org/10.1016/j.funbio.2015.02.006>
- Indrakeerthi S.R.P. & Adikaram N.K.B. (2011). Control of crown rot of banana using *Carica papaya* latex. *Journal of the National Science Foundation of Sri Lanka* **39**(2): 155–162.
DOI: <https://doi.org/10.4038/jnsfsr.v39i2.3176>
- Johnston A. & Booth C. (ed.) (1983). *Plant Pathologist's Handbook*, 2nd edition, pp. 333–334. Commonwealth Mycological Institute, UK.
- Kumar A.S., Tomer V.D., Gat Y. & Kumar V. (2018). *Ficus religiosa*: A wholesome medicinal tree. *Journal of Pharmacognosy and Phytochemistry* **7**(4): 32–37.
- Kumar S., Stecher G. & Tamura K. (2016). MEGA7: molecular evolutionary genetics analysis version 7.0 for bigger datasets. *Molecular Biology and Evolution* **33**(7): 1870–1874.
DOI: <https://doi.org/10.1093/molbev/msw054>
- Lee S.B. & Taylor J.W. (1990). Isolation of DNA from fungal mycelia and single spores. In: *PCR Protocols: A Guide to Methods and Applications* (eds. M.A. Innis, D.H. Gelfand, J.J. Sninsky & T.J. White), pp. 282–287. Academic Press, San Diego, USA.
DOI: <https://doi.org/10.1016/B978-0-12-372180-8.50038-X>
- Linders E.G.A., Van Damme J.M.M. & Zadoks J. C. (1996). Transmission and over seasoning of *Diaporthe adunca* on *Plantago lanceolata*. *Plant Pathology* **45**(1): 59–69.
DOI: <https://doi.org/10.1046/j.1365-3059.1996.d01-92.x>
- Maharachchikumbura S.S.N. & Adikaram N.K.B. (2009). Occurrence of leaf blotch disease (*Botryosphaeria* sp.) in *Ficus religiosa* in Sri Lanka. *Ceylon Journal of Science (Bio. Sci.)* **38**(2): 51–56.
DOI: <https://doi.org/10.4038/cjsbs.v38i2.1858>
- Maharachchikumbura S.S.N. et al. (41 authors) (2016). Families of Sordariomycetes. *Fungal Diversity* **79**: 1–317.
DOI: <https://doi.org/10.1007/s13225-016-0369-6>
- Miller M.A., Pfeiffer W. & Schwartz T. (2012). The CIPRES science gateway: enabling high impact science for phylogenetics researchers with limited resources. In: *Proceedings of the 1st Conference of the Extreme Science and Engineering Discovery Environment: Bridging from the Extreme to the Campus and Beyond*, pp. 1–8.
DOI: <https://doi.org/10.1145/2335755.2335836>
- Nayab M. & Akhtar N. (2016). First report of *Curvularia aerea* causing leaf spot of *Ficus religiosa* in Pakistan. *Plant Disease* **100**(12): 2530.
DOI: <https://doi.org/10.1094/PDIS-05-16-0650-PDN>
- Panwar N.S., Chand J.N., Singh H. & Paracer S. (1970). Phomopsis fruit rot of brinjal (*Solanum melongena* L.) in Punjab. I. Variability of fungus and role of seed in disease development. *Ludhiana Journal of Agriculture* **7**: 641–643.
- Rambaut A. (2014). FigTree v1.4.2, A Graphical Viewer of Phylogenetic Trees. Available at <http://tree.bio.ed.ac.uk/software/figtree/>
- Rossmann A.Y., Farr D.F. & Castlebury L.A. (2007). A review of the phylogeny and biology of the Diaporthales. *Mycoscience* **48**: 135–144.
DOI: <https://doi.org/10.1007/s10267-007-0347-7>
- Santos J.M., Vrandečić K., Cosic J., Duvnjak T. & Phillips A.J. (2011). Resolving the *Diaporthe* species occurring on soybean in Croatia. *Persoonia* **27**: 9–19.
DOI: <https://doi.org/10.3767/003158511X603719>
- Sharma P., Singh N. & Verma O.P. (2011). First report of leaf blight on *Ficus religiosa* caused by *Phyllosticta* sp. *Journal of Plant Pathology and Microbiology* **2**: 106.
DOI: <https://doi.org/10.4172/2157-7471.1000106>
- Singh R.S. (ed.) (1987). *Plant Pathogens*, 2nd edition. Oxford and IBH Publishing Company, New Delhi, India.
- Stamatakis A. (2014). RAxML version 8: a tool for phylogenetic analysis and post-analysis of large phylogenies. *Bioinformatics* **30**: 1312–1313.
DOI: <https://doi.org/10.1093/bioinformatics/btu033>
- Torres C., Camps R., Aguirre R. & Besoain X.A. (2016). First report of *Diaporthe rudis* in Chile causing stem-end rot on ‘Hass’ avocado fruit imported from California, USA. *Plant Disease* **100**: 1951.
DOI: <https://doi.org/10.1094/PDIS-12-15-1495-PDN>
- Udayanga D., Liu X., McKenzie E.H.C., Chuakeatirote E., Bahkali A.H.A. & Hyde K.D. (2011). The genus *Phomopsis*: biology, applications, species concepts and names of common phytopathogens. *Fungal Diversity* **50**: 189–225.
DOI: <https://doi.org/10.1007/s13225-011-0126-9>
- White T.J., Bruns T., Lee S. & Taylor J. (1990). Amplification and direct sequencing of fungal ribosomal RNA genes for phylogenetics. In: *PCR Protocols: A Guide to Methods and Applications* (eds. M.A. Innis, D.H. Gelfand, J.J. Sninsky & T.J. White), pp. 282–287. Academic Press, San Diego, USA.
DOI: <https://doi.org/10.1016/B978-0-12-372180-8.50042-1>

RESEARCH ARTICLE

Low dose radioiodine therapy: A review of dosimetry and evaluation of potential shielding materials for neck collars

S Mubarak¹, D Nanayakkara², C Jayalath¹ and V Sivakumar^{1*}

¹ Department of Physics, Faculty of Science, University of Peradeniya, Peradeniya.

² Nuclear Medicine Unit, Faculty of Medicine, University of Peradeniya, Peradeniya.

Submitted: 21 July 2020; Revised: 25 June 2021; Accepted: 03 August 2021

Abstract: Radioactive Iodine (¹³¹I) has become the most widely used radionuclide for the treatment of patients with thyroid cancer in Sri Lanka. This study aims to measure radiation dose rate emitted from the ¹³¹I treated patients at the Nuclear Medicine Unit (NMU), University of Peradeniya, Sri Lanka and synthesise a lead-free material to be used as a shielding collar to minimize the radiation exposure to the family members and the general public. Routinely, an average activity of 1110 MBq (30 mCi) is administered orally to thyroid cancer patients following a thyroidectomy. A total number of 40 patients including 17.5% males and 82.5% females were monitored for radiation dose rate after administering the radioiodine. The dose rate was measured at 1.0 m distance from the patient's neck, after 1 hour of ¹³¹I administration. The results showed moderately high dose rates (mean $50.01 \pm 11.50 \mu\text{Sv h}^{-1}$) from these patients when compared to permissible dose rates to the general public in other countries. Hence, measures should be taken to reduce the dose rates at the releasing time of the patients. Four types of shielding materials were synthesised to make a collar. The best shielding material identified was iodine incorporated silicon-based rubber with a reduction percentage of 38.48%.

Keywords: ¹³¹I treatment, nuclear medicine, radiation protection, shielding materials, thyroid cancer.

INTRODUCTION

According to the World Health Organization (WHO), cancer is the second leading cause of death globally and is responsible for an estimated 9.6 million deaths in 2018

(Bangkok Post, 2019; Ulinskiene *et al.*, 2019; Sharma *et al.*, 2020; WHO report, 2020). Approximately 70% of the deaths from cancer occur in low and middle-income countries (Sloan & Gelband, 2007; GHEC, 2008; Bray *et al.*, 2018; Knaul *et al.*, 2018; WHO report, 2020). According to the American Cancer Society (ACS), thyroid cancer has seized the ninth place in worldwide rankings for incidence (Bray *et al.*, 2018). As claimed by the International Agency for Research on Cancer under the supervision of WHO, thyroid cancer is the fifth most common cancer among Sri Lankans in 2018 (GLOBOCAN, 2018; Gunasekera *et al.*, 2018). Also, it is the second most common cancer among women in Sri Lanka (NCCP, 2014; GLOBOCAN, 2018; Jayarajah *et al.*, 2018).

Radioactive iodine (RAI) therapy for thyroid cancer is widely accepted and is the most frequently used treatment modality in the world (Muhammad *et al.*, 2006). ¹³¹I is administered to patients with thyroid carcinoma to ablate residual functioning thyroid tissues as well as to destroy the residual cancer cells after completion of (total or near-total) thyroidectomy (Hackshaw *et al.*, 2007). The administered RAI is absorbed mainly by the thyroid tissues and later excreted by the renal system (Pashnehsaz *et al.*, 2016; Haghigatafshar *et al.*, 2018). The absorbed dose and radiation emission (dose rate) by the thyroid tissues might differ from person to person depending on many factors (Hewamanna *et al.*, 2014).

* Corresponding author (vsiva@sci.pdn.ac.lk;  <https://orcid.org/0000-0002-8473-767X>)



This article is published under the Creative Commons CC-BY-ND License (<http://creativecommons.org/licenses/by-nd/4.0/>). This license permits use, distribution and reproduction, commercial and non-commercial, provided that the original work is properly cited and is not changed in anyway.

The administration of low dose RAI is relatively inexpensive and convenient for the patient with minimum side effects (Muhammad *et al.*, 2006). However, one of the risks of using ^{131}I to treat thyroid cancer is that the patients may act as a mobile radiation source. If precautions were not taken, radiation exposure to family members, caregivers and the general public is inevitable. Thus, standard regulations are made when releasing those patients from the hospital. According to the International Atomic Energy Agency (IAEA) Safety Series No. 63 (IAEA, 2009; HERCA, 2010), patients should not be discharged from the hospital unless the ^{131}I activity is less than or equal to 1100 MBq (~30 mCi). At the same time, some countries follow the safety level of 400 MBq (~11 mCi) as a measure of good practice (IAEA, 2009). Table 1 gives a list of some countries, that discharge RAI administered patients on activity basis (Brian, 2014).

Table 1: Activity based release criteria followed by some countries after RAI administration

Country	Activity at the time of release [MBq (mCi)]
China	400 (10.8)
France, United Kingdom, Poland, Spain, New Zealand	800 (21.6)
Germany	250 (6.8)
Malaysia, Bangladesh	1100 (29.7)

Some countries use the dose rate measured at a fixed distance as a criterion for releasing patients (Zanzonico *et al.*, 2000; Hewamanna *et al.*, 2014). The fixed distance may vary from 1–2 m away from the patient, e.g. Poland measures the dose rate at 1.0 m from the patient whereas Germany measures at 2.0 m distance (Brian, 2014). However, in any case, at the time of release, ^{131}I treated patients are strictly advised on necessary precautions to be taken for the protection of whom they may come in contact with, especially pregnant women and children.

The radiation exposure to the general public from a ^{131}I administered patient mainly depends on the patient's behaviour and understanding of radiation effects as the public is not necessarily aware of the patient's status. Considering the socio-economic conditions, extended family system, nature of the job, mode of transportation, and cultural bindings, releasing ^{131}I treated patients is a common problem in this part of the world. Currently, many countries have formed their own criteria for

releasing patients after RAI therapy according to their own necessities (Brian, 2014).

Sri Lanka Atomic Energy Board (SLAEB), the regulatory body of radiation protection in Sri Lanka in compliance with the IAEA recommendations has imposed an activity-based limit of 1100 MBq (~30 mCi) at the discharge of ^{131}I administered patients from the hospitals (AEA, 1996). The Nuclear Medicine Unit (NMU) of the University of Peradeniya, which treats only out-patients in concurrence with the regulations of the recently established regulatory council, Sri Lanka Atomic Energy Regulatory Council (SLARC) and treats with an average ^{131}I activity of 1110 MBq (30 mCi).

According to de Klerk (2000), there is a possibility for the caregivers and family members, especially toddlers and pre-schoolers, to exceed the annual maximum dose limit (Radiation Protection 97, 1998) from ^{131}I treated patients during their stay at home. For example, family members can be exposed to radiation by cross contamination while using the same bathroom or washing facilities. Usually, before Iodine administration, the patients are advised on their behaviour during the time of their isolated stay at home. While following these instructions a feasible precaution that could be taken to reduce the exposure risk is covering the neck area of the patient using a suitable shielding material.

Usage of lead collars by radioactive patients has been a known practice in developed countries over the past years, owing to the high blocking ability of lead from gamma radiation. However, due to the disadvantages such as high cost, cumbersomeness, disposal difficulties, lead toxicity, etc. currently, the usage of lead for radiation protection is replaced by other materials (Nambiar & Yeow, 2012; Nambiar *et al.*, 2012; Ambika & Nagaiah, 2017). The main aspects expected in synthesising shielding materials are to be more flexible, comfortable, cost-efficient and non-toxic, so that it could be easily disposed.

In this study, an effort has been made to analyse the measured radiation dose rate at the releasing time of ^{131}I treated patients administered with an activity of 1110 MBq (30 mCi). Moreover, an attempt has been made to synthesise a cost-effective, affordable and lead-free shielding material, which can be used as a collar by the patient. This collar can be used as a radiation protection shield by the ^{131}I treated patients at the releasing time in order to minimize the exposure to the caregivers, family members and the general public.

METHODOLOGY

Dose measurement

Ethics approval was not obtained for this study, as it does not require any extra data other than the regular data collected by the NMU, University of Peradeniya for clinical and other safety purposes. Data did not contain any identifiers, which can reveal the personal identity of the subjects. No changes in protocols were adopted for the benefit of this study.

The study used secondary data of 40 thyroid cancer patients (17.5% males and 82.5% females) who have undergone a total or near-total thyroidectomy and were referred to the NMU of the University of Peradeniya. Patients had been administered with radioactive Iodine (^{131}I) having a mean activity of 1043.4 MBq (28.2 mCi) and a median of 1036 MBq (28 mCi) with a standard deviation (SD) of 61.42 MBq (1.66 mCi).

Dose rates emitted from each patient after 1 hour had been recorded at 1.0 m distance away from the neck,

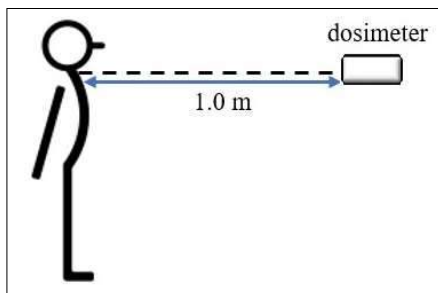


Figure 1: The figure shows the arrangement to take dose rates at the neck area

while the patient was in a standing position (Figure 1), according to the IAEA protocol (IAEA, 2009). Calibrated, portable dose rate meter type - RadEye™ PRD was used to measure the dose rate in $\mu\text{Sv h}^{-1}$. Here, the readings of the RadEye were cross-checked with a dose rate meter (Nuclear Enterprises Portable Dose Rate Meter Type PDR 1) available at the NMU. The dose rate meter at the NMU is calibrated annually at the SLAEB. Background radiation was subtracted from the measurements.

According to the protocol followed by the NMU, patients are allowed to go home after 1 hour from the time of administration.

Collar material

Polyethylene glycol, ethylene glycol and rubber were used as matrix media for the protective collar. Locally available fillers such as bone powder, calcium and phosphate compounds and elements such as Iodine were systematically incorporated into the matrix media.

The alumina incorporated polymer sample was prepared as follows. Alumina (Sigma-Aldrich) (1.28 g) was vacuum dried using the vacuum oven at a temperature of 50 °C for 2 h and was ground well using an agate mortar and pestle. Polyethylene glycol (Sigma-Aldrich) (5.12 g) and ethylene glycol (Sigma-Aldrich) (1.28 g) dissolved in ethanol was added to a beaker along with the ground alumina and DI water. The mixture was thoroughly mixed using a magnetic stir for 2 h to ensure uniform dispersion of alumina in the mixture and was poured into a mold.

In order to prepare the samples with bone powder, first the chloroprene rubber (commercially available) was mixed with dichloromethane (to reduce the thickness) and a small volume was poured into a Perspex mold to get a thin layer. Then to get a composition ratio

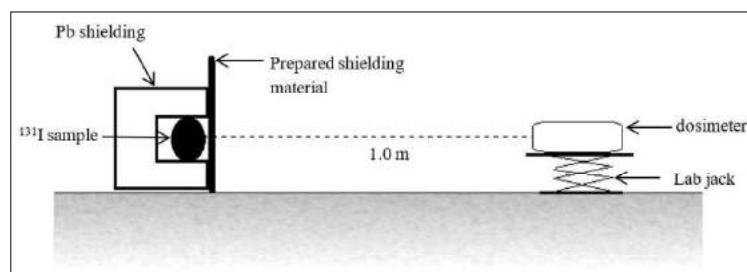


Figure 2: Experimental setup used to calculate the dose rate reduction of the shielding materials prepared

of Ca:P:S:C equals to 6:2:1:1 (wt%), bone powder was dusted upon the chloroprene rubber layer using a metal sieve and allowed to dry. The above-mentioned layers were repeated one after the other until the thickness of 5.0 mm was obtained. The bones were purchased from the local market and were powdered using a laboratory ball mill and sieved using a sieve shaker machine.

To prepare the iodine incorporated silicon rubber (Dow Corning) sample, 20 mL of slime-6178 base and 0.30 mL of catalyst-9600 (1.5% volume of the slime) were mixed in a beaker. Iodine crystals (5 g) (99%, C&G chemicals) were powdered and added to the beaker. The mixture was poured into a Perspex mold and allowed to dry. In all the samples the filler to matrix medium weight ratio was maintained around 1:4 ratio.

Out of the material combinations used, silicon-rubber-based media incorporated with iodine powder (I_2 , 99%, C&G chemicals) and bone powder (purchased from the local market) gave the best shielding ability. The collar was tested using a ^{131}I source while keeping the collar very close to the source and measuring the dose rate at 1.0 m away from the collar using the same dosimeter (Figure 2).



Figure 3: Prototype collar prepared from Iodine incorporated Si-rubber

Usage of collar

Figure 3 depicts the usage of a collar (not with a real patient) that contains the shielding material to cover the thyroid gland. In this prototype, the material blocks the radiation emitted from the front part of the neck. However, it is possible to make the entire collar using the same material so that it can cover the entire neck region. It must be noted that, similar to previously reported studies (Grigsby *et al.*, 2000; Loutfi *et al.*, 2003), testing the collar with real patients and exposure to caregivers

and household members were not undertaken as it required ethical approval.

RESULTS AND DISCUSSION

Dose rate readings

Forty patients were included in the study. The study population consisted of 17.5% males and 82.5% females, ranging in age from 17 to 71 years (mean 40.3 ± 13.16 years). Mean activity of 1043.4 MBq (28.2 mCi) [SD 61.42 MBq (1.66 mCi)] ^{131}I was administered to the patients. The mean dose rate measured at a 1.0 m distance from the patient's neck area after 1 hour of ^{131}I administration was $50.01 \mu Sv h^{-1}$ (SD $11.50 \mu Sv h^{-1}$) with the range 37.3–80.0 $\mu Sv h^{-1}$. By using the reported effective half-life of 5.5 days for ^{131}I by Hewamanna *et al.* (2014), the calculated mean activity after 1 hour of post administration was 1037.94 MBq (28.05 mCi).

A histogram of the normalized dose rate ($\mu Sv / h$ MBq) of each patient at 1.0 m distance at the time of discharge is given in Figure 4. The histogram shown in Figure 5 represents the fluctuation of the dose rate values ($\mu Sv h^{-1}$) at the time of discharge, measured at 1 m distance along with dose rate limits at the discharge practiced in some countries. Also, the figure shows the deviation of the above dose rate limits with respect to the mean value of our measured dose rates. These deviations show that the mean of dose rates measured at the release of the patients at the NMU of University of Peradeniya is moderately high.

Over the past decade, total or near-total surgical removal of the thyroid gland (thyroidectomy) followed by radioactive iodine therapy for ablation of remnant thyroid cells has been the standard treatment for differentiated thyroid cancer (Hewamanna *et al.*, 2014; Pacini *et al.*, 2015). The main concern of using RAI is the radiation exposure risk to the caregivers and the general public due to the ionizing radiation emitted from the ^{131}I administered patients.

Previous studies conducted in Sri Lanka on radiation dose rates emitted from the ^{131}I treated patients were on in-ward patients who received high dose RAI from 3700–11100 MBq (100–300 mCi) at various radiation therapy units (Hettiarachchi, 2008) and at the National Cancer Hospital in Sri Lanka (Hewamanna *et al.*, 2014). For the first time, this study reveals the dose rates emitted from the patients who received low dose 1100 MBq (30 mCi) RAI as out-patient basis at NMU, University of Peradeniya, Sri Lanka.

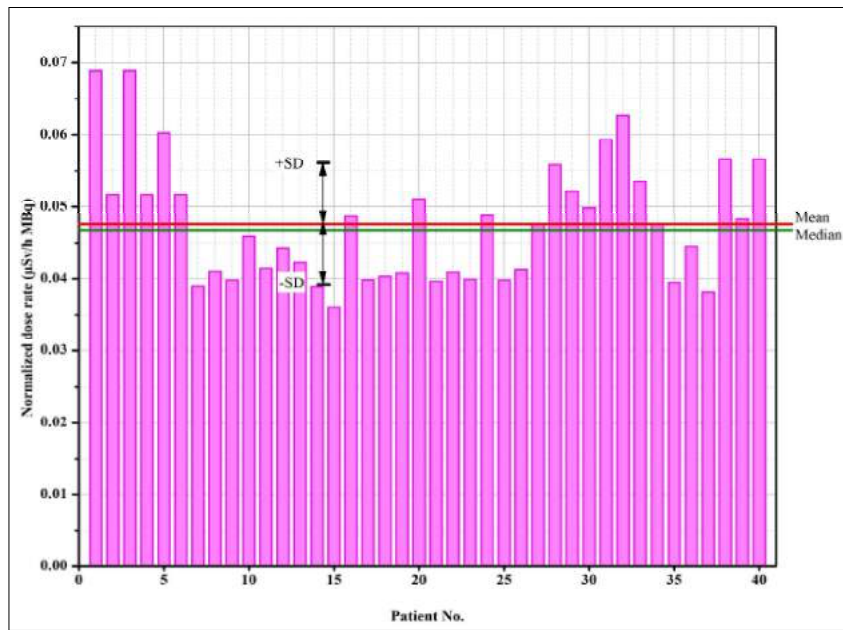


Figure 4: Histogram of the normalized dose rate ($\mu\text{Sv/h MBq}$) of each patient measured at 1.0 m distance at the time of release

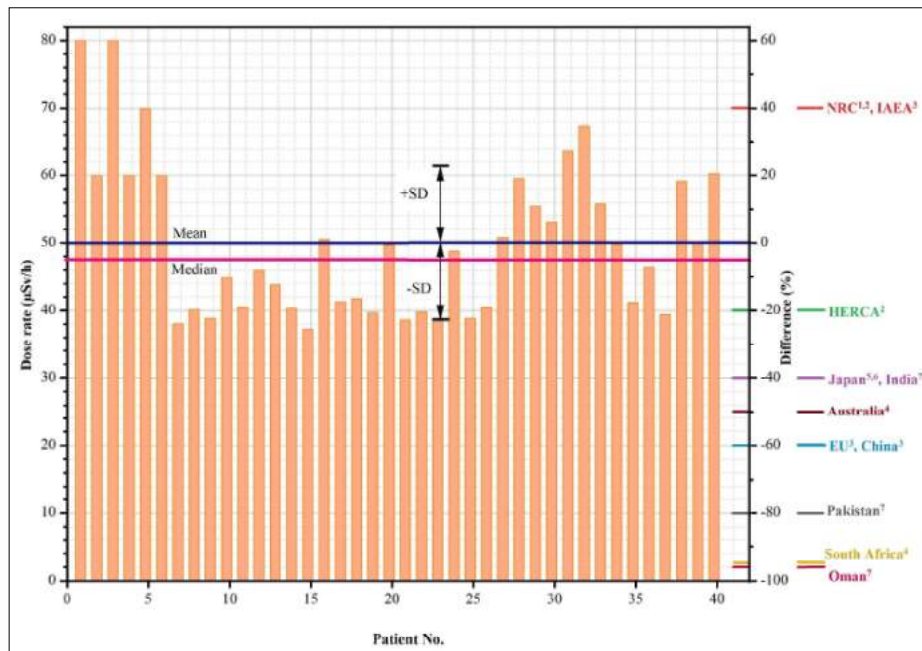


Figure 5: Measured radiation dose rates ($\mu\text{Sv h}^{-1}$) emitted from each patient at 1.0 m distance at the time of release (on the left axis) and the percentage difference (%) of dose limits practiced in some countries with respect to the mean of the measured dose rate (on the right axis).

¹ Lee *et al.*, 2010; ² Nosheen *et al.*, 2016; ³ Zhang *et al.*, 2014; ⁴ Brian, 2014; ⁵ IAEA, 2009; ⁶ Muhammad *et al.*, 2006; ⁷ Al-Maskery & Bererhi, 2009

Figure 4 proclaims a histogram of the normalized dose rate ($\mu\text{Sv/h MBq}$) of each patient measured at 1.0 m distance at the time of release. Here, the emitted dose rate per unit of administered activity has been calculated for each patient involved in this study. Previous studies (Hewamanna *et al.*, 2014) have pointed out that many variables such as the administered ^{131}I activity, patient's gender, age, body weight, percentage of remnant thyroid cells, that differ from patient to patient affect the dose rates emitted from these patients. In our study too, one could observe the variation in the emitted dose rate from the ^{131}I treated patients. We did not excogitate the emitted dose rate dependency on them, as it was not the scope of this study. However, Figure 4 and 5 indicates important information on radiation protection purpose considering that it is directly linked to the risk of managing these ^{131}I treated patients.

According to Hewamanna *et al.* (2014) some studies conducted on discharged patients administered with more than 1110 MBq (30 mCi) ^{131}I have concluded that for most of the patients, 35–75% of the ^{131}I is cleared from the body within the first 24 hours. According to Memon *et al.* (2017), the recommended dose rate on discharging ^{131}I treated patients to avoid unwanted radiation exposure to family members was around 20–30 $\mu\text{Sv h}^{-1}$ at 1.0 m distance. Barrington *et al.* (1996) recommended that ^{131}I administered patients should be separated from children less than 2 years of age for at least 16 days. It has been calculated that the dose to such a child if the advice is not heeded, will be 33 mSv which is a considerably high value compared to the annual maximum dose limit for children (1 mSv y^{-1}) (Barrington *et al.*, 1996; Radiation Protection 97, 1998; Memon *et al.*, 2017). The same implies to the working staff and the caregivers who are being exposed, yet the maximum instructed limit for them is 5 mSv y^{-1} (Radiation Protection 97, 1998). According

to the protocols followed at the National Cancer Institute (NCI) of Sri Lanka, all the patients are discharged from the hospital only when the dose rate measured at 1.0 m from their bodies is less than 30 $\mu\text{Sv hr}^{-1}$ (Hewamanna *et al.*, 2014).

Complying with the regulations of SLARC, patients administered with ^{131}I are discharged with strict instructions only if the activity is less than or equal to 1110 MBq (30 mCi) (AEA, 1996). Moreover, ^{131}I administered patients are observed 1 hour after the administration as a routine practice at the NMU premises.

It is visible that the dose rate values emitted from the ^{131}I administered patients from NMU are greater than that of most countries recommended value on discharging the patients from the hospitals (Figure 5). Thus, as a precautionary measure to this problem; we have suggested using a protective collar by the patients to reduce the emitted dose rate to a certain extent. This is in addition to the radiation protection advice given to the patients at the time of discharge.

Shielding materials

The materials synthesized incorporating different kinds of composites are presented in Table 2. Here, these sample materials were tested using a ^{131}I source (~10 mCi) that emits gamma rays at an average photon energy of 360 keV. The prepared samples were categorised into 4 main types; alumina incorporated polymers, bone composition with chloroprene rubber, bone powder with chloroprene rubber, and iodine incorporated silicon rubber. The maximum reduction percentage of radiation (1) calculated for each type of sample using equation is also shown in Table 2. Here, the measurements were taken while using the materials as a shield in front of the source (Figure 2) and without using any shield.

$$\text{Reduction} = \frac{(\text{dose rate before shielding}) - (\text{dose rate after shielding})}{\text{dose rate before shielding}} \times 100\% \quad \dots(1)$$

Table 2: The maximum reduction percentage of different types of samples prepared

Material	Thickness (mm)	Maximum reduction (%)
lumina incorporated polymer	4.21	6.75
Bone composition with chloroprene rubber	4.21	22.79
Bone powder with chloroprene rubber	4.02	30.10
Iodine incorporated Si-rubber	5.21	38.48

In this study, the first collar material was prepared by incorporating alumina into a biocompatible polymer matrix where it gave a dose rate reduction of 6.75% while measuring at 1.0 m distance from the ^{131}I source (Figure 2). Commercially available chloroprene rubber incorporated with different compositions of calcium and phosphate (to obtain bone composition) gave reduction percentages that varied from 14% to 23%. The maximum reduction 22.79% was obtained while using Ca: P: S: C ratio 6: 2:1: 1 wt.% (bone composition) along with chloroprene rubber. Actual bone powder incorporated in chloroprene rubber gave a reduction percentage of 30.10%. However, the major drawback of using chloroprene rubber as the matrix medium was that it became harder and rigid when the thickness was increased.

Iodine incorporated silicon rubber-based sample displayed a reduction percentage up to a maximum of 38.48%. To have an inkling, the reduction percentage value was compared with the reported value of He *et al.* (2016), where an evaluation has been performed to find the shielding effectiveness of lead aprons used in nuclear medicine clinics. It has been concluded that depending on whether the aprons are really made of lead or lead equivalent thickness, the reduction percentage might vary between 19–24% for gamma rays with energy of 356 keV. Hence, considering these factors, the reduction percentage obtained for the iodine incorporated silicon rubber-based sample seems to be persuasive. This convincing reduction percentage may be due to the absorption edges of the iodine incorporated (Kane, 2009). In addition to this level of attenuating the radiation, the material is also flexible, and cost-efficient.

CONCLUSION

The results show emission of moderately high dose rates (mean $50.01 \mu\text{Sv h}^{-1}$ and median $47.65 \mu\text{Sv h}^{-1}$ with SD $11.50 \mu\text{Sv h}^{-1}$) from RAI treated patients at the time of discharge from the NMU, University of Peradeniya. In order to minimize the radiation exposure to the general public and caregivers, wearing a neck collar as a radiation shield by these patients is proposed. Among the four types of shielding materials synthesized with the aim of producing a lead-free, flexible and cost-effective collar, the best shielding material was the iodine incorporated silicon-based rubber with a reduction percentage of 38.48%.

Conflicts of interest

The authors have no conflict of interest to disclose.

REFERENCES

- AEA Regulations on Ionizing Radiation Protection (1996). Available at https://www.aeb.gov.lk/web/images/stories/article/srlregulations_2000_webversion.pdf, Accessed 10 October 2019.
- Al-Maskery I. & Bererhi H. (2009). Radiation exposure levels in family members of Omani patients with thyrotoxicosis treated with radioiodine (^{131}I) as outpatients. *Sultan Qaboos University Medical Journal* **9**(2): 148–152.
- Ambika M.R. & Nagaiah N. (2017). Gamma shielding ability and chemical stability of polyester-based polymer composites. *Indian Journal of Advances in Chemical Science* **S2**: 23–27.
DOI: <https://doi.org/10.22607/IJACS.2017.S02006>
- Bangkok Post Public Company Limited (2019). Cancer in the workplace: eliminating cancer anxieties. Available at <https://www.bangkokpost.com/business/1762479/cancer-in-the-workplace-eliminating-cancer-anxieties>, Accessed 17 November 2019.
- Barrington S.F., Kettle A.G., Odoherty M.J., Wells C.P., Somer E.J.R. & Coakley A.J. (1996). Radiation dose rates from patients receiving iodine-131 therapy for carcinoma of the thyroid. *European Journal of Nuclear Medicine* **23**(2): 123–130.
DOI: <https://doi.org/10.1007/bf01731834>
- Bray F., Ferlay J., Soerjomataram I., Siegel R.L., Torr L.A. & Jemal A. (2018). Global cancer statistics 2018: GLOBOCAN estimates of incidence and mortality worldwide for 36 cancers in 185 countries. *CA: A Cancer Journal for Clinicians* **68**(6): 394–424.
DOI: <https://doi.org/10.3322/caac.21492>
- Brian E.H. (2014). International patient release practices following iodine-131 therapy. Available at <https://www.nrc.gov/docs/ML1421/ML14217A350.pdf>, Accessed 25 January 2020.
- de Klerk J.M.H. (2000). ^{131}I therapy: inpatients or outpatients? *Journal of Nuclear Medicine* **41**(11): 1876–1878.
- GHEC (2008). Cancer control in low and middle-income countries. Available at https://www.cugh.org/sites/default/files/17_Cancer_Control_In_Low_And_Middle_Income_Countries_FINAL_0.pdf, Accessed 10 November 2019.
- GLOBOCAN (2018). Fact sheets-Sri Lanka. Available at <http://gco.iarc.fr/today/data/factsheets/populations/144-sri-lanka-fact-sheets.pdf>, Accessed 22 November 2019.
- Grigsby P.W., Siegel A., Baker S. & Eichling J.O. (2000). Radiation exposure from outpatient radioactive iodine (^{131}I) therapy for thyroid carcinoma. *Jama* **283**(17): 2272.
DOI: <https://doi.org/10.1001/jama.283.17.2272>
- Gunasekera S., Seneviratne S., Wijeratne T. & Booth C.M. (2018). Delivery of cancer care in Sri Lanka. *Journal of Cancer Policy* **18**: 20–24.
DOI: <https://doi.org/10.1016/j.jcpc.2018.10.001>
- Hackshaw A., Harmer C., Mallick U., Haq M. & Franklyn J.A. (2007). ^{131}I activity for remnant ablation in patients with differentiated thyroid cancer: a systematic

- review. *The Journal of Clinical Endocrinology and Metabolism* **92**(1): 28–38.
DOI: <https://doi.org/10.1210/jc.2006-1345>
- Haghighatafshar M., Banani A., Zeinali-Rafsanjani B., Etemadi Z. & Ghaedian T. (2018). Impact of the amount of liquid intake on the dose rate of patients treated with radioiodine. *Indian Journal of Nuclear Medicine* **33**(1): 10–13.
DOI: https://doi.org/10.4103/ijnm.IJNM_90_17
- He X., Zhao R., Rong L., Yao K., Chen S. & Wei B. (2016). Answers to if the lead aprons are really helpful in nuclear medicine from the perspective of spectroscopy. *Radiation Protection Dosimetry* **174**(4): 558–564.
DOI: <https://doi.org/10.1093/rpd/ncw255>
- HERCA (2010). 131I therapy: Patient release criteria. Available at https://www.herca.org/docstats/Annexe%20I_HERCA-OH_2011_0005_HERCA_Release%20criteria%2030062010.pdf, Accessed 18 February 2020.
- Hettiarachchi M. (2008). Radiation protection in nuclear medicine: a review on present situation in Sri Lanka. *Galle Medical Journal* **13**(1): 33–35.
DOI: <https://doi.org/10.4038/gmj.v13i1.892>
- Hewamanna R., Loganathan N. & Perera D. (2014). Releasing thyroid cancer patients from the hospital based on dose rate measurement after 131I activity administration. *Journal of the National Science Foundation of Sri Lanka* **42**(2): 137.
DOI: <https://doi.org/10.4038/jnsfsr.v42i2.6993>
- IAEA (2009). Safety Report Series No.63: Release of Patients After Radionuclide Therapy. Available at https://www-pub.iaea.org/MTC'D/publications/PDF/pub1417_web.pdf, Accessed 6 December 2019.
- Jayarajah U., Fernando A., Prabashani S., Fernando E.A. & Seneviratne S.A. (2018). Incidence and histological patterns of thyroid cancer in Sri Lanka 2001-2010: an analysis of national cancer registry data. *BMC Cancer* **18**(1): 163.
DOI: <https://doi.org/10.1186/s12885-018-4083-5>
- Kane S.A. (2009). *Introduction to Physics in Modern Medicine*, 2nd edition. CRC Press, Taylor and Francis Group, USA.
- Knaul F.M., Arreola-Ornelas H., Rodriguez N.M., Méndez-Carniado O., Kwete X.J., Puentes-Rosas E. & Bhadelia A. (2018). Avoidable mortality: the core of the global cancer divide. *Journal of Global Oncology* **4**: 1–12.
DOI: <https://doi.org/10.1200/jg-o.17.00190>
- Lee J. & Park S. (2010). Estimation of the release time from isolation for patients with differentiated thyroid cancer treated with high-dose I-131. *Nuclear Medicine and Molecular Imaging* **44**(4): 241–245.
DOI: <https://doi.org/10.1007/s13139-010-0041-0>
- Loutfi I., Sakr M. & Al-Shummari A.M. (2003). Minimizing radiation exposure from patients treated with Iodine-131 for hyperthyroidism using a lead collar: a simple and effective approach. *Medical Principles and Practice* **12**(4): 203–207.
DOI: <https://doi.org/10.1159/000072284>
- Memon S.A., Laghari N.A., Mangi F.H., Hussain M.M. & Nohario S.H. (2017). Isolation period of 131I administered patients at NIMRA Jamshoro Pakistan. *International Journal of Radiology and Radiation Therapy* **2**(1): 1.
DOI: <https://doi.org/10.15406/ijrrt.2017.02.00011>
- Muhammad W., Faaruq S., Matiullah H.A. & Khan A.A. (2006). Release criteria from hospitals of 131I thyrotoxicosis therapy patients in developing countries—case study. *Radiation Protection Dosimetry* **121**(2): 136–139.
DOI: <https://doi.org/10.1093/rpd/ncl003>
- Nambiar S. & Yeow J.T.W. (2012). Polymer-composite materials for radiation protection. *ACS Applied Materials & Interfaces* **4**(11): 5717–5726.
DOI: <https://doi.org/10.1021/am300783d>
- Nambiar S., Osei E.K. & Yeow J.T.W. (2012). Polymer nanocomposite-based shielding against diagnostic X-rays. *Journal of Applied Polymer Science* **127**(6): 4939–4946.
DOI: <https://doi.org/10.1002/app.37980>
- NCCP (2014). Cancer incidence data, Sri Lanka 2014. Ministry of Health, Colombo. Available at https://www.nccp.health.gov.lk/pdf/publications/cancer_incidece/Cancer_Incidence_in_Sri_Lanka_2014.pdf, Accessed 23 February 2020.
- Nosheen F., Maseeh U.Z., Areeba Z., Unaiza Z., Rabia T. & Wajiha S. (2016). Factors predicting early release of thyroid cancer patients from the isolation room after radioiodine-131 treatment. *Asian Pacific Journal of Cancer Prevention* **17**: 125.
DOI: <https://doi.org/10.7314/APJCP.2016.17.1.125>
- Pacini F., Brianzoni E., Durante C., Elisei R., Ferdeghini M., Fugazzola L., Mariotti S. & Pellegriti G. (2015). Recommendations for post-surgical thyroid ablation in differentiated thyroid cancer: a 2015 position statement of the Italian Society of Endocrinology. *Journal of Endocrinological Investigation* **39**: 341–347. DOI: <https://doi.org/10.1007/s40618-015-0375-7>
- Pashnehsaz M., Takavar A., Izadyar S., Zakariaee S.S., Mahmoudi M., Paydar R. & Geramifar P. (2016). Gastrointestinal side effects of the radioiodine therapy for the patients with differentiated thyroid carcinoma two days after prescription. *World Journal of Nuclear Medicine* **15**(3): 173–178. DOI: <https://doi.org/10.4103/1450-1147.174703>
- Radiation Protection 97 (1998). *Radiation Protection Following Iodine 131 Therapy*. European Commission. Available at https://ec.europa.eu/energy/sites/ener/files/documents/097_en.pdf, Accessed 29 January 2020
- Sharma B., Parajuli P. & Podila R. (2020). Rapid detection of urokinase plasminogen activator using flexible paper-based graphene-gold platform. *Biointerphases* **15**(1): 011004.
DOI: <https://doi.org/10.1116/1.5128889>
- Sloan F.A. & Gelband H. (2007). *Cancer Control Opportunities in Low- and Middle-Income Countries*. National Academies Press, Washington DC, USA.
DOI: <https://doi.org/10.17226/11797>
- Ulinskiene D.L., Patasius A., Zabuliene L., Stukas R. & Smailyte G. (2019). Increased risk of site-specific cancer in people with type 2 diabetes: a national cohort study. *Endocrine Abstracts*. *International Journal of Environmental, Research and Public Health* **17**: 246.
DOI: <https://doi.org/10.3390/ijerph17010246>

WHO report (2020). Cancer. Available at https://www.who.int/health-topics/cancer#tab=tab_1, Accessed 15 October 2109.

Zanzonico P.B., Siegal J.A. & St Germain J.A. (2000). generalized algorithm for determining the time of release and the duration of post-release radiation precautions following radionuclide therapy. *Health Physics* **78**: 648–659.

DOI: <https://doi.org/10.1097/00004032-200006000-00007>
Zhang H., Jiao L., Cui S., Wang L., Tan J., Zhang G., He Y., Ruan S., Fan S. & Zhang W. (2014). The study of external dose rate and retained body activity of patients receiving ¹³¹I therapy for differentiated thyroid carcinoma. *International Journal of Environmental Research and Public Health* **11**(10): 10991–11003.

DOI: <https://doi.org/10.3390/ijerph111010991>

RESEARCH ARTICLE

Effects of particle size and concentration on the pulsation characteristics of transformer oil

C Bin^{1*} and L Ge²

¹ School of Mechanical & Electrical, Hebei Key Laboratory of Safety Monitoring of Mining Equipment, North China Institute of Science and Technology, Hebei, 065201, China.

² Heibei Key Laboratory of Hazardous Chemicals Safety and Control Technology, School of Chemical and Environmental Engineering, North China Institute of Science and Technology, Hebei, 065201, China.


Submitted: 28 July 2020; Revised: 09 April 2021; Accepted: 24 September 2021

Abstract: The presence of particulate matter in oil has a great impact on the pulsation characteristics of oil. The effects of particle size and concentration on the pulsation characteristics of oil were studied to ensure the safe operation of oil equipment. According to the ISO 4406 standard for oil contamination, oil samples containing Cu, Fe, and SiO₂ with particle sizes of 5, 15, 25, and 50 μm and concentrations of 6.58, 4.57, 3.00, 0.971, 0.648 ppm were configured. Oil flow with different particle sizes and concentrations was tested in a square tube using PIV measurement technology. The instantaneous velocity vector data of the flow field were acquired in oil with different sizes and concentrations of the particles, and the distributions of the pulsation intensity of oil along the streamwise and normal directions were analysed. The time-frequency curves of the transient velocity and average velocity were discussed. The results showed that the distribution of the streamwise pulsation intensity of oil changes more gently along the normal direction in the centre region and changes more steeply in the near-wall area. With increasing particle concentration, the streamwise pulsation intensity of oil decreases gradually. The distribution of the normal pulsation intensity of oil along the normal direction is rough 'w'-shaped under different particle diameters. With increasing particle concentration, the main frequency trend of the oil speed along with the streamwise and normal directions decreases, and the streamwise average speed of the oil increases. The change in the normal average speed of oil decreases when the particle concentration is under 3.00 ppm. The normal velocity of oil increases when the particle concentration is over 3.00 ppm.

Keywords: Oil flow, particle concentration, particle size, PIV measurement, pulsation characteristics.

INTRODUCTION

The power transformer is the core equipment of power transmission and conversion that plays a significant role in ensuring the safe operation of the power grid. However, the transformer pulsates due to the influence of various factors, such as core loosening and winding deformation, which will significantly reduce the ability of the transformer to withstand short-circuit impact and then cause power system faults. Therefore, monitoring the pulsation of transformers and evaluating the state of core and winding is of great significance for the stable operation of transformers. The vibration of a transformer is caused by winding deformation due to the electromagnetic force on the winding through the transformer oil to the tank wall or loose core due to magnetostriction phenomenon of silicon steel sheet by the same transformer oil to the tank wall, so the transformer pulse monitoring can be done by detecting the transformer oil pulsation (Bagheri, 2018). In the industry, various methods are usually used to detect the pulsation of transformer oil to obtain the fault information of a transformer indirectly because the pulsation of transformer oil is not only related to

* Corresponding author (hustchb@ncist.edu.cn;  <https://orcid.org/0000-0001-5196-1221>)



This article is published under the Creative Commons CC-BY-ND License (<http://creativecommons.org/licenses/by-nd/4.0/>). This license permits use, distribution and reproduction, commercial and non-commercial, provided that the original work is properly cited and is not changed in anyway.

the function of the transformer switching switch but also plays a vital role in the pulsation of oil due to the characteristics of the oil, particle size and concentration in the oil (Zeng, 2018).

As an arc extinguishing medium, transformer oil is bound to produce carbon particles, polar impurities, and charging colloids and other ageing products. Moreover, with the increase of switching switch or selector switch connection conversion times, there must be mechanical friction and wear in the oil. Mechanical wear debris, mainly copper, iron, and other metal particles directly adulterate the transformer oil. These particles are very fine, and some of them can float in the oil for a long time without settling. Moreover, iron dust, even by the transformer winding adsorption, seriously affects the insulation performance of the transformer (Borges, 2015). Therefore, it is necessary to carry out studies to understand the influence of the size and concentration of particles in the transformer oil on the pulsation characteristics of oil for the safe operation of the transformer.

The effect of particle size and concentration on the pulsation characteristics of oil belongs to a sparse solid-liquid two-phase flow field, on which many scholars have carried out theoretical simulation and experimental research (Abiev & Galushko, 2013; Eschmann *et al.*, 2015; Wang *et al.*, 2016; Yuan *et al.*, 2016). These results have a specific reference value to investigate the influence of particle size and concentration in oil with higher viscosity on the pulsation characteristics of the oil.

Papadopoulos *et al.* (2016) conducted a direct numerical simulation of sinusoidal pulsation turbulence in a straight tube with a low-volume Reynolds number and a high-frequency, indicating the evolution of the average velocity and fluid pulsation over time. Tian *et al.* (2016) obtained the variation trend of vibration displacement and the velocity of a pipeline system by establishing an analysis method of pressure pulsation in the channel and the coupling interaction of tube flow. Yan *et al.* (2012) studied the interaction between quasiperiodic large-scale vortex structures and flow pulsation in a rectangular channel. The conclusions indicated that the pulsation of the vortex structure and the flow velocity pulsation could be enhanced by an adjacent velocity interface. Zhao *et al.* (2016) studied the unsteady flow field in a channel using direct numerical simulation and found that the contributions of the low-frequency vortices to the flow direction and normal pulsation velocity increase with increasing normal

height; the pulsation of the spanwise velocity at the near-wall surface exhibited a large pulsation strength in the logarithmic layer and the viscous bottom layer. Ghadi *et al.* (2016) conducted jet oscillating flow experiments and showed that pulsating flow forms a coherent periodic structure. The pulsation frequency has a significant influence on the formation, size, and dynamics of a vortex structure. Hsu *et al.* (2014) measured a jet field using high-speed particle image velocimetry (PIV). They found that with the change in the jet exit velocity, the jet produced vibration within a pulsating period and induced a periodic wavy flow structure in the downstream region. Yang *et al.* (2013) believed that the change in frequency of wind-sand flow was at least greater than 100 Hz, and the effect of atmospheric turbulent pulsation on sediment concentration was related to the sand grain size; the smaller the particle size was, the greater the effect of wind speed fluctuation.

Two-phase flow in pipelines has been studied for the generation and development of flow field pulsation and the interaction of vortex structures in flow fields at home and abroad. However, due to the random nature of oil movement and the complexity of its interaction with particles, the understanding of the pulsation characteristics of oil with different particle sizes and concentrations remains in the qualitative or semiquantitative stage. Moreover, there is little literature that analyses the pulsation characteristics of oil with higher viscous fluids. Therefore, it is necessary to investigate the pulsation characteristics of oil in the flow direction and for the normal pulsation strength, as well as the instantaneous velocity and the average velocity based on the vector field data measured by the PIV of the oil-containing particles in pipelines. Additionally, understanding the pulsation movement of oil at different concentrations and particle sizes reveals the interaction between particles and oil and lays a foundation for understanding the physical essence of the formation and development of oil pollution. This enables effective detection and diagnosis of transformer pulsation, early detection and elimination of hidden faults, avoiding unexpected accidents, and is vital for the safe operation of the transformer.

METHODOLOGY

The PIV experimental equipment for oils containing different particle sizes and particle concentrations are shown in Figure 1. It is mainly divided into two parts: experimental pipeline and PIV testing device. The coordinate origin is the vertex at the lower left corner of the experimental pipeline, x-direction is the flow direction of oil, y-direction is the spanwise direction,

and z-direction is the normal direction of oil. The experimental pipeline is a square tube with a total length of 500 mm and a cross-section of 40×40 mm, the oil inlet section of the pipeline is the development section 200 mm long and the middle is the test section 100 mm

long, the bottom and back wall of the test section is made of a steel plate, the front wall and top surface are made of glass and can be disassembled for PIV laser incidence and testing. 2DPIV system from TSI (USA) is used for the PIV test device,

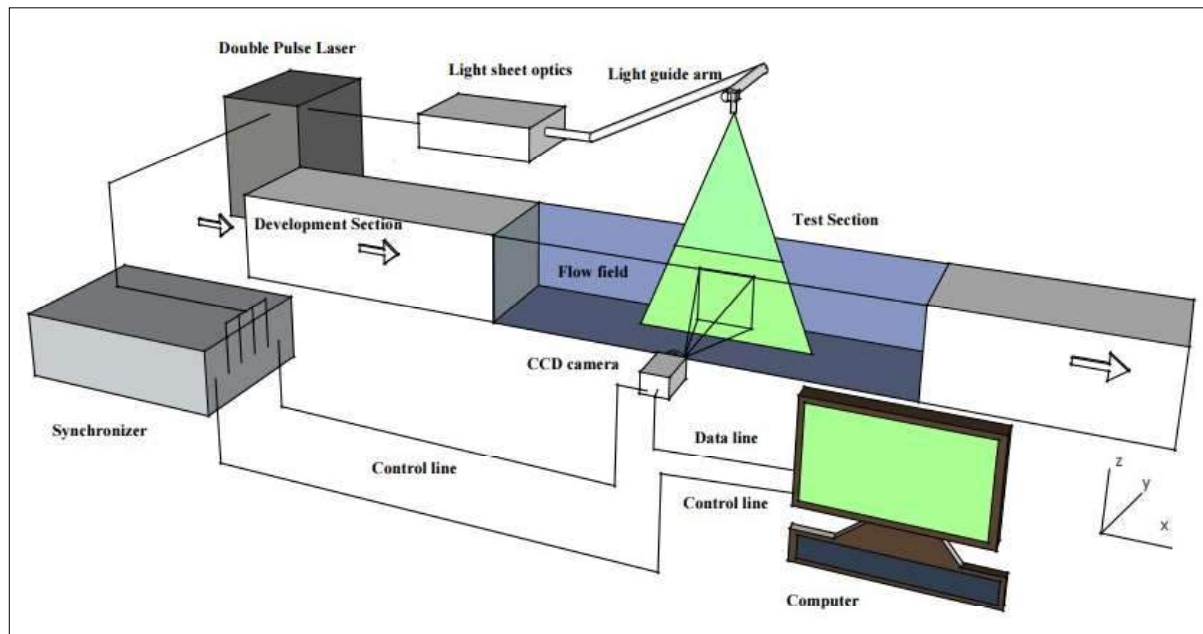


Figure 1: PIV experimental equipment for oil liquid

The 2DPIV system consists of a double yttrium aluminum garnet laser (200 mJ, pulse frequency 15 Hz, laser wavelength 532 nm), light guide arm, sheet light source lens (focal length from 30–3000 mm, two sets of cylindrical lenses 15 mm F.L. and -25 mm F.L., and divergence angles 25° and 14° , respectively), a Nikon CCD camera (15 frames per sec, 50 mm/ F1.8 lens, $2K \times 2K$ pixel resolution) and TSI Insight4G image acquisition, analysis and display software platform. The coordinate frame of the camera is three-dimensional and is automatically controlled by a microcomputer with a movement accuracy of 0.01 mm. The laser light emitted from the laser passes through the light guide arm and the light source lens to form a 1-mm thick sheet light, which is irradiated from the normal direction (z-direction) of the pipe test section. Then, oil image information is obtained by the camera positioned in the direction of the pipe (y-direction). In addition, the synchronization controller (time resolution of 0.25 ns) is set to trigger the laser and the camera synchronously.

25# transformer oil was used as the test fluid (colourless and transparent for the PIV test). First, the oil was treated by a vacuum filter to obtain an initial oil sample. Then, Cu, Fe, and SiO_2 powders (Beijing Focus Yingchuang Technology Co., Ltd., China) of different particle sizes were selected as particulate matter to simulate metallic and non-metallic contaminants in transformer oil. According to the ISO 4406 standard for oil contamination, the particulate matter in oil was divided into several size segments of 5, 15, 25, and $50 \mu\text{m}$ according to different contamination levels. The concentration of particulate matter in the measured oil sample was converted into the corresponding volume fraction of particulate matter in oil according to the test results of different contamination levels. The volume fraction of the particulate matter in oil was obtained as 6.58, 4.57, 3.00, 0.971, 0.648 ppm in several volume concentrations of oil samples. In this method, 0.02 g of Cu, Fe, and SiO_2 powder were mixed with 1 L 25# transformer oil and oscillated evenly in an ultrasonic oscillator for 8 hours (temperature kept at

30–60 °C). Then, the mixed solution was separated using a filter paper having different pore diameters to obtain oil samples of medium diameter of 5, 15, 25, and 50 μm and a concentration of 14.40 ppm. Next, the initial oil sample was added to the oil sample at a certain volume ratio, and ultrasonic vibration was evenly distributed over 8 hours (temperature kept at 30–60 °C). Oil samples containing particles having a gradient concentration of 6.58, 4.57, 3.00, 0.971, and 0.648 ppm of different medium-diameter particles were eventually obtained.

Since the pulsation amplitude of transformer oil in the operational process is small at about 100 μm , and lower pulsation frequency of about 100 Hz, the oil in the transformer is in laminar flow. So, the initial velocity of the oil inlet is set as $V_0 = 0.0362$ m/s. As the dynamic viscosity μ of transformer oil is 10.58 mPa.s, density ρ is 895 kg/m^3 , equivalent diameter d of the experimental pipe section is 0.0452 m, corresponding Reynolds number $Re = \rho d V_0 / \mu = 138.3$, and the oil in the pipeline is in laminar flow. Since the temperature did not change much during an experiment, the influence of temperature was not considered. The oil samples to be tested were thoroughly mixed and fed into the test pipeline through a peristaltic pump. As the particle size is up to 50 μm , the dynamic viscosity of transformer oil 10.58 mPa.s is larger, thus after flowing through the pipeline development section of 200 mm long, a uniform liquid-solid two-phase suspension flow was formed in the test section, and then entered the oil tank through the tail section to form a circulation. After several experimental tests, the system was run for 30 minutes before the PIV test, ensuring that the oil and particles were fully and uniformly mixed during the PIV measurement period.

As the particle size in oil is less than 100 μm , the particles follow good behaviour and uniform distribution of light scattering, so no tracer particles were needed to be added during the test. The acquired image adopts the algorithms of multigrid iterative mutual correlation and multiadaptive deformation window. To obtain the original velocity vector, the image query area adopts pipeline horizontal and vertical initial query windows of 72×64 pixels, a final query window of 64×48 pixels and 50% overlap to eliminate the impact of the query window boundary. The method of processing the error vector is to use a local average verification method, and this vector is replaced by the mean in the adjacent 5×5 -pixel range. The measurement position is 300 mm from the inlet of the pipeline; the measurement area is (flow direction \times normal direction) 85.86×22.20 mm, while the centre of the area is (flow direction \times normal direction) 300×30 mm. In addition, 200 image frames were captured in each test period.

RESULTS AND DISCUSSION

The instantaneous velocity vector field data were averaged over time, and the mean square of the flow velocity and normal pulsation velocity were obtained. The flow pulsation intensity and normal pulsation intensity were as follows:

$$\sigma_u = \sqrt{\frac{1}{C} \sum_{x=1}^C \left[u(x, y, t) - \frac{1}{N} \sum_{i=1}^N u(x, y, t) \right]^2},$$

$$\sigma_v = \sqrt{\frac{1}{C} \sum_{x=1}^C \left[v(x, y, t) - \frac{1}{N} \sum_{i=1}^N v(x, y, t) \right]^2} \quad \dots(1)$$

In the formulas, σ_u and σ_v indicate the fluctuation intensity of the flow and normal pulsation intensities, respectively; $u(x, y, t)$ and $v(x, y, t)$ represent the flow instantaneous velocity and normal instantaneous velocity at a certain position (x,y) at a certain time t, respectively, that PIV acquires in the flow field; N is the period of PIV acquisition, and C is the number of acquisitions in the PIV field of view.

Distribution of flow pulsation intensity along the normal direction

When the particle size in the oil is 5, 15, 25, and 50 μm while the particle concentration is 0.65, 0.97, 3.00, 6.58, and 14.40 ppm, the distribution curves of the flow pulsation intensity along the normal direction are shown in Figure 2. The horizontal axes of the graphs show the ratio of the flow pulsation intensity to the fluid inlet velocity V_0 , and the vertical coordinate represents the normal dimensionless pipe length.

Figure 2(a) shows the distribution of the flow pulsation intensity of the oil along the normal direction with different particle concentrations for a particle size of 5 μm . The figure shows that the flow pulsation intensity of the PIV acquisition oil field is relatively slow to change along the normal direction in the central region due to the presence of particulate matter, while the change is steep in the near-wall area, and this trend becomes increasingly obvious as the particle concentration increases. On the other hand, when the particle concentration is lower, the flow pulsation intensity of the oil field is larger in the near-wall area and gradually decreases toward the centre of the pipe; however, this trend becomes less obvious as the particle concentration increases. At the same concentration near the $y/d = 0.25$ normal position, the flow pulsation intensity of the oil appears as a maximum.

Overall, with increasing particle concentration, the flow pulsation intensity of the oil successively decreases. If the particle concentration is too large (such as 6.58 and 14.40 ppm), the difference in flow pulsation intensity is smaller. The reason is that at a constant concentration near the $y/d = 0.25$ normal position is the normal centre of the oil laminar flow. The flow intensity of the oil appears as a parabolic flow pattern, thus having a maximum value at this position. The particles in oil in the near-wall area increase the flow velocity of the oil. To maintain mass conservation, the oil flow velocity in the central region decreases. Additionally, coupled with the blocking action of the oil particles, the flow pulsation

intensity of the oil is steeply distributed in the near-wall region along the normal direction, while this intensity is relatively gentle in the centre area (Ling & Zhong, 1999). In addition, with increasing particle concentration in oil, the effect of near-wall particles on oil flow velocity growth is attenuated due to decreasing viscous shear force, which weakens the tendency of oil flow pulsation intensity growth in the near-wall area. Therefore, as the particle concentration reaches 3.00 ppm or more, the tendency of the flow pulsation intensity distribution along the normal direction becomes slower. This finding also indicates that the flow pulsation of the flow field in the pipeline is greatly affected by the wall surface.

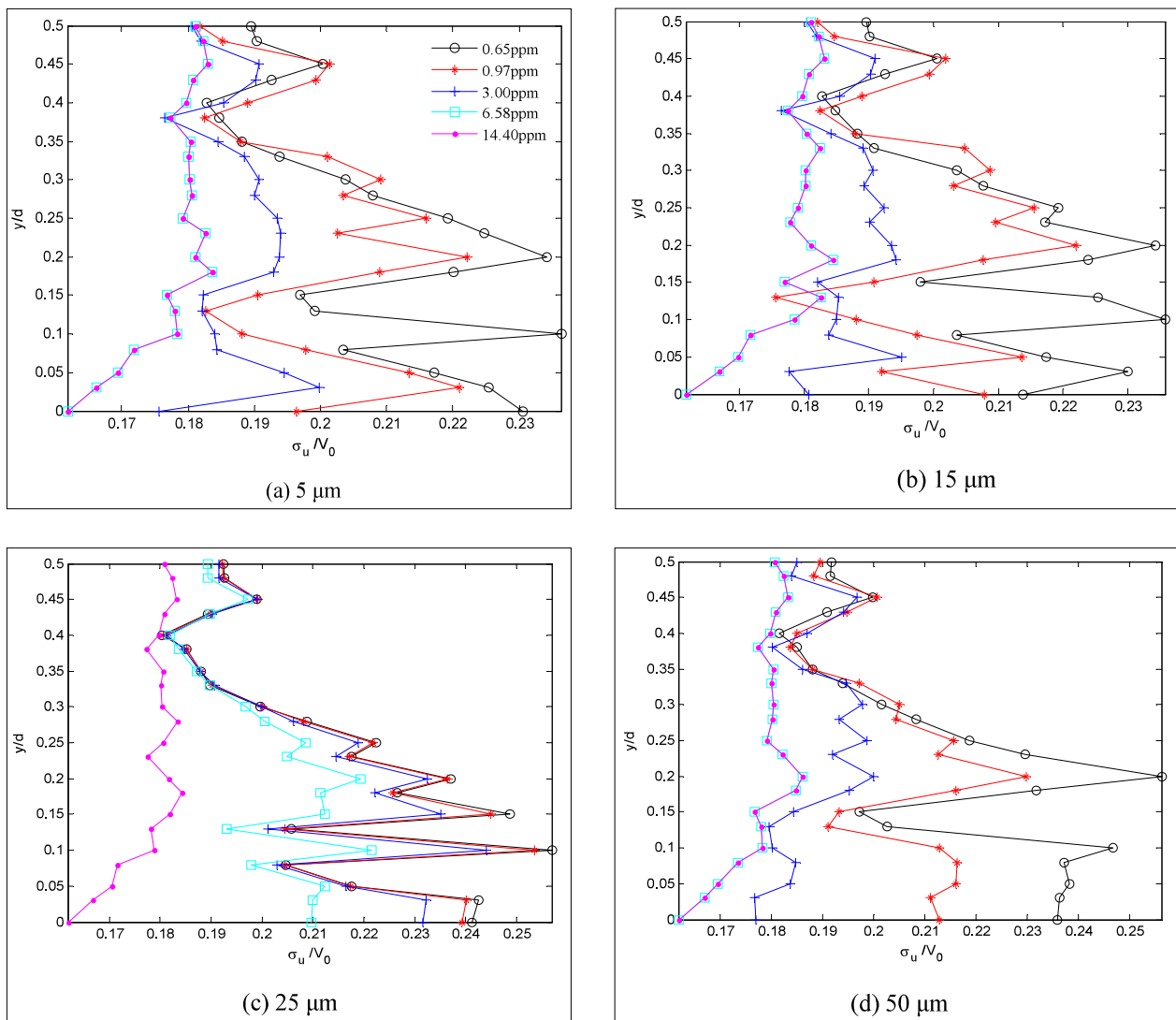


Figure 2: The distribution of streamwise mean intensity along the normal direction

According to the effect of the 15 μm particle size on the flow pulsation intensity of oil as shown in Figure 2(b), the effect of different particle concentrations on the intensity distribution along the normal direction is consistent with that of the 5 μm particle size shown in Figure 2(a). The difference is that in the case of low particle concentration, the maximum value of the flow pulsation intensity is larger for the 15 μm particle size. For example, the maximum value of the flow pulsation intensity for the 5 μm particle size under 0.65 ppm particle concentration is 0.233, while the maximum flow pulsation intensity for the 15 μm particle size is 0.236. The reason is that the larger the particle size is, the greater the viscous shearing force of the oil, so the particles in the near-wall region increase the role of oil flow velocity growth.

Figure 2(c) shows the effect of different particle concentrations on the flow pulsation intensity of the oil when the particle size is 25 μm . The effect of the 25 μm particle size on the flow pulsation intensity of the oil is similar to the trends shown in Figure 2(a) and (b). However, for the case of the particle size of 25 μm , the flow pulsation intensity is larger in the near-wall region and has a value of 0.256, and then, the 5 μm and 15 μm amplitudes are increased by 9.95 and 8.56%, respectively. In addition, when the particle concentration is 6.58 ppm, the flow pulsation intensity of oil is larger. This finding indicates that the particle size in the oil has less attenuation effect on the viscous shear force of oil when the particle size is 25 μm . However, the effect of the particles in the near-wall area on the oil growth rate is enhanced when the particle size exceeds 25 μm , due to the increase in particle size to enhance its gravitational sedimentation, and thus under the combined effect of viscous shear and gravity when the particle size is 50 μm as shown in Figure 2(d), the amplitude of the flow pulsation intensity under each particle concentration decreases greatly, except for the particle concentration of 0.65 ppm. Moreover, when the particle concentration is 6.58 ppm, the flow pulsation intensity is the same as that for 14.40 ppm.

The results in Figure 2 show that the flow pulsation intensity decreases with increasing particle concentration, and the difference decreases gradually for oil with different particle concentrations. The intensity of flow pulsation increases simultaneously with the increase of particle size.

Normal pulsation intensity distribution along the normal direction

Figure 3 shows the distribution curves of the normal pulsation intensity along the normal direction when the particle sizes are 5, 15, 25, and 50 μm and the particle concentrations are 0.65, 0.97, 3.00, 6.58, and 14.40 ppm. The horizontal axes in the figures show the ratio of the normal pulsation intensity to the oil inlet velocity V_0 , and the vertical coordinate represents the dimensionless length of the pipeline.

Figure 3 shows that the distribution of the normal pulsation intensity of oil with different particle sizes along the normal direction is roughly of the shape of a 'W'. The amplitude of the normal pulsation intensity in the central region and the near-wall region is largely within the field of view tested by PIV. Moreover, the particle concentration has a non-unidirectional effect on the distribution of the normal pulsation intensity. The normal pulsation intensity is also affected by the pipeline wall, but the distribution of the normal pulsation intensity shows a parabolic shape due to the action of the central mainstream.

Figure 3(a) shows the effect of different particle concentrations on the distribution of the normal pulsation intensity when the particle size is 5 μm . The particle concentration (6.58 and 14.40 ppm) is larger, and the variation in the normal pulsation intensity of the oil is greater in the near-wall area. In contrast, when the particle concentration (0.65, 0.97, and 3.00 ppm) is smaller, the variation range of the normal pulsation intensity in the central region is greater. This is because increasing the particle concentration makes the wall surface prone to the rough surface, and this effect enhances the turbulent burst behaviour near the wall, thus leading to a significant increase in the normal pulsation intensity near the wall (Li *et al.*, 2012).

Figure 3(b) shows the distribution of the normal pulsation intensity of the oil under the diameter of 15 μm particle size along the normal direction. The influence of different particle concentrations is similar to that of 5 μm . Figures 3(c) and (d) show that as the particle size increases, the amplitude of the normal pulsation intensity increases slightly, which indicates that the particle size influences the normal pulsation intensity of the oil.

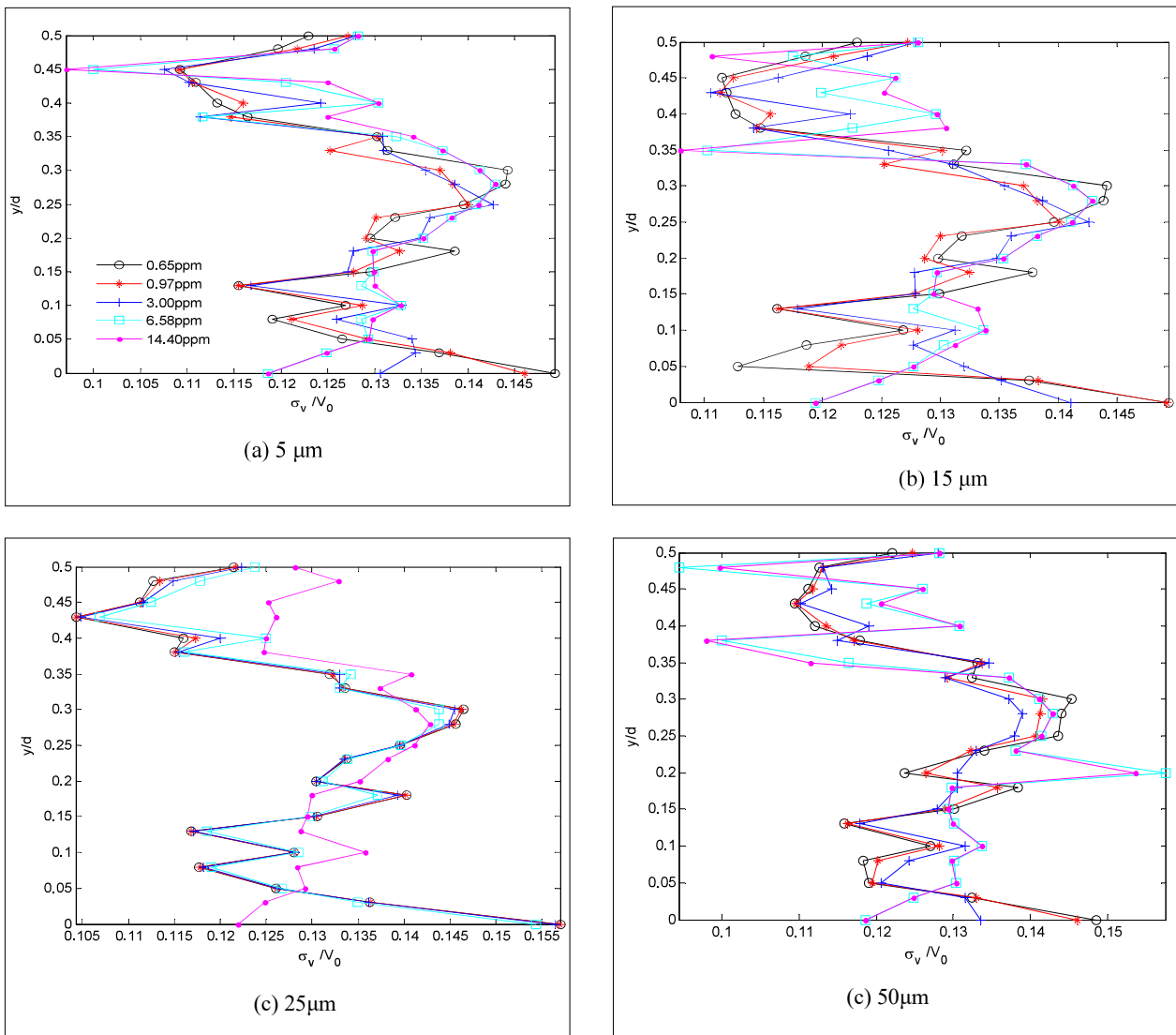


Figure 3: The distribution of the normal pulse velocity along the normal direction

Figure 3(c) shows that due to a decrease in the viscous shear force of 25 μm particles in the near-wall region, the distribution of the normal pulsation intensity for different particle concentrations increases with increasing particle concentration. However, in the central region, due to the retardation role of the particles increases, so the normal pulsation intensity decreases as the particle concentration increases.

Time-frequency curves of transient velocity

The distribution of pulsation intensity in the flow direction and normal direction shows that the pulsation intensity

in the flow direction and normal direction increases simultaneously with the increase of particle size. The particle size of 25 μm has a more obvious effect on them. In order to characterize the development of the pulsation characteristics of the oil flow field containing particles in the pipeline with time, according to the transient velocity vector of the PIV test of the flow field in the pipeline, the oil sample with the particle size of 25 μm in the oil is taken as an example. The pulsation frequency of the flow field is set to 0.12 Hz and a point (0.9, 0.25) near the centre of the test field is randomly selected. Time-frequency analysis of the instantaneous flow velocity and normal velocity at different particle concentrations of

0.65 ppm, 0.97 ppm, 3.00 ppm, 6.58 ppm, and 14.40 ppm are shown in Figures 4–8, respectively. Figures 4–8, (a) shows the time curve of the instantaneous flow velocity of the oil, (b) shows the time curve of the instantaneous

normal velocity of the oil, (c) presents the spectrum curve of the instantaneous flow velocity of the oil, and (d) presents the spectral curve of the instantaneous normal velocity of the oil.

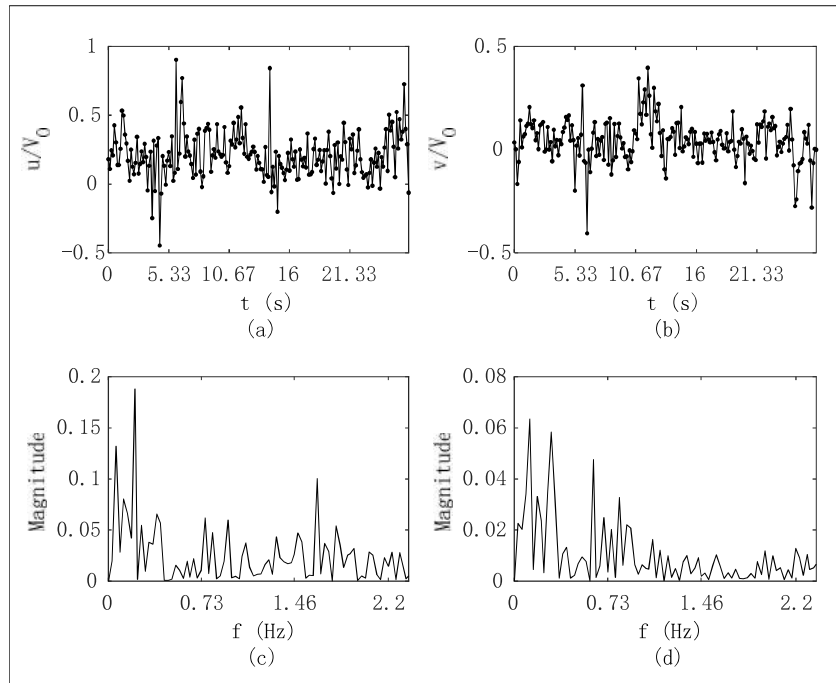


Figure 4: The time-frequency variation in the transient velocity of oil when the concentration is 0.65 ppm

Figure 4 shows the variation in the time-frequency curves of the instantaneous flow velocity and the instantaneous normal velocity when the particle concentration is 0.65 ppm. Figure 4(a) presents the change in the instantaneous flow velocity over time. The instantaneous flow velocity fluctuates at approximately 0.2099 under the action of a flow field pulsation base frequency of 0.12 Hz [as shown in Figure 4(c)], and the flow velocity appears to have a reflow phenomenon (having a negative velocity) in the first cycle; however, the distribution of the flow velocity tends to be gentle after this cycle. Due to the small particle concentration, the viscous shear force has little effect on the oil, where this force made the pulsation degree increase from -0.4474 to 0.9041 , namely, a change of 1.3515 . In addition, Figure 4(c) shows that the flow velocity pulsation frequency is mainly 0.21 Hz, approximately two times the base frequency.

Figure 4(b) presents the change in the instantaneous normal velocity with time, and this figure shows that the

instantaneous normal velocity at this point fluctuated around 0.0436, indicating that the velocity distribution in the central region is relatively balanced in the normal direction. The change in the amplitude of the normal velocity is relatively flat, from 0.4058 to 0.3965, with a range of 0.8023. Figure 4(d) shows that the normal velocity pulsation frequency of the oil mainly includes the base frequency of 0.12 Hz, and 0.21 Hz, approximately two times of the base frequency.

The time-frequency variations in the instantaneous flow velocity and normal velocity when the particle concentration is 0.97 ppm are shown in Figure 5. The instantaneous flow velocity changes over time, as shown in Figure 5(a), and the instantaneous flow velocity of the point fluctuation is near the value of 0.1683. Under the action of the flow pulsation base frequency of 0.12 Hz [as shown in Figure 5(c)], the flow velocity appears to reflow in the first two cycles. Compared with Figure 4(a), as the particle concentration increases and the

viscous shear force increases, the flow velocity pulsation intensity decreases from -0.3985 to 0.8943; namely, the variation range is 1.2928. In addition, the flow velocity pulsation frequency is 0.18 Hz, which is 1.5 times the base frequency (shown in Figure 5(c)).

Figure 5(b) shows the curve of the change in the instantaneous normal velocity over time. The instantaneous normal velocity of the point fluctuates

near the value of 0.0299, which shows that the normal velocity distribution in the central region is balanced concerning that of Figure 4(b). However, the magnitude of the change in the normal velocity is relatively large, ranging from -0.4759 to 0.4649, with a variation of 0.9408. Figure 5(d) shows that the normal velocity pulsation frequency mainly includes the subharmonic frequency of 0.09 Hz, and 0.21Hz, approximately twice the base frequency.

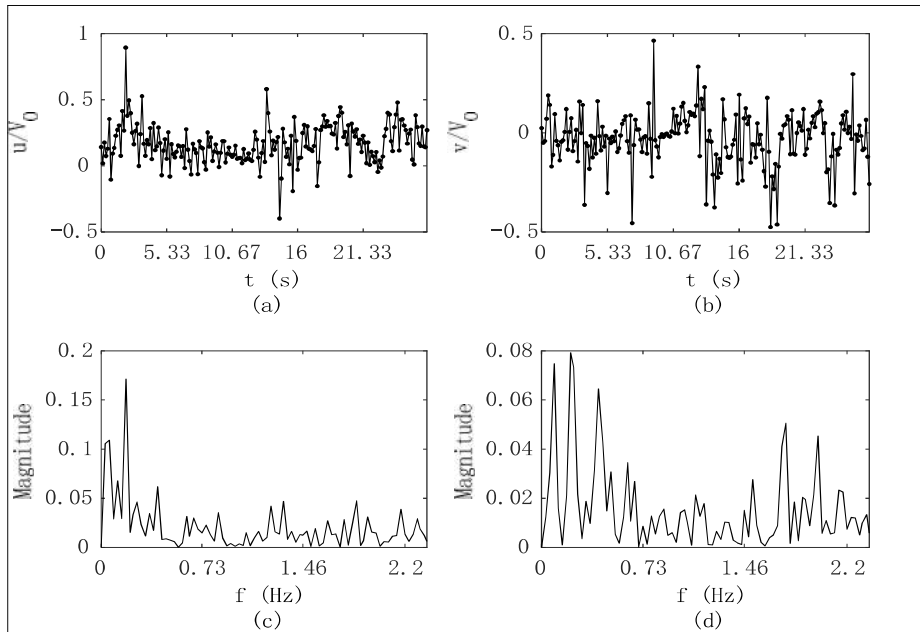


Figure 5: The time-frequency variation in the transient velocity of oil when the concentration is 0.97 ppm

Figure 6 shows the time-frequency variations in the instantaneous flow velocity and normal velocity when the particle concentration is 3.00 ppm. The instantaneous flow velocity changes over time, as shown in Figure 6(a), and the transient flow velocity of the point fluctuates near a value of 0.1635. Under the action of the flow field base pulsation frequency of 0.12 Hz [as shown in Figure 6(c)], the flow velocity amplitude in the first period has a large fluctuation phenomenon, and the reflow phenomenon occurs in the third cycle. As the particle concentration increases and the viscous shear force of the oil increases, the flow velocity pulsation degree of the oil shown in Figure 6(a) relative to that of Figure 4(a) and Figure 5(a) decreases from -0.1292 to 0.8407, with a varied range of 0.9699. In addition, Figure 6(c) shows that the flow velocity pulsation frequency is mainly 0.09 Hz, which is a subharmonic frequency of the base frequency.

In Figure 6(b), the instantaneous normal velocity at a randomly selected point (0.9, 0.25) near the centre of the test field fluctuates around -0.0387 over time, which indicates that the velocity distribution in the central region has a negative trend in the normal direction relative to that of Figure 4(b) and Figure 5(b). However, the magnitude of the change in the normal velocity is relatively small, from -0.3491 to 0.3944, with a varied range of 0.7435. Figure 6(d) shows that the normal velocity pulsation frequency is 0.06 Hz, which is a subharmonic frequency of the base frequency.

Figure 7 shows the time-frequency variations in the instantaneous flow velocity and normal velocity when the particle concentration is 6.58 ppm. The instantaneous flow velocity of the point shown in Figure 7(a) fluctuates near 0.161 over time. Under the action of

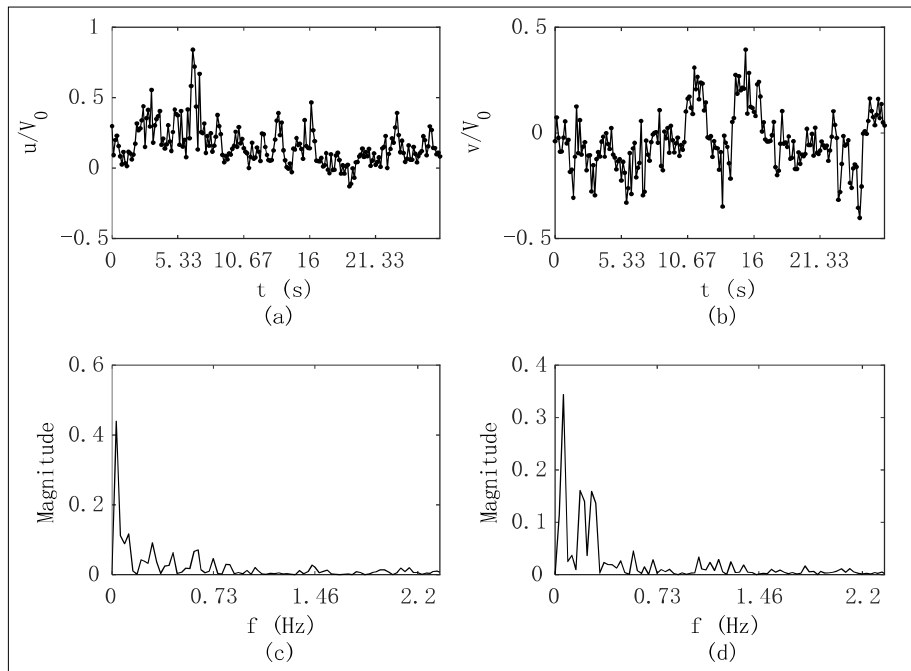


Figure 6: The time-frequency variation in the transient velocity of oil when the concentration is 3.00 ppm

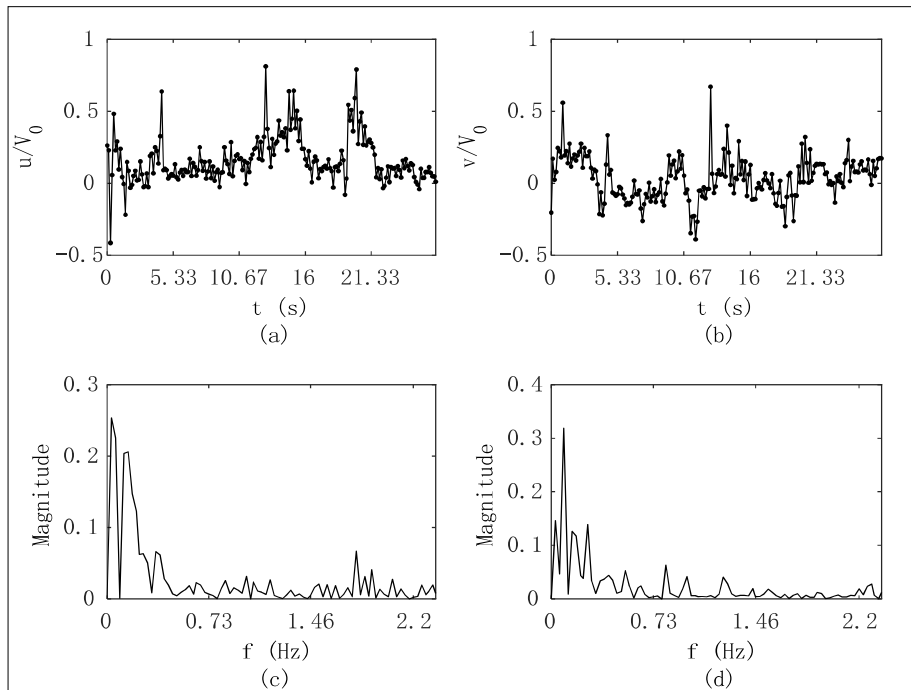


Figure 7: The time-frequency variation in the transient velocity of oil when the concentration is 6.58 ppm

the flow field pulsation frequency of 0.12 Hz [as shown in Figure 7(c)], the amplitude of the flow velocity in the latter two periods has a large fluctuation phenomenon. As the particle concentration increases and the viscous shear force increases, the flow velocity pulsation degree is reduced from 0.0807 to 0.8113 relative to that of Figures 4–6(a), with a varied range of 0.8920. In addition, Figure 7(c) shows that the flow velocity pulsation frequency is mainly a subharmonic frequency of 0.03 Hz and a base frequency of 0.12 Hz.

In Figure 7(b), the instantaneous normal velocity of the point fluctuates near 0.032 over time, which shows that in the central region, the normal upward velocity distribution has a positive trend relative to the trend of Figure 4–6 (b). However, the magnitude of the change in the normal velocity is relatively higher from -0.3905 to 0.6698, with a range of 1.0603. In addition, Figure 7(d) shows that the normal velocity pulsation frequency is mainly the subharmonic frequency of 0.09 Hz and is approximately twice the frequency of 0.26 Hz of the base frequency.

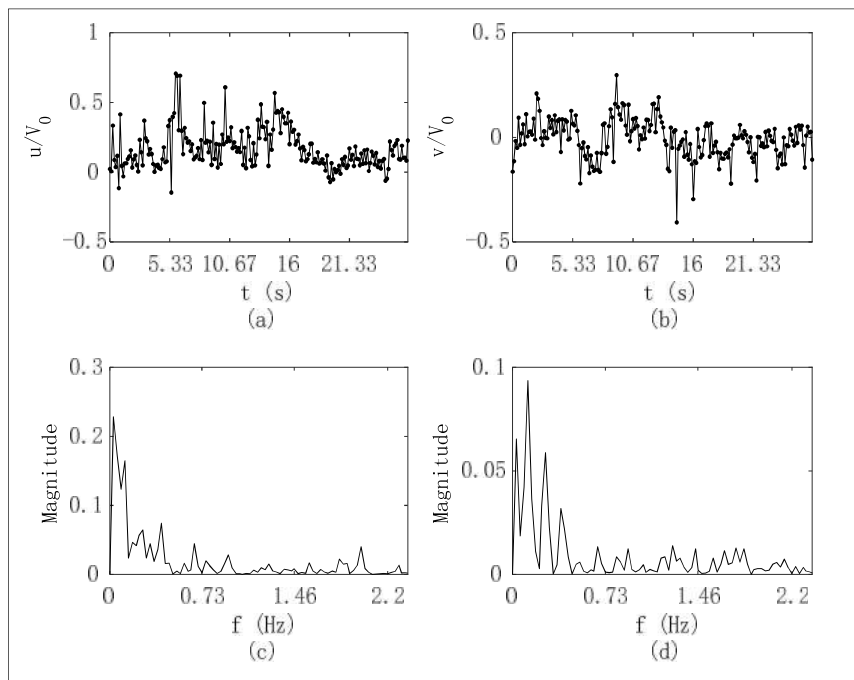


Figure 8: The time-frequency variation in the transient velocity of oil when the concentration is 14.40 ppm

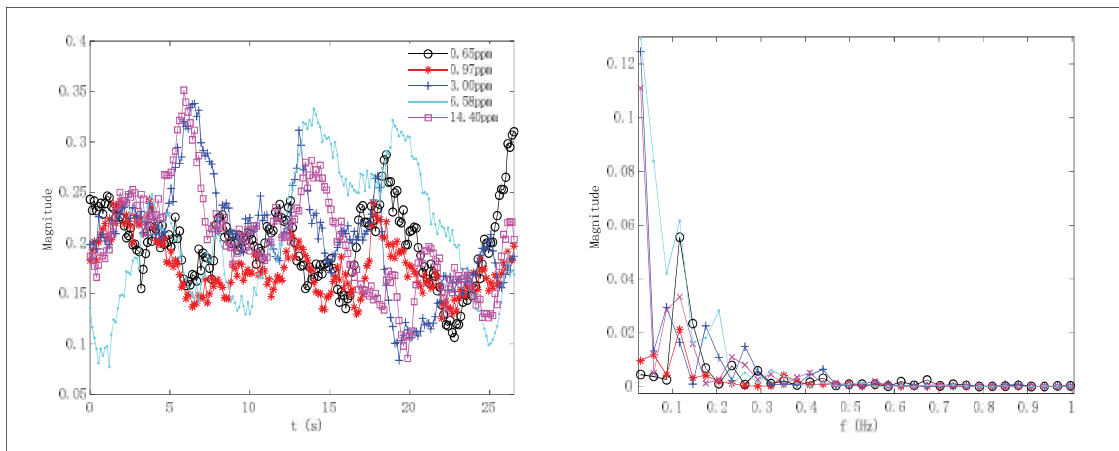
Table 1: Fluctuation frequency of the transient velocity in the flow field

Velocity	Concentration (ppm)	Subharmonic	Base frequency	Second-time frequency	Third-time frequency	Fourth-time frequency	Fifth-time frequency	Other times frequency
Flow velocity	0.65	0.06	0.12	0.21	0.41			0.76
	0.97	0.06	0.12	0.18	0.41			0.85
	3.00	0.03	0.12	0.29	0.44		0.62	0.73
	6.58	0.03	0.12	0.26	0.35		0.64	0.85
	14.40	0.03	0.12	0.26	0.41		0.67	0.94
Normal velocity	0.65	0.03	0.12	0.29	0.41	0.53	0.62	0.82
	0.97	0.09	0.12	0.21	0.41	0.50	0.62	0.88
	3.00	0.06	0.18	0.26	0.47	0.56		0.70
	6.58	0.09	0.18	0.26	0.41	0.53		0.82
	14.40	0.03	0.12	0.26	0.38	0.53	0.67	0.82

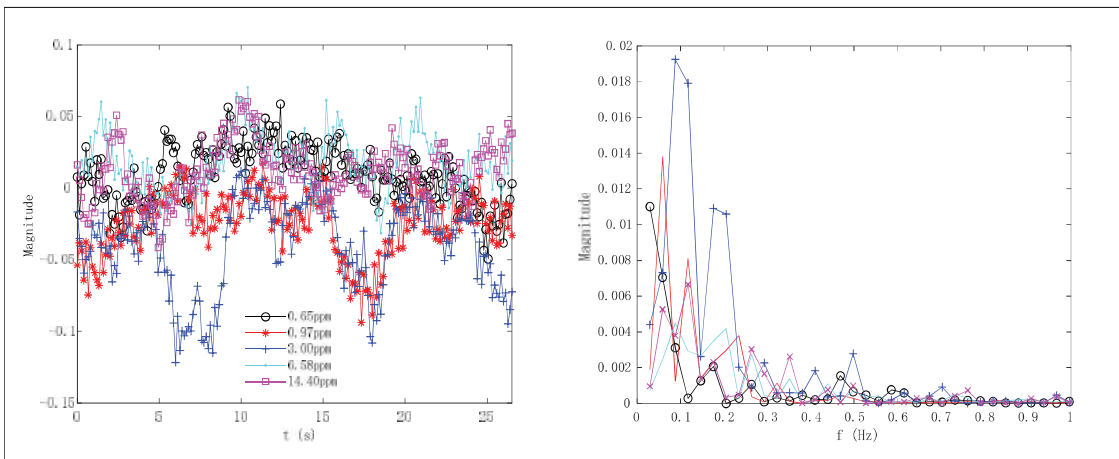
Figure 8 shows the time-frequency variations in the instantaneous flow velocity and normal velocity when the particle concentration is 14.40 ppm. As shown in Figure 8(a), the instantaneous flow velocity at this point fluctuates around 0.166 over time. Under the action of the flow field pulsation frequency of 0.12 Hz [as shown in Figure 8(c)], the flow velocity amplitude appears to exhibit large fluctuations in the first two cycles. As the particle concentration increases and the viscous shear force increases, the flow velocity pulsation degree decreases concerning that of Figures 4–7(a), from -0.1459 to 0.6922 with a varied range of 0.8381.

In addition, Figure 8(c) shows that the flow pulsation frequency is mainly a subharmonic frequency of 0.03 Hz and a base frequency of 0.12 Hz.

As shown in Figure 8(b), the instantaneous normal velocity at this point fluctuates around -0.008, which indicates that the normal velocity distribution in the central region is relatively balanced concerning that of Figure 4–7(b). However, the magnitude of the change in the normal velocity is relatively small, ranging from -0.4071 to 0.2982 with a varied range of 0.7053. In addition, Figure 8(d) shows that the normal velocity



(a) The time-domain distribution of the average flow velocity (b) The frequency-domain distribution of the average flow velocity



(c) The time-domain distribution of the normal average velocity (d) The frequency-domain distribution of the normal average velocity

Figure 9: The time-frequency curves of the mean velocity of oil

pulsation frequency is mainly the subharmonic frequency of 0.03 Hz and is approximately twice the frequency of 0.26 Hz of the base frequency.

The above results show that with increasing particle concentration in oil, the mean value of the magnitude of the instantaneous flow velocity pulsation is gradually reduced, and the varying amplitude simultaneously decreases. On the other hand, the changes in the mean and variance amplitude of the instantaneous normal velocity pulsation are not obvious due to the influence of the flow field structure.

Table 1 shows the main frequencies of the instantaneous flow velocity and normal velocity for different particle concentrations. The base frequency of 0.12 Hz is reflected in the frequency domain of the flow velocity. As the particle concentration increases, the main frequency of the flow velocity decreases from twice the base frequency to the subharmonic frequency, which shows an attenuation trend. Similarly, with increasing particle concentration, the main frequency of the normal velocity of oil decreases from the base frequency to the subharmonic frequency, which also shows an attenuation trend.

The speed-frequency curve of average velocity

The instantaneous velocity vectors for different particle concentrations obtained by the PIV test are averaged in the flow direction and the normal direction to obtain the corresponding time-frequency curves of the average flow velocity and normal average velocity of oil in the time of the PIV test, as shown in Figure 9.

Figure 9(a) shows the time-domain distribution of the average flow velocity under different particle concentrations; it is obvious that the distribution of the average flow velocity is periodic. In addition, the base frequency of the flow field is 0.12 Hz, as shown in Figure 9(b). With increasing particle concentration, the change in the average flow velocity is non-unidirectional, but the overall trend is that the average velocity of the oil gradually increases. The reason is that due to the increase in the particle concentration, the particle inertia increases the average velocity in the near-wall region, so the thickness of the turbulent viscous bottom layer decreases and the flow velocity gradient increases (Li *et al.*, 2012), which lead to an increase in the flow pulsation peak value.

The time-domain distribution of the average normal velocity for different particle concentrations is shown in Figure 9(c). As the particle concentration increases, the

change in the average normal velocity decreases up to a particle concentration of 3.00 ppm, while this change increases when the particle concentration exceeds 3.00 ppm. This is because when the particle concentration reaches a certain level (3.00 ppm) in the horizontal pipeline, the sedimentation of the particles causes the wall surface to form a rough wall surface, which enhances the release of the oil with a sudden turbulence behaviour in the near-wall region and results in increasing the normal average velocity. Figure 9(d) shows that the main frequency of the normal average velocity is concentrated in a subharmonic frequency of 0.09 Hz and a base frequency of 0.12 Hz, which is consistent with the main frequency of the transient normal velocity.

CONCLUSIONS

Faults of power transformer such as loose cores and coil deformation can be detected by transformer pulsation. Compared to detecting pulsation of the transformer body, detecting pulsation of the transformer oil is more accurate. However, the inevitable presence of metallic and non-metallic particles in transformer oil, their particle size, and concentration also plays a non-negligible influence on the pulsation of the oil. Therefore, it is important to research the influence of factors such as particle size and concentration on the pulsation characteristics of the oil for the safe operation of the transformer. According to the ISO 4406 standard for oil contamination, oil samples containing Cu, Fe, and SiO₂ powders with particle sizes of 5, 15, 25 and 50 μm and concentrations of 6.58, 4.57, 3.00, 0.971, and 0.648 ppm were prepared and tested in an experimental test setup using the 2DPIV measurement technique for different oil samples in a square tube, to obtain the transient velocity vectors of the oil flow field containing particles of different particle sizes and concentrations. The distribution of the oil flow direction and normal pulsation intensity, as well as the transient and average velocities, were analysed. It was found that the distribution of the oil flow pulsation intensity along the normal direction changes slowly in the central region, while the change in the near-wall region is steep, and this trend becomes more obvious with increasing particle concentration. In addition, the flow direction pulsation intensity of oil decreases with increasing particle concentration, and the difference gradually decreases. The distribution of the normal pulsation strength of oil in the normal direction for different particle sizes is roughly of the shape of a 'W'. The amplitude of the normal pulsation intensity fluctuates greatly in the central region and near-wall region. In addition, the influence of particle concentration on the distribution of the normal pulsation intensity is non-unidirectional. With

increasing particle concentration, the mean value of the fluctuation amplitude of the instantaneous flow velocity gradually decreases, and the varying amplitude decreases simultaneously. However, the fluctuation amplitude of the instantaneous normal velocity is not obvious. With increasing particle concentration, the main frequencies of the flow direction and normal direction velocities show a decreasing trend. The distribution periodicity of the average flow velocity of oil is more obvious. As the particle concentration increases, the average flow velocity gradually increases. When the particle concentration is below 3.00 ppm, the average normal velocity decreases with increasing particle concentration, while when the particle concentration exceeds 3.00 ppm, the average normal velocity of the oil shows an increasing trend. It can be seen that the influence of particles on the transformer oil pulsation is large. For the transformer pulsation test it is necessary to consider the influence of these factors in order to accurately obtain the operating state of the transformer for safe operation of the transformer.

Acknowledgements

This study was funded by Local Science and Technology Development Fund projects guided by the central government (206Z5201G), Chongqing Basic Research and Frontier Exploration Project (cstc2018jcyjAX0121), and Fundamental Research Funds for the Central Universities (3142019001, 3142019055).

REFERENCES

- Abiev R.S. & Galushko A.S. (2013). Hydrodynamics of pulsating flow type apparatus: Simulation and experiments. *Chemical Engineering Journal* **229**: 285–295. DOI: <https://doi.org/10.1016/j.cej.2013.05.105>
- Bagheri M., Nezhivenko S., Naderi M.S. & Zollanvari A. (2018). A new vibration analysis approach for transformer fault prognosis over cloud environment. *International Journal of Electrical Power and Energy Systems* **100**: 103–116. DOI: <https://doi.org/10.1016/j.ijepes.2018.02.026>
- Borges G.R., Farias G.B., Braz T.M., Santos L.M., Amaral M.J., Fortuny M., Franceschi E., Dariva C. & Santos A.F. (2015). Use of near-infrared for evaluation of droplet size distribution and water content in water-in-crude oil emulsions in pressurized pipeline. *Fuel* **147**: 43–52. DOI: <https://doi.org/10.1016/j.fuel.2015.01.053>
- Eschmann G., Kuntze A., Uffrecht W., Kaiser E. & Odenbach S. (2015). Experimental and numerical investigation of heat transfer coefficients in gaseous impinging jets – First test of a recent sensor concept for steady and unsteady flow. *International Journal of Thermal Sciences* **96**: 290–304. DOI: <https://doi.org/10.1016/j.ijthermalsci.2015.03.016>
- Ghadi S., Esmailpour K., Hosseinalipour S.M. & Mujumdar A. (2016). Experimental study of formation and development of coherent vortical structures in pulsed turbulent impinging jet. *Experimental Thermal and Fluid Science* **74**: 382–389. DOI: <https://doi.org/10.1016/j.expthermflusci.2015.12.007>
- Hsu C.M., Huang R.F. & Loretero M.E. (2014). Unsteady flow motions of an oscillating jet in crossflow. *Experimental Thermal and Fluid Science* **55**: 77–85. DOI: <https://doi.org/10.1016/j.expthermflusci.2014.02.016>
- Li J., Wang H., Liu Z., Chen S. & Zheng C. (2012). An experimental study on turbulence modification in the near-wall boundary layer of a dilute gas-particle channel flow. *Experiments in Fluids* **53**(5): 1385–1403. DOI: <https://doi.org/10.1007/s00348-012-1364-7>
- Ling L. & Zhong X. (1999). Effect of particle concentration and size on distribution of velocity for the gas-particle two-phase flow in a vertical square duct. *Journal of Hydrodynamics* **14**(2): 154–161.
- Papadopoulos P.K. & Vouros A.P. (2016). Pulsating turbulent pipe flow in the current dominated regime at high and very-high frequencies. *International Journal of Heat and Fluid Flow* **58**: 54–67. DOI: <https://doi.org/10.1016/j.ijheatfluidflow.2015.12.007>
- Tian J., Yuan C., Yang L., Wu C., Liu G. & Yang Z. (2016). The vibration analysis model of pipeline under the action of gas pressure pulsation coupling. *Engineering Failure Analysis* **66**: 328–340. DOI: <https://doi.org/10.1016/j.engfailanal.2016.05.017>
- Wang G., Evans G.M. & Jameson G.J. (2016). Bubble-particle detachment in a turbulent vortex I: Experimental. *Minerals Engineering* **92**: 196–207. DOI: <https://doi.org/10.1016/j.mineng.2016.03.011>
- Yan B.H., Gu H.Y. & Yu L. (2012). Numerical simulation of large scale vortex structure and flow pulsation in rectangular channels. *Progress in Nuclear Energy* **54**(1): 29–35. DOI: <https://doi.org/10.1016/j.pnucene.2011.09.006>
- Yang B., Zhang W. & Zhang Y. (2013). Experiment study of the wind fluctuation's effect on the sand concentration in unsteady wind-sand flow. *Journal of Experiments in Fluid Mechanics* **27**(3): 47–50.
- Yuan H., Tan S., Wen J. & Zhuang N. (2016). Heat transfer of pulsating laminar flow in pipes with wall thermal inertia. *International Journal of Thermal Sciences* **99**: 152–160. DOI: <https://doi.org/10.1016/j.ijthermalsci.2015.08.014>
- Zeng L., Yu Z., Zhang H., Zhang X. & Chen H. (2018). A high sensitive multi-parameter micro sensor for the detection of multi-contamination in hydraulic oil. *Sensors and Actuators: A. Physical* **282**: 197–205. DOI: <https://doi.org/10.1016/j.sna.2018.09.023>
- Zhao H., Wei A., Luo S. & Fan J. (2016). Velocity fluctuations in the near-wall region of the turbulent channel flow. *Journal of Engineering Thermal Physics* **37**(3): 551–555.

RESEARCH ARTICLE

Bioethanol production from Palmyrah (*Borassus flabellifer*) wastes using yeast

EJSBA Christy¹, S Mahilrajan², G Chandrasena¹ and R Kapilan^{3*}

¹ Uva Wellassa University, Passara Road, Badulla.

² Palmyrah Research Institute, Kandy Road, Kaithady, Jaffna.

³ Department of Botany, Faculty of Science, University of Jaffna, Thirunelvely, Jaffna.


Submitted: 17 December 2019; Revised: 27 May 2021; Accepted: 20 December 2021

Abstract: This study describes bioethanol production from palmyrah (*Borassus flabellifer* L.) waste using yeast and optimization of fermentation conditions to increase the yield. When subjected to different pre-treatment conditions with various alkaline and acidic solutions, significantly higher reducing sugar contents were obtained from palmyrah coir dust with H₂SO₄ and HNO₃ pre-treatments. H₂SO₄ pre-treatment at 3%, 5% and 7% concentrations for 15, 30, and 45 minutes respectively were given to the coir dust, and a significantly higher quantity of sugar was produced with 3% H₂SO₄ after 45 minutes of reaction. Among the acids and bases used for the pre-treatment, H₂SO₄ is the best hydrolysing agent for coir dust. When fermentation was done with the coir dust hydrolysed solution under optimized conditions [30 °C and pH 5.0 with baker's yeast (6×10^6 cells mL⁻¹) and incubated in peptone, yeast extract and nutrient (PYN) medium at 30 °C for 7 days], a significantly higher amount of alcohol was produced on the 4th day than the respective non-optimized conditions. Similarly, molasses and fruit pulp of palmyrah also produced significantly higher quantities of ethanol individually under similar optimized conditions used for coir dust on the 6th and 4th day of fermentation respectively, than the respective non-optimized conditions. The efficiency of alcohol fermentation by yeast with palmyrah coir dust acid hydrolysate was 19%. Therefore, coir dust could also be used as a long-term substrate for bioethanol production, considering the excess availability of this under-utilized waste material.

Keywords: Bioethanol, coir dust, fermentation, molasses, palmyrah, pre-treatment.

INTRODUCTION

Population growth and increased industrial activities have resulted in a rising concentration of greenhouse gases in the atmosphere causing the greenhouse effect. Bioethanol produced from biomass sources are one of the best alternatives for petroleum-based fuels and recently, they have been commonly used for transportation in many countries (Hill *et al.*, 2006). Bioethanol is basically produced from first- or second-generation feedstocks. First generation bioethanol is produced from some cereals and legumes such as corn, sugar beet, wheat, and barley, which are used also as food sources. Sugars which are obtained from the first-generation feedstocks such as sugarcane, molasses, sugar beet, and fruits can be fermented via yeast directly. The advantages of these raw materials are, high sugar yields and low conversion cost. The disadvantage is limited availability of the raw materials during certain period of the year. While 25 gallons of ethanol is produced from an average of 1 ton sugar beet, 20 gallons of ethanol is produced from 1 ton of sweet sorghum stalk (Sarkar *et al.*, 2012). Usage of this first-generation feedstock for bioethanol production has raised concerns about increasing food prices and occupation of agricultural land. These problems are solved partially by using second-generation feedstock lignocellulosic materials

* Corresponding author (ranganat@ualberta.ca;  <https://orcid.org/0000-0002-7608-1615>)



This article is published under the Creative Commons CC-BY-ND License (<http://creativecommons.org/licenses/by-nd/4.0/>). This license permits use, distribution and reproduction, commercial and non-commercial, provided that the original work is properly cited and is not changed in anyway.

such as waste or forest residues (Nigam & Singh, 2011). Second-generation feedstocks have some advantages over the first-generation feedstocks due to not being used as food sources and less land requirement. However, their harvesting, purification and various pre-treatment needs have made their production quite challenging and not economical (Daroch *et al.*, 2013). During the past ten to fifteen years, biofuel has drawn attention as a potential environmentally friendly fuel because of diminishing petroleum reserves in the world, and the deleterious environmental effects of exhaust gases from petroleum (Vasudevan, 2008). Time has come to explore diverse natural plant and agricultural substrates that could produce biofuels efficiently (Kapilan, 2015). During the past five decades there has been a significant increase in studies on biofuel production by fermentation using diverse plant-based substrates including rice, corn, whey, molasses, sea weeds and cellulosic biomass (Qureshi & Blaschek, 2005).

Palmyrah (*Borassus flabellifer* L.) is a tropical palm, belonging to the family Arecaceae and all its parts are of potential economic value (Mohanadas, 2002). Palmyrah palms are economically useful and widely cultivated, especially in Southeast Asia. Of the estimated 11 million palmyrah palms in Sri Lanka, 90% are found in the three Districts of Jaffna, Mannar and Kilinochchi. Palmyrah palm has multiple uses: timber for construction, leaves for fencing, roofing and woven handicrafts, fibre for rope and sap for drinking. If the sap is left to ferment for a few hours, it becomes a mildly alcoholic, fragrant toddy. The young palmyrah roots are high in calcium and consumed as a snack, and is also ground to make flour for porridge called *khool*. Jaggery, a delicious golden-coloured unrefined palm sugar is made from unfermented palmyrah toddy. The germinated seeds of palmyrah palm form fleshy sprouts below the surface that can be boiled and eaten as a fibrous, nutritious food. The crunchy watery kernel is also edible and sweeter. The kernel inside the hard shell is an edible jelly that is rich in minerals. From the fleshy crown of the tree, cakes can be made. Products obtained from palmyrah are classified into edible and non-edible products (Asiri Nisansala *et al.*, 2021). Among the palmyrah products are, expired bottled palmyrah fruit pulp (PFP), and molasses, which is the mother liquor left after the crystallization of juice. This dark coloured viscous liquid contains about 60% fermentable sugar that could be used for ethanol production. PFP is extracted from the ripe fruit and molasses is obtained from the sugar candy producing centres. Fibre is one of the non-edible products obtained from basal sheath of the palmyrah leaf. Fibres are mainly vascular bundles or groups of sclerenchymatous fibre cells. In Sri Lanka, until 1991, fibre was extracted

manually from young (5–10 years old) palm trees. During the extraction of Coir fibre, dust is generated as the main waste (Theivendirarajah, 2008). Palmyrah coir dust is a spongy material which could be used for the production of bioethanol (Theivendirarajah, 2008). Lignocellulosic waste materials obtained from forestry and agricultural industries are generally not used as raw materials for the production of second-generation bioethanol. Even though coir dust is the principal and excessive waste material generated during the extraction of fibre from palmyrah palm, its utilization is very limited in the palmyrah palm growing regions (Theivendirarajah, 2008). The objective of this study was to produce bioethanol from palmyrah wastes; expired palmyrah fruit pulp, molasses and coir dust, using baker's yeast and to optimize the pre-treatment conditions to increase the yield

METHODOLOGY

Collection of raw materials

Palmyrah coir dust was collected from Sarasalai fibre industry, Jaffna District, Sri Lanka and molasses and expired PFP 3 months after expiry date (PEP shelf life is 12 months), were obtained from the Palmyrah Development Board, Jaffna, Sri Lanka.

Chemical analysis

Determination of reducing sugar

The reducing sugar content was determined by using 3, 5-Dinitrosalicylic acid (DNS) method. A series of standard glucose solutions were prepared by diluting different volumes ranging from 0.2–1.0 mL of a stock glucose solution (1.0 gL⁻¹) in a series of labelled test tubes. The total volume was made up to 1.0 mL with distilled water. DNS reagent (1.0 mL) was added, and the tubes were heated in a boiling water bath for 5 min. The tubes were cooled, distilled water (10.0 mL) was added, and the absorbance was measured spectrometrically (Spectronic 21D) against a reagent blank at 550 nm. The reagent blank was prepared by taking 1.0 mL of distilled water instead of standard glucose solution. Solutions of unknown concentrations (samples) were treated similarly, and their glucose concentrations were determined using the standard curve for glucose (Miller, 1959).

Determination of acidity

Acidity of the sample was measured by titrating with 0.1 M NaOH solution using phenolphthalein as the indicator. Percentage acidity is expressed as millimoles of NaOH used per 100 mL of sap solution.

$$\text{Percentage acidity} = \frac{\text{Volume of NaOH (mL)} \times 0.1}{\text{Volume of sap solution (mL)}} \times 100$$

pH

A sample was taken in a clean beaker (25 mL) and its pH was measured by using a digital pH meter (Sension PH 31-Spain) at room temperature (28 ± 2 °C). The sample was returned to the fermentation vessel after measurement.

Determination of alcohol

Alcohol content of the fermented sample was determined directly for each sample by using Dujardin-Salleron ebulliometer and expressed in terms of percentage (v/v).

Determination of brix

The total soluble sugar content of the molasses and bottled PFP was analysed using a refractometer (Atago, Germany).

Ethanol production from coir dust

Size Reduction

Small sized particles of coir dust were chosen by filtering the coir dust using a sieve plate (40 mm diameter) for an efficient pre-treatment and hydrolysis.

Pre-treatment of coir dust

Alkaline hydrolysis

Alkaline hydrolysis of the coir dust was carried out by using NaOH and Ca(OH)_2 . Coir dust (10 g) was placed in a 250 mL Erlenmeyer flask and 100 mL of 5% (w/v) alkaline solution was added separately. Then the flasks were plugged with cotton and autoclaved at 121 °C for 15 min. The substance obtained after treatment was dark in colour which was then filtered through muslin cloth and washed under running distilled water until no colour was observed in the wash water and made up to 100 mL. Reducing sugar was determined by using the DNS method.

Acid hydrolysis

The same procedure used for alkaline hydrolysis was followed with three acid solutions; sulfuric acid, nitric acid and hydrochloric acid for acid hydrolysis of the coir dust, and the acids that produced high reducing sugar content were selected for further studies.

Optimization of acid hydrolysis condition

Coir dust (10g) was inoculated with different concentration of sulphuric acid (3, 5 and 7%) and hydrolysed at different time intervals (15, 30 and 45 min). Then the hydrolysate was filtered through a muslin cloth and washed under running distilled water until no colour was observed in the wash water and made up to 100 mL. DNS method was used to determine the reducing sugar content. This experiment was repeated with nitric acid. Acid that resulted the highest reducing sugar content was selected as the best treatment for further studies.

Preparation of yeast inoculum

Peptone, yeast extract, and nutrient (PYN) medium (Balakumar & Arasaratnam, 2009) was prepared and sterilized at 121 °C for 15 min. It was then inoculated with one loop of baker's yeast (*Saccharomyces cerevisiae*), incubated at 30 °C for 18 h and used as the inoculum. The inoculum contained a cell density of 6×10^6 cells mL^{-1} .

Table 1: Composition of peptone, yeast extract and nutrient (PYN) medium (pH = 5.0)

Medium	g/L
Peptone	3.5
Yeast extract	3
MgSO_4	1
KH_2PO_4	2
(NH_4SO_4)	1
Glucose	50

Ethanol production from molasses and expired PFP

Initial total soluble solid (TSS) content of molasses and PFP was adjusted to °15 brix with sterile water and used for the fermentation studies.

Fermentation

Acid hydrolysate (100 mL) obtained from selected treatments of coir dust (with sulphuric acid and nitric acid), 100 mL of molasses and PFP were taken into separate conical flasks and adjusted to pH 5.0 using 0.4 M NaOH. Fermentation medium was added in the ratio of 10 mL of yeast inoculum to 100 mL of pre-treated sample (1:10). Samples were taken at intervals of 24 hours for determination of alcohol, acidity, pH and reducing sugar.

Efficacy of fermentation

Efficiency of alcohol fermentation was determined as follows.

$$\text{Efficiency of fermentation} = \frac{\text{Actual ethanol content}}{\text{Theoretical value}} \times 100$$

$$\text{Theoretical ethanol content} = \text{Total fermentable sugar} \times 0.64$$

Statistical analysis

Each experiment was performed in triplicate and standard deviation for each experimental result was calculated using Microsoft Excel for graphical representation. Acid pre-treatments of coir dust were optimized using general full factorial design. Altogether nine treatments were carried out for one acid. Results obtained from the entire treatment was analysed using one way ANOVA and least significance difference (LSD) was tested using Turkeys comparison at 5% confidence level using Minitab 17 software.

RESULTS AND DISCUSSION

Results

Based on the amount of reducing sugar production during hydrolysis at 121 °C for 15 min, H₂SO₄ and HNO₃ were selected as best hydrolysing agents since the production of reducing sugar was significantly higher with H₂SO₄ and HNO₃ (more than 30 mg/mL reducing sugar) than the other agents (Table 2).

Table 2: Production of reducing sugars from palmyrah coir dust by different pre-treatment agents

Pre-treatment	Agent	Reducing sugar (mg/mL)
Alkaline hydrolysis	Ca(OH) ₂	4.15 (±0.05)
	NaOH	0.54 (±0.06)
Acid hydrolysis	HCL	13.39 (±0.05)
	HNO ₃	36.19 (±0.12)
	H ₂ SO ₄	34.92 (±0.11)

Optimization of sulphuric acid (H₂SO₄) pre-treatment

Optimization of acid hydrolysis with H₂SO₄ was carried out with different concentrations of acid (3, 5 and 7%) and different hydrolysis times (15, 30 and 45 min). Altogether there were nine treatments as listed in Table 3. Main effects plot (Figure 1a) of response means for reducing sugar of each factor indicate that different levels of each factor affect the reducing sugar content.

According to the interaction plot (Figure 1b), it could be confirmed that there is an interaction between concentrations of acid and times of hydrolysis for the production of reducing sugar from coir dust. Treatment 7 (3% and 45 min) that produced significantly higher amount of reducing sugar was selected for further fermentation studies.

Table 3: Design for sulphuric acid pre-treatments with different concentrations of acid and different hydrolysed time for the production of reducing sugar from coir dust

Std order	Run Order	Blocks	Hydrolysed time	Concentration	Reducing sugar (mg/mL)
1	1	1	1	1	34.628
2	2	1	1	2	0.991
3	3	1	1	3	0.34
4	4	1	2	1	41.953
5	5	1	2	2	0.545
6	6	1	2	3	0.199
7	7	1	3	1	40.154
8	8	1	3	2	2.531
9	9	1	3	3	2.021

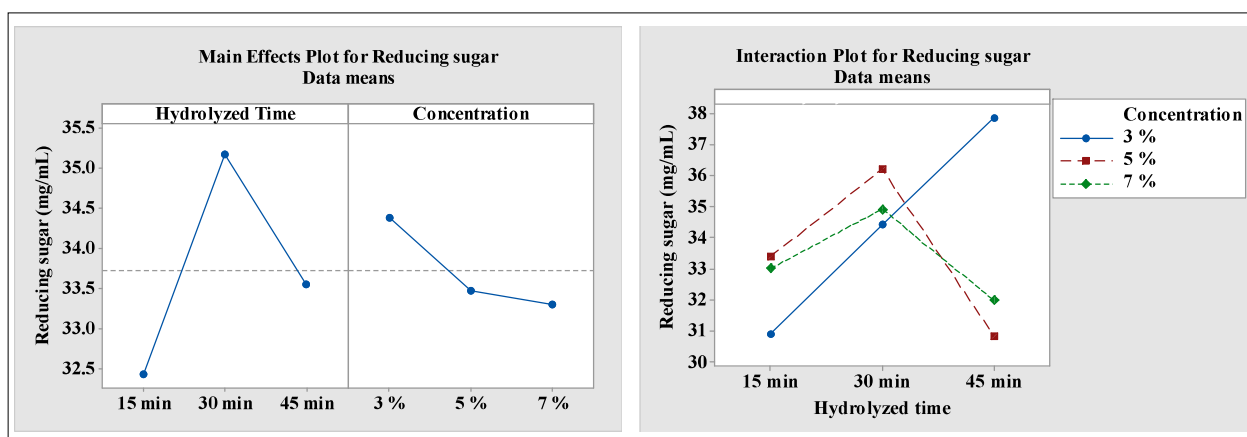


Figure 1: Effect of different concentrations and time on formation of reducing sugar with H₂SO₄ pre-treatment from coir dust

Table 4: Design for nitric acid pre-treatments with different concentrations of acid percentage and different hydrolysed time for the production of reducing sugar from coir dust

Std order	Run order	Blocks	Hydrolysed Time	Concentration	Reducing sugar (mg/mL)
1	1	1	1	1	30.892
2	2	1	1	2	33.385
3	3	1	1	3	33.002
4	4	1	2	1	34.408
5	5	1	2	2	36.199
6	6	1	2	3	34.920
7	7	1	3	1	37.861
8	8	1	3	2	30.828
9	9	1	3	3	31.979

Factor 1: Hydrolysed time (Level 1: 15 min, Level 2: 30 min, Level 3: 45 min)

Factor 2: Concentration (Level 1: 3%, Level 2: 5%, Level 3: 7%)

Optimization of nitric acid (HNO₃) pre-treatment

Optimization of acid hydrolysis with HNO₃ was carried out with different concentrations of acid (3, 5 and 7%) and different hydrolysed times (15, 30 and 45 min). Altogether there were nine treatments (Table 4).

According to the interaction plot and main plot (Figure 2) of HNO₃ pre-treatment, treatment 4 (3% at 30 min) that produced significantly higher amount of sugar was selected for further fermentation studies.

Production of alcohol from coir dust acid hydrolysed solution

Alcohol was not produced from HNO₃ acid hydrolysed solution while 0.4% of alcohol was obtained at the 4th day of fermentation from H₂SO₄ hydrolysed solution (Table 5). Although the concentration of reducing sugar was similar for HNO₃ hydrolysed solution and H₂SO₄ hydrolysed solution, there was no alcohol production in HNO₃ hydrolysed solution, probably due to the formation of toxic by-products during hydrolysis (Taherzadeh & Karimi, 2007).

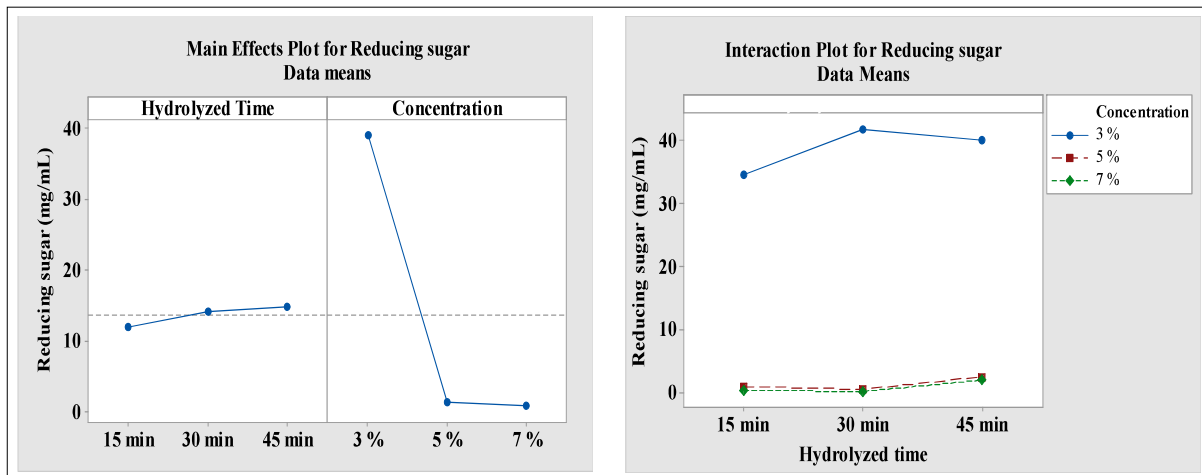


Figure 2: Effect of different concentrations and time on formation of reducing sugar with HNO₃ pre-treatment from coir dust

Table 5: Changes in chemical characteristics of H₂SO₄ hydrolysed medium during fermentation

Fermentation period (days)	Alcohol (%)	Acidity (%)	Reducing sugar (mg/mL)	pH
2	0.1 (±0.008)d	3.17 (±0.03)b	33.3298 (±91.38)a	5.05 (±0.02)c
3	0.2 (±0.009)c	2.87 (±0.08)c	22.2287 (±171.25)b	5.14 (±0.01)b
4	0.4 (±0.01)a	2.64 (±0.07)d	14.9823 (±9.19)c	5.19 (±0.02)a
5	0.4 (±0.01)a	3.16 (±0.08)b	0.9889 (±29.53)d	5.10 (±0.01)b
6	0.3 (±0.009)b	4.85 (±0.05)a	0.9886 (±29.50)d	4.94 (±0.03)d

Each value in the table is represented as mean ± SD (n = 3). Values in the same column followed by a different letter (a-d) are significantly different (p < 0.05).

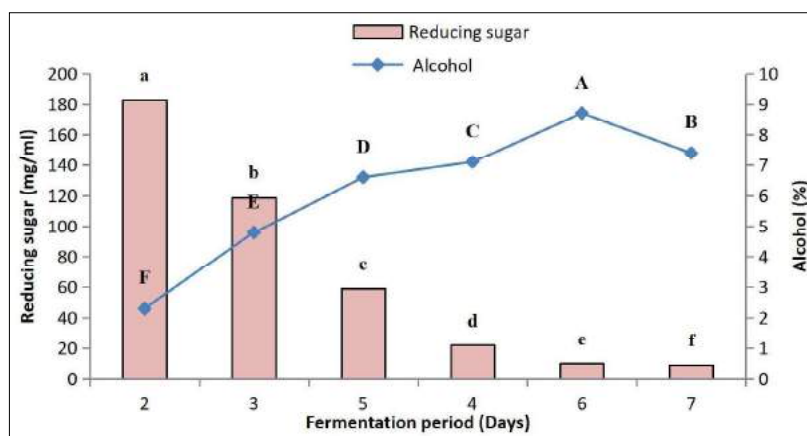


Figure 3: Changes in alcohol and reducing sugar content during fermentation of palmyrah molasses using baker’s yeast. Values indicated by different letters (a-f), (A-F) are significantly different (p < 0.05)

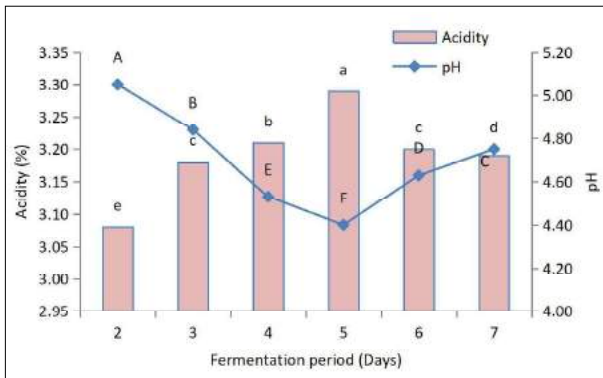


Figure 4: Changes in alcohol and reducing sugar content during fermentation of palmyrah molasses using baker's yeast. Values indicated by different letters (a-f), (A-F) are significantly different ($p < 0.05$)

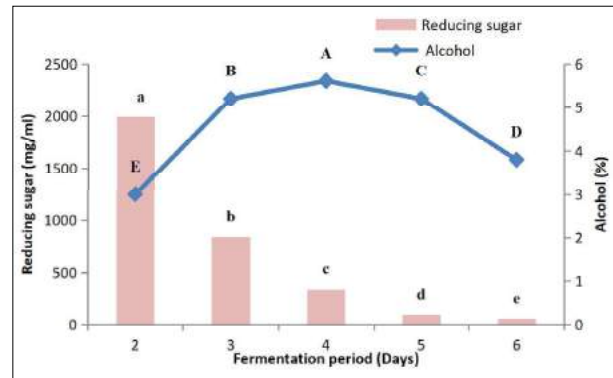


Figure 5: Changes in alcohol and reducing sugar content during fermentation of palmyrah fruit pulp (PFP) using baker's yeast. Values indicated by different letters (a-c), (A-E) are significantly different ($p < 0.05$).

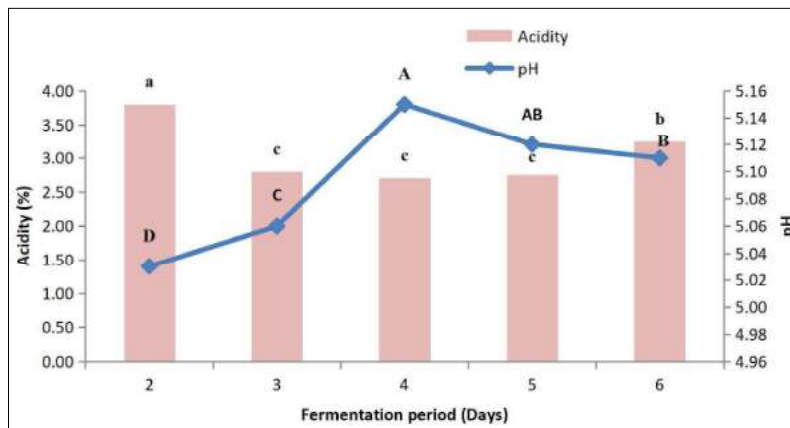


Figure 6: Changes in acidity and pH value during fermentation of palmyrah fruit pulp (PFP) using baker's yeast. Values indicated by a different letters (a-c), (A-D) are significantly different ($p < 0.05$)

Production of alcohol from molasses

Production of alcohol from molasses (brix°15) increased from the 2nd to 6th day of fermentation (Figure 3). The maximum production of alcohol was obtained on the 6th day of fermentation. The amount of reducing sugar decreased from 2nd to 7th day of fermentation.

The total acid produced with molasses increased from the 2nd to the 5th day of fermentation. It then decreased from 6th to the 7th day of fermentation. The pH value decreased from the 2nd to the 5th day of fermentation and increased from 6th to 7th day of fermentation (Figure 4).

Production of alcohol from PFP

Production of alcohol increased from the 2nd to 4th day of fermentation and then it decreased. The highest alcohol production was (5.5%) observed on the 4th day of fermentation. The amount of reducing sugar from PFP decreased during fermentation (Figure 5). The pH of the PFP added media increased from 2nd to 4th day of fermentation and then decreased from 5th to 6th day of fermentation. The acidity decreased from 2nd to 3rd day of fermentation and remained without any significant change on the 3rd, 4th and 5th day of fermentation, and then increased on the 6th day of fermentation (Figure 6).

Table 6: Efficiency of alcohol fermentation from different palmyrah waste materials

	Initial total sugar content (g)	Expected value (V/V)	Observed value V/V)	Efficiency (%)
Molasses	15.51	9.92	8.6	86.6
PFP	10.57	6.76	5.5	81.2
Coir dust acid hydrolysed	3.28	2.09	0.4	19.0

Efficiency of fermentation

The efficiency of alcohol fermentation by yeast was significantly lower (19%) in coir dust acid hydrolysate when compared with molasses (86.6%) and expired PFP pulp (81.2%) of palmyrah (Table 6).

Discussion

There have been continuous studies to investigate the effects of diverse lignocellulosic substrates in the production of bioethanol (Azzam, 1987; Wright, 1988; Cadoche & López, 1989; Reshamwala *et al.*, 1995; Bjerre *et al.*, 1996; Kathirgamanathan *et al.*, 2017). Conversion of natural lignocellulosic material to ethanol includes two steps: hydrolysis of cellulose to fermentable reducing sugars and fermentation of the sugars to ethanol. In this research, coir dust was used for the secondary ethanol production. Further as a comparison, molasses obtained from sugar candy production and expired PFP were also used for the primary ethanol production.

The aim of the pre-treatment of coir dust was to break down the structure of lignin and interrupt the crystalline structure of cellulose as this will facilitate the acids or bases to easily hydrolyse the cellulosic materials (Duff & Murray, 1996). Dilute acid hydrolysis could be used for pre-treatment of lignocellulosic materials, and this can achieve higher reaction rates and significantly improve cellulose hydrolysis (Mosier *et al.*, 2005). In this study, 3% H₂SO₄ acid was selected as the best pre-treatment agent at 121 °C for 45 min. It produced a small but significant amount of ethanol. However, there was no alcohol produced from the HNO₃ pre-treated hydrolysate. This may be due to the formation of toxic substances or inhibitors (Taherzadeh & Karimi, 2007). Some pre-treatments carried out particularly at low pH would lead to the formation of different types of inhibitors such as carboxylic acids, furans and phenolic

compounds (Esteghlalian *et al.*, 1997). These chemicals may not affect the enzymatic hydrolyses, but they usually inhibit the microbial growth and fermentation, resulting less ethanol yield.

During the initial fermentation period of pulp and molasses, there was an increase in the alcohol content, and this may be due to fermentation where yeasts grow on sugar to release pyruvic acid via glycolysis. Then the acetaldehyde produced will be reduced by nicotinamide adenine dinucleotide (NAD) to form ethyl alcohol (Singh *et al.*, 2003). Metabolic activities of yeasts that produce the ethanol and other metabolic by-products such as esters, ketones and higher alcohols are due to the efficient fermentation mechanism (Hansen, 1999; Piškur *et al.*, 2006; Fernando & Kapilan, 2019). During prolonged fermentation of the pulp, the amount of alcohol and acid produced showed a decrease, and this may be due to the formation of esters and higher alcohols.

The fermentation efficiency of coir dust was low compared with molasses and PFP. This may be due to the formation of inhibitors during the acid pre-treatment that inhibits or prevent the process of fermentation. In the presence of higher sugar concentration, furfural, a pentose degradation product and 5-hydroxymethylfurfural (HMF), a hexose degradation product will act as inhibitors. Lignin degradation products are formed during the fermentation of coir dust, and this leads to the reduction of ethanol yield from coir dust to a considerable amount. Therefore, it could be suggested that formation of inhibitors needs to be avoided or their effect minimized by a detoxification process. Inhibition of fermentation is a multifactor effect that depends on different internal and external factors of palmyrah such as the type of substrate, type and amount of microorganisms present in the substrate, surface exposed to microbial interaction and the biochemical reaction between the substrates and the microorganisms (Parekh *et al.*, 2000, Kapilan,

2015, Kapilan *et al.*, 2015, Sarathadevi *et al.*, 2018). During the hydrolysis of coir dust, non-fermentable sugars were also produced, which lowered the efficiency of fermentation of coir dust acid hydrolysate, when compared with molasses and expired PFP. Bioethanol production from coir dust substrate could be improved by developing enzymatic pre-treatment technologies in addition to the acid hydrolysis and optimization of fermentation medium (Panday, 1992; Parekh *et al.*, 2000; Kathirgamanathan *et al.*, 2017). Because of the absence or minimal level of accumulation of inhibitory substances in molasses and PFP, the amount of ethanol yield was significantly higher in molasses and PFP of palmyrah than in coir dust during fermentation. When the feasibility and the economics are considered, there will not be any issue in using molasses and PFP of the palmyrah palm as the raw material for bioethanol production. However, the novelty of this study is the usage of coir dust as a raw material for bioethanol production. With planning, obtaining coir dust from the palm can be made easy and cost-effective. Among the different palmyrah waste materials for bioethanol production, molasses and PFP could be treated as primary substrates and coir dust could be a secondary substrate.

CONCLUSION

Among the palmyrah palm wastes tested as starting materials for bioethanol production, molasses and palmyrah fruit pulp were more efficient than coir dust. Among the acids H_2SO_4 , HNO_3 and HCl and bases $NaOH$ and $Ca(OH)_2$ used for the pre-treatment, H_2SO_4 is the best hydrolysing agent for coir dust. Although the efficiency of alcohol production from coir dust was comparatively low, it could also be considered as a substrate for bio-ethanol production considering the excessive amount under-utilized in regular practice. This preliminary study concludes that the pre-treatment of palmyrah coir dust with 3% H_2SO_4 for 45 min and fermentation by yeast on PYN medium at pH 5.0 and at 30 °C for 4 days could be effectively used for bioethanol production from coir dust with further optimization.

Conflict of interests

The authors declare that they have no competing interests.

Acknowledgements

The authors express their sincere gratitude to the Ministry of Prison Reforms, Rehabilitation, Resettlement and Hindu Religious Affairs, Sri Lanka for the financial support.

REFERENCES

- Azzam A.M. (1987). Saccharification of bagasse cellulose pretreated with $ZnCl_2$ and HCl . *Biomass and Bioenergy* **12**: 71–77.
DOI: [https://doi.org/10.1016/0144-4565\(87\)90009-6](https://doi.org/10.1016/0144-4565(87)90009-6)
- Asiri Nisansala D., Piraveena G. & Kapilan R. (2021). Palmyrah (*Borassus flabellifer*) Nature's Gift for Life. Aarani Publishers, Jaffna.
- Barker H.A., Ruben S. & Kamen M.D. (1940). The reduction of radioactive carbon dioxide by methane-producing bacteria. *Proceedings of the National Academy of Sciences of USA* **26**: 426–430.
DOI: <https://doi.org/10.1073/pnas.26.6.426>
- Balakumar S. & Arasaratnam V. (2009). Comparison of industrial scale ethanol production from a palmyrah-based carbon source by commercial yeast and a mixed culture from palmyrah toddy. *Journal of the Institute of Brewing* **115**(2): 105–110.
DOI: <https://doi.org/10.1002/j.2050-0416.2009.tb00353.x>
- Bjerre A.B., Olesen A.B. & Fernqvist T. (1996). Pre-treatment of wheat straw using combined wet oxidation and alkaline hydrolysis resulting in convertible cellulose and hemicellulose. *Biotechnology and Bioengineering* **49**: 568–577.
DOI: [https://doi.org/10.1002/\(SICI\)1097-0290\(19960305\)49:5<568::AID-BIT10>3.0.CO;2-6](https://doi.org/10.1002/(SICI)1097-0290(19960305)49:5<568::AID-BIT10>3.0.CO;2-6)
- Cadoche L. & López G.D. (1989). Assessment of size reduction as a preliminary step in the production of ethanol from lignocellulosic wastes. *Biological Wastes* **30**: 153–157.
DOI: [https://doi.org/10.1016/0269-7483\(89\)90069-4](https://doi.org/10.1016/0269-7483(89)90069-4)
- Chan L., Kit N.C.V, Khim W.C.X., Kent L.H. & Yip C.H. (2011). *Determination of Acid Content in Vinegar - Volumetric Titration*. University Malaysia Sabah, Malaysia.
- Cortes T.R., Cuervo-Parra J.A., Robles-Olvera V.J., Cortes E.R. & López Pérez P.A. (2018). Experimental and kinetic production of ethanol using mucilage juice residues from cocoa processing. *International Journal of Chemical Reactor Engineering* **16** (11).
- Daroch M., Geng S. & Wang G. (2013). Recent advances in liquid biofuel production from algal feed stocks. *Applied Energy* **102**: 1371–1381.
DOI: <https://doi.org/10.1016/j.apenergy.2012.07.031>
- Duff S.J.B. & Murray W.D. (1996). Bioconversion of forest products industry waste cellulose to fuel ethanol: a review. *Bioresource Technology* **55**: 1–33.
DOI: [https://doi.org/10.1016/0960-8524\(95\)00122-0](https://doi.org/10.1016/0960-8524(95)00122-0)
- Esteghlalian A., Hashimoto A.G., Fenske J.J. & Penner M.H. (1997). Modeling and optimization of the dilute-sulfuric-acid pre-treatment of corn stover, poplar and switch grass. *Bioresource Technology* **59**(2): 129–136.
DOI: [https://doi.org/10.1016/S0960-8524\(97\)81606-9](https://doi.org/10.1016/S0960-8524(97)81606-9)
- Fernando M.N. & Kapilan R. (2019). Biodiesel production from *Sargassum* sp. a SriLankan marine flora and optimization of conditions for yield enhancement, *Proceedings of the Vavuniya Campus International Research Symposium*, pp. 99–103.

- Hansen J. (1999). Inactivation of MXR1 abolishes formation of dimethyl sulfide from dimethyl sulfoxide in *Saccharomyces cerevisiae*. *Applied and Environmental Microbiology* **65**: 3915–3919.
DOI: <https://doi.org/10.1128/AEM.65.9.3915-3919.1999>
- Hill J., Nelson E., Tilman D., Polasky S. & Tiffany D. (2006). Environmental, economic, and energetic costs and benefits of biodiesel and ethanol biofuels. *Proceedings of the National Academy of Sciences* **103**(30): 11206–11210.
DOI: <https://doi.org/10.1073/pnas.0604600103>
- Kapilan R. (2015). Optimization of the usage of commercial lime for the inhibition of fermentation of sweet sugary saps of *Borassus flabellifer* and *Caryota urens*. *International Journal for Advanced Research in Biological Sciences* **2**(12): 60–66.
- Kapilan R., Robika K., Mahilrajana S. & Srivijeindran S. (2015). Efficient fermentation inhibitor of sweet phloem sap of Palmyrah (*Borassus flabellifer* L.) in Sri Lanka. *International Journal of Advanced Research in Biological Sciences* **2**(10): 89–95.
DOI: <https://doi.org/10.12983/ijrsas-2015-p0166-0174>
- Kapilan R. (2015). Solid state fermentation for microbial products: A review. *Archives of Applied Science Research* **7**(8): 21–25.
- Kathirgamanathan M., Abhayasekera C.L., Kulasoorya S.A., Wanigasekera A. & Ratnayake R.R. (2017). Evaluation of 18 isolates of basidiomycetes for Lignocellulose degrading enzymes. *Ceylon Journal of Science* **46**(4): 77–84.
DOI: <https://doi.org/10.4038/cjs.v46i4.7470>
- Miller G.L. (1959). Use of dinitrosalicylic acid reagent for determination of reducing sugar. *Analytical Chemistry* **31**(3): 426–428.
DOI: <https://doi.org/10.1021/ac60147a030>
- Mohanadas K. (2002). The palmyrah palm and the composition of palmyrah fruit pulp. Sivapathasuntharam Mageswaran Memorial Lecture. University of Jaffna.
- Mosier N.S., Wyman Dale B., Elander R., Lee Y.Y., Holtzapple M. & Ladisch M.R. (2005). Features of promising technologies for pre-treatment of lignocellulosic biomass. *Bioresource Technology* **96**: 673–686.
DOI: <https://doi.org/10.1016/j.biortech.2004.06.025>
- Nigam P.S. & Singh A. (2011). Production of liquid biofuels from renewable resources. *Progress in Energy and Combustion Science* **37**(1): 52–68.
DOI: <https://doi.org/10.1016/j.peccs.2010.01.003>
- Parekh S., Vinci V.A. & Strobel R.J. (2000). Improvement of microbial strains and fermentation processes. *Applied Microbiology and Biotechnology* **54**(3): 287–301.
DOI: <https://doi.org/10.1007/s002530000403>
- Pandey A. (1992). Recent process developments in solid-state fermentation. *Process Biochemistry* **27**: 12–17.
DOI: [https://doi.org/10.1016/0032-9592\(92\)80017-W](https://doi.org/10.1016/0032-9592(92)80017-W)
- Piškur J., Rozpędowska E., Polakova S., Merico A. & Compagno C. (2006). How did *Saccharomyces* evolve to become a good brewer? *Trends in Genetics* **22**: 183–186.
DOI: <https://doi.org/10.1016/j.tig.2006.02.002>
- Potrich E. & Amaral L.S. (2018). Activation energy, half-life and yield of the hydrolysis reaction of sucrose catalyzed by the enzyme invertase produced by yeast *Saccharomyces cerevisiae*. *International Journal of Current Microbiology and Applied Sciences* **7**(2): 806–816.
DOI: <https://doi.org/10.20546/ijcmas.2018.702.102>
- Qureshi N. & Blaschek H.P. (2005). Butanol production from agricultural biomass. In: *Food Biotechnology* (eds. K. Shetty, A. Pometto & G. Paliyath), pp. 525–551. Taylor and Francis Group, Boca Raton, Florida, USA.
DOI: <https://doi.org/10.1201/9781420027976.ch1.20>
- Refai-El A.H., El-Abyad M.S., El-Diwanly A.I., Sallam L.A. & Allam F. (1992). Some physiological parameters for ethanol production from beet molasses by *Saccharomyces cerevisiae* Y-7. *Bioresource Technology* **42**(3): 183–189.
DOI: [https://doi.org/10.1016/0960-8524\(92\)90021-O](https://doi.org/10.1016/0960-8524(92)90021-O)
- Reshamwala S., Shawky B.T. & Dale B.E. (1995). Ethanol production from enzymatic hydrolysates of AFEX-treated coastal Bermuda grass and switch grass. *Applied Biochemistry and Biotechnology* **51/52**: 43–55.
DOI: <https://doi.org/10.1007/BF02933410>
- Sarathadevi R., Kapilan R. & Vasantharuba S. (2018). Papaw fruit juice as source for single cell protein production using natural palmyrah toddy yeast. *Ceylon Journal of Science* **47**(4): 379–386.
DOI: <https://doi.org/10.4038/cjs.v47i4.7556>
- Sarkar N., Ghosh S.K., Bannerjee S. & Aikat K. (2012). Bioethanol production from agricultural wastes: An overview. *Renewable Energy* **37**(1): 19–27.
DOI: <https://doi.org/10.1016/j.renene.2011.06.045>
- Singh D.P. & Trivedi R.K. (2003). Acid and alkaline pre-treatment of lignocellulosic biomass to produce ethanol as biofuel. *International Journal of Chem Tech Research* **5**: 727–734.
- Taherzadeh M.J. & Karimi K. (2007). Acid-based hydrolysis processes for ethanol from lignocellulosic materials: A review. *BioResources* **2**: 472–499.
- Theivendirarajah K. (2008). *Palmyrah Palm*, 1st edition. Graph Arts Print, Jaffna.
- Vasudevan P.T. & Briggs M. (2008). Biodiesel production: current state of the art and challenges. *Journal of Industrial Microbiology and Biotechnology* **35**: 421–430.
DOI: <https://doi.org/10.1007/s10295-008-0312-2>
- Wright J.D. (1988). Ethanol from biomass by enzymatic hydrolysis. *Chemical Engineering Progress* **84**(8): 62–74.

List of Referees - Volume 49 (2021)

Prof. Chamil Abeykoon
Dept. of Materials
Univ. of Manchester, UK

Prof. Ajith Abeysekera
Univ. of Sri Jayewardenepura

Prof. Charmalie Abeysekera
Dept. of Botany
Univ. of Peradeniya

Prof. Chrishantha Abeysena
Dept. of Public Health
Univ. of Kelaniya

Prof. P.D. Abeyasinghe
Dept. of Botany
Univ. of Ruhuna

Dr Hemalika T.K. Abeysondera
Dept. of Statistics & Computer Science
Univ. of Peradeniya

Dr Sachith Abeysondera
Dept. of Statistics & Computer Science
Univ. of Peradeniya

Prof. NKB Adikaram
National Institute of Fundamental Studies
Kandy

Dr Janaka Alawatugoda
Dept. of Computer Engineering
Univ. of Peradeniya

Dr Upali Amarasinghe
International Water Management Institute
Colombo

Prof. HBS Ariyaratne
Dept. of Basic Veterinary Science
Univ. of Peradeniya

Prof. KKIU Arunakumara
Dept. of Crop Science
Univ. of Ruhuna

Dr MDT Attygalle
Dept. of Statistics
Univ. of Colombo

Dr Oluwafemi Samson Balogun
University of Eastern Finland Finland

Dr Janaka Bamunawala
Dept. of Civil Engineering
Univ. of Moratuwa

Dr CS Bandara
Dept. of Civil Engineering
Univ. of Peradeniya

Dr GG Tushara Chaminda
Dept. of Civil & Environmental Engineering
Univ. of Ruhuna

Prof. Rohana Chandrajith
Dept. of Geology
Univ. of Peradeniya

Prof. GAP Chandrasekera
Dept. of Applied Nutrition
Wayamba University

Prof. Upali Chandrasekera
Dept. of Zoology & Environmental
Management
Univ. of Kelaniya

Prof. Chandima Dangalle
Dept. of Zoology & Environment Sciences
Univ. of Colombo

Dr Maheshi Danthurebandara
Dept. of Chemical and Process Engineering
Univ. of Peradeniya

Dr D Anupama Daranagama
Dept. of Plant & Molecular Biology
Univ. of Kelaniya

Prof. PN Dassanayake
Dept. of Botany
Univ. of Sri Jayewardenepura

Prof. WB Daundasekera
Dept. of Mathematics
Univ. of Peradeniya

Dr NW Nuwan Dayananda
Dept. of Electronic & Telecommunication
Engineering
Univ. of Moratuwa

Prof. E Dilip de Silva
Dept. of Chemistry
Univ. of Colombo

Prof. GSY De Silva
Dept. of Civil & Environmental Engineering
Univ. of Ruhuna

Dr Kaushika de Silva
Dept. of Mathematics
Univ. of Sri Jayewardenepura

Prof. P Mangala CS De Silva
Dept. of Zoology
Univ. of Ruhuna

Dr PSN de Silva
Lanka Electrical Company

Prof. Subashi de Silva
Dept. of Civil & Environmental Engineering
Univ. of Ruhuna

Dr MP Dhanapala
No 25, Hanwella Road
Ovitigama, Pugoda

Prof. RS Dharmakeerthi
Dept. of Soil Science
Univ. of Peradeniya

Dr USS Dharmapriya
Dept. of Manufacturing and Industrial
Engineering
Univ. of Peradeniya

Prof. Gihan Dias
Dept. of Computer Engineering
Univ. of Moratuwa

Dr DMPV Dissanayaka
Dept. of Statistics & Computer Science
Univ. of Kelaniya

Prof. Jayanthi Edirisinghe
Univ. of Peradeniya

Prof. JP Eeswara
Department of Crop Science
University of Peradeniya

Prof. JB Ekanayake
Dept. of Electrical & Electronic Engineering
Univ. of Peradeniya

Dr Serdar Erken
Atatürk Central Horticultural Research
Institute

Dr Aruna Fernando
General Sir John Kotelawala Defence
University

Dr EY Fernando
Dept. of Biological Sciences
Rajarata University

Prof. MARM Fernando
Dept. of Electrical & Electronic Engineering
Univ. of Peradeniya

Dr K Menaka C Fernando
Dept. of Crop Science
Univ. of Ruhuna

Dr Narmada Fernando
Institute of Biochemistry, Molecular Biology
& Biotechnology
Univ. of Colombo

Dr NC Ganegoda
Dept. of Mathematics
Univ. of Sri Jayewardenepura

Prof. S.M Ganehiarachchi
Dept. of Zoology & Environmental
Management
Univ. of Kelaniya

Dr Nalaka Geekiyanage
Dept. of Plant Sciences
Rajarata University

Dr T. Geretharan
Dept. of Crop Science
Eastern University

Prof. KB Gunaherath
The Open University of Sri Lanka

Prof. Sudarshanee Geekiyanage
Dept. of Agricultural Biology
Univ. of Ruhuna

Dr Thilanka Gunaratne Dept. of Botany Univ. of Peradeniya	Prof. Leslie Jayasekara Dept. of Mathematics Univ. of Ruhuna	Dr C. I. Keppitiyagama Univ. of Colombo School of Computing
Prof. K.D. Prasanna P. Gunatilake Dept. of Food Science & Technology Wayamba University	Prof. DKDD Jayasena Dept. of Animal Science Uva Wellassa University	Prof. Peter E. Kloeden Univ. of Tubingen Germany
Dr A.A.J.K. Gunatilake Dept. of Geology University of Peradeniya	Dr Chathuri Jayasinghe Dept. of Statistics Univ. of Sri Jayewardenepura	Prof. ND Kodikara Univ. of Colombo School of Computing
Prof. Mangala Gunatilake Dept. of Physiology Univ. of Colombo	Prof. Jeevani Jayasinghe Dept. of Electronics Wayamba University	Prof. Nisha Kottearachchi Dept. of Biotechnology Wayamba University
Prof. Savithri Gunatillake Dept. of Botany Univ. of Peradeniya	Prof. U.L. Jayasinghe National Institute of Fundamental Studies	Dr Sunil Kulatunga Dept. of Radiography Univ. of Peradeniya
Prof. Shiroma Handunnetti Institute of Biochemistry, Molecular Biology and Biotechnology Univ. of Colombo	Mr M.C.N. Jayasooriya Dept. of Food Science & Technology Sabaragamuwa University	Prof. S.A.S. Kulathilaka Dept. of Civil Engineering Univ. of Moratuwa
Dr Kasun T. Hemachandra Dept. of Electronic & Telecommunication Engineering Univ. of Moratuwa	Dr Dimanthi Jayatilake Dept. of Agricultural Biology Univ. of Peradeniya	Dr Terney Pradeep Kumara Dept. of Oceanography and Marine Geology Univ. of Ruhuna
Dr Damayanthi Herath Dept. of Computer Engineering Univ. of Peradeniya	Dr Eranda Jayatunga Dept. of Electrical and Information Engineering Univ. of Ruhuna	Prof. PVR Kumarasiri Dept. of Community Medicine Univ. of Peradeniya
Prof. Sanath Hettiarachchi Dept. of Biological Sciences Rajarata University	Dr Wasana Isuri Jayawardena Dept. of Physics Open University of Sri Lanka	Prof. WGD Lakmini Dept. of Crop Science Univ. of Ruhuna
Dr TM Bandula Heva Department of Civil & Environmental Engineering Univ. of Ruhuna	Dr Piyankarage Viraj Jayaweera SPD Laboratory Inc. Japan	Prof. DAL Leelamanie Dept. of Soil Science Univ. of Ruhuna
Dr AP Hewaarachchi Dept. of Statistics & Computer Science Univ. of Kelaniya	Dr Jeyasingam Jeyasugiththan Dept. of Nuclear Science Univ. of Colombo	Dr Tissa Liyanage Master Hellie's Engineering Consultants Battaramulla
Dr Kai Kwong Hon Hong Kong Observatory Hong Kong	Ms Humaira Kalsoom Dept. of Mathematics Zhejiang Normal University China	Dr DN Magana-Arachchi National Institute of Fundamental Studies Kandy
Prof. OA Ieperuma Univ. of Peradeniya	Prof. R. Kapilan Dept. of Botany Univ. of Jaffna	Dr Shahid Mahmood Sarhad University of Science & Information Technology Pakistan
Prof. JRP Jayakody Dept. of Physics Univ. of Kelaniya	Prof. AL Karunanayake Dept. of Anatomy Univ. of Kelaniya	Prof. Ajith Malalasekera Department of Anatomy Univ. of Colombo
Dr B Janarthanan Dept. of Civil Engineering Univ. of Jaffna	Dr P Kathirgamanathan Dept. of Electrical & Electronic Engineering Univ. of Jaffna	Prof. Pathmalal M. Manage Dept. of Zoology Univ. of Sri Jayewardenepura
Dr Sampath Jayarathna Dept. of Computer Science Old Dominion University, USA	Dr B Prabhu Kavim Sri Ramachandra Institute of Higher Education India	Dr Faiz Marikkar General Sir John Kotelawala Defence University
Prof. HTR Jayasooriya Dept. of Zoology The Open University of Sri Lanka	Prof. Syed Asad Raza Kazmi Government College University Pakistan	Dr DA Meedeniya Dept. of Computer Science & Engineering Univ. of Moratuwa
		Dr Malik Muhammad International Islamic University Islamabad Pakistan

Dr R.G.N. De S. Munasinghe
Dept. Materials Science and Engineering
Univ. of Moratuwa

Prof. S.B. Navaratne
Dept. of Food Science and Technology
Univ. of Sri Jayewardenepura

Dr GWRMR Palamakumbura
Dept. of Engineering Mathematics
Univ. of Peradeniya

Dr Ajith Pasqual
Dept. of Electronic and Telecommunication
Engineering

Prof. Asoka Pathiratne
Dept. of Zoology & Environmental
Management
Univ. of Kelaniya

Prof. Sriyani Peiris
School of Natural Sciences
SLIIT

Prof. Aloy Perera
Dept. of Physics
Univ. of Kelaniya

Dr Indika Perera
Dept. of Computer Science and Engineering
Univ. of Moratuwa

Dr Ishara Perera
Dept. of Agriculture
Peradeniya

Prof. Niranjalie Perera
Dept. of Food Science & Technology
Wayamba University

Prof. PIP Perera
Department of Horticulture and Landscape
Gardening
Wayamba University

Dr Srinath Perera
WSO2
Colombo 03

Dr SVT Janaka Perera
Dept. of Civil Engineering
SLIIT

Prof. Vasanthi Pinto
Dept. of Anaesthesiology & Critical Care
Univ. of Peradeniya

Dr Poorna Piyathilaka
Dept. of Environmental Technology
Univ. of Colombo

Dr WD Prasad
Dept. of Electrical Engineering
Univ. of Moratuwa

Prof. Dammini Premachandra
Dept. of Zoology
Univ. of Ruhuna

Dr US Premarathne
Dept. of Electrical and Computer
Engineering
Open University of Sri Lanka

Prof. WAP J Premaratne
Dept. of Chemistry
Univ. of Kelaniya

Prof. Ranjith Premasiri
Dept. of Earth Resources Engineering
Univ. of Moratuwa

Prof. Namal Priyantha
Dept. of Chemistry
Univ. of Peradeniya

Prof. Chandrika Nanayakkara
Dept. of Plant Sciences
Univ. of Colombo

Prof. SMA Nanayakkara
Dept. of Civil Engineering
Univ. of Moratuwa

Prof. Udeni Nawagamuwu
Dept. of Civil Engineering
Univ. of Moratuwa

Dr Indrajith Nissanka
Dept. of Mechanical Engineering
Univ. of Moratuwa

Prof. Robert M Norton
Univ. of Melbourne
Australia

Ravinder Krishna Raina
M. P. University of Agriculture and Technology
India

Prof. Rupika Rajakaruna
Dept. of Zoology
Univ. of Peradeniya

Dr RDAA Rajapaksha
Dept. of Electronics
Wayamba University

Prof. Udaya Ralapanawa
Dept. of Medicine
Univ. of Peradeniya

Dr A Ramanan
Dept. of Computer Science
Univ. of Jaffna

Dr Shantha Ramanayake
210/11, Kandy Road
Geliyoa

Dr AKRN Ranasinghe
Dept. of Surveying & Geodesy
Sabaragamuwa University

Dr Menaka Ranasinghe
Dept. of Electrical and Computer
Engineering
The Open University of Sri Lanka

Dr EM Ranatunga
Dept. of Physics
Univ. of Ruhuna

Prof. Lanka Ranawake
Dept. of Agricultural Biology
Univ. of Ruhuna

Prof. KKDS Ranaweera
Dept. of Food Science and Technology
Univ. of Sri Jayewardenepura

Dr RHG Ranil
Dept. of Crop Science
Univ. of Peradeniya

Prof. Sudheera Ranwala
Dept. of Plant Sciences
Univ. of Colombo

Prof. P Ravirajan
Dept. of Physics
Univ. of Jaffna

Dr TM Rengarasu
Dept. of Civil and Environmental
Engineering
Univ. of Ruhuna

Prof. Upali Samarajeewa
Univ. of Peradeniya

Dr Dulani Samaranyake
Dept. of Community Medicine
Univ. of Colombo

Mrs IR Samarathunga
Institute of Technology
Univ. of Moratuwa

Prof. MB Samarawickrama
Dept. of Anatomy
Univ. of Ruhuna

Dr Channa Senanayake
Dept. of Medical Microbiology and
Immunology
Univ. of Colombo

Prof. Gamini Senanayake
Dept. of Agriculture Biology
Univ. of Ruhuna

Dr Jayantha Senanayake
Rice Research Development Institute
Bathalagoda

Prof. Priyanganie Senanayake
Dept. of Plant & Molecular Biology
Univ. of Kelaniya

Prof. WTPSK Senarath
Dept. of Botany
Univ. of Sri Jayewardenepura

Prof. Jayamini Seneviratne
Lady Ridgeway Hospital for Children
Colombo 08

Prof. NAKPJ Seneviratne
Dept. of Chemistry
Univ. of Kelaniya

Dr Jeewanthi Sirisena
Dept. of Water Engineering and Management
Univ. of Twente, The Netherlands

Prof. Upul Subasinghe
Dept. Forestry and Environmental Science
Univ. of Sri Jayewardenepura

Prof. N.P. Sunil Chandra
Dept. of Medical Microbiology
Univ. of Kelaniya

Prof. S.N Surendran
Dept. of Zoology
Univ. of Jaffna

Prof. K. Tennakoon
Tapodarama Road
Kandy

Prof. Kamani H Tennekoon
Institute of Biochemistry, Molecular Biology
and Biotechnology,
Univ. of Colombo

Dr K. Thabotharan
Dept. of Computer Science
Univ. of Jaffna

Prof. Ira Thabrew
University of Kelaniya

Dr RDN Thilakarathna
Dept. of Mathematics
Univ. of Colombo

Prof. Preethi Udagama
Dept. of Zoology and Environment Sciences
Univ. of Colombo

Prof. Disala Uduwawala
Dept. of Electrical and Electronic
Engineering
Univ. of Peradeniya

Dr Ahsan-Ul-Haq
National College of Arts Lahore
Pakistan

Prof. Wasim Ul-Haq
Dept. of Mathematics
Majmaah University
Saudi Arabia

Dr Nagarajah Varathan
Dept. of Mathematics and Statistics
Univ. of Jaffna

Dr CK Walgampaya
Dept. of Engineering Mathematics
Univ. of Peradeniya

Dr KS Wanniarachchi
Department of Civil & Environmental
Engineering
University of Ruhuna

Prof. PC Weeraddana
Dept. of Electronic & Telecommunication
Engineering
Univ. of Moratuwa

Prof. Aruni Weerasinghe
Dept. of Plant Sciences
Rajarata University

Prof. Devaka Weerakoon
Dept. of Zoology and Environmental
Science
Univ. of Colombo

Dr TC Weeraratne
Dept. of Zoology
Univ. of Peradeniya

Prof. Aruni Weerasinghe
Dept. of Plant Sciences
Rajarata University

Dr Pasindu Weerasinghe
Dept. of Civil Engineering
Univ. of Moratuwa

Prof. Jayantha Welihinda
Dept. of Biochemistry and Molecular
Biology
Univ. of Colombo

Prof. Rajitha Wickramasinghe
Dept. of Public Health
Univ. of Kelaniya

Dr WMADB Wickramasinghe
27/4, Wijayasiri Mawatha
Kulugammana

Dr Lidula Widanagama Arachchige
Dept. of Electrical Engineering
Univ. of Moratuwa

Prof. Dimuthu Wijeyaratne
Dept. of Zoology & Environmental
Management
Univ. of Kelaniya

Dr Prasad Wimalaratne
Univ. of Colombo School of Computing

Dr SP Withanage
Dept. of Genetics & Plant Breeding
Rubber Research Institute of Sri Lanka

Dr Sanjeeva Witharana
Dept. of Mechanical Engineering
Univ. of Moratuwa

Dr WAU Witharana
Dept. of Soil Science
Univ. of Peradeniya

Prof. Wipula Yapa
Dept. of Zoology
Univ. of Colombo

Prof. SK Yatigammana
Dept. of Zoology
Univ. of Peradeniya

Dr Abdullah M. Zeyad
Dept. of Civil Engineering
Jazan University
Saudi Arabia

AUTHOR INDEX - VOL. 49 – 2021

Aananda GKS *see* Jayarathne HSM *et al.* (2021)

Abayaratne CP, Wickramarathna AVUA & Jayananda MK - Solar luminance distribution in the principal plane for different wavelengths at two locations in Sri Lanka **49**: 361-368 (2021)

Abayasekara CL *see* Hettiarachchi CS *et al.* (2021)

Abayasekara CL *see* Jayasekara SK *et al.* (2021)

Adikaram N, Maharachchikumbura S, Vithanage ISK, Yakandawala D & Jayasinghe L - A new foliar disease of *Ficus religiosa* caused by *Diaporthe acutispora*, identified using molecular phylogeny based multigene DNA sequence analyses **49**: 573-581 (2021)

Ahmad SA *see* Khan H *et al.* (2021)

Amaradasa HS *see* Vithana PVSC *et al.* (2021)

Amarasekera DABN *see* Sandamal S *et al.* (2021)

Arachchi UPE *see* Perera PIP *et al.* (2021)

Arivazhagan S, Arun M & Rathina D - Recognition of handwritten characters using deep convolution neural network **49**: 503-511 (2021)

Arun M *see* Arivazhagan S *et al.* (2021)

Attanayaka DPSTG *see* Dissanayaka DMS *et al.* (2021)

Attanayaka DPSTG *see* Perera PIP *et al.* (2021)

Aziz U *see* Khan H *et al.* (2021)

Bako SP *see* Buba T *et al.* (2021)

Balaban P, Viduka D, Ristic V, Maksin M, Radic V, Vladislavljevic R, Vulic M, Josimovic M & Radivojevic NZ - Mechanical and barrier properties of flexible packaging materials after the flexo printing process **49**: 513-523 (2021)

Bandara KMJ *see* Diyes GCP *et al.* (2021)

Bandarage VP *see* Vithana PVSC *et al.* (2021)

Bandupriya D & Waidyarathne P - Improved protocol for efficient regeneration of coconut (*Cocos nucifera* L.) anther derived embryos **49**: 383-391 (2021)

Bhatti SH *see* Javed M *et al.* (2021)

Bin C & Ge L - Effects of particle size and concentration on the pulsation characteristics of transformer oil **49**: 593-606 (2021)

Buba T, Gaya AE, Bako SP & Sabo MU - Responses and recovery among seedlings of some arid land woody legumes under combined effects of sudden drought and nutrient stress **49**: 51-60 (2021)

Chandrasekharan N *see* Dewasurendra R *et al.* (2021)

Chandrasena G *see* Christy EJSBA *et al.* (2021)

Chang KH *see* Chen LC *et al.* (2021)

Chen LC, Chang KH & Yang SC - An integrated corpus-based text mining approach used to process military technical information for facilitating EFL troopers' linguistic comprehension: US anti-tank missile systems field manual as an example **49**: 403-417 (2021)

Christy EJSBA, Mahilrajana S, Chandrasena G & Kapilana R - Bioethanol production from Palmyrah (*Borassus flabellifer*) wastes using yeast **49**: 607-616 (2021)

De Alwis N *see* Jayatissa R *et al.* (2021)

De Silva KH *see* Jayatissa R *et al.* (2021)

de Silva MPKSK & Senaarachchi WARK - Rice bran in the diet as an enriching source of long chain Omega 3 poly unsaturated fatty acids (LC n-3 PUFAs) in fillets of genetically improved farmed Tilapia (GIFT) **49**: 17-24 (2021)

- De Silva SNT *see* Dissanayaka DMS *et al.* (2021)
- Deifel KS *see* Kulathunga MRDL *et al.* (2021)
- Dewasurendra R, Sepulveda N, Chandrasekharan N, Karunaweera N & Gunawardena S - Polymorphisms in rs915941 and rs915942: Are they associated with increased risk of G6PD enzyme deficiency in the Sri Lankan population? **49**: 157-168 (2021)
- Dharmasena WGBP & Munasinghe DHH - Identification of potential TALEN and CRISPR/Cas9 targets of selected genes of some human pathogens which cause persistent infections **49**: 451-464 (2021)
- Dharmawardana IVP *see* Jayasumana MTLK *et al.* (2021)
- Dheerasinghe DSAF *see* Vithana PVSC *et al.* (2021)
- Din Q *see* Ozair M *et al.* (2021)
- Dissanayaka DMS, De Silva SNT, Attanayaka DPSTG & Vimukthi EMM - Production and characterization of β -galactosidase from the fungus *Thielaviopsis ethacetica* Went. **49**: 563-571 (2021)
- Dissanayaka MP & Yapa HD - Numerical prediction of early age concrete temperature via 3D finite difference simulation **49**: 539-550 (2021)
- Diyes GCP, Bandara KMJ, Rajakaruna RS & Karunaratne SHPP - Acaricide resistance in the spinose ear tick, *Otobius megnini* (Acari: Argasidae) infesting racehorses in Sri Lanka **49**: 551-561 (2021)
- Donchev T *see* Ozair M *et al.* (2021)
- Dunuwila DMUNK *see* Jayasumana MTLK *et al.* (2021)
- Ekanayake EMHGS *see* Hettiarachchi CS *et al.* (2021)
- Fernando BR *see* Karunaratne NB *et al.* (2021)
- Fernando CN *see* Perera PIP *et al.* (2021)
- Fernando E *see* Vithana PVSC *et al.* (2021)
- Fernando R *see* Muthugala V *et al.* (2021)
- Galappaththi MO, Jayasuriya KMGG & Gama-Arachchige NS - Effect of priming with neem seed extract on seeds of four traditional rice varieties of Sri Lanka; Kaluheenati, Kurulurthuda, Madathawalu and Maa-wee **49**: 525-538 (2021)
- Gama-Arachchige NS *see* Galappaththi MO *et al.* (2021)
- Gamlath L, Siriwardana T & Sudasinghe BH - A baseline survey on food safety hazards in commonly consumed food items in Sri-Lanka **49**: 241-254 (2021)
- Gaya AE *see* Buba T *et al.* (2021)
- Gayathree THI *see* Jayarathne HSM *et al.* (2021)
- Ge L *see* Bin C & Ge L (2021)
- Ghosh I *see* Maurya N & Ghosh I (2021)
- Goonetilleke IA, Subasinghe HCS, Ratnayake AS & Jayawardana DT - Acid-assisted leaching of iron and manganese from Sri Lankan laterite: a potential source of alumina production **49**: 303-310 (2021)
- Gowthamy P, Indraratne SP, Weerasooriya R & Mapa RB - Characterisation of clay mineralogy of the major soils in the Northern region of Sri Lanka **49**: 351-360 (2021)
- Gunaratne HMA *see* Hettiarachchi CS *et al.* (2021)
- Gunasekera MY *see* Nadeeshani E & Gunasekera MY (2021)
- Gunawardena S *see* Dewasurendra R *et al.* (2021)
- Gunawardhana WPDS *see* Perera PIP *et al.* (2021)
- Hammer GL *see* Kulathunga MRDL *et al.* (2021)

Hettiarachchi CS, Abayasekara CL, Saravana Kumar P, Rajapakse S, Kulasoorya SA, Ekanayake EMHGS, Kumara RKGK & Gunaratne HMA - Nitrogen fertiliser replacement by single and multi-strain rhizobial inoculants for black gram, green gram and soybean cultivation in Sri Lanka **49**: 323-336 (2021)

Hussain T *see* Ozair M *et al.* (2021)

Indraratne SP *see* Gowthamy P *et al.* (2021)

Irfan M *see* Javed M *et al.* (2021)

Javed M, Irfan M & Bhatti SH - On optimal classes of estimators in the presence of some non-sampling errors **49**: 281-294 (2021)

Jayalath C *see* Mubarak S *et al.* (2021)

Jayananda MK *see* Abayaratne CP *et al.* (2021)

Jayarathne HSM, Ranaweera LT, Gayathree THI, Karunaratne SI, Aananda GKS, Ranasinghe RDGA, Thilakarathne SMNM, Wijesundara WWMUK, Weebadde CK & Sooriyapathirana SDSS - Assessment of the organoleptic properties, species delimits and varietal identities of pennyworts in Sri Lanka **49**: 227-240 (2021)

Jayasekara SK, Madusanka TGY, Rupasinghe CP, Weerasinghe HAS, Abayasekara CL, Seneweera S & Ratnayake RR - Bagasse and vinasse, factory wastes from sugarcane industry as potential substrates for bioethanol production **49**: 169-182 (2021)

Jayasinghe L *see* Adikaram N *et al.* (2021)

Jayasumana MTLK, Dunuwila DMUNK, Palkumbura PGAS, Mudalige R, Dharmawardana IVP, Wijesundera RRMKK & Jinadasa HRN - Detection of *Mycobacterium bovis* in cattle lungs from two abattoirs in Western and North Central provinces of Sri Lanka **49**: 99-109 (2021)

Jayasuriya KMGG *see* Galappaththi MO *et al.* (2021)

Jayathilaka KMDC *see* Kafi FSB *et al.* (2021)

Jayatissa R, Santos JA, Rannan-Eliya RP, Trieu K, Perera AG, De Alwis N, Ranasingha S, Jayawardana R & De Silva KH - A method to monitor the national salt reduction efforts in Sri Lanka and status of salt, potassium and iodine intake in an adult Sri Lankan community **49**: 111-122 (2021)

Jayawardana DT *see* Goonetilleke IA *et al.* (2021)

Jayawardana R *see* Jayatissa R *et al.* (2021)

Jinadasa HRN *see* Jayasumana MTLK *et al.* (2021)

Josimovic M *see* Balaban P *et al.* (2021)

Kafi FSB, Jayathilaka KMDC, Wijesundera RP & Siripala W - Effect of pre-surface treatments on p-Cu₂O/Au Schottky junctions **49**: 61-66 (2021)

Kapilan R *see* Christy EJSBA *et al.* (2021)

Karunaratne NB, Perera IA, Nayomi NT, Munasinghe DMS, Silva SSP, Strashnov I & Fernando BR - Occurrence of enrofloxacin and ciprofloxacin residues in broiler meat sold in Sri Lanka **49**: 479-492 (2021)

Karunaratne P, Yakandawala D & Samaraweera P - Fruit morphology helps identifying evolutionary groups in Alpinieae (Zingiberaceae): inferences from phylogenetic analysis of gingers in Sri Lanka **49**: 337-350 (2021)

Karunaratne SI *see* Jayarathne HSM *et al.* (2021)

Karunaratne SHPP *see* Diyes GCP *et al.* (2021)

Karunaratne SHPP *see* Marasinghe JP & Karunaratne SHPP (2021)

Karunaweera N *see* Dewasurendra R *et al.* (2021)

Khan H, Koreshi ZU, Aziz U, Sheikh SR & Ahmad SA - Energy deposition and dose enhancement using Monte Carlo derivative sampling: applications in brachytherapy **49**: 493-501 (2021)

Khan H, Koreshi ZU, Sheikh SR & Khan MY - Characteristic photon yields from thermal neutron activation of explosives for a portable detection system **49**: 209-218 (2021)

Khan MY *see* Khan H *et al.* (2021)

Koreshi ZU *see* Khan H *et al.* (2021)

- Koreshi ZU *see* Khan H *et al.* (2021)
- Kulasooriya SA *see* Hettiarachchi CS *et al.* (2021)
- Kulathunga MRDL, van Oosterom EJ, Hammer GL & Deifel KS - Transpiration efficiency of sorghum [*Sorghum bicolor* (L.) Moench] in relation to plant type and genotype **49**: 183-193 (2021)
- Kumara RKGK *see* Hettiarachchi CS *et al.* (2021)
- Kumara TN *see* Shafana MS *et al.* (2021)
- Lakmini MC & Mahanama KRR - Safety concerns of lead chromate in enamel paints: A study based on the Sri Lankan enamel paints industry after the lead paint regulatory enforcement **49**: 311-320 (2021)
- Madusanka TGY *see* Jayasekara SK *et al.* (2021)
- Mahanama KRR *see* Lakmini MC & Mahanama KRR (2021)
- Maharachchikumbura S *see* Adikaram N *et al.* (2021)
- Mahilrajan S *see* Christy EJSBA *et al.* (2021)
- Maksin M *see* Balaban P *et al.* (2021)
- Manage PM *see* Serasinghe DSW & Manage PM (2021)
- Mapa RB *see* Gowthamy P *et al.* (2021)
- Marambe B *see* Sandamal S *et al.* (2021)
- Marasinghe JP & Karunaratne SHPP - Evaluation of insecticide resistance and underlying resistance mechanisms in selected whitefly populations in Sri Lanka **49**: 469-478 (2021)
- Marasinghe S & Sivakanesan R - Paraoxonase 1 phenotype distribution in a cohort of healthy Sri Lankan population **49**: 419-427 (2021)
- Maurya N & Ghosh I - Dexamethasone induced glaucoma associated features exhibited differentially in retinal ganglion cells and human trabecular meshwork cells **49**: 295-302 (2021)
- Mubarak S, Nanayakkara D, Jayalath C & Sivakumar V - Low dose radioiodine therapy: a review of dosimetry and evaluation of potential shielding materials for neck collars **49**: 583-591 (2021)
- Mudalige R *see* Jayasumana MTLK *et al.* (2021)
- Munasinghe DHH *see* Dharmasena WGBP & Munasinghe DHH (2021)
- Munasinghe DMS *see* Karunarathna NB *et al.* (2021)
- Muthugala V, Wadduwage DP, Wijayapala A & Fernando R - Identification of coherent groups of generators for out-of-step protection using online measurements **49**: 3-15 (2021)
- Nadeeshani E & Gunasekera MY - Environmental performance comparison of parboiled rice production **49**: 137-155 (2021)
- Nanayakkara D *see* Mubarak S *et al.* (2021)
- Naseemdeen SH *see* Vithana PVSC *et al.* (2021)
- Nayomi NT *see* Karunarathna NB *et al.* (2021)
- Ng CK *see* Sutharsini U *et al.* (2021)
- Noor KI *see* Saliu A & Noor KI (2021)
- Ozair M, Din Q, Donchev T & Hussain T - Stability, control and discretization for a smoking model **49**: 25-38 (2021)
- Palkumbura PGAS *see* Jayasumana MTLK *et al.* (2021)
- Pathirana R *see* Perera PIP *et al.* (2021)
- Perera AG *see* Jayatissa R *et al.* (2021)

Perera IA *see* Karunarathna NB *et al.* (2021)

Perera ND, Prathapan SP, Wass DA & Wijewickrama A - Construct validity and reliability of the Sinhala version of the Chalder fatigue questionnaire in a cohort following dengue infection in Sri Lanka **49**: 441-450 (2021)

Perera PIP, Attanayaka DPSTG, Yakandawala K, Yakandawala DMD, Fernando CN, Arachchi UPE, Gunawardhana WPDS & Weerasinghe WDCD - *In vitro* culture of *Nymphaea nouchali* seeds; a conservation approach for a vulnerable species **49**: 393-402 (2021)

Perera PIP, Pathirana R & Vidhanaarachchi VRM - Somatic embryogenesis in anther-derived fast-growing callus as a long-term source for doubled-haploid production of coconut (*Cocos nucifera* L.) **49**: 39-49 (2021)

Perera S *see* Vithana PVSC *et al.* (2021)

Prathapan SP *see* Perera ND *et al.* (2021)

Radic V *see* Balaban P *et al.* (2021)

Radivojevic NZ *see* Balaban P *et al.* (2021)

Ragel RG *see* Shafana MS *et al.* (2021)

Rajakaruna RS *see* Diyes GCP *et al.* (2021)

Rajapakse S *see* Hettiarachchi CS *et al.* (2021)

Ramesh S *see* Sutharsini U *et al.* (2021)

Ranasingha S *see* Jayatissa R *et al.* (2021)

Ranasinghe RDGA *see* Jayarathne HSM *et al.* (2021)

Ranasinghe RS - Simulation of breaking waves over different seabed configurations using phase-resolving wave models **49**: 67-78 (2021)

Ranaweera LT *see* Jayarathne HSM *et al.* (2021)

Rannan-Eliya RP *see* Jayatissa R *et al.* (2021)

Rathina D *see* Arivazhagan S *et al.* (2021)

Ratnasekera D *see* Sandamal S *et al.* (2021)

Ratnayake AS *see* Goonetilleke IA *et al.* (2021)

Ratnayake AS *see* Wijesinghe UMP *et al.* (2021)

Ratnayake NP *see* Wijesinghe UMP *et al.* (2021)

Ratnayake RR *see* Jayasekara SK *et al.* (2021)

Ristic V *see* Balaban P *et al.* (2021)

Rupasinghe CP *see* Jayasekara SK *et al.* (2021)

Sabo MU *see* Buba T *et al.* (2021)

Saliu A & Noor KI - Radii problems and some other properties of certain classes of analytic functions with boundary rotation **49**: 429-439 (2021)

Samarakoon PN *see* Vithana PVSC *et al.* (2021)

Samaraweera P *see* Karunarathne P *et al.* (2021)

Sandamal S, Tennakoon A, Amarasekera DABN, Marambe B & Ratnasekera D - Functional trait diversity of wild rice species in Sri Lanka: implications for field identification and application **49**: 369-382 (2021)

Santos JA *see* Jayatissa R *et al.* (2021)

Saravana Kumar P *see* Hettiarachchi CS *et al.* (2021)

Senaarachchi WARK *see* de Silva MPKSK & Senaarachchi WARK (2021)

- Seneweera S *see* Jayasekara SK *et al.* (2021)
- Sepulveda N *see* Dewasurendra R *et al.* (2021)
- Serasinghe DSW & Manage PM - Feasibility of biodegradation of Azamethiphos; odour and fly controlling chemical used in open solid waste dumpsite at Karadiyana, Colombo, Sri Lanka **49**: 123-134 (2021)
- Shafana MS, Ragel RG & Kumara TN - An effective feature set for enhancing printed Tamil character recognition **49**: 195-208 (2021)
- Sheikh SR *see* Khan H *et al.* (2021)
- Sheikh SR *see* Khan H *et al.* (2021)
- Silva SSP *see* Karunaratna NB *et al.* (2021)
- Siripala W *see* Kafi FSB *et al.* (2021)
- Siriwardana T *see* Gamlath L *et al.* (2021)
- Sivakanesan R *see* Marasinghe S & Sivakanesan R (2021)
- Sivakumar V *see* Mubarak S *et al.* (2021)
- Sooriyapathirana SDSS *see* Jayarathne HSM *et al.* (2021)
- Strashnov I *see* Karunaratna NB *et al.* (2021)
- Subasinghe HCS *see* Goonetilleke IA *et al.* (2021)
- Sudasinghe BH *see* Gamlath L *et al.* (2021)
- Sutharsini U, Thanahaichelvan M, Ramesh S & Ng CK - Surface yttria content and hydrothermal ageing behaviour of two step sintered 3Y-TZP ceramics **49**: 219-225 (2021)
- Tennakoon A *see* Sandamal S *et al.* (2021)
- Thanahaichelvan M *see* Sutharsini U *et al.* (2021)
- Thilakarathne SMNM *see* Jayarathne HSM *et al.* (2021)
- Trieu K *see* Jayatissa R *et al.* (2021)
- van Oosterom EJ *see* Kulathunga MRDL *et al.* (2021)
- Vidanagamachchi SM - An improved method with higher efficiency for protein biomarker discovery and verification workflow **49**: 255-271 (2021)
- Vidhanaarachchi VRM *see* Perera PIP *et al.* (2021)
- Viduka D *see* Balaban P *et al.* (2021)
- Vimukthi EMM *see* Dissanayaka DMS *et al.* (2021)
- Vithana PVSC, Bandarage VP, Dheerasinghe DSAF, Perera S, Samarakoon PN, Amaradasa HS, Naseemdeen SH & Fernando E - Cervical cancer: five-year survival and associated prognostic factors in the Western Province of Sri Lanka **49**: 273-279 (2021)
- Vithanage ISK *see* Adikaram N *et al.* (2021)
- Vladislavljevic R *see* Balaban P *et al.* (2021)
- Vulic M *see* Balaban P *et al.* (2021)
- Wadduwage DP *see* Muthugala V *et al.* (2021)
- Waidyarathne P *see* Bandupriya D & Waidyarathne P (2021)
- Wass DA *see* Perera ND *et al.* (2021)
- Weebadde CK *see* Jayarathne HSM *et al.* (2021)
- Weerasinghe HAS *see* Jayasekara SK *et al.* (2021)

Weerasinghe WDCD *see* Perera PIP *et al.* (2021)

Weerasooriya R *see* Gowthamy P *et al.* (2021)

Wickramarathna AVUA *see* Abayaratne CP *et al.* (2021)

Wijayapala A *see* Muthugala V *et al.* (2021)

Wijesinghe UMP, Ratnayake AS & Ratnayake NP - Geochemistry of Negombo Lagoon sediments in Sri Lanka: implications for environmental monitoring **49**: 89-98 (2021)

Wijesundara WWMUK *see* Jayarathne HSM *et al.* (2021)

Wijesundera RP *see* Kafi FSB *et al.* (2021)

Wijesundera RRMKK *see* Jayasumana MTLK *et al.* (2021)

Wijewickrama A *see* Perera ND *et al.* (2021)

Yakandawala D *see* Adikaram N *et al.* (2021)

Yakandawala D *see* Karunaratne P *et al.* (2021)

Yakandawala DMD *see* Perera PIP *et al.* (2021)

Yakandawala K *see* Perera PIP *et al.* (2021)

Yang SC *see* Chen LC *et al.* (2021)

Yapa HD *see* Dissanayaka MP & Yapa HD (2021)

Yapage N - A study on some geometrical and statistical properties of the continuous power-law distribution with a comparison of similar properties of a particular exponential distribution **49**: 79-87 (2021)

SUBJECT INDEX 2021

δ Scuti

Determination of oscillation frequencies and stellar properties of three Delta Scuti variable stars using Kepler data (Adassuriya J, Jayaratne KPSC & Cooray PTLV & Attygalle MLC) **48**: 367-378 (2020)

Acceleration mean square value

Comfort evaluation of bridge based on stochastic process theory (Tan Y, Qin S, Zhang Z, Wang H & Wang Q) **48**: 239-249 (2020)

Accuracy assessment

Google Earth imagery coupled with on-screen digitisation for urban land-use mapping: case study of Hambantota, Sri Lanka (Madarasinghe SK, Yapa KKAS & Jayatissa LP) **48**: 357-366 (2020)

Ae. cogilli

First record of the presence of *Aedes* (Phagomyia) *cogilli* (Edwards, 1922) in Sri Lanka (Jayadas TTP, Thiruchenthooran V, Tharsan A, Sivabalakrishnan K, Santhirasekaram S & Surendran SN) **48**: 327-331 (2020)

Aedes aegypti

The scope of Rp EPIC markers in population genetic studies: a preliminary study with dengue vectors (Nirmani MD, Perera NS & Galhena GH) **48**: 275-288 (2020)

Aedes albopictus

The scope of Rp EPIC markers in population genetic studies: a preliminary study with dengue vectors (Nirmani MD, Perera NS & Galhena GH) **48**: 275-288 (2020)

Age hardening

Effect of precipitate size distribution on hardness of aluminium 6063 alloy (Dilrukshi LWUR & De Silva GIP) **48**: 305-313 (2020)

Agronomic effectiveness

Use of single superphosphate fertiliser produced using Eppawala rock phosphate as a source of phosphorous for rice cultivation (Udawatte CP, Panagoda PVA, Wickramasinghe WMADB, Wijewardena JDH, Sirisena DN, Emitiyagoda S & Bandara HRUD) **48**: 131-142 (2020)

Air voids

Effect of air voids on permeability and durability of hot mix asphalt (Ahmad N, Haroon W & Abid MM) **48**: 463-474 (2020)

Al 6063 alloy

Effect of precipitate size distribution on hardness of aluminium 6063 alloy (Dilrukshi LWUR & De Silva GIP) **48**: 305-313 (2020)

Altitude

Relative production efficiency of maize-legume intercroppings at different altitudes (Arshad M, Nawa R, Ahmad S, Razaq A, Ranamukhaarachchi S & Rahman Sur) **48**: 409-420 (2020)

Altitudinal preferences

Species diversity and altitudinal preferences of lichens on selected substrata in Ritigala Strict Natural Reserve (Gunawardene KW & Wijeyaratne SC) **48**: 49-56 (2020)

Anacardiaceae

Molecular phylogeny and chromosomal evolution of endemic species of Sri Lankan Anacardiaceae (Ariyaratne M, Yakandawala D, Barfuss M, Heckenhauer J & Samue R) **48**: 289-303 (2020)

Antifungal

In vitro antifungal efficacy of selected essential oils in controlling fungi associated with the stem-end rot disease of mango (cv. Karutha Colomban) fruits and characterisation of antifungal components (Kodituwakku TD, Ekanayake GCM, Abeywickrama KP & Jayakody R) **48**: 101-111 (2020)

Anti-leptospiral antibodies

A novel approach for qualitative biosensing of anti-leptospiral IgG antibodies in human sera using functionalised silver nanoparticles (Madushani V, Dahanayake H, Gamage CD, Sirimuthu NMS & Jayasundera ACA) **48**: 437-447 (2020)

Aspergillus aculeatus

Decolourisation and detoxification of CI Direct Blue 201 textile dye by two fungal strains of genus *Aspergillus* (Ekanayake EMMS & Manage PM) **48**: 69-80 (2020)

Aspergillus nomius

Decolourisation and detoxification of CI Direct Blue 201 textile dye by two fungal strains of genus *Aspergillus* (Ekanayake EMMS & Manage PM) **48**: 69-80 (2020)

Bay of Bengal

A mini-warm pool during spring in the Bay of Bengal (Pathirana G & Priyadarshani K) **48**: 345-355 (2020)

Begomovirus

Transmission and host range of *Horsegram yellow mosaic virus* (HgYMV) causing common bean (*Phaseolus vulgaris L.*) yellowing disease in Sri Lanka (Rienzie R, De Costa MD & Wickramaarachchi WART) **48**: 81-92 (2020)

Bemisia tabaci Genn

Transmission and host range of *Horsegram yellow mosaic virus* (HgYMV) causing common bean (*Phaseolus vulgaris L.*) yellowing disease in Sri Lanka (Rienzie R, De Costa MD & Wickramaarachchi WART) **48**: 81-92 (2020)

Bias

A new improved difference-cum-exponential ratio type estimator in systematic sampling using two auxiliary variables (Shabbir J, Masood S & Gupta S) **48**: 27-36 (2020)

Biodiversity

New additions to leafy liverwort flora (Marchantiophyta, Jungermanniopsida) of Sri Lanka (Bandaranayake BMSK, Ruklani NCS & Rubasinghe SCK) **48**: 187-198 (2020)

Biomarker

Use of liver histological alterations and erythrocytic nuclear abnormalities of two native fish species in Kelani River, Sri Lanka as biomarkers for pollution impact assessments (Ruvinda KMS & Pathiratne A) **48**: 15-26 (2020)

Bioremediation

Decolourisation and detoxification of CI Direct Blue 201 textile dye by two fungal strains of genus *Aspergillus* (Ekanayake EMMS & Manage PM) **48**: 69-80 (2020)

Bivariate distributions

Bivariate Gompertz generator of distributions: statistical properties and estimation with application to model football data (Eliwa MS, Alhussain ZA, Ahmed EA, Salah MM, Ahmed HH & El-Morshedy M) **48**: 149-162 (2020)

Bryophytes

New additions to leafy liverwort flora (Marchantiophyta, Jungermanniopsida) of Sri Lanka (Bandaranayake BMSK, Ruklani NCS & Rubasinghe SCK) **48**: 187-198 (2020)

Camptosperma zeylanica

Molecular phylogeny and chromosomal evolution of endemic species of Sri Lankan Anacardiaceae (Ariyaratne M., Yakandawala D., Barfuss M., Heckenhauer J, & Samue R.) **48**: 289-303 (2020)

Characterisation

Topp-Leone moment exponential distribution: properties and applications (Abbas S, Jahngeer A, Shahbaz SH, Afify AZ & Shahbaz MQ) **48**: 265-274 (2020)

Chen distribution

The odd Chen generator of distributions: properties and estimation methods with applications in medicine and engineering (El-Morshedy M, Eliwa MS & Afify AZ) **48**: 113-130 (2020)

Chromosome counts

Molecular phylogeny and chromosomal evolution of endemic species of Sri Lankan Anacardiaceae (Ariyaratne M, Yakandawala D, Barfuss M, Heckenhauer J, & Samue R) **48**: 289-303 (2020)

Chronic kidney disease

Cadmium and arsenic levels in edible fishes, *Oreochromis niloticus* (Nile Tilapia) and *Ompok bimaculatus* (Butter catfish) from Padaviya Reservoir, Sri Lanka and human health risk assessment associated with their dietary exposure (Weerasekara KAWS, Pathiratne A & Kithsiri HMP) **48**: 335-344 (2020)

CI Direct Blue 201 textile dye

Decolourisation and detoxification of CI Direct Blue 201 textile dye by two fungal strains of genus *Aspergillus* (Ekanayake EMMS & Manage PM) **48**: 69-80 (2020)

Coefficient of permeability

Effect of air voids on permeability and durability of hot mix asphalt (Ahmad N, Haroon W & Abid MM) **48**: 463-474 (2020)

COI

First record of the presence of *Aedes* (Phagomyia) *cogilli* (Edwards, 1922) in Sri Lanka (Jayadas TTP, Thiruchenthooran V, Tharsan A, Sivabalakrishnan K, Santhirasekaram S & Surendran SN) **48**: 327-331 (2020)

Comfort

Comfort evaluation of bridge based on stochastic process theory (Tan Y, Qin S, Zhang Z, Wang H & Wang Q) **48**: 239-249 (2020)

Common bean Yellowing disease

Transmission and host range of *Horsegram yellow mosaic virus* (HgYMV) causing common bean (*Phaseolus vulgaris L.*) yellowing disease in Sri Lanka (Rienzie R, De Costa MD & Wickramaarachchi WART) **48**: 81-92 (2020)

Cryo injuries

Recovery, histological observations and genetic integrity in coconut (*Cocos nucifera* L.) embryogenic calli cryopreserved using encapsulation-dehydration procedure (Welewanni I, Perera C, Jayasekera A & Bandupriya D) **48**: 175-186 (2020)

Daldinia eschscholzii

A secondary metabolite with in vitro radical scavenging activity from endolichenic fungus *Daldinia eschscholzii* found in lichen, *Parmotrema* sp. in Sri Lanka (Manthirathna MATP, Kandiah R, Gunasekera DS, Samanthi KAU, Welideniya DT, Maduranga HAK & Paranagama PA) **48**: 143-148 (2020)

Dawkinsia singhala

Use of liver histological alterations and erythrocytic nuclear abnormalities of two native fish species in Kelani River, Sri Lanka as biomarkers for pollution impact assessments (Ruvinda KMS & Pathiratne A) **48**: 15-26 (2020)

Decolourisation

Decolourisation and detoxification of CI Direct Blue 201 textile dye by two fungal strains of genus *Aspergillus* (Ekanayake EMMS & Manage PM) **48**: 69-80 (2020)

Diversity

First record of the presence of *Aedes* (Phagomyia) *cogilli* (Edwards, 1922) in Sri Lanka (Jayadas TTP, Thiruchenthooran V, Tharsan A, Sivabalakrishnan K, Santhirasekaram S & Surendran SN) **48**: 327-331 (2020)

Durability

Effect of air voids on permeability and durability of hot mix asphalt (Ahmad N, Haroon W & Abid MM) **48**: 463-474 (2020)

Dynamic reconfiguration

Implementation of data cache block (DCB) in shared processor using field-programmable gate array (FPGA) (Karthick R & Meenalochini P) **48**: 475-479 (2020)

Efficiency

A new improved difference-cum-exponential ratio type estimator in systematic sampling using two auxiliary variables (Shabbir J, Masood S & Gupta S) **48**: 27-36 (2020)

Endolichenic fungus

A secondary metabolite with in vitro radical scavenging activity from endolichenic fungus *Daldinia eschscholzii* found in lichen, *Parmotrema* sp. in Sri Lanka (Manthirathna MATP, Kandiah R, Gunasekera DS, Samanthi KAU, Welideniya DT, Maduranga HAK & Paranagama PA) **48**: 143-148 (2020)

Essential amino acids

Total and free amino acid contents of popular rice varieties (*Oryza sativa* L.) consumed in the capital city of Sri Lanka (Liyanaarachchi GVV, Mahanama KRR, Somasiri HPPS, Punyasiri PAN & Kottawa-Arachchi JD) **48**: 199-211 (2020)

Essential oils

In vitro antifungal efficacy of selected essential oils in controlling fungi associated with the stem-end rot disease of mango (cv. Karutha Colomban) fruits and characterisation of antifungal components (Kodituwakku TD, Ekanayake GCM, Abeywickrama KP & Jayakody R) **48**: 101-111 (2020)

ESSP

Use of single superphosphate fertiliser produced using Eppawala rock phosphate as a source of phosphorous for rice cultivation (Udawatte CP, Panagoda PVA, Wickramasinghe WMADB, Wijewardena JDH, Sirisena DN, Emitiyagoda S & Bandara HRUD) **48**: 131-142 (2020)

Estimation

Topp-Leone moment exponential distribution: properties and applications (Abbas S, Jahngeer A, Shahbaz SH, Afify AZ & Shahbaz MQ) **48**: 265-274 (2020)

Estimation methods

The odd Chen generator of distributions: properties and estimation methods with applications in medicine and engineering (El-Morshedy M, Eliwa MS & Afify AZ) **48**: 113-130 (2020)

Etroplus Suratensis

Use of liver histological alterations and erythrocytic nuclear abnormalities of two native fish species in Kelani River, Sri Lanka as biomarkers for pollution impact assessments (Ruvinda KMS & Pathiratne A) **48**: 15-26 (2020)

Exact solution

Mathematical model of eyring fluid in a scraped surface heat exchanger (Imran A, Siddiqui AM, Numan M, Rana MA & Waheed A) **48**: 3-14 (2020)

Eyring fluid

Mathematical model of eyring fluid in a scraped surface heat exchanger (Imran A, Siddiqui AM, Numan M, Rana MA & Waheed A) **48**: 3-14 (2020)

Finite element method

MHD natural convection nanofluid flows in a wavy trapezoidal porous enclosure With differentially heated side walls (Reddy ES & Panda S) **48**: 57-68 (2020)

First record

Cicindelinae of Sri Lanka: New record of the arboreal tiger beetle *Tricondyla gounellei* Horn, 1900 (Abeywardhana DL, Dangalle CD and Mallawarachchi YW) **48**: 213-216 (2020)

Full memory method

An efficient numerical method for fractional ordinary differential equations - based on exponentially decreasing random memory on uniform meshes (Somathilake LW) **48**: 163-174 (2020)

Fractional derivatives

An efficient numerical method for fractional ordinary differential equations - based on exponentially decreasing random memory on uniform meshes (Somathilake LW) **48**: 163-174 (2020)

Fractional differential equation

An efficient numerical method for fractional ordinary differential equations - based on exponentially decreasing random memory on uniform meshes (Somathilake LW) **48**: 163-174 (2020)

Functionalisation

A novel approach for qualitative biosensing of anti-leptospirosis IgG antibodies in human sera using functionalised silver nanoparticles (Madushani V, Dahanayake H, Gamage CD, Sirimuthu NMS & Jayasundera ACA) **48**: 437-447 (2020)

Future demand analysis

Optimising usage of Salinized Lands in the lower part of the river basin for the coastal community in Bentota, Sri Lanka (Ranasinghe TKGP & Piyadasa RUK) **48**: 379-396 (2020)

GABA

Total and free amino acid contents of popular rice varieties (*Oryza sativa* L.) consumed in the capital city of Sri Lanka (Liyanarachchi GVV, Mahanama KRR, Somasiri HPPS, Punyasiri PAN & Kottawa-Arachchi JD) **48**: 199-211 (2020)

GC-MS

In vitro antifungal efficacy of selected essential oils in controlling fungi associated with the stem-end rot disease of mango (cv. Karutha Colomban) fruits and characterisation of antifungal components (Kodituwakku TD, Ekanayake GCM, Abeywickrama KP & Jayakody R) **48**: 101-111 (2020)

Genetic differentiation

The scope of Rp EPIC markers in population genetic studies: a preliminary study with dengue vectors (Nirmani MD, Perera NS & Galhena GH) **48**: 275-288 (2020)

Genetic fidelity

Recovery, histological observations and genetic integrity in coconut (*Cocos nucifera* L.) embryogenic calli cryopreserved using encapsulation-dehydration procedure (Welewanni I, Perera C, Jayasekera A & Bandupriya D) **48**: 175-186 (2020)

Geographic information system

Hotspots of land use/land cover change around Bolgoda wetland, Sri Lanka (Athapaththu AHLCM, Wickramasinghe D & Somachandra MGMC) **48**: 219-226 (2020)

Gompertz-H family of distributions

Bivariate Gompertz generator of distributions: statistical properties and estimation with application to model football data (Eliwa MS, Alhussain ZA, Ahmed EA, Salah MM, Ahmed HH & El-Morshedy M) **48**: 149-162 (2020)

Google distance matrix

Challenges faced in heterogeneous traffic data collection: a comparison of traffic data collection technologies (Jayaratne DND, Vidanapathirana CJ & Pasindu HR) **48**: 227-237 (2020)

Google earth imagery

Google Earth imagery coupled with on-screen digitisation for urban land-use mapping: case study of Hambantota, Sri Lanka (Madarasinghe SK, Yapa KKAS & Jayatissa LP) **48**: 357-366 (2020)

Hardness

Effect of precipitate size distribution on hardness of aluminium 6063 alloy (Dilrukshi LWUR & De Silva GIP) **48**: 305-313 (2020)

Hazard rate function

The odd Chen generator of distributions: properties and estimation methods with applications in medicine and engineering (El-Morshedy M, Eliwa MS & Afify AZ) **48**: 113-130 (2020)

Heavy metal

Cadmium and arsenic levels in edible fishes, *Oreochromis niloticus* (Nile Tilapia) and *Ompok bimaculatus* (Butter catfish) from Padaviya Reservoir, Sri Lanka and human health risk assessment associated with their dietary exposure (Weerasekera KAWS, Pathiratne A & Kithsiri HMP) **48**: 335-344 (2020)

Heat generation/absorption

Rheology of hydro-magnetic polymeric material with heat generation/absorption and chemical reaction (Awais M, Awais SE, Irum S, Shoaib M, Ali H & Raja MAZ) **48**: 397-407 (2020)

Heterogeneous traffic

Challenges faced in heterogeneous traffic data collection: a comparison of traffic data collection technologies (Jayaratne DND, Vidanapathirana CJ & Pasindu HR) **48**: 227-237 (2020)

High performance liquid chromatography

Monolithic columns with incorporated titanium dioxide nanoparticles for hydrophilic interaction liquid chromatography (Ganewatta N & El Rassi Z) **48**: 315-325 (2020)

Histology

Recovery, histological observations and genetic integrity in coconut (*Cocos nucifera* L.) embryogenic calli cryopreserved using encapsulation-dehydration procedure (Welewanni I, Perera C, Jayasekera A & Bandupriya D) **48**: 175-186 (2020)

Horsegram yellow mosaic virus (HgYMV)

Transmission and host range of *Horsegram yellow mosaic virus* (HgYMV) causing common bean (*Phaseolus vulgaris* L.) yellowing disease in Sri Lanka (Rienzie R, De Costa MD & Wickramaarachchi WART) **48**: 81-92 (2020)

Host range

Transmission and host range of *Horsegram yellow mosaic virus* (HgYMV) causing common bean (*Phaseolus vulgaris* L.) yellowing disease in Sri Lanka (Rienzie R, De Costa MD & Wickramaarachchi WART) **48**: 81-92 (2020)

Hotspots

Hotspots of land use/land cover change around Bolgoda wetland, Sri Lanka (Athapaththu AHLICM, Wickramasinghe D & Somachandra MGMC) **48**: 219-226 (2020)

Hydraulic conductivity

Effect of air voids on permeability and durability of hot mix asphalt (Ahmad N, Haroon W & Abid MM) **48**: 463-474 (2020)

Hydrophilic interaction liquid chromatography

Monolithic columns with incorporated titanium dioxide nanoparticles for hydrophilic interaction liquid chromatography (Ganewatta N & El Rassi Z) **48**: 315-325 (2020)

ICP-MS

Cadmium and arsenic levels in edible fishes, *Oreochromis niloticus* (Nile Tilapia) and *Ompok bimaculatus* (Butter catfish) from Padaviya Reservoir, Sri Lanka and human health risk assessment associated with their dietary exposure (Weerasekera KAWS, Pathiratne A & Kithsiri HMP) **48**: 335-344 (2020)

Image classification

Google Earth imagery coupled with on-screen digitisation for urban land-use mapping: case study of Hambantota, Sri Lanka (Madarasinghe SK, Yapa KKAS & Jayatissa LP) **48**: 357-366 (2020)

Innovative trend analysis

Streamflow trends of Kelani River basin in Sri Lanka (1983-2013) (Jayasekera SM, Abeysingha NS & Meegastenna TJ) **48**: 449-462 (2020)

In vitro

Recovery, histological observations and genetic integrity in coconut (*Cocos nucifera* L.) embryogenic calli cryopreserved using encapsulation-dehydration procedure (Welewanni I, Perera C, Jayasekera A & Bandupriya D) **48**: 175-186 (2020)

Isolation

Isolation improvement of compact LTE MIMO terminal using combination of neutralisation line and modified ground structure (Singh HS & Shubair RM) **48**: 251-263 (2020)

Kelani River

Toxic hazards of industrial waste receiving canal system in the lower catchment of Kelani River basin, Sri Lanka (Kuruppuarachchi HD & Pathiratne A) **48**: 37-47 (2020)

Kelani River

Use of liver histological alterations and erythrocytic nuclear abnormalities of two native fish species in Kelani River, Sri Lanka as biomarkers for pollution impact assessments (Ruvinda KMS & Pathiratne A) **48**: 15-26 (2020)

Land use

Hotspots of land use/land cover change around Bolgoda wetland, Sri Lanka (Athapaththu AHLICM, Wickramasinghe D & Somachandra MGMC) **48**: 219-226 (2020)

Land-use classes

Google Earth imagery coupled with on-screen digitisation for urban land-use mapping: case study of Hambantota, Sri Lanka (Madarasinghe SK, Yapa KKAS & Jayatissa LP) **48**: 357-366 (2020)

Land use pattern

Optimising usage of Salinized Lands in the lower part of the river basin for the coastal community in Bentota, Sri Lanka (Ranasinghe TKGP & Piyadasa RUK) **48**: 379-396 (2020)

Landsat 8 imagery

Google Earth imagery coupled with on-screen digitisation for urban land-use mapping: case study of Hambantota, Sri Lanka (Madarasinghe SK, Yapa KKAS & Jayatissa LP) **48**: 357-366 (2020)

Leafy liverworts

New additions to leafy liverwort flora (Marchantiophyta, Jungermanniopsida) of Sri Lanka (Bandaranayake BMSK, Ruklani NCS & Rubasinghe SCK) **48**: 187-198 (2020)

Leptospirosis

A novel approach for qualitative biosensing of anti-leptospiral IgG antibodies in human sera using functionalised silver nanoparticles (Madushani V, Dahanayake H, Gamage CD, Sirimuthu NMS & Jayasundera ACA) **48**: 437-447 (2020)

Lichen diversity

Species diversity and altitudinal preferences of lichens on selected substrata in Ritigala Strict Natural Reserve (Gunawardene KW & Wijeyaratne SC) **48**: 49-56 (2020)

Lie group analysis

Rheology of hydro-magnetic polymeric material with heat generation/absorption and chemical reaction (Awais M, Awan SE, Irum S, Shoaib M, Ali H & Raja MAZ) **48**: 397-407 (2020)

Linear Programming model

Optimising usage of Salinized Lands in the lower part of the river basin for the coastal community in Bentota, Sri Lanka (Ranasinghe TKGP & Piyadasa RUK) **48**: 379-396 (2020)

Localised surface plasmon resonance

A novel approach for qualitative biosensing of anti-leptospiral IgG antibodies in human sera using functionalised silver nanoparticles (Madushani V, Dahanayake H, Gamage CD, Sirimuthu NMS & Jayasundera ACA) **48**: 437-447 (2020)

LTE

Isolation improvement of compact LTE MIMO terminal using combination of neutralisation line and modified ground structure (Singh HS & Shubair RM) **48**: 251-263 (2020)

Lubrication approximation theory

Mathematical model of Eyring fluid in a scraped surface heat exchanger (Imran A, Siddiqui AM, Numan M, Rana MA & Waheed A) **48**: 3-14 (2020)

Magnetic field effects

Rheology of hydro-magnetic polymeric material with heat generation/absorption and chemical reaction (Awais M, Awan SE, Irum S, Shoaib M, Ali H & Raja MAZ) **48**: 397-407 (2020)

Mango

In vitro antifungal efficacy of selected essential oils in controlling fungi associated with the stem-end rot disease of mango (cv. Karutha Colomban) fruits and characterisation of antifungal components (Kodituwakku TD, Ekanayake GCM, Abeywickrama KP & Jayakody R) **48**: 101-111 (2020)

Mann-Kendall test

Streamflow trends of Kelani River basin in Sri Lanka (1983-2013) (Jayasekara SM, Abeysingha NS & Meegastenna TJ) **48**: 449-462 (2020)

Marker assisted breeding

Assessment on variation of performance indicators under phosphorus-starved conditions in a core-set of rice cultivars and their diversity in *pup1*-linked DNA marker-haplotypes (Jayarathne HSM, Rathnayake PGRG, Ranaweera LT, Nizam R, Rathnayake RMSK, Kannangara SK, Udawela UAKS, Weebadde CK & Sooriyapathirana SDSS) **48**: 421-435 (2020)

Marshall-Olkin shock model

Bivariate Gompertz generator of distributions: statistical properties and estimation with application to model football data (Eliwa MS, Alhussain ZA, Ahmed EA, Salah MM, Ahmed HH & El-Morshedy M) **48**: 149-162 (2020)

Maximum likelihood estimators

The odd Chen generator of distributions: properties and estimation methods with applications in medicine and engineering (El-Morshedy M, Eliwa MS & Afify AZ) **48**: 113-130 (2020)

Maximum likelihood method

Bivariate Gompertz generator of distributions: statistical properties and estimation with application to model football data (Eliwa MS, Alhussain ZA, Ahmed EA, Salah MM, Ahmed HH & El-Morshedy M) **48**: 149-162 (2020)

Maximum likelihood method

Google Earth imagery coupled with on-screen digitisation for urban land-use mapping: case study of Hambantota, Sri Lanka (Madarasinghe SK, Yapa KKAS & Jayatissa LP) **48**: 357-366 (2020)

MHD

Rheology of hydro-magnetic polymeric material with heat generation/absorption and chemical reaction (Awais M, Awan SE, Irum S, Shoaib M, Ali H & Raja MAZ) **48**: 397-407 (2020)

MHD nanofluid flow

MHD natural convection nanofluid flows in a wavy trapezoidal porous enclosure with differentially heated side walls (Reddy ES & Panda S) **48**: 57-68 (2020)

Microsatellites

The scope of Rp EPIC markers in population genetic studies: a preliminary study with dengue vectors (Nirmani MD, Perera NS & Galhena GH) **48**: 275-288 (2020)

MIMO antenna

Isolation improvement of compact LTE MIMO terminal using combination of neutralisation line and modified ground structure (Singh HS & Shubair RM) **48**: 251-263 (2020)

Mini-warm pool

A mini-warm pool during spring in the Bay of Bengal (Pathirana G & Priyadarshani K) **48**: 345-355 (2020)

Molecular phylogeny

Molecular phylogeny and chromosomal evolution of endemic species of Sri Lankan Anacardiaceae (Ariyaratne M, Yakandawala D, Barfuss M, Heckenhauer J, & Samue R) **48**: 289-303 (2020)

Moment exponential

Topp-Leone moment exponential distribution: properties and applications (Abbas S, Jahngeer A, Shahbaz SH, Afify AZ & Shahbaz MQ) **48**: 265-274 (2020)

MPSoC

Implementation of data cache block (DCB) in shared processor using field-programmable gate array (FPGA) (Karthick R & Meenalochini P) **48**: 475-479 (2020)

MSE

A new improved difference-cum-exponential ratio type estimator in systematic sampling using two auxiliary variables (Shabbir J, Masood S & Gupta S) **48**: 27-36 (2020)

Mungbean

Relative production efficiency of maize-legume intercroppings at different altitudes (Arshad M, Nawa R, Ahmad S, Razaq A, Ranamukhaarachchi S & Rahman Sur) **48**: 409-420 (2020)

Multiprocessor

Implementation of data cache block (DCB) in shared processor using field-programmable gate array (FPGA) (Karthick R & Meenalochini P) **48**: 475-479 (2020)

Nanoparticles

A novel approach for qualitative biosensing of anti-leptospiral IgG antibodies in human sera using functionalised silver nanoparticles (Madushani V, Dahanayake H, Gamage CD, Sirimuthu NMS & Jayasundera ACA) **48**: 437-447 (2020)

Natural convection

MHD natural convection nanofluid flows in a wavy trapezoidal porous enclosure with differentially heated side walls (Reddy ES & Panda S) **48**: 57-68 (2020)

Neutralisation line

Isolation improvement of compact LTE MIMO terminal using combination of neutralisation line and modified ground structure (Singh HS & Shubair RM) **48**: 251-263 (2020)

New records

New additions to leafy liverwort flora (Marchantiophyta, Jungermanniopsida) of Sri Lanka (Bandaranayake BMSK, Ruklani NCS & Rubasinghe SCK) **48**: 187-198 (2020)

Nitrogen

Relative production efficiency of maize-legume intercroppings at different altitudes (Arshad M, Nawa R, Ahmad S, Razaq A, Ranamukhaarachchi S & Rahman Sur) **48**: 409-420 (2020)

North Central Province

Cadmium and arsenic levels in edible fishes, *Oreochromis niloticus* (Nile Tilapia) and *Ompok bimaculatus* (Butter catfish) from Padaviya Reservoir, Sri Lanka and human health risk assessment associated with their dietary exposure (Weerasekara KAWS, Pathiratne A & Kithsiri HMP) **48**: 335-344 (2020)

Optimising salinized lands

Optimising usage of Salinized Lands in the lower part of the river basin for the coastal community in Bentota, Sri Lanka (Ranasinghe TKGP & Piyadasa RUK) **48**: 379-396 (2020)

Organic polymer based monolith

Monolithic columns with incorporated titanium dioxide nanoparticles for hydrophilic interaction liquid chromatography (Ganewatta N & El Rassi Z) **48**: 315-325 (2020)

Oscillation modes

Determination of oscillation frequencies and stellar properties of three Delta Scuti variable stars using Kepler data (Adassuriya J, Jayaratne KPSC & Cooray PTLV & Attygalle MLC) **48**: 367-378 (2020)

Padaviya reservoir fish

Cadmium and arsenic levels in edible fishes, *Oreochromis niloticus* (Nile Tilapia) and *Ompok bimaculatus* (Butter catfish) from Padaviya Reservoir, Sri Lanka and human health risk assessment associated with their dietary exposure (Weerasekera KAWS, Pathiratne A & Kithsiri HMP) **48**: 335-344 (2020)

Pedestrian bridge

Comfort evaluation of bridge based on stochastic process theory (Tan Y, Qin S, Zhang Z, Wang H & Wang Q) **48**: 239-249 (2020)

Phosphorus efficient rice

Assessment on variation of performance indicators under phosphorus-starved conditions in a core-set of rice cultivars and their diversity in pup1-linked DNA marker-haplotypes (Jayarathne HSM, Rathnayake PGRG, Ranaweera LT, Nizam R, Rathnayake RMSK, Kannangara SK, Udawela UAKS, Weebadde CK & Sooriyapathirana SDSS) **48**: 421-435 (2020)

Phosphorus fertiliser crisis

Assessment on variation of performance indicators under phosphorus-starved conditions in a core-set of rice cultivars and their diversity in pup1-linked DNA marker-haplotypes (Jayarathne HSM, Rathnayake PGRG, Ranaweera LT, Nizam R, Rathnayake RMSK, Kannangara SK, Udawela UAKS, Weebadde CK & Sooriyapathirana SDSS) **48**: 421-435 (2020)

Photometry

Determination of oscillation frequencies and stellar properties of three Delta Scuti variable stars using Kepler data (Adassuriya J, Jayaratne KPSC & Cooray PTLV & Attygalle MLC) **48**: 367-378 (2020)

Pollution impact assessment

Use of liver histological alterations and erythrocytic nuclear abnormalities of two native fish species in Kelani River, Sri Lanka as biomarkers for pollution impact assessments (Ruvinda KMS & Pathiratne A) **48**: 15-26 (2020)

Population forecasting

Optimising usage of Salinized Lands in the lower part of the river basin for the coastal community in Bentota, Sri Lanka (Ranasinghe TKGP & Piyadasa RUK) **48**: 379-396 (2020)

Population genetics

The scope of Rp EPIC markers in population genetic studies: a preliminary study with dengue vectors (Nirmani MD, Perera NS & Galhena GH) **48**: 275-288 (2020)

Porous medium

MHD natural convection nanofluid flows in a wavy trapezoidal porous enclosure with differentially heated side walls (Reddy ES & Panda S) **48**: 57-68 (2020)

Polymeric liquid

Rheology of hydro-magnetic polymeric material with heat generation/absorption and chemical reaction (Awais M, Awan S E, Irum S, Shoaib M, Ali H & Raja MAZ) **48**: 397-407 (2020)

Precipitate size distribution

Effect of precipitate size distribution on hardness of aluminium 6063 alloy (Dilrukshi LWUR & De Silva GIP) **48**: 305-313 (2020)

Principal component analysis

Toxic hazards of industrial waste receiving canal system in the lower catchment of Kelani River basin, Sri Lanka (Kuruppuarachchi HD & Pathiratne A) **48**: 37-47 (2020)

Pup1 qtl

Assessment on variation of performance indicators under phosphorus-starved conditions in a core-set of rice cultivars and their diversity in pup1-linked DNA marker-haplotypes (Jayarathne HSM, Rathnayake PGRG, Ranaweera LT, Nizam R, Rathnayake RMSK, Kannangara SK, Udawela UAKS, Weebadde CK & Sooriyapathirana SDSS) **48**: 421-435 (2020)

Radical scavenging activity

A secondary metabolite with in vitro radical scavenging activity from endolichenic fungus *Daldinia eschscholzii* found in lichen, *Parmotrema* sp. in Sri Lanka (Manthirathna MATP, Kandiah R, Gunasekera DS, Samanthi KAU, Welideniya DT, Maduranga HAK & Paranagama PA) **48**: 143-148 (2020)

Rainfall

Streamflow trends of Kelani River basin in Sri Lanka (1983-2013) (Jayasekara SM, Abeysingha NS & Meegastenna TJ) **48**: 449-462 (2020)

Random vibration

Comfort evaluation of bridge based on stochastic process theory (Tan Y, Qin S, Zhang Z, Wang H & Wang Q) **48**: 239-249 (2020)

Relative yield

Relative production efficiency of maize-legume intercroppings at different altitudes (Arshad M., Nawa R., Ahmad S., A Razaq A., Ranamukhaarachchi S. & Rahman Sur) **48**: 409-420 (2020)

Reliability

Topp-Leone moment exponential distribution: properties and applications (Abbas S, Jahngeer A, Shahbaz SH, Afify AZ & Shahbaz MQ) **48**: 265-274 (2020)

Remote sensing

Hotspots of land use/land cover change around Bolgoda wetland, Sri Lanka (Athapaththu AHLCM, Wickramasinghe D & Somachandra MGMC) **48**: 219-226 (2020)

Rice

Total and free amino acid contents of popular rice varieties (*Oryza sativa* L.) consumed in the capital city of Sri Lanka (Liyanarachchi GVV, Mahanama KRR, Somasiri HPPS, Punyasiri PAN & Kottawa-Arachchi JD) **48**: 199-211 (2020)

Rice

Use of single superphosphate fertiliser produced using Eppawala rock phosphate as a source of phosphorous for rice cultivation Udawatte CP, Panagoda PVA, Wickramasinghe WMADB, Wijewardena JDH, Sirisena DN, Emitiyagoda S & Bandara HRUD) **48**: 131-142 (2020)

Rice landraces

Assessment on variation of performance indicators under phosphorus-starved conditions in a core-set of rice cultivars and their diversity in pup1-linked DNA marker-haplotypes (Jayarathne HSM, Rathnayake PGRG, Ranaweera LT, Nizam R, Rathnayake RMSK, Kannangara SK, Udawela UAKS, Weebadde CK & Sooriyapathirana SDSS) **48**: 421-435 (2020)

Risk assessment

Cadmium and arsenic levels in edible fishes, *Oreochromis niloticus* (Nile Tilapia) and *Ompok bimaculatus* (Butter catfish) from Padaviya Reservoir, Sri Lanka and human health risk assessment associated with their dietary exposure (Weerasekara KAWS, Pathiratne A & Kithsiri HMP) **48**: 335-344 (2020)

Ritigala strict natural reserve

Species diversity and altitudinal preferences of lichens on selected substrata in Ritigala Strict Natural Reserve (Gunawardene KW & Wijeyaratne SC) **48**: 49-56 (2020)

Row pattern

Relative production efficiency of maize-legume intercroppings at different altitudes (Arshad M, Nawa R, Ahmad S, Razaq A, Ranamukhaarachchi S & Rahman Sur) **48**: 409-420 (2020)

SAR

Isolation improvement of compact LTE MIMO terminal using combination of neutralisation line and modified ground structure (Singh HS & Shubair RM) **48**: 251-263 (2020)

Seawater intrusion

Optimising usage of Salinized Lands in the lower part of the river basin for the coastal community in Bentota, Sri Lanka (Ranasinghe TKGP & Piyadasa RUK) **48**: 379-396 (2020)

Secondary metabolites

A secondary metabolite with in vitro radical scavenging activity from endolichenic fungus *Daldinia eschscholzii* found in lichen, *Parmotrema* sp. in Sri Lanka (Manthirathna MATP, Kandiah R, Gunasekera DS, Samanthi KAU, Welideniya DT, Maduranga HAK & Paranagama PA) **48**: 143-148 (2020)

Security touchpoints

A security specific knowledge modelling approach for secure software engineering (Abeyrathna A, Samarage C, Dahanayake B, Wijesiriwardana C & Wimalaratne P) **48**: 93-98 (2020)

Semecarpus species

Molecular phylogeny and chromosomal evolution of endemic species of Sri Lankan Anacardiaceae (Ariyaratne M, Yakandawala D, Barfuss M, Heckenhauer J, & Samue R) **48**: 289-303 (2020)

Short memory principle

An efficient numerical method for fractional ordinary differential equations - based on exponentially decreasing random memory on uniform meshes (Somathilake LW) **48**: 163-174 (2020)

Simple sequence repeats

Recovery, histological observations and genetic integrity in coconut (*Cocos nucifera* L.) embryogenic calli cryopreserved using encapsulation-dehydration procedure (Welewann I, Perera C, Jayasekera A & Bandupriya D) **48**: 175-186 (2020)

Simulation

The odd Chen generator of distributions: properties and estimation methods with applications in medicine and engineering (El-Morshedy M, Eliwa MS & Afify AZ) **48**: 113-130 (2020)

Simultaneous sowing

Relative production efficiency of maize-legume intercroppings at different altitudes (Arshad M, Nawa R, Ahmad S, A Razaq A, Ranamukhaarachchi S & Rahman Sur) **48**: 409-420 (2020)

Size homoplasy

The scope of Rp EPIC markers in population genetic studies: a preliminary study with dengue vectors (Nirmani MD, Perera NS & Galhena GH) **48**: 275-288 (2020)

Software security

A security specific knowledge modelling approach for secure software engineering (Abeyrathna A, Samarage C, Dahanayake B, Wijesiriwardana C & Wimalaratne P) **48**: 93-98 (2020)

Spring inter-monsoon

A mini-warm pool during spring in the Bay of Bengal (Pathirana G & Priyadarshani K) **48**: 345-355 (2020)

Sri Lanka

Cicindelinae of Sri Lanka: New record of the arboreal tiger beetle *Tricondyla gounellei* Horn, 1900 (Abeywardhana DL, Dangalle CD and Mallawarachchi YW) **48**: 213-216 (2020)

Sri Lanka

First record of the presence of *Aedes* (Phagomyia) *cogilli* (Edwards, 1922) in Sri Lanka (Jayadas TTP, Thiruchenthooran V, Tharsan A, Sivabalakrishnan K, Santhirasekaram S & Surendran SN) **48**: 327-331 (2020)

Sri Lanka

Total and free amino acid contents of popular rice varieties (*Oryza sativa* L.) consumed in the capital city of Sri Lanka (Liyanaarachchi GVV, Mahanama KRR, Somasiri HPPS, Punyasiri PAN & Kottawa-Arachchi JD) **48**: 199-211 (2020)

Staggered sowing

Relative production efficiency of maize-legume intercroppings at different altitudes (Arshad M, Nawa R, Ahmad S, A Razaq A, Ranamukhaarachchi S & Rahman Sur) **48**: 409-420 (2020)

Static code analysis

A security specific knowledge modelling approach for secure software engineering (Abeyrathna A, Samarage C, Dahanayake B, Wijesiriwardana C & Wimalaratne P) **48**: 93-98 (2020)

Stellar pulsations

Determination of oscillation frequencies and stellar properties of three Delta Scuti variable stars using Kepler data (Adassuriya J, Jayaratne KPSC & Cooray PTLV & Attygalle MLC) **48**: 367-378 (2020)

Stem-end rot

In vitro antifungal efficacy of selected essential oils in controlling fungi associated with the stem-end rot disease of mango (cv. Karutha Colomban) fruits and characterisation of antifungal components (Kodituwakku TD, Ekanayake GCM, Abeywickrama KP & Jayakody R) **48**: 101-111 (2020)

Streamflow

Streamflow trends of Kelani River basin in Sri Lanka (1983-2013) (Jayasekara SM, Abeysingha NS & Meegastenna TJ) **48**: 449-462 (2020)

Systematic sampling

A new improved difference-cum-exponential ratio type estimator in systematic sampling using two auxiliary variables (Shabbir J, Masood S & Gupta S) **48**: 27-36 (2020)

Taxonomy

New additions to leafy liverwort flora (Marchatiophyta, Jungermanniopsida) of Sri Lanka (Bandaranayake BMSK, Ruklani NCS & Rubasinghe SCK) **48**: 187-198 (2020)

Threat modelling

A security specific knowledge modelling approach for secure software engineering (Abeyrathna A, Samarage C, Dahanayake B, Wijesiriwardana C & Wimalaratne P) **48**: 93-98 (2020)

TIRTL

Challenges faced in heterogeneous traffic data collection: a comparison of traffic data collection technologies (Jayaratne DND, Vidanapathirana CJ & Pasindu HR) **48**: 227-237 (2020)

Titanium dioxide nanoparticles

Monolithic columns with incorporated titanium dioxide nanoparticles for hydrophilic interaction liquid chromatography (Ganewatta N & El Rassi Z) **48**: 315-325 (2020)

Topp-Leone-G family

Topp-Leone moment exponential distribution: properties and applications (Abbas S, Jahngeer A, Shahbaz SH, Afify AZ & Shahbaz MQ) **48**: 265-274 (2020)

Total amino acids

Total and free amino acid contents of popular rice varieties (*Oryza sativa* L.) consumed in the capital city of Sri Lanka (Liyanarachchi GVV, Mahanama KRR, Somasiri HPPS, Punyasiri PAN & Kottawa-Arachchi JD) **48**: 199-211 (2020)

Toxic hazard

Toxic hazards of industrial waste receiving canal system in the lower catchment of Kelani River basin, Sri Lanka (Kurupparachchi HD & Pathiratne A) **48**: 37-47 (2020)

Trapezoidal wavy enclosure

MHD natural convection nanofluid flows in a wavy trapezoidal porous enclosure with differentially heated side walls (Reddy ES & Panda S) **48**: 57-68 (2020)

Traffic data collection

Challenges faced in heterogeneous traffic data collection: a comparison of traffic data collection technologies (Jayaratne DND, Vidanapathirana CJ & Pasindu HR) **48**: 227-237 (2020)

TRAZER

Challenges faced in heterogeneous traffic data collection: a comparison of traffic data collection technologies (Jayaratne DND, Vidanapathirana CJ & Pasindu HR) **48**: 227-237 (2020)

Tricondyla gounellei

Cicindelinae of Sri Lanka: New record of the arboreal tiger beetle *Tricondyla gounellei* Horn, 1900 (Abeywardhana DL, Dangalle CD and Mallawarachchi YW) **48**: 213-216 (2020)

TSP

Use of single superphosphate fertiliser produced using Eppawala rock phosphate as a source of phosphorous for rice cultivation Udawatte CP, Panagoda PVA, Wickramasinghe WMADB, Wijewardena JDH, Sirisena DN, Emitiyagoda S & Bandara HRUD) **48**: 131-142 (2020)

Urban development

Google Earth imagery coupled with on-screen digitisation for urban land-use mapping: case study of Hambantota, Sri Lanka (Madarasinghe SK, Yapa KKAS & Jayatissa LP) **48**: 357-366 (2020)

UV-visible spectroscopy

A novel approach for qualitative biosensing of anti-leptospirosis IgG antibodies in human sera using functionalised silver nanoparticles (Madushani V, Dahanayake H, Gamage CD, Sirimuthu NMS & Jayasundera AA) **48**: 437-447 (2020)

Virus transmission

Transmission and host range of Horsegram yellow mosaic virus (HgYMV) causing common bean (*Phaseolus vulgaris* L.) yellowing disease in Sri Lanka (Rienzie R, Costa DMD & Wickramaarachchi WART) **48**: 81-92 (2020)

Viscous and joule dissipation

MHD natural convection nanofluid flows in a wavy trapezoidal porous enclosure with differentially heated side walls (Reddy ES & Panda S) **48**: 57-68 (2020)

Water pollution

Toxic hazards of industrial waste receiving canal system in the lower catchment of Kelani River basin, Sri Lanka (Kurupparachchi HD & Pathiratne A) **48**: 37-47 (2020)

Weighted least squares estimators

The odd Chen generator of distributions: properties and estimation methods with applications in medicine and engineering (El-Morshedy M, Eliwa MS & Afify AZ) **48**: 113-130 (2020)

Wetlands

Hotspots of land use/land cover change around Bolgoda wetland, Sri Lanka (Athapaththu AHLICM, Wickramasinghe D & Somachandra MGMC) **48**: 219-226 (2020)



JOURNAL OF THE NATIONAL SCIENCE FOUNDATION OF SRI LANKA

GUIDANCE TO CONTRIBUTORS

GENERAL INFORMATION

Scope

The Journal of the National Science Foundation of Sri Lanka publishes the results of research in all aspects of Science and Technology. It is open for publication of Research Articles, Reviews, Research Communications and Correspondence.

Categories of manuscripts

Research Articles: Research Articles are papers that present complete descriptions of original research. Research Articles should include an Abstract, Keywords, Introduction, Methodology, Results and Discussion, Conclusion and Recommendations where relevant. References should be prepared according to the “Guidelines for the preparation of manuscripts”. Maximum length of the article should be limited to 25 pages with a word count of 10,000 including references, figures and tables. Any articles above this limit will be returned.

Reviews: Reviews are critical presentations on selected topics of Science or Technology. They should be well focused and organized and avoid general “textbook” style. As reviews are intended to be critical presentations on selected topics, reviewers need to have had substantial leadership in research supported by a publication track record in the areas covered by the review. A person/s wishing to submit a Review Article should obtain prior approval from the Editorial Board by submitting a concise summary of the intended article, along with a list of the author’s publications in the related area (jnsf@nsf.gov.lk). Maximum length of the article should be limited to 40 pages with a word count of 12,000 including references, figures and tables. Any articles above this limit will be returned.

Research Communications: Research Communications are intended to communicate important new findings in a specific area of limited scope that are worthy of rapid dissemination among the scientific community. The article should include an Abstract, Keywords, Introduction, Methodology, Results & Discussion, Conclusion and References. Maximum length of the article should be limited to 10 pages with a word count of 2,500 including references, figures and tables. Any articles above this limit will be returned.

Correspondence: Correspondence will be accepted regarding one or more articles in the preceding four issues of the Journal, as well as Letters to the Editor. Articles covering important scientific events or any other news of interest to scientists, reviews of books of scientific nature, articles presenting views on issues related to science and scientific activity will also be considered. Publication will be made at the discretion of the Editor-in-Chief. Maximum length of the article should be limited to 05 pages with a word count of 1,500 including references, figures and tables. Any articles above this limit will be returned.

SUBMISSION OF MANUSCRIPT

Authors submitting articles to the JNSF should first create an account in the Sri Lanka Journals Online System (<https://jnsfsl.sljol.info/>). All manuscripts in MS Word format must be electronically submitted to the journal’s online platform at <https://jnsfsl.sljol.info/submit/start/>. Submissions via emails are not encouraged. Please make sure that no author information is mentioned in the article submitted. The names and details of affiliations of all authors and contact information of the corresponding author must be fed into the system during the online submission process. Authors (at least the corresponding author) are required to provide their personal, validated ORCID ID (by obtaining an ORCID ID from <https://orcid.org/>) when submitting the manuscript. No change to the authors or order of authors will be accepted after the submission. All those who have made significant contributions should be listed as co-authors. The corresponding author should ensure that all contributing co-authors are included in the author list and have approved the final version of the paper and have agreed to its submission for publication.

All submissions should be in English. If the manuscript conforms to the guidelines specified, the date received will be the date that the manuscript was submitted to the online system.

Submissions are accepted for processing on the understanding that they will be reviewed and that they have not been submitted for publication elsewhere (including publication as a full paper or extended abstract as a part of Conference Proceedings). The JNSF does not accept manuscripts that have already been submitted to pre-print servers.

Suggesting potential reviewers by authors

The authors may suggest up to three names of referees when submitting their manuscript, in the Cover Letter space provided at the bottom of the page in the first stage of online submission. Referees should not be from the institution where the work was carried out and should not have been co-authors in previous publications. The address, institutional affiliation and e-mail of the suggested referees should be supplied. Please note that the JNSF is not bound to select all or any of the suggested referees for sending the manuscript for reviewing

Authorship

All authors designated as authors should be eligible for authorship. Those who have made a substantial contribution to the concept or design of the work; or acquisition, analysis or interpretation of data are recognized as Authors.

The corresponding author should be prompt and ensure adherence to timelines when responding to requests, queries and recommendation of reviewers conveyed by or on behalf of the Editor-in Chief and Editorial Board.

Supplementary materials

Any experimental data necessary to evaluate the claims made in the paper but not included in the paper should be provided as supplementary materials. Supplementary materials will be sent to the reviewers and published online with the manuscript if accepted. The supplementary materials should conform to Journal guidelines and should be uploaded as separate files. Authors should number Supplementary Tables and Figures as, for example, 'Supplementary Table S1'. Refer to each piece of supplementary material at the appropriate point(s) in the main article. Supplementary Materials may include description of the materials and methods, controls, or tabulated data presented in Tables or Figures, and programming codes.

Peer review

The manuscripts submitted to the JNSF will initially be screened by the Editorial Board and, if suitable, will be referred to at least two subject experts in the relevant field. The peer-review process of the JNSF is double-blind.

When revision of a manuscript has been requested, the revised manuscript should be submitted on or before the stated deadline. If the revised manuscript is not received on time, the manuscript will not be processed further. The authors' response to the comments of referees should be tabulated with the comment, response and the line number/s for reference. The decision of the Editorial Board shall be final.

Accepted papers are subject to editing. The date of acceptance will be the date when the Editorial Board has decided it to be acceptable for publication.

Article publication fee and complementary copies

A publication fee of US\$ 150 will be levied for each manuscript other than where the corresponding author is affiliated to a Sri Lankan Institute, to cover the publication cost.

A complimentary copy of the Journal issue carrying the respective article will be supplied to each of the authors.

Authors' declaration

When an article is accepted for publication, the authors are required to submit the Authors' Declaration signed by all the authors.

Copyright

Articles in JNSF are published under the Creative Commons License CC-BY-ND. This license permits use, distribution and reproduction of articles for commercial and non-commercial purposes, provided that the original work is properly cited and is not changed in anyway. The copyright of the article is with the National Science Foundation of Sri Lanka. Therefore, authors are requested to check with institution's copyright and publication policy before submitting an article to the JNSF. Authors secure the right to reproduce any material that has already been published or copyrighted elsewhere. When an article is accepted for publication, the authors are required to submit the Transfer of Copyright document signed by all the authors.

Post-publication corrections

The Editorial Board reserves the right to take action on publishing an erratum or corrigendum. If serious errors are identified in a published article, the Journal may consider a retraction or publishing a correction.

STRUCTURE OF MANUSCRIPT

Manuscript

The manuscript should be free of errors and prepared in single column, using double-spaced text of Times New Roman 12 font throughout with line numbers, leaving at least 2 cm margins on both sides, and liberal spacing at the top and bottom of each page. Pages should be numbered consecutively.-

a. Style

The paper should be written clearly and concisely. The style of writing should conform to scholarly writing. Slang, jargon, unauthorized abbreviations, abbreviated phrasings should not be used. In general, the impersonal form should be used. Poor usage of language will result in rejection of the manuscript during initial screening.

b. Layout

Manuscripts other than review articles should be generally organized as follows: Title, Abstract, Keywords, Introduction, Methodology, Results and Discussion, Conclusions and Recommendations (where relevant), Acknowledgements and References. Pages should be arranged in the following order:

Title page should include the title of manuscript, and no author information should be mentioned in the title page. If a major part of the research has been published as an abstract in conference proceedings, it should be cited as a footnote on the title page. Authors must also indicate the **general and specific research area** of the manuscript in the title page. In order to highlight the significance of the manuscript, authors are required to provide the following highlights in brief. (1) Why was this study conducted? (2) What are the new findings? (3) Possible applications of the findings. Please limit your answers to 25-30 words for each.

Title: Should accurately and concisely reflect the contents of the article.

Running title: Should be a shortened title (limited to a maximum of 50 characters) that could be printed at the top of every other page of the Journal article.

Abstract: Should be between 200 - 250 words for full length articles and written as a single paragraph. It should not contain any references and should be able to stand on its own. It should outline objectives and methodology together with important results and conclusions. A Review Article should carry a summary of not more than 300 words.

Keywords: Include a maximum of six keywords, which may include the names of organisms (common or scientific), methods or other important words or phrases relevant to the study.

Introduction: This should state the reasons for performing the work with a brief review of related research studies in the context of the work described in the paper. Objectives of the study should be clearly stated.

Materials and Methods: This section should give the details of how you conducted your study. New methods may be described in detail with an indication of their limitations. Established methods can be mentioned with appropriate references. Sufficient details should be included to allow direct repetition of the work by others. Where human subjects are involved, they should be referred to by numbers or fictitious names. A paper reporting the results of investigations on human subjects or on animals must include a statement to the effect that the relevant national or other administrative and ethical guidelines have been adhered to, and a copy of the ethical clearance certificate should be submitted. Methods of statistical analyses used should be mentioned where relevant.

Results and Discussion: Results: the results should be concisely and logically presented. Repetition of the same results in figures, tables or text should be avoided.

Discussion: data essential for the conclusions emerging from the study should be discussed. Long, rambling discussions should be avoided. The discussion should deal with the interpretation of results. It should logically relate new findings to earlier ones. Unqualified statements and conclusions not completely supported by data should be avoided.

Molecular sequence data, such as gene or rDNA sequences, genome sequences, metagenomic sequences etc. must be deposited in a public molecular sequence repository, such as GenBank, that is part of the International Nucleotide Sequence Database Collaboration (INSDC). The accession numbers obtained must be cited in the text, Table or on Figures of phylogenetic trees of the manuscript.

Conclusion: The conclusion should be brief, highlight the outcomes of the study and should be aligned with the objectives of the study. It should not contain references.

Conflict of interest statement: All authors should include a statement on conflict of interest disclosing any financial or other substantive conflicts of interest that may be construed to influence the results or interpretation of their research. All sources of financial support for the project should be disclosed.

Acknowledgement: Should be brief and made for specific scientific, financial and technical assistance only. If a significant part of the research was performed in an institution other than in those indicated by the authors' affiliations given in the title page, this fact should be acknowledged. All those who have made substantial contribution to the research but do not qualify to be authors should be acknowledged.

References :

All research work of other authors, when used or referred to or cited, should be correctly acknowledged in the text and in the References.

Citing references in the text:

- References to the literature must be indicated in the text and tables as per the Author-Year System, by the author's last name and year, in parenthesis (i.e. Able, 1997) or (Able & Thompson, 1998).
- Citation to work by more than two authors should be abbreviated with the use of *et al.* (i.e. Able *et al.*, 1997).
- Multiple publications by the same first author in the same year should be coded by letters, (i.e. Thompson, 1991a; b).
- Multiple citations should be made in chronological order and separated by a semi-colon, (i.e. Zimmerman *et al.*, 1986; Able *et al.*, 1997).
- Reference to unpublished work, work in preparation or work under review should be cited in italics as (*unpublished data*) or, with the author's initials and surname given; such works should not be included in the Reference section.
- Personal communications may be mentioned in the text with the date of communication as (*Personal communication*, 2 June 2000).

List of references:

- The list of References should be arranged in alphabetical order based on the last name of the first author.
- Names of all the authors should be given except when there are more than 10 authors. When there are more than 10 authors, only the name of the first author can be given followed by *et al.*
- All the initials of the author must be given after the last name and the year of publication should follow in parentheses.
- This should be followed by the full title of the referred publication.
- When journal articles are listed, the journal name should be given in full and in italics and followed by the volume number in bold type, issue number in parentheses and then the inclusive pages.
- Where there are several publications by the same author(s) and published in the same year they should be differentiated by adding a lower-case letter after the year. When books are listed, the order should be: author(s), year, book title, volume number, edition, pagination/ inclusive pages, publisher and place of publication. The book title should be in italics. When sections of a book are listed, the order should be: author(s) of chapter, year, title of the section, title of the book, edition, inclusive pages, publisher and place of publication.
- Digital object identifiers (DOIs) should be included for all references where available.
- References should only be cited as 'in press' if the paper has been accepted for publication.

Examples of correct forms of references are given below.

Journal Articles

Boutin C. & Harper J.L. (1991). A comparative study of the population dynamics of five species of *Veronica* in natural habitats. *Journal of Ecology* 79(01): 199 – 221.

DOI: <https://doi.org/10.2307/2260793>

Books

Burnham K.P. & Anderson D.R. (2002). *Model Selection and Multimodal Inference*, 2nd edition, pp. 488. Springer Science and Business Media, Inc., New York, USA.

Book Chapters

Hinrichsen R.A. & Holmes E.E. (2009). Using multivariate state-space models to study spatial structure and dynamics. In: *Spatial Ecology* (eds. R.S. Cantrell, C. Cosner & S. Ruan), pp. 145 – 166. CRC/ Chapman Hall, Florida, USA.

DOI: <https://doi.org/10.1201/9781420059861.ch8>

Edited Books

Kimati H., Amorim L., Rezende J.A.M., Bergamin Filho A. & Camargo L.E.A. (eds.) (2005). *Manual de Fitopatologia*, volume 2. Doenças das Plantas Cultivadas, 4th edition. Ceres, São Paulo, Brazil.

Conference Papers

Weaver D. (2002). Implementation of a learning management system using an integrated approach to professional development. In: Winds of change in the sea of learning. *Proceedings of the 19th Annual Conference of the Australasian Society for Computers in Learning and Tertiary Education (ASCILITE)* (eds. A. Williamson, C. Gunn, A. Young & T. Clear), volume 2, Auckland, New Zealand, 8-11 December. Unitec Institute of Technology, Auckland, New Zealand, pp. 711-720.

Agency Publications

U.S. Census Bureau (2009). *World Population: 1950 – 2050*. U.S. Census Bureau, Washington DC, USA.

Department of Health (2008). *Health Inequalities: Progress and Next Step* (pdf). Department of Health, London, UK. Available at http://PublicationsPolicyAndGuidance/DH_08_5307, Accessed 9 June 2008.

Other

Robinson L.J. (2003) Spatial scale and depletion models of farmland birds in a fragmented landscape. *PhD thesis*, University of Reading, Reading, UK.

Efford M.G. (2008). Density 4.3: software for spatially explicit capture-recapture. Available at <http://www.otago.ac.nz/density>, Accessed 15 March 2009.

Abbreviations and Symbols: Unless common, these should be defined when first used, and not included in the abstract. The SI System of units should be used wherever possible. If measurements were made in units other than SI, the data should be reported in the same units followed by SI units in brackets, e.g. 5290 ft (1610 m).

Formulae and Equations: Equations should be typewritten and quadruple spaced. They should be started on the left margin and the number placed in parentheses to the right of the equation.

Nomenclature: Scientific names of plants and animals should be printed in italics. In the first citation, genus, species and authority must be given. e.g. *Borassus flabellifer* Linn. In latter citations, the generic name may be abbreviated, for example, *B. flabellifer* L.

Tables and figures: Tables and Figures should be clear and intelligible and kept to a minimum, and should not repeat data available elsewhere in the paper. Any reproduction of illustrations, tabulations, pictures etc. in the manuscript should be acknowledged.

Tables: Tables should be numbered consecutively with Arabic numerals and placed at the appropriate position in the manuscript. If a Table must be continued, a second sheet should be used and all the headings repeated. The number of columns or rows in each Table should be minimized. Each Table should have a title, which makes its general meaning clear, without reference to the text. All Table columns should have explanatory headings. Units of measurement, if any, should be indicated in parentheses in the heading of each column. Vertical lines should not be used and horizontal lines should be used only in the heading and at the bottom of the table. Footnotes to Tables should be placed directly below the Table and should be indicated by superscript lower case italic letters (^{*a*}, ^{*b*}, ^{*c*}, etc.).

Figures: All illustrations are considered as figures, and each graph, drawing or photograph should be numbered consecutively with Arabic numerals and placed at the appropriate position in the manuscript. Any lettering to appear on the illustrations should be of a suitable size for reproduction and uniform lettering should be used in all the Figures of the manuscript. Scanned figures or photographs should be of high quality (**300 dpi**), to fit the proportions of the printed page (12 × 17 cm). Each figure should carry a legend so that the general meaning of the figure can be understood without reference to the text. Where magnifications are used, they should be stated.

Units of measurement

Length: km, m, mm, μ m, nm

Area: ha, km², m²

Capacity: kL, L, mL, μ L

Volume: km³, m³, cm³

Mass: t, kg, g, mg, μ g

Time: year(s), month(s), wk(s),
d(s), h, min, s

Concentration: M, mM, N, %, g/L, mg/L, ppm

Temperature: °C, K

Gravity: x g

Molecular weight: mol wt

Others: Radio-isotopes: 32P

Radiation dose: Bq

Oxidation-reduction potential: rH

Hydrogen ion concentration: pH